CHEMICAL LASERS

V. K. Ablekov, Yu. N. Denisov,
and V. V. Proshkin

INTRODUCTION

Lasers, known also as *optical quantum generators*, are finding increasing use from year to year in commercial technology, medicine, communication, geodesy, and other branches of science and technology. Quantum techniques are used in holography, in sounding of remote objects and measuring large distances in astronomy, in research on transmission of television images with the aid of a light beam, etc. Promising results were obtained for the use of quantum generators for use in thermonuclear fusion [1].

The expanding fields of application of quantum generators is accompanied by modernization of the already produced systems and by the development of quantum generators using new active media and new physical and chemical principles Industry is now producing solid-state, gas-discharge, semiconductor, and dye lasers.

The development of stimulated-emission generators and amplifiers for the visible and infrared bands [2-7] evolved from the basic researches of N. G. Basov, A. M. Prokhorov, and Townes and coworkers, who obtained coherent radiation [8, 9] in the microwave band on the basis of amplification of electromagnetic waves [10, 11].

Methods other than those using optical or electric energy were developed for pumping of quantum generators. The most promising among them are thermal and chemical pumping. In the first, thermal energy is converted into the energy of coherent stimulated emission, and in the second the pumping energy is released in exothermic reactions in which atoms and molecules are produced in excited states [12-15].

A *chemical* quantum generator is a device in which population inversion and radiation generation are effected either directly, as a result of a chemical reaction, or after a reaction in which energy is exchanged between components of a medium, at least one of which is a product of this reaction.

The branch of science dealing with chemical quantum generators includes quantum mechanics, physics, chemical kinetics, optics, and hydro-, gas-, and plasmadynamics. With respect to the features of the energochemical transformations of reagents A, B, C, D, and G, the main processes in chemical lasers can be illustrated by the following scheme [16]:

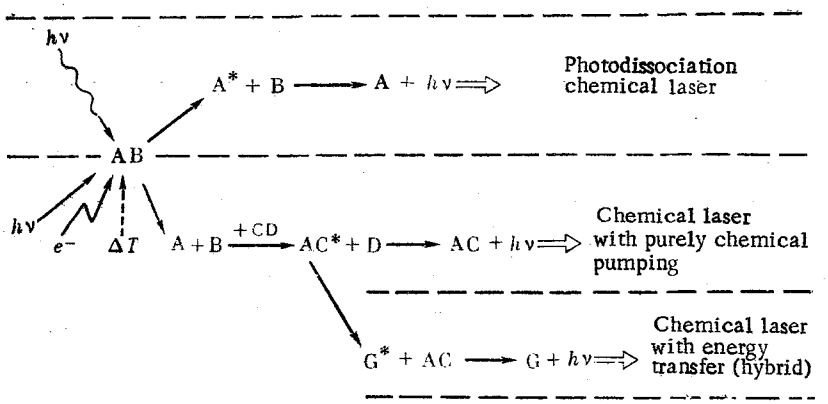

Translated from Khimicheskie Lazery, pp. 3-222, 1980.

0270-2010/83/0404-0287$07.50

Most chemical reactions are relatively slow and are therefore not suitable for population inversion. The excited particles (marked with an asterisk) have no time to accumulate and relax to the ground state, and no quantum-mechanical radiation is generated. Chemical lasers can therefore work only with rapid reactions, such as molecule photodissociation or other chemical reactions initiated by the action of light ($h\nu$), combustion, explosion (ΔT), electric discharge (e^-), or a chemical reaction between atoms or molecules, e.g., in colliding beams of atoms or molecules of various substances.

The chemical method of population inversion makes the construction of a laser with high efficiency and high output power possible. Particularly high power can be obtained from a laser with an explosive chemical reaction.

In a chemically pumped laser, chemical energy is directly converted into optical radiation. Among the advantages of such chemical lasers over other known lasers is also that they generate a broad wavelength spectrum in the range from 2 [17, 18] to 100 μm [19]. Advances in research into chemical lasers extends this range to the ultraviolet and millimeter regions of the spectrum.

The spectra of the coherent emission of chemical lasers coincide with the regions of the vibrational frequencies of many molecules. This makes it possible to use chemical lasers for a purposeful stimulation of chemical reactions by applying radiation to selected vibrational degrees of freedom [20].

Chemical lasers can be used to study the distribution and transport of energy in chemical reactions, and to obtain information on the nature of excited particles by wavelengths. Methods were developed for the measurement of the cross sections of relaxational and other chemical-kinetics processes, based on the use of chemical-laser radiation and on the salient features of spectral and temporal characteristics.

Chemical lasers make use of exothermic processes, in the course of which excited reaction products with inverted populations are obtained. Therefore, the chemical-laser properties cited above include also the fact that the energy required for the excitation is produced by a chemical reaction proper, and not by an external source, as, e.g., in solid-state and gas lasers. Later trends in science and technology have shown, however, that chemical lasers constitute a larger class of quantum mechanical systems, including some with external energy sources (such as γ-rays, electrons, and others), which initiate the chemical reactions, inasmuch as the reactions can be, e.g., photolytic or radiolytic. If account is also taken of matter conversion in the course of the reaction, excimer lasers can also be regarded as chemical. Inversion can also be obtained in plasmochemical reactions induced by the products of nuclear fission in energy releasing elements – nuclear fuel rods.

One more qualitatively new possibility of chemical pumping of lasers is indicated in [22]. It is proposed to use in lasers phototransitions that occur upon collision of two molecules capable of exothermic conversion. These phototransitions correspond to changes in the chemical bonds in molecules, i.e., they are identical to elementary chemical acts. Stimulation of a phototransition by light leads to photostimulation of the chemical process itself.

Included in [23] among the chemical lasers are also detonation lasers in which the detonation products serve as the active medium.

In this book, Chaps. 1 and 2 are devoted to an exposition of the laws governing the gas-phase chemical reactions typical of chemical lasers, under various conditions; to the principles of the quantum-mechanical description of molecular systems; and to certain processes in which excited particles are produced in the course of nonequilibrium chemical reactions. These chapters cast light on the concepts and processes used in the subsequent exposition of the material. The kinetics of the processes in chemical lasers is presented in Chapter 3.

This is followed by the development of a classification, indicated in [23, 24], of lasers in accord with their hydro- and gas-dynamic attributes, with description of both the construction of chemical-laser systems and their operating principles. Chapter 4 is therefore devoted to chemical lasers with an immobile working medium – static gaseous chemical lasers. In Chap. 5 chemical lasers with subsonic forced flow of the medium are considered, and in Chap. 6 lasers with diffusion of the component in a supersonic stream are considered. Chapter 7 is devoted to detonation chemical lasers.

The limited size of the book makes it impossible to present a more exhaustive exposition of an appreciable number of papers published to date on chemical lasers. The reader can fill this gap by becoming acquainted with the monographs [16, 25], the reviews [23, 24, 26-42], and topical articles [43]. An analysis of different trends in chemical laser development and their history are given in [44].

This book uses the SI system of units. The principal and derived units of this system (N, J, W, Hz, V, F, Ω, etc.) are listed in Soviet standard SÉV 1052-78 and are familiar to the reader, with the exception of the recently introduced measurement unit for pressure, the Pascal (Pa). We therefore present a conversion of this unit into the previously employed units not included in the SI system, viz., atm, bar, and mm Hg: 1 Pa = $9.8692 \cdot 10^{-6}$ atm (physical) = $10.1972 \cdot 10^{-6}$ bar (commercial) = $7.5006 \cdot 10^{-3}$ mm Hg.

For approximate estimates it is convenient to use the relations 1 MPa ≈ 10 atm (technical atmospheres) and 1 kPa ≈ 7.5 mm Hg.

LITERATURE CITED

1. N. G. Basov and O. N. Krokhin, "Conditions for plasma heating by laser radiation," Zh. Eksp. Teor. Fiz., 46, 171 (1964); P. P. Pashinin and A. M. Prokhorov, "Production of a high-temperature plasma by laser heating of a special gas target," Preprint No. 160, FIAN, Moscow (1970); Zh. Eksp. Teor. Fiz., 60, 1630 (1971); E. P. Velikhov and A. A. Filyukov, "New approach to the use of lasers for controlled fusion," in: Problems of Laser Thermonuclear Fusion [in Russian], Atomizdat, Moscow (1976), pp. 3-14.
2. A. M. Prokhorov, "Molecular amplifier and generator using submillimeter waves," Zh. Eksp. Teor. Fiz., 34, No. 6, 1658 (1958).
3. N. G. Basov, O. N. Krokhin, and Yu. M. Popov, "Generation, amplification, and display of infrared and optical radiation with the aid of quantum systems," Usp. Fiz. Nauk, 72, No. 2, 161-209 (1960); N. G. Basov, B. M. Vul, and Yu. M. Popov, "Quantum-mechanical semiconductor generators and amplifiers of electromagnetic oscillations," Zh. Eksp. Teor. Fiz., 37, No. 2, 587-588 (1959).
4. A. L. Schawlow and C. H. Townes, "Infrared and optical masers," Phys. Rev., 112, No. 6, 1940-1949 (1958).
5. T. H. Maiman, "Stimulated optical radiation in ruby," Nature, 168, No. 4736, 493-494 (1960).
6. V. K. Ablekov, M. S. Pesin, and I. L. Fabelinskii, "Realization of a medium with a negative absorption coefficient," Zh. Eksp. Teor. Fiz., 39, No. 3, 892-893 (1960).
7. A. Javan, W. R. Bennett, and D. R. Harriott, Jr., "Population inversion and continuous optical maser oscillations in a gas discharge containing a He-Ne mixture," Phys. Rev. Lett., 6, No. 3, 106-110 (1961).
8. N. G. Basov and A. M. Prokhorov, "Use of molecular beams for microwave-spectroscopy study of rotational spectra of molecules," Zh. Eksp. Teor. Fiz., 27, No. 4, 431-438 (1954); "Molecular generator and amplifier," Usp. Fiz. Nauk, 57, No. 3, 481-501 (1955).
9. J. P. Gordon, H. J. Zeiger, and C. H. Townes, "Molecular microwave oscillator and new hyperfine structure in the microwave spectrum of NH_3," Phys. Rev., 95, No. 1, 282-284 (1954).
10. V. A. Fabrikant, "Mechanism of gas-discharge radiation," Tr. VEI, No. 41, 236 (1940).
11. V. A. Fabrikant, M. M. Budynskii, and F. A. Butaeva, "Method of amplifying electromagnetic radiation," Inventor's Certificate No. 123209, Disclosure No. 5767491 of 18 June (1951); Byull. Izobret., No. 29, 29 (1959). "Amplification of electromagnetic waves," Discovery Diploma No. 12-18.6.51, Byull. Izobret., No. 8 (1962).
12. J. C. Polanyi, "Proposal for an infrared maser dependent on vibrational excitation," J. Chem. Phys., 34, No. 1, 347-348 (1961).
13. A. N. Oraevskii, "Production of negative temperatures in chemical reactions," Zh. Eksp. Teor. Fiz., 45, No. 2(8), 177 (1963).
14. V. L. Tal'roze, "Concerning generation of coherent induced radiation in chemical reactions," Kinet. Katal., 5, No. 1, 11-27 (1964).
15. J. V. V. Kasper and G. C. Pimentel, "HCl chemical laser," Phys. Rev. Lett., 14, No. 10, 352-354 (1965).
16. K. I. Kompa, Chemical Lasers, Springer-Verlag, Berlin (1973).
17. S. N. Suchard and G. C. Pimentel, "Deuterium fluoride overtone chemical laser," Appl. Phys. Lett., 18, 530-531 (1971).
18. F. G. Sadie, P. A. Bürger, and O. G. Malan, "Continuous-wave overtone bands in a CS_2–O_2 chemical laser," J. Appl. Phys., 43, 2906-2907 (1972).

19. N. Skribanowitz, I. P. Herman, R. M. Osgoot,Jr., et al., "Anisotropic ultrahigh gain emission observed in rotational translations in optically pumped HF gas," Appl. Phys. Lett., 20, 428-432 (1972).
20. V. L. Tal'roze and P. P. Barashev, "Chemical actions of laser radiation," Zh. Vses. Khim. O-va im. D. I. Mendeleeva, 8, No. 1, 5 (1973).
21. L. I. Gudzenko and S. I. Yakovlenko, Plasma Lasers [in Russian], Atomizdat (1978).
22. S. I. Pekar, "Chemical high-pressure lasers and optically stimulated chemical reactions, Dokl. Akad. Nauk SSSR, 187, No. 3, 555-557 (1969).
23. W. R. Warren, Jr., "Chemical lasers," Astron. Aeron., 13, No. 4 (1975).
24. W. H. Christiansen, D. A. Russell, and A. Hertzberg, "Flow lasers," Ann. Rev. Fluid Mech., 7, 115-139 (1975).
25. A. S. Bashkin et al., "Chemical lasers," in: Progress in Science and Engineering [in Russian], Vol. 8, VINITI (1975), p. 382
26. A. N. Oraevskii, "Chemical lasers," Khim. Vys. Energ., 8, No. 1, 3-20 (1974).
27. S. Solimeno, "Chemical lasers," Phys. Bull., Nov., 517-520 (1974).
28. M. S. Dzhidzhoev , V. T. Platonenko, and R. V. Khokhlov, "Chemical lasers," Usp. Fiz. Nauk, 100, No. 4, 641-679 (1970).
29. O. S. Heavens, "Some recent development in gas lasers," Contemp. Phys., 17, No. 6, 529-552 (1976).
30. T. A. Cool, "The transfer chemical lasers: a review of recent research," IEEE J. Quantum Electron., QE-1, No. 1, 72-83 (1973).
31. V. N. Karnyushin and R. I. Soloukhin, "Use of gasdynamic flows in laser technology," Fiz. Goreniya Vzryva, No. 2, 163-202 (1972).
32. C. R. Jones and H. P. Broida, "Chemical lasers in the visible," Laser Focus, 10, No. 3, 37-47 (1974).
33. N. G. Basov et al., "Dynamics of chemical lasers (a review)," Kvantovaya Elektron (Moscow), No. 2, 3-24 (1971).
34. A. N. Chester, "Chemical lasers: a survey of current research," Proc. IEEE, 61, No. 4, 414-422 (1973); A. N. Chester and L. D. Hess, "Study of the HF chemical lasers by pulse-delay measurements," IEEE J. Quantum Electron., QE-8, No. 1, 3-13 (1972).
35. R. W. F. Gross and J. F. Bott (eds.), Handbook of Chemical Lasers, Wiley-Interscience (1976).
36. J. J. Ewing, "New laser sources," in: Chemical and Biochemical Applications of Lasers (C. B. Moore, ed.), Academic Press, Vol. II (1972), pp. 241-278.
37. R. I. Soloukhin, "Present status and prospects for the development of combustion gas-dynamic lasers," in: Combustion and Explosion [in Russian], Nauka (1977), pp. 30-49.
38. A. N. Oraevskii, "Chemical lasers," in: Laser Handbook [in Russian] (A. M. Prokhorev, ed.), Vol. 1, Sovet-Skoe Radio (1978), pp. 158-183.
39. Chemical and molecular lasers," J. Opt . Soc. Am., 68, No. 5, 651-656 (1978).
40. A. V. Eletskii, "Excimer lasers," Usp. Fiz. Nauk, 125, No. 2, 279-314 (1978).
41. "UV and excimer lasers, I," J. Opt. Soc. Am., 68, No. 5, 702-706 (1978); II, ibid., 711-718.
42. I. N. Knyazev and V. S. Letokhov, "Gas lasers in the UV and VUV regions of the spectrum," in: Laser Handbook [in Russian] (A. M. Prokhorov, ed.), Vol. 1, Sovet-skoe Radio (1978), pp. 197-220.
43. A. S. Bashkin, N. L. Kupriyanov, and A. N. Oraevskii, "Chemical lasers in the visible, based on chain reactions," Kvantovaya Elektron (Moscow), 6, No. 12, 2611-2619 (1978); "Use of excited atoms in thermally initiated chemical lasers in the visible," ibid., 2567-2576.
44. I. M. Dunskaya, Lasers and Chemistry [in Russian], Nauka (1979).

CHAPTER 1

LAWS OF KINETICS OF GAS-PHASE CHEMICAL REACTIONS

1.1. Law of Effective Masses

The processes in chemical lasers take place mainly in the gas phase, and to assess the chemical reactions in chemical lasers one must know the rates and the ratios at which the initial gases react and the compositions of the intermediate and resultant products. We therefore consider the laws governing the chemical reactions in gaseous media.

Reaction Rate. Rate Constant. Consider a gas consisting in the general case of the chemical components A_i ($i = 1, 2, \ldots, n$), i.e., of N_1 molecules of component A_1, N_2 molecules of component A_2, N_3 molecules of component A_3, etc. The chemical reaction of conversion of the initial substances $A_1, A_2, \ldots, A_i$ into the reaction products $A_1', A_2', \ldots, A_i'$ can then be described by the stoichiometric equation

$$\sum_{i=1}^{N} r_i A_i \rightarrow \sum_{i=1}^{N} r_i' A_i', \tag{1.1}$$

where r_i and r_i' are the *stoichiometric coefficients* of the reaction for the i-th substance in the states of the initial reagent and of the reaction product, respectively.

For a system with a fixed volume V and composition, the connection between the change of the concentration of any two substances i and j participating in the reaction is expressed, on the basis of Eq. (1.1), in the form

$$\bar{w}_i/(r_i' - r_i) = \bar{w}_j/(r_j' - r_j). \tag{1.2}$$

Here $\bar{w} = V^{-1}\,\Delta N/\Delta t$ mole/(cm^3•sec) is the change of the molar concentration $c = N/V$ of the substance during the time Δt, i.e., the average rate of the chemical reaction.

The chemical reaction rate w is in the general case a function of the concentrations of the reacting substances, of the pressure, and of the temperature [1]. The dependence of the reaction rate on the concentration of the reagents is determined by the law of effective masses: *The reaction rate is proportional to the product of the concentrations of the reacting substances*. Thus, for a reaction of the general form (1.1),

$$w = kc_1^{r_1} c_2^{r_2} \ldots = k \prod_{i=1}^{N} c_i^{r_i}, \tag{1.3}$$

where k is the rate constant or the specific reaction rate. The value of k usually increases rapidly with increasing temperature.

Simple Reaction. Order of Reaction. Molecularity. According to the derivation of the *law of effective masses* from the kinetic theory of gases, the number of simultaneous collisions produced when r_1 molecules of substance A_1 (concentration c_1) interact with r_2 molecules of substance A_2 (concentration c_2), etc., is proportional to the product $c_1^{r_1} c_2^{r_2} \ldots$. Conversely, the rate of the single-stage reactions that include the simultaneous interaction of $r_1 + r_2 + \ldots = r$ molecules should be expressed by the law of effective masses [2]. The reactions that satisfy this condition are called *simple reactions*.

By definition,

$$dc_i/dt = w_i, \qquad i = 1, \ldots, N, \tag{1.4}$$

and in the elementary stage of the reaction,

$$w_i = (r_i' - r_i)\, w. \tag{1.5}$$

Taking (1.3) and (1.5) into account we obtain in lieu of (1.4), for the substances i and j,

$$dc_i/dt = [(r_i' - r_i)k] \prod_{j=1}^{N} c_j^{r_j}, \tag{1.6}$$

where $(r_i' - r_i)k$ is a constant for isothermal systems. Usually, measurements of the value of dc_i/dt in isothermal reactions lead to

$$dc_i/dt \sim \prod_{j=1}^{N} c_j^{n_j}, \tag{1.7}$$

where the exponents n_j are constants. In such cases the number n_i is called the *order of the reaction* for the i-th substances, and $n \equiv \sum_{i=1}^{N} n_i$ is the *summary order* or simply the order of the reaction.

It can be seen from (1.6) and (1.7) that if the reaction is simple then $n_i = r_i$. The quantity n_i is then the molecularity of the reaction relative to the substance i, and n is the summary molecularity of the reaction. Thus, the molecularity of a reaction is determined by the number of molecules that participate in the process: at r = 1 the reaction is of first order or monomolecular, at r = 2 it is of second order, etc.

A relation of the form (1.7) frequently takes place even when Eq. (1.6) does not hold, i.e., when the reaction consists of several stages. In such cases the connection between the order of the reaction and the molecularities becomes more complicated and n_i can take on non-integer values [3].

1.2. Mechanisms of Simple Reactions

First-Order Reactions. When the rate of change of the concentration is proportional to the concentration, one refers to a first-order reaction. Such a reaction is the simplest chemical process. According to the law of effective masses (1.3), the rate of a first-order reaction for a reagent A_1 (i = 1) is

$$w = -dc_1/dt = kc_1, \tag{1.8}$$

where

$$[\sec^{-1}] > 0.$$

Integrating (1.8), we obtain, if the concentration c_1^0 at the initial instant of time t = 0 is known,

$$c_1 = c_1^0 \exp(-kt) = c_1^0 \exp(-t/\tau). \tag{1.9}$$

From (1.9) follows an expression for the reaction rate constant

$$k = (1/t) \ln (c_1^0/c_1). \tag{1.10}$$

At $t = \tau$ the concentration of the reagent A_1 is decreased by a factor e. The quantity $\tau_e = 1/k$ is called the *characteristic reaction time*. The rate of a chemical reaction can also be assessed from the *half-life* $\tau_{1/2}$ of the reaction, or the time during which the initial concentration c_1^0 is decreased to one-half: $\tau_{1/2} = \ln 2/k$. The simplest type of reaction that obeys Eq. (1.8) is the monomolecular decomposition of a substance*

$$AB \rightarrow A + B. \tag{1.11}$$

The molecule AB is assumed constant and should not decay spontaneously into reaction products. What is then the mechanism of a monomolecular process?

It is assumed that not all molecules are subject to decomposition, but only those that are specially activated and have an internal energy exceeding a certain threshold value,

*Here and elsewhere we designate the reagents A_i and their products A_i' not only by numerical subscripts, but also by different letters A, B, C, ..., AB, BC, ...

namely an *activation energy* E_a. Such molecules are called *active*. According to [4], many monomolecular reactions proceed in two stages:

$$AB + M \underset{k_2}{\overset{k_1}{\rightleftarrows}} AB^* + M; \tag{1.12}$$

$$AB^* \xrightarrow{k_3} AB^{\neq} \rightarrow A + B, \tag{1.13}$$

the first of which is the activation (k_1) and deactivation (k_2) of the molecules, and the second is their decay (k_3). The letter M in (1.12) and (1.13) denotes an arbitrary molecule, and the asterisk marking AB means that the molecule is in an excited (in this case, unstable) state, while the symbols above and below the arrows indicate the values of the specific rate constants k_1, k_2, and k_3 for the elementary stages of the reaction.

During the second stage (1.13), owing to the intramolecular redistribution of the energy, a monomolecular transformation takes place. Since the realization of such a transformation requires that the active-particle energy be concentrated on definite degrees of freedom, one introduces the concept of the *activated molecule* $AB^{\neq}$, which is the instantaneous state of the active molecule; transition through this state completes the reaction.

The first-order reactions and the second-order reactions described below play an essential role in chemical kinetics, since most elementary stages constitute mono- or bimolecular reactions.

Reactions of Second and Higher Orders. When molecules A_1 and A_2 form in the reaction (1.1) molecules of type A' and at the same time the reaction rate is proportional to the concentration of both initial substances, the process is referred to as a second-order reaction.

The kinetics of a second-order chemical reaction, for reagents A_1 and A_2, is described by the equation

$$-\frac{dc_1}{dt} = -\frac{dc_2}{dt} = kc_1c_2, \tag{1.14}$$

where k has the dimensionality [cm³/mole•sec].

After integration of (1.14), we obtain, in analogy with (1.9) and (1.10), for known initial conditions $c_1 = c_1^0$ and $c_2 = c_2^0$:

$$\frac{c_1}{c_2} = \frac{c_1^0}{c_2^0}\exp[-(c_2^0 - c_1^0)kt]. \tag{1.15}$$

The expression for the rate constant of the reaction is then

$$k = \frac{1}{t}\frac{1}{c_2^0 - c_1^0}\ln\frac{c_2c_1^0}{c_2^0c_1}. \tag{1.16}$$

Examples of second-order reactions are the bimolecular decomposition of hydrogen iodide $2HI \rightarrow H_2 + I_2$ and the thermal decomposition of chlorine oxide $2Cl_2O \rightarrow 2Cl_2 + O_2$.

We now consider the n-th order reaction

$$A + B + C + \ldots \rightarrow \text{reaction products.}$$

If $c_1^0 = c_2^0 = \ldots = c^0$, the reaction rate is

$$-dc/dt = kc^n. \tag{1.17}$$

Integrating (1.17), we obtain an expression for the reaction rate constant

$$k = \frac{1}{t(n-1)}\left(\frac{1}{c^{(n-1)}} - \frac{1}{(c^0)^{(n-1)}}\right), \tag{1.18}$$

the dimensionality of which is $[(\text{cm}^3/\text{mole})^{(n-1)}\cdot\text{sec}^{-1}]$. For $c = c^0/2$, $t = \tau_{1/2}$ we have

$$k = \frac{(2^{(n-1)} - 1)}{\tau_{1/2}(n-1)}\frac{1}{(c^0)^{(n-1)}} \tag{1.19}$$

and

$$\tau_{1/2} = \frac{(2^{(n-1)} - 1)}{k(n-1)} \frac{1}{(c^0)^{(n-1)}}. \tag{1.20}$$

Thus, for the general case of an n-th order reaction

$$\tau_{1/2} \sim (c^0)^{-(n-1)}, \tag{1.21}$$

i.e., the form of the dependence of the reaction half-life on the initial concentration describes the actual order of the reaction. It is not very likely that reactions with molecularity larger than three can play a role in chemical processes, since high-molecularity reactions are exceedingly slow.

1.3. Chemical Equilibrium

Equilibrium Conditions and the Equilibrium Constant. Since chemical reactions proceed in both direct and reverse directions, Eq. (1.1) should be written in the form

$$\sum_{i=1}^{N} r_i A_i \underset{k_b}{\overset{k_f}{\rightleftarrows}} \sum_{i=1}^{N} r_i' A_i', \tag{1.22}$$

i.e., besides the direct reaction (1.1) there proceeds also its reverse reaction.

If we denote the equilibrium constants by c_{ie} and c_{je}, the condition for the equilibrium of the direct and reverse reactions is

$$k_f \prod_{i=1}^{N} c_{ic}^{r_i} = k_b \prod_{j=1}^{N} c_{je}^{r_j'}. \tag{1.23}$$

From this we get the *equilibrium constant*

$$K_c = \frac{k_f}{k_b} = \prod_{j=1}^{N} c_{je}^{r_j'} \Big/ \prod_{i=1}^{N} c_{ie}^{r_i}. \tag{1.24}$$

Tables and handbooks usually list equilibrium constants K_p expressed in terms of the partial pressures p_i and p_j of the substances that take part in the reaction

$$K_p = \prod_{j=1}^{N} p_j^{r_j'} \Big/ \prod_{i=1}^{N} p_i^{r_i}. \tag{1.25}$$

The Arrhenius Law. From [5] follows the temperature dependence of the equilibrium constant at constant volume as a function of the reaction heat Q

$$d \ln K/dT = -Q/RT^2. \tag{1.26}$$

Here R is the gas constant.

Arrhenius [6] proposed to use for the reaction rate constant k vs the temperature an analogous equation

$$d \ln k/dT = E_a/RT^2,$$

where E_a is the difference between the energies of the active and inactive molecules of the initial substances, i.e., the *activation energy*. If E_a is constant, then

$$\ln k = \text{const} - E_a/RT,$$

or, putting const = ln A, we obtain

$$k = A \exp(-E_a/RT), \tag{1.27}$$

where A is the frequency factor or the preexponential factor.

In the Arrhenius law (1.27) the value of A can depend little on the temperature T. For all reactions one can then use within the experimental error the equation

$$A = BT^{\alpha} \tag{1.28}$$

with account taken of the fact that B = const, α = const and $0 \leqslant \alpha \lesssim 1$.

An idea of the order of magnitude of the preexponential factor can be obtained from the results [7] of the decay and isomerization of substances.

In general, in accord with the transition-state method [8-10], the preexponential factor A is represented as a product of the *gas-kinetic collision number* Z_0 and the so-called *steric factor* P, which describes the effectiveness of one collision of the molecules relative to the chemical reaction, or the directivity of the interaction that leads to formation of the chemical bond.

The reactions proceed sometimes with the preexponential factor A deviating considerably from the usual values 10^{12}-10^{15} sec^{-1}. It is assumed for specially large values of A [11] that the reaction only appears to be monomolecular, and proceeds actually via a chain mechanism.

The Arrhenius law (1.27) can be theoretically proved by using the premises of the kinetic theory of gases (see, e.g., [12]).

Activation Energy. Only a small fraction of the colliding molecules take part in the reaction, only those whose summary collisional kinetic energy exceeds a certain critical value E_a. The number of these molecules is smaller the more this energy exceeds the average energy of the system ((3/2) $k^{\circ}T$ for monatomic gases and (5/2)$k^{\circ}T$ for diatomic, where k° is Boltzmann's constant). The value of E_a for a reaction usually amounts to several times ten thousand joules per mole, whereas the average energy at an approximate temperature 1000°C reaches only several thousand. This means that on the Maxwellian velocity distribution curve of the molecules the reaction is characterized only by the branch in which the velocities exceed a certain critical value.

Thus, at $E_a \approx 84$ kJ/mole the fraction of the molecules capable of entering in the reaction is only 0.0045% at 1000°C and reaches 0.67% at 2000°C.

It follows from the notions concerning the molecular structure of matter that a homogeneous reaction in an ideal gas takes place when two or three molecules collide. The collision and the subsequent reaction are described by a Schrödinger equation in which the independent variables are the coordinates of all the electrons and nuclei contained in the interacting molecules. For a sufficiently slow collision process, such that the solution of the nonstationary Schrödinger equation hardly differs from that of the stationary one and the kinetic energy of each nucleus is small compared with that of the electrons, it can be assumed that the nuclei move along trajectories on the *potential energy surface* (PES).

The height of the energy barrier of the reaction on the PES is equal to the activation energy E_a needed to restructure the intramolecular bonds. As an illustration of this definition, we can consider the interchange of the energy states in the bimolecular chemical reaction A + BC → AB + C, using as coordinates the potential energy E_p (Fig. 1.1) and the running time t of the reaction.

If the atom A has a rather high energy, total breaking of the bonds between the atoms A, B, and C takes place, namely, dissociation of the molecule BC (upper curve of Fig. 1.1). If a chemical reaction takes place between A and BC, the potential energy reaches a maximum (middle curve of Fig. 1.1), there is no complete breaking of the interatomic bonds, and the system is in an unstable equilibrium — in the activated state A–B–C. Next, depending on the type of reaction, the process will follow the middle or the lower curve. In the former case the reaction is endothermic, and in the latter exothermic.

The activation energies of the direct and reverse reactions are different. It follows from Fig. 1.1 that the endothermic reaction that is the reverse of an exothermic one has an activation energy $E_r = E_a + Q_{ex}$, where Q_{ex} is the *thermal effect of the reaction*.

1.4. Complex Reactions

Successive Reactions. The simplest kinetic equations of first, second, and third order describe only an extremely small number of processes. Most chemical reactions go through individual mono- or bimolecular stages in which intermediate products are formed.

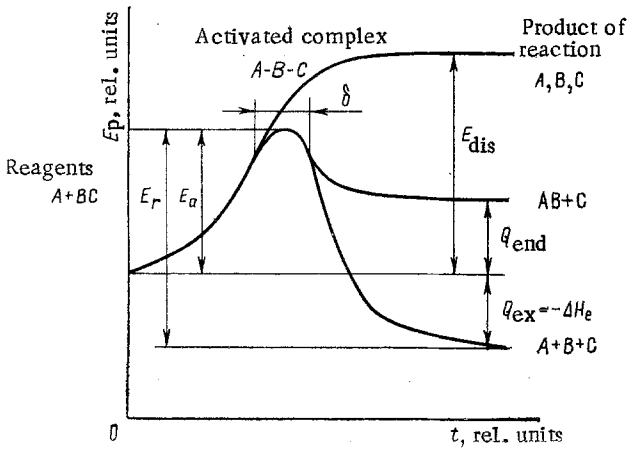

Fig. 1.1. Change of potential energy of the system in the collision of A with BC.

Many complex reactions have two or several stages that follow one another:

$$A \xrightarrow{k_1} B \xrightarrow{k_2} C \text{ etc.}$$

or

$$A + B \xrightarrow{k_1} C + D \xrightarrow{k_2} M + N.$$

These reactions are called reactions with successive stages. In these reactions, the substance produced in the first stage is capable of continuing a chemical reaction, and the subsequent chemical transformation is effected in the subsequent stages of the reaction. Such substances are called *intermediate substances*.

It follows from [13] that each stage has its own PES independent of the others. The reacting systems that go through the highest energy barriers need not necessarily pass through all the intermediate stages. Therefore, the rate of a reaction with successive stages is determined by the rate of passage of the activated complex through the highest energy barrier.

Parallel Reactions. The simplest type of parallel reactions is those in which the initial substance is transformed via two or more independent ways, which result in either identical or different reaction products:

$$A \underset{k_2}{\overset{k_1}{\rightrightarrows}} \begin{matrix} M \\ N \end{matrix}.$$

We write down the kinetic equations for such reactions, assuming each to be monomolecular:

$$dc_M/dt = k_1 c_A, \quad dc_N/dt = k_2 c_A. \tag{1.29}$$

Dividing one equation by the other and integrating, we get

$$c_M/c_N = k_1/k_2, \tag{1.30}$$

i.e., the yields of the products of the parallel reactions have the same ratio as the rate constants of these reactions.

We determine the rate constant of such a combined reaction:

$$-dc_A/dt = dc_M/dt + dc_N/dt = (k_1 + k_2)\, c_A = kc_A. \tag{1.31}$$

Consequently, the rate constant of the combined reaction in the case of two or several stages is equal to the sum of the rate constants of these stages, $k = \Sigma k_i$.

Coupled Reactions. Chemical Induction. A feature of a number of widely encountered parallel chemical reactions is that one of these stages (A + B) can proceed only in the presence of another parallel reaction in the system (A + C). These reactions are called *coupled*; this phenomenon is called in chemistry *chemical induction*. The inducing reaction (A + B) is knows as *primary*, and the coupled induced reaction (A + C) as *secondary*. The substance A, which participates in both reactions, is called the *actor*; the substance B, the interaction

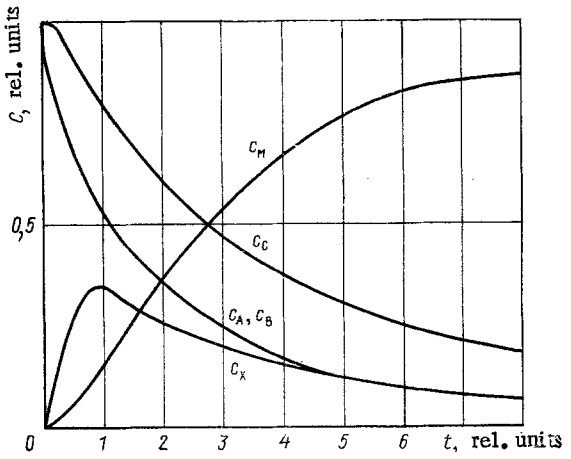

Fig. 1.2. Kinetic curves for coupled reactions.

of which with the actor induces the secondary reaction, is called the *inductor*; C is called the *acceptor*.

Such a process is described by an *induction factor*, which is the ratio of the actor fraction that participates in the reaction to the actor fraction that participates in the transformation of the inductor.

The simultaneous oxidation of carbon and hydrogen is cited in [2] as an example of coupled reactions. The reaction $2CO + O_2 = 2CO_2$ in the absence of impurities does not take place up to very high temperatures, but is easily realized in the presence of hydrogen in the mixture [14, 15]. In these reactions hydrogen is the inductor, CO the acceptor, and O_2 the actor, which takes part in reactions with both H_2 and CO. The induction factors is the ratio of the amounts of the produced CO_2 and H_2O.

The chemical induction phenomenon is based on the formation, in the course of the primary reaction, of intermediate substances that directly transfer the inductive influence of the primary reaction to the secondary [16].

On the basis of these concepts, coupled reactions are described by a set of two elementary processes A + B = X + ..., X + C = M + ... (A is the actor; B, inductor; C, acceptor; X, intermediate substance; M, reaction product), for which the following equations hold:

$$\left.\begin{aligned} -dc_A/dt = -dc_B/dt &= k_1 c_A c_B; \\ dc_X/dt &= k_1 c_A c_B - k_2 c_C c_X; \\ -dc_C/dt &= dc_M/dt = k_2 c_C c_X. \end{aligned}\right\} \qquad (1.32)$$

At $c_A^\circ = c_B^\circ = c_C^\circ = c^\circ$, we have

$$\left.-dc_A/dt = k_1 c_A^2;\ dc_X/dt = k_1 c_A^2 - k_2 (c_A + c_X) c_X.\right\} \qquad (1.33)$$

It can be seen from the solution of these differential equations (Fig. 1.2) that the acceptor C is consumed more slowly than the actor A and the inductor B. The consumption curve is S-shaped, i.e., it can be assumed that the substance C gets involved in the reaction only via the intermediate substance X whose concentration is low at the initial instant. The limiting case of coupled reaction can be taken to be homogeneous catalytic reactions, inasmuch as in any case an active intermediate substance is produced in the primary interaction between the actor and the inductor-catalyst. This inductor is a *positive catalyst* if the reaction is accelerated, and a *negative catalyst* or *inhibitor* if it is slowed down. Reactions break up frequently into macroscopic stages separated in time, with the inhibitor influencing only the first — initiating — stage [17]. In certain reactions [18, 19] the catalyst accumulates as the reaction proceeds and is a product of the reaction itself. This leads to self-acceleration of the reaction — *autocatalysis*. In most cases the autocatalysis kinetic equations do not describe the real reaction mechanism. Thus, it is shown in [20, 21] that branched-chain reactions with a complicated mechanism also correspond to the kinetics of autocatalysis.

1.5 Chain Reactions

Kinetics of Chain Reactions. A set of consecutive reactions sometimes has a rate that exceeds the rate of the chain reaction as given by the stoichiometric equation (1.1). This occurs when the active particles or *centers* A are replenished during one or several stages of the reaction 1 → 3, as shown in Fig. 1.3. In this case an active particle A is produced simultaneously with the molecule of the reaction product C. The rate of such a reaction can be expressed in the stationary case (see Fig. 1.3a) by the equation

$$w = w_0 P_1 P_3 + w P_1 P_3, \tag{1.34}$$

where w_0 is the rate of thermal activation of the molecule, and P_i is the probability of each of the i = 1, 2, 3, 4 elementary processes.

Introducing the chain length l_c, we obtain from (1.34)

$$w = \frac{w_0}{[(1/P_1 P_3) - 1]} = w_0 l_c, \tag{1.35}$$

$$l_c = \frac{1}{[(1/P_1 P_3) - 1]} = \frac{P_1 P_3}{(1 - P_1 P_3)}. \tag{1.36}$$

It has been shown experimentally that the principal active centers of such *chain reactions* are chemically unsaturated fragments of molecules – *free atoms and radicals*. The chains produced by them are called *radical chains*.

Simple Chain Reactions. The reactions described by expressions (1.34)-(1.36) are called *simple chain reactions*. In each link of the chain no more than one center is newly produced for each consumed active center.

In chain-reaction kinetics [21] the probability that the reaction will follow the path 1 is called the *probability* $P_1 = \alpha_c$ *of chain continuation* with a stationary-reaction rate

$$w = \frac{dc_C}{dt} = \frac{w_0 \alpha_c}{1 - \varepsilon \alpha_c} = w_0 l_c, \tag{1.37}$$

where

$$l_c = \alpha_c/(1 - \varepsilon\alpha_c). \tag{1.38}$$

For simple reactions, ε = 1 and the chain length l_c is the average number of links per active center, i.e., *the average chain length*. The probability of continuation of a chain of s links is

$$P_s = \alpha_c^s (1 - \alpha_c). \tag{1.39}$$

Here $1 - \alpha_c = \beta_c$ is the chain-breaking probability.

The evolution of the reaction in time is described by the following expression for the reaction rate:

$$w = \nu_1^{\alpha_c} c_A = \frac{w_0 \alpha_c}{1 - \varepsilon \alpha_c} \left[1 - \exp\left(-\frac{t}{\tau}\right)\right] = w_0 l_c \left[1 - \exp\left(-\frac{t}{\tau}\right)\right], \tag{1.40}$$

where ν^{α_c} is the frequency of the particle-interaction acts and τ is the lifetime of the active center.

If the chain is broken, we have for the chain reaction $\alpha_c < 1$. The chain-breaking probability β_c is then inversely proportional to the chain length l_c:

$$\beta_c \sim l_c^{-1}. \tag{1.41}$$

Active particles whose mean free path is smaller than the vessel dimensions move to the vessel walls with a diffusion flux

$$q_D = -D dc_A/dx, \tag{1.42}$$

where D is the diffusion coefficient and dc_A/dx is the gradient of the concentration of the active centers along the normal to the vessel-wall surface.

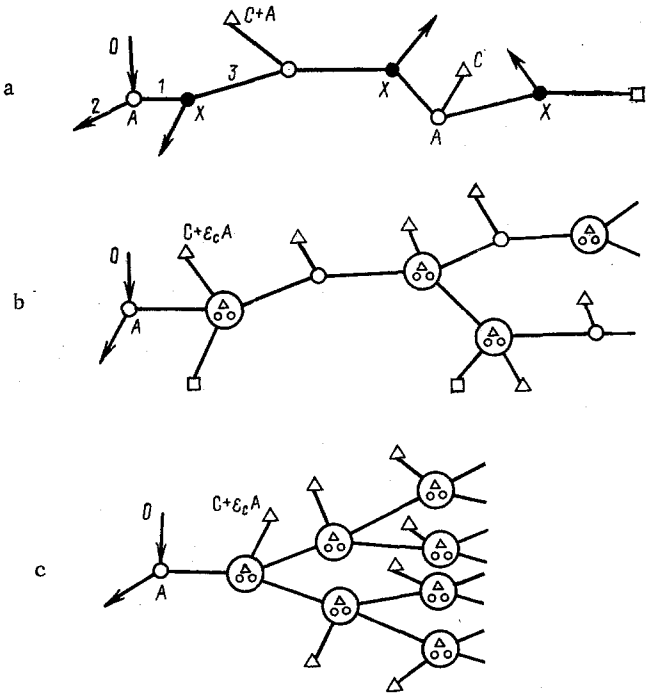

Fig. 1.3. Diagrams of simple $\varepsilon_c = 1$ (a); branched $2 > \varepsilon_c > 1$ (b) and repeatedly branched $\varepsilon_c = 2$ (c) chain reactions: ○) active centers A; △) reaction products C; □) reaction by-products; ●) intermediate substance.

If we consider now the process along this normal and introduce the concept of a "reduced film" of thickness Δ [22], it follows from (1.42) that

$$q_D = (D/\Delta)(c_A - c'_A), \tag{1.43}$$

where c'_A is the concentration of the active centers near the surface.

Equating, in the stationary case, q_D to flux due to the breaking of the chains at the wall surface, we obtain

$$(D/\Delta)(c_A - c'_A) = kc'_A, \tag{1.44}$$

whence

$$c'_A = \frac{D/\Delta}{k+(D/\Delta)} c_A, \tag{1.45}$$

and the reaction rate is

$$w = kc'_A = \frac{kD/\Delta}{k+(D/\Delta)} c_A. \tag{1.46}$$

Denoting by k* the effective rate constant, we have

$$k^* = \frac{kD/\Delta}{k+(D/\Delta)} \quad \text{or} \quad \frac{1}{k^*} = \frac{1}{k} + \frac{1}{D/\Delta}, \tag{1.47}$$

where k^{-1} and $(D/\Delta)^{-1}$ are, respectively, the *diffusion* and the *kinetic resistances*.

It can be seen from (1.46) and (1.47) that at $k \gg D/\Delta$ we have $k^* = D/\Delta$ and the reaction rate is determined by the diffusion. In this case it is said that the reaction takes place in the *diffusion region* with $c'_A \ll c_A$. At $k \ll D/\Delta$ we have $k^* = k$ and the total reaction rate is determined by the rate of the chemical process itself, i.e., the reaction takes place in the *kinetic region* with a concentration c'_A almost equal to c_A.

Reactions with Branched Chains. Chain reactions in which more than one center is produced on the average per consumed active center are *branched*. We denote the branching probability for one link of the chain by [21]

$$\delta_c = \varepsilon_c - 1. \tag{1.48}$$

At $\delta_c > 0$ branchings take place from time to time on individual sections of the chain, and additional active centers initiate second branched chains (see Fig. 1.3b). At $\delta_c = 1$ ($\varepsilon_c = 2$) branching takes place in each link of the chain (see Fig. 1.3c). The chains obtained in this manner are called *repeatedly branched*.

We now calculate the length l'_c of a branched chain, i.e., the number of elementary reactions caused by the appearance of one primary active center. The effective chain-breaking probability is the difference $(\beta_c - \delta_c)$. Consequently, with allowance for (1.41),

$$l'_c = 1/(\beta_c - \delta_c) = l_c/(1 - l_c\delta_c); \tag{1.49}$$

$$w = c_A^0 l'_c = c_A^0 l_c/(1 - l_c\,\delta_c). \tag{1.50}$$

Since β_c and δ_c are functions of temperature and pressure, it is possible to have under certain conditions $\beta_c - \delta_c \cong 0$, and then the chain length is $l'_c \to \infty$. This means that if at least one branching takes place over the length of a simple chain, i.e., $l_c\delta_c = 1$, an explosive process is produced.

Limiting Phenomena. At a certain vapor pressure of a phosphorus–oxygen mixture, the ignition region is bounded by two limiting oxygen pressures $(p_{O_2})_1$ and $(p_{O_2})_2$. Outside this region, the phosphorus vapor is not ignited. A quantitative investigation of this process [23-25], together with a study of the ignition of a stoichiometric mixture of hydrogen with oxygen [26-28], led to N. N. Semenov's pioneering theoretical description of the phenomenon [21, 29].

The existence of such limiting pressures — lower and upper limits of ignition of substances — is due to the peculiarities of the kinetics and mechanism of the branched chain reaction. Thus, whereas in a simple chain reaction ($\varepsilon_c\alpha_c < 1$) the rate of the relatively slow stationary reaction is $w = w_0\alpha_c/(1 - \varepsilon_c\alpha_c)$, in a branched chain reaction ($\varepsilon_c\alpha_c \geqslant 1$) the reaction rate (1.40) is

$$w = w_0 \frac{\alpha_c}{\varepsilon_c\,\alpha_c - 1}(\exp \varphi t - 1), \tag{1.51}$$

or

$$\varphi = -\frac{1}{\tau} = (\nu_1^{\alpha_c} + \nu_2^{\alpha_c})(\varepsilon_c\,\alpha_c - 1). \tag{1.52}$$

From (1.51) and (1.52) follows, for $\varphi t \gg 1$, and recognizing that $\alpha_c = P_1 = \nu_1^{\alpha c}/(\nu_1^{\alpha c} + \nu_2^{\alpha c})$, *Semenov's law*:

$$w = \frac{w_0\,\nu_1^{\alpha_c}}{\varphi} \exp \varphi t. \tag{1.53}$$

At $\varepsilon_c\alpha_c > 1$ the reaction becomes rapid and self-accelerating, ending in explosion. The transition from the stationary to the nonstationary process is determined by the condition

$$\varepsilon_c\,\alpha_c = 1. \tag{1.54}$$

Hence, taking into account (1.48) and the relation for the chain-continuation probability $\alpha_c = \nu_1^{\alpha c}/(\nu_1^{\alpha c} + \nu_2^{\alpha c})$, we obtain

$$\delta_c\,\nu_1^{\alpha_c} = \nu_2^{\alpha_c}. \tag{1.55}$$

The dependences of $\nu_1^{\alpha c}$ and $\nu_2^{\alpha c}$ on the pressure can be written in the form

$$\nu_1^{\alpha_c} = ap \quad \text{and} \quad \nu_2^{\alpha_c} = bp^2 + b', \tag{1.56}$$

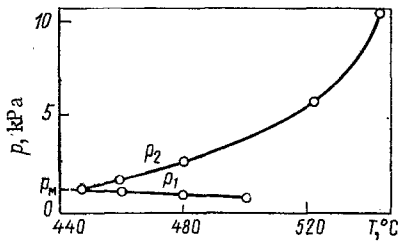

Fig. 1.4. Ignition peninsula of the mixture $2H_2/O_2$.

where $\nu_2^{\alpha c}$ is expressed by a sum of terms, the first of which characterizes the volume chain-breaking via the ternary-collision mechanism, and the second characterizes chain breaking at the walls in the kinetic region of the reaction.

From (1.55) and (1.56) follows

$$p^2 - \delta ap/b + b'/b = 0, \tag{1.57}$$

whose solutions are in fact the pressures at the lower (p_1) and upper (p_2) ignition limits:

$$p_1 = \delta a/2b - \sqrt{\delta^2 a^2/4b^2 - b'/b}, \tag{1.58}$$

$$p_2 = \delta a/2b + \sqrt{\delta^2 a^2/4b^2 - b'/b}. \tag{1.59}$$

The plot of p_1 and p_2 vs T (Fig. 1.4) is arbitrarily called the "ignition peninsula" and $p = p_M$ is called the "cape of the peninsula."

1.6. Elementary Processes of System Excitation in Chemical Reactions

Principles of the Quantum-Mechanical Description of Molecular Systems. Quantum mechanics describes the connection between the structures of atoms or molecules and their spectra and elucidates the distribution of the energy in a molecular system, its excitation, relaxation, and chemical reactivity. The transition of a system from one state to another is accompanied by the absorption or emission of an energy

$$h\nu = E_2 - E_1, \tag{1.60}$$

where h is Planck's constant; $\nu = c/\lambda$, quantum frequency; λ, wavelength; and c, speed of light. Alternately, using in place of ν the wave number $\omega = \nu/c$ [cm^{-1}], we have

$$\omega = (E_2 - E_1)/ch. \tag{1.61}$$

Absorption, by a molecular system, of light quanta, depending on their energies, changes the rotational (R) energy of the molecule at absorbed-quantum energies 0.125-1.25 kJ/mole, the vibrational energy (V) at 1.25-50 kJ/mole, and the electron energy (E) at energies on the order of tens and hundreds of kJ/mole.

Corresponding to these energy changes are the energy-level and transition schemes shown in Figs. 1.5a-c as well as the regions of the electromagnetic radiation spectrum (Fig. 1.5d). The far IR, millimeter, and microwave regions correspond here to the rotational R spectra (a); the IR region, to the vibrational–rotational spectra V-R (b); and the near infrared, visible, and ultraviolet, to the electron (E) and electron–vibrational–rotational (E–V-R) spectra (c).

The molecule can be represented as a harmonic oscillator having an energy

$$E_v = hc\omega_e (v + 1/2), \tag{1.62}$$

where v = 0, 1, 2, 3, ... is the *vibrational quantum number*, which determines the level of the vibrational energy; ω_e corresponds to the ground state v = 0 with energy $E_0 = (1/2)hc\omega_e$, which exists also at zero temperature. For a harmonic oscillator, the difference between the energies of neighboring states is

$$E_{v+1} - E_v = hc\omega_e. \tag{1.63}$$

From (1.61) we have

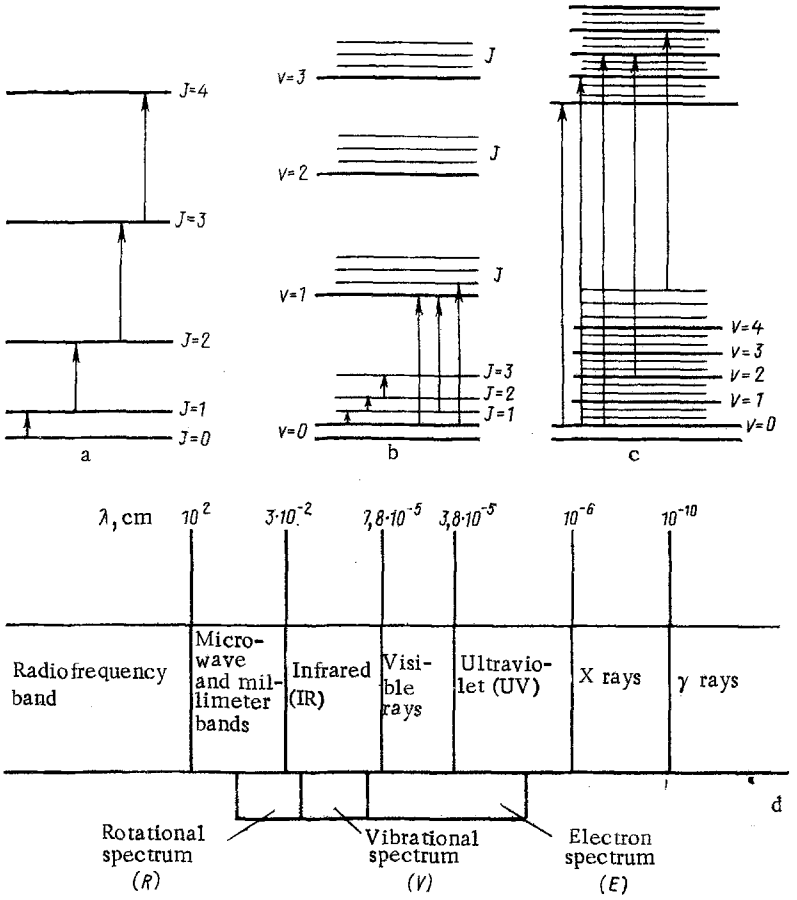

Fig. 1.5. Energy levels and transitions of the R (a), V–R (b), and E–V–R (c) spectra and the corresponding electromagnetic radiation regions (d).

$$E_{v+1} - E_v = hc\omega, \tag{1.64}$$

i.e., $\omega = \omega_e$.

The model of a real molecule, however, is an anharmonic oscillator, and ω should differ from ω_e, but this difference is small at small values of the vibrational quantum number v.

Owing to the anharmonicity, the V energy levels come closer together with increasing v, and (1.62) is replaced by the two-term formula

$$E_v = hc\omega_e (v + 1/2) - hc\omega_e x_e (v + 1/2)^2 \tag{1.65}$$

with a constant $x_e \ll 1$ that characterizes the anharmonicity. Transitions with $\Delta v > 1$, or *overtones*, are then possible. With further increase of v the molecule energy reaches a value E_{max}, and at $E_{max} - E_o = D_o$ the molecule dissociates.

The R structure of the vibrational band is determined by the change of the rotational energy $E_J = BJ(J + 1)$ in the V transition:

$$E'_J - E''_J = B'J'(J' + 1) - B''J''(J'' + 1), \tag{1.66}$$

where J = 0, 1, 2, ... is the *rotational quantum number* and B is the *rotational constant*.

For dipole radiation $\Delta J = J' - J'' = 0, \pm 1$ we obtain, correspondingly, three spectrum branches $\mathcal{Q}$, $\mathcal{R}$, $\mathcal{P}$. But since transitions with $\Delta J = 0$ are forbidden for most diatomic molecules in the electronic ground state, only a positive $\mathcal{R}$- and a negative $\mathcal{P}$-branch are observed.

The E or E–V–R energy of molecules is connected in a complicated manner with their structure, and the electronic energy states of the molecules are classified by the type of

their symmetry. Thus, electronic states or terms of diatomic and axisymmetric linear polyatomic molecules are classified in accordance with the following:

a) the quantum numbers Λ, which represent the absolute values of the total orbital momentum **L** on the molecule axis (in units of $\hbar = h/2\pi$). The quantum number Λ can take on values $\Lambda = 0, 1, 2, 3, \ldots, L$, designated, respectively, by Σ, Π, Δ, and Φ;

b) the multipolarity $2S + 1$, where S is the quantum number of the total spin of all the electrons of the molecules; the multipolarity is marked on the upper right of the state symbol, e.g., $^3\Sigma$;

c) the total orbital momentum **L + S**, marked by a subscript on the right for terms different from Σ, e.g., $^3\Pi_2$;

d) the symmetry of the electronic eigenfunction of the molecule, marked by a "+" or "–" right-hand superscript for the state Σ; in any plane passing through the line joining the nuclei, the electronic eigenfunction either remains unchanged (Σ^+) or reverses sign (Σ^-);

e) the even (g) or odd (u) state for molecules whose nuclei have like charges, e.g., $^1\Sigma_g^+$, $^1\Sigma_u^+$.

In the PES system the electronic state whose minimum is lowest is called the ground state and is designated by the letter X, which is placed before the symbol of the state ($X\,^1\Sigma_g^+$), and the sequence of the excited electronic states is marked by the letters A, B, C, ... For light molecules the sequence of excited states that differ in multipolarity from the ground state is marked by the letters *a*, b, c, ..., and those of like multipolarity are marked A, B, C, ... The lowest energy is possessed by the state with the largest value of S possible for the given electron configuration and with the largest (at the given S) value of L (Hund's rule).

Since the energies of the electrons, of the vibrations of the nuclei, and of the rotations of the molecule are quantized, the total energy is also quantized:

$$E = E_{el} + E_{vib} + E_{tot}. \tag{1.67}$$

The quantity $|E_i|/hc$ for each i-th level is called the *term*. The corresponding term can be represented as a sum of three terms:

$$T = E_i/hc = T_{el} + G(v) + F(J), \tag{1.68}$$

where T_{el}, G(v), F(J) are, respectively, the electronic, vibrational, and rotational terms.

In E transitions in molecules, as can be seen from Fig. 1.5d, an optical quantum is radiated in the UV and in the visible, and less frequently in the near IR. Superposition of V and R transitions on electronic transitions gives the fine structure of the electronic spectrum (see Fig. 1.5c).

The V–R system (see Fig. 1.5b) can be obtained when solving the Schrödinger equation for the molecule in the nonrigid rotator–anharmonic-vibrator approximation. In this case the potential energy is substituted in the Schrödinger equation in the form of a certain function of the distance r between the nuclei. A potential-energy curve for diatomic molecules was proposed in [30] in the empirical form

$$E_p(r) = D_0\{1 - \exp[-a(r - r_e)]\}^2, \tag{1.69}$$

where D_0 is the dissociation energy; r_e, equilibrium distance; and *a*, constant of the molecule. Also used is the Lennard–Jones potential, which is close to the real one,

$$E_p(r) = 4\varepsilon[(\sigma/r)^{12} - (\sigma/r)^6], \tag{1.70}$$

where ε is the strength function and σ is the average diameter of the colliding spheres.

Distribution of the Chemical-Reaction-Products Energy. The energy released in elementary chemical processes is distributed among different energy levels or degrees of freedom of the reaction products [13, 31-33]. The character of this distribution determines, e.g., the nonequilibrium emission, in the course of a reaction in the visible or in the UV region, of cold flames from hydrocarbons and CS_2 [14, 34, 35]. In combustion reactions, nonequilibrium emission is observed in the IR region of the spectrum [36] corresponding to V transitions.

Reactions can be divided into two types: those proceeding within the limits of one PES and usually accompanied by V excitation (*adiabatic reactions* [37]), and reactions that involve more than one PES and are frequently accompanied by E excitation (*nonadiabatic reactions*).

The representation of a reaction in the form of a curve or a PES is particularly convenient in those cases when the coupling between the E and V motions is weak. Knowing the potential energy, the electron energy of the system can be obtained for arbitrary fixed positions of the nuclei. The PES is calculated or else determined from available experimental data [38]. This involves the solution of two problems: determination of the surface and its use to describe the experimental results.

To interpret the experimental data, however, knowledge of the total structure of the surfaces is not mandatory. The distribution of the reaction products in energy can be obtained from qualitative characteristics of the surfaces, such as the effective radius of the forces, the relative slopes of the PES parts corresponding to the initial reagents and the products, and the energy parameters [39]. Let us consider [40-44] the distribution of the products in energy, using as an example a typical chemical-laser substitution reaction such as

$$A + BC \rightleftarrows AB + C. \tag{1.71}$$

This reaction can be divided into three stages: first — approach of the atom A to the complex BC; second — intermediate stage, in which the B–C bond is stretched as the approach distance decreases; third — departure of the reaction products AB and C. Let E_1, E_2, E_3 be the energies released in these three stages of the process. The relations between E_1, E_2, and E_3 depend essentially on the form of the potential energy $E_p(r_{AB}, r_{BC})$. The principal part E_1 is released in vibrational form, E_3 in the form of kinetic energy, and the fraction E_2, which goes over into the E_{vib} of the molecules, is larger the heavier the atom A compared with B and C [41]. For example, in the case of the H + Cl_2 interaction, the greater part of the energy is released during the second and third stages [40, 41]. Of interest for chemical lasers are reactions with high ratios E_{vib}/E_{kin}. Large values of E_{vib}/E_{kin} can be obtained in reactions in which the hydrogen atom is replaced by a heavier one, say deuterium or a metal, and also in the reactions F + H_2, Cl + HI and others.

PES of a system of atoms are shown in Fig. 1.6 in the attraction (a), repulsion (b), and mixed energy-release stages (c). The solid curves are equal-energy lines, the dash-dot curve is the coordinate of the reaction (the potential energy increases on either side of this curve), and a dashed curve is a possible trajectory of the system in the course of the reaction (1.71). If the system energy insignificantly exceeds the reaction activation energy, these trajectories pass near the PES saddle point marked by the cross.

If the form of the function E_p (r_{AB}, r_{BC}) corresponds to Fig. 1.6a, the most probable trajectories are those with energy release during the stage of the approach of A to BC, for after the system passes through the potential barrier, r_{AB} decreases and r_{BC} changes little, i.e., energy is released here in the attraction phase.

For the reaction corresponding to Fig. 1.6b, r_{AB} changes little after passing through the potential barrier, while r_{BC} increases, i.e., the energy release occurs in the dissociation stage, i.e., in the repulsion phase.

In the intermediate case (Fig. 1.6c) we have a mixed energy release in the plot of the reaction, Fig. 1.6d, where the attraction and repulsion phases are marked A and R, respectively. For energy release in the region M, the character of the most probable trajectories depends to a considerable degree on the relation between the particle masses.

Adiabatic and Nonadiabatic Interactions, Energy Resonance. If the relative velocities of two or more colliding particles are small compared with the electron orbital velocities, the electrons have time to adjust themselves to the instantaneous positions of the nuclei and their energy depends as a result only on the relative positions of the nuclei of the atoms. This simplification is known as the *Born–Oppenheimer approximation*. It is applicable not only to slow molecular collisions, but also to rotational and vibrational motions of nuclei in one molecule. According to this approximation the nuclei have, relative to one another, certain potentials, an approximate form of which for two different E states is shown by the solid curves of Fig. 1.7 [45]. Such a slow collision without E transitions is called adiabatic (B–A). Obviously, adiabatic collisions between two atoms are elastic, i.e., the atoms move apart if no energy is expended on a third particle or radiation. Adiabatic collisions of polyatomic molecules can be accompanied by rotational or vibrational excitation or by a

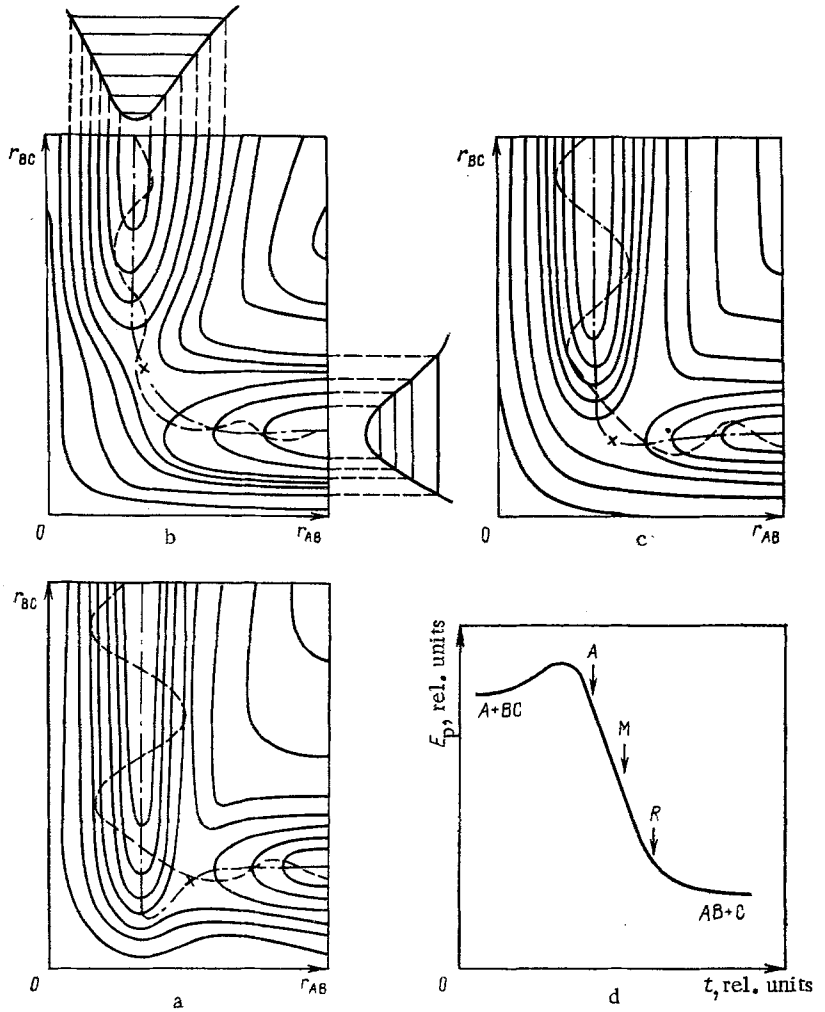

Fig. 1.6. EPS of an atom system in the attraction (a), repulsion (b), mixed energy-release phases (c), and plot of the reaction (d).

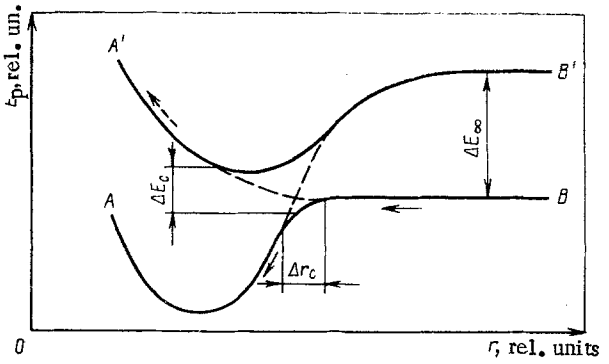

Fig. 1.7. Potential curves of nuclear collisions: B—A) adiabatic process; B—A') nonadiabatic process.

chemical reaction. At sufficiently fast collisions, however, the electrons have no time to become adjusted and the nuclei follow the dashed curve B—A' — a nonadiabatic collision. If the relative velocity u of the diverging particles is still large, the nuclei, following the same curve, will land again in the state B and the collision turns out again to be elastic.

To obtain an E transition from B to B', the nuclei should move as the solid curve as thev converge and the dashed one as they diverge, or vice versa. Consequently, the degree of excitation has a maximum at certain intermediate velocities, when the probabilities of follow-

ing the solid or the dashed curves are equal. A quantum-mechanical analysis shows that this takes place if the time of stay in the intersection region $\Delta r_c/u$ is approximately equal to the characteristic time $h(2\pi\Delta E_c)$ of energy exchange (see Fig. 1.7). Under these conditions the cross section can be practically equal to the gas-kinetic value.

The approach of the potential curves can take place at very small ΔE_∞, i.e., when energy resonance exists between the initial and final states. At thermal energies, however, the existence of resonance is neither a necessary nor a sufficient condition for a large excitation cross section. The potential curves, which are far from each other at large internuclear distances, can come much closer when these distances decrease. The inverse situation can also be realized. This is confirmed by careful measurements in exothermic chemical reactions and in "quenching" reactions [46-48].

In the course of the electronic excitation the molecule goes from the ground electronic state to an excited one. The question as to just which rotational state the molecule goes to, or as to whether it is preserved or dissociates, is answered by the *Franck–Condon principle*. According to this principle, the change of the state of the electron shell of the molecule proceeds so rapidly compared with the vibrations of the atomic nuclei that neither the velocities of the nuclei nor their positions manage to change in an E transition [49]. The relative excitation probabilities of the rotational levels, called Franck–Condon factors, were calculated for many important transitions (see, e.g., [50]).

In nonadiabatic transitions, a transition complex A–B–C can be formed, which can also radiate. This mechanism is preferable for the conversion of the chemical-bond energy into radiation energy, since it does not include competing energy-dissipation processes. It can also be seen from the PES (see Fig. 1.6) that the lower potential curves AB and C can be repulsive, meaning that the complex A–B–C does not have a lower level in the usual sense of the word, and exists only in an excited state.

Such complexes, consisting of elements of groups I and VII of the periodic table, were observed in [51]. The spectra of the chemiluminescence produced in a continuous-flow system of Na and a halogen X were investigated. The spectra of Na + F (0.6-0.81 μm) and Na + Cl_2 (0.42-0.55 μm) have a vibrational structure. It was concluded that the carrier of the bands is the NaX_2 molecule formed in the reaction in an electron-excited state.

1.7. Chemical Reactions in a Closed Volume and in a Stream

Exothermic Reaction in a Closed Volume. Heat of Reaction. In contrast to the rarely observed isothermal chain explosion [52], the cause of a thermal explosion of a gas mixture in a closed volume V is the temperature rise when the heat-release rate q^+ exceeds the heat-removal rate q^-. A general idea of such a process is given in a quantitative theory [53] that takes into account the equalization of the temperature in the volume.

The explosion conditions are characterized by the balance of q^+ and q^-

$$Qw(T_2) = \alpha_Q (S/V)(T_2 - T_0) \tag{1.72}$$

and by the equalities of the derivatives with respect to temperature at the point T_2

$$Q(dw/dT) = \alpha_Q (S/V), \tag{1.73}$$

where T_2 is the combustion-zone temperature corresponding to the explosion; α_Q, heat-transfer coefficient; and S, wall surface area.

For the fast processes in chemical lasers, interest attaches to the adiabatic conditions of the reaction initiated in the closed volume [2]. Under these conditions, all the heat released by the reaction goes to heating of the mixture, i.e.,

$$c_V dT = -Qdc, \tag{1.74}$$

where c_V is the specific heat of the mixture at constant volume.

Introducing the total-combustion temperature T_{max}, we can obtain

$$dT/dt = k_0 (c_V/Q)^{n-1} (T_{max} - T)^n \exp(-E/RT). \tag{1.75}$$

Solution of this equation shows that during a certain time interval – *the ignition induction period* – the gas temperature increases slowly, after which the reaction proceeds with fast flow rate of the reagent and with rise of temperature.

The heat released in a closed system is equal to the *heat of reaction* $-Q \equiv -\int dQ$. It follows from thermodynamics that $dQ = dH_e - Vdp$, so that for isobaric processes $Q = \int dH_e \equiv \Delta H_e$, the increase of the system enthalpy during the time of the reaction. For any reaction in an ideal gas the heat released can be calculated from the formula

$$-\Delta H_e = -\sum_{i=1}^{N} (r_i' - r_i)\,\Delta H_{f,i}, \tag{1.76}$$

where $\Delta H_{f,i}$ are the tabulated values of the heat of formation of the molecules i.

Exothermic Reaction in a Stream. For a reacting mixture of ideal gases of density ρ, moving with an average velocity $\mathbf{u}$, the following are satisfied [3]:

the continuity equation
$$\partial\rho/\partial t + \nabla(\rho\mathbf{u}) = 0; \tag{1.77}$$

the angular-momentum conservation equation with allowance for the external force $\mathbf{f}_i$ acting on a unit mass of the fraction of the component Y_i and for the stress tensor P

$$\partial\mathbf{u}/\partial t + \mathbf{u}\nabla\mathbf{u} = -\nabla P/\rho + \sum_{i=1}^{N} Y_i \mathbf{f}_i; \tag{1.78}$$

the energy-conservation equation, including the specific internal energy u_e and taking into account the diffusion velocity $\mathbf{u}_i^D$ of the i-th component

$$\rho\partial u_e/\partial t + \rho(\mathbf{u}\nabla)u_e = -(\nabla\mathbf{q}) - P:(\nabla\mathbf{u}) + \rho\sum_{i=1}^{N} Y_i(\mathbf{f}_i\mathbf{u}_i^D) \tag{1.79}$$

[the colon (:) denotes a doubly contracted tensor]; and

the equation of continuity of the chemical components

$$\partial Y_i/dt + (\mathbf{u}\nabla)Y_i = w_i/\rho - (1/\rho)(\nabla\rho\, Y_i\mathbf{u}_i^D). \tag{1.80}$$

The stress tensor P is defined by the formula

$$P = [p + (2\eta/3 - \eta')(\nabla\mathbf{u})]U - \eta[(\nabla\mathbf{u}) + (\nabla\mathbf{u})^T], \tag{1.81}$$

where η and η' are, respectively, the shear and bulk viscosity coefficients; U is a unit tensor and T denotes the transpose of a tensor.

The heat flux density vector $\mathbf{q}$ in Eq. (1.79), neglecting radiative heat transfer, is given by

$$\mathbf{q} = -\lambda_Q\nabla T + \rho\sum_{i=1}^{N}(h_e)_i Y_i\mathbf{u}_i^D + RT\sum_{i=1}^{N}\sum_{j=1}^{N}\left(\frac{X_j D_{T,i}}{\mu_i D_{ij}}\right)(\mathbf{u}_i^D - \mathbf{u}_j^D), \tag{1.82}$$

where λ_Q is the thermal conductivity coefficient; $(h_e)_i$ and μ_i are, respectively, the specific energy and the molar mass of the i-th component; X_j is the molar fraction of the j-th component; $D_{T,i}$, thermal diffusion coefficient of the i-th component; and D_{ij}, coefficient of binary diffusion of the components.

The quantity $\mathbf{u}_i^D$ in (1.79) and (1.80) for i = 1, 2, ..., N components is determined from the formula

$$\nabla X_i = \sum_{j=1}^{N}\left(\frac{X_i X_j}{D_{ij}}\right)(\mathbf{u}_j^D - \mathbf{u}_i^D) + (Y_i - X_i)\left(\frac{\nabla p}{p}\right) + \left(\frac{\rho}{p}\right)\sum_{j=1}^{N} Y_i Y_j(\mathbf{f}_i - \mathbf{f}_j) + \sum_{j=1}^{N}\left[\left(\frac{X_i X_j}{\rho D_{ij}}\right)\left(\frac{D_{T,j}}{Y_j} - \frac{D_{T,i}}{Y_i}\right)\right]\left(\frac{\nabla T}{T}\right). \tag{1.83}$$

The external forces $\mathbf{f}_i$ are assumed given, and w_i in Eq. (1.80) is determined, in accordance with the chemical-kinetics law (1.3) and with allowance for (1.27) and (1.28), by the expression

$$w_i = \mu_i \sum_{k=1}^{M} (r'_{i,k} - r_{i,k}) B_k T^{\alpha_k} \exp(-E_k/RT) \prod_{j=1}^{N} (X_j p/RT)^{r_{j,k}} \tag{1.84}$$

(M is the total number of chemical reactions).

The determined variables in Eqs. (1.77)-(1.80) can be the quantities Y_i, ρ, T, and $\mathbf{u}$. The other variables can then be expressed in their terms with the aid of the equation of state of an ideal gas

$$p = \rho RT \sum_{i=1}^{N} \frac{Y_i}{\mu_i}, \tag{1.85}$$

the expression for the specific internal energy of the gas mixture

$$u_e = \sum_{i=1}^{N} (h_e)_i Y_i - p/\rho, \tag{1.86}$$

the caloric equation of state, which includes the heat of formation $(h_f)_i$ of the i-th component at the temperature T_0

$$(h_e)_i = (h_f)_i + \int_{T_0}^{T} c_{p,i}\, dT \tag{1.87}$$

($c_{p,i}$ is the specific heat of the component i at constant pressure), and the relation

$$X_i = Y_i \left(\mu_i \sum_{j=1}^{N} \frac{Y_j}{\mu_j} \right)^{-1}. \tag{1.88}$$

In the case of one-dimensional nonviscous stationary flow without mass forces, Eqs. (1.77)-(1.83) are greatly simplified.

From (1.77), we obtain

$$\rho u = \text{const}. \tag{1.89}$$

Equation (1.78) is transformed into

$$\rho u du/dx + dp/dx = 0, \tag{1.90}$$

the integral of which is $\rho u^2 + p = \text{const}$. Equation (1.79) yields

$$\rho u (h_e + u^2/2) + q = \text{const}, \tag{1.91}$$

and from (1.80) we have

$$\frac{d}{dx} \left[\rho Y_i (u + u_i^D) \right] = w_i. \tag{1.92}$$

If we neglect the conductive heat transfer and assume q = 0, then in the case of steady flow of a nonviscous medium, Eqs. (1.90)-(1.92) take, respectively, the form

$$\frac{u du}{dx} = -\frac{1}{\rho} \frac{dp}{dx}; \tag{1.93}$$

$$\frac{d}{dx} \left(h_e + \frac{u^2}{2} \right) = 0; \tag{1.94}$$

$$udY_i/dx = w_i/\rho. \tag{1.95}$$

For a channel with variable cross section S(x) the continuity equation is of the form

$$d(\rho uS)/dx = 0. \tag{1.96}$$

The equation of state (1.85) and Eqs. (1.86) and (1.87) together with the relation $h_e = u_e + p/\rho$ connect the thermodynamic parameters h_e and p with the quantities ρ, T, **u**, and Y_i (i = 1, 2, ..., N). Then Eqs. (1.93)-(1.96) are a system of N + 3 ordinary differential equations of first order for the N + 3 unknowns Y_i, T, ρ, and u. Specifying, in some section of the stream, all its parameters, and the area S as a function of x, we can obtain the characteristics of the flow at any other point of the channel by integrating Eqs. (1.93)-(1.96) and taking relations (1.84)-(1.88) into account.

A more accurate calculation should take into account the boundary layer on the channel wall, the ratio of the nonviscous flow displacement thickness to the momentum-loss thickness, and the local coefficient of friction against the wall in the case of flow of a relaxing gas [54]. In this case one uses as an approximation the similarity parameters obtained for laminar or turbulent flow near a flat plate [55].

Photochemical Reactions. As indicated in Sec. 1.2, only activated molecules are subject to chemical transformation. Whereas the molecules are activated in the thermal process of, e.g., the type described above on account of energy redistribution in the collisions, the molecule-activation energy needed in photochemical processes is obtained by absorption of radiation from an external source of intensity I_ν.

In this case the *Stark–Einstein photochemical equivalence law* is satisfied: In a photochemical system acted upon by radiation of frequency ν each absorbed photon $h\nu$ activates one molecule.

Thus, the kinetics of photochemical reactions is governed by the laws of light absorption by matter and is connected with the *reaction quantum yield* φ, defined as the ratio of the number of reacting molecules to the number of quanta absorbed by the molecules. When one absorbed quantum causes transformation of one molecule we have $\varphi = 1$. Actually, $\varphi < 1$, owing to deactivation. Conversely, $\varphi \gg 1$ in the case of photoinitiation of secondary exothermic chain reactions. If radiation is generated by photolytic or some other initiation of a chemical reaction, the *generation quantum yield* φ_g is defined as the ratio of the number of quanta participating in the reaction per unit volume of the medium to the concentration n_a of the active centers produced by the initiation source

$$\varphi_g = \frac{\varepsilon_g/h\nu_g}{n_a} \tag{1.97}$$

(ε_g and ν_g are, respectively, the specific energy and the frequency of the generated radiation).

Critical phenomena are inherent in many reactions with pulsed photoinitiation: depending on the initial conditions (initiation energy, temperature, reagent concentration, total mixture pressure), either an explosive regime is realized with complete chemical transformation, or else a regime with a rather small degree of transformation of the reagents.

The transition from one regime to the other has a certain threshold. A quantitative description of such critical phenomena and of the kinetics of the mixture of the photoinitiated reaction $F_2 + D_2$ (H_2) inhibited by O_2 is given in [56, 57], where use is made of the concepts of thermal acceleration of the reaction, which are the basis of the theory of thermal explosion [21].

The photoinitiated chain reaction regime is considered in [57] in the adiabatic approximation in the absence of gradients of the temperature and of the concentrations of the active particles. It is assumed that the reaction proceeds via one active center, and that the active centers are generated by photoinitiation that is uniform over the volume. It follows from the solution of the equations for the concentration of the active particles and for the heat balance of the reaction that the kinetic character of the curves is greatly changed by small changes of the heating near its critical value. A characteristic of a branched reaction is an abrupt growth of the curves, due to the strongly pronounced period of reaction induction.

The existence of a critical condition is due to the competition between the thermal acceleration of the reaction and its slowdown because of the loss of active centers. Such a pulsed-photoinitiated chemical reaction under conditions of progressive self-acceleration as a result of accumulation of heat or active centers in the system is a photothermal explosion [57].

Nonequilibrium Effects in a Chemical Reaction. Chemical Reactions in an Electric Discharge. Real chemical reactions proceed under essentially nonequilibrium conditions, i.e., when the Maxwell–Boltzmann distribution function of the particles in velocity and in internal state is violated. This violation follows naturally from the fact that the molecules capable of reacting are those with energy higher than E_a, so that the high-energy part of the distribution function is continuously depleted on account of the vanishing of the molecules after reacting.

The solution of the equations that describe the change of the distribution function in nonequilibrium chemical processes presents mathematical difficulties. Various simplifications of the problem are therefore resorted to in the analysis of relaxation processes. Thus, the system is divided into subsystems: equilibrium, "frozen," and relaxing.

In a number of cases it suffices to consider the distribution function of the number n of the particles at energy n_A (E) dE, i.e., the probability of observing in a system with an excess of molecules B relaxing molecules A in states with energy close to E in an interval dE. The rate of change of population is then

$$\frac{dn_A(E)}{dt} = -c_B \int P(E, E') n_A(E) dE' + c_B \int P(E', E) n_A(E') dE', \tag{1.98}$$

where P(E, E') is the transition probability per unit time at unity concentrations A and B of the molecule A from the energy level E to levels in the energy interval E', E' + dE' at unity concentration of the molecules B. These probabilities satisfy the relation

$$\frac{P(E, E')}{P(E', E)} = \frac{\rho(E')}{\rho(E)} \exp\left[-\frac{E'-E}{k_0 T}\right], \tag{1.99}$$

which includes the density ρ(E) of the energy levels of the relaxing degrees of freedom of the molecule A.

If the relaxation and reaction overlap, the kinetic equations expressed in terms of the concentrations are not valid at all, although even in this case it is possible to reduce the problem to macroscopic equations that describe the changes of both the concentrations and the parameters of the nonequilibrium distribution function, e.g., the temperatures corresponding to different types of degree of freedom [58-63].

It is chemical reactions with strong disequilibrium of the reaction-product parameters which are responsible for the processes in chemical lasers. Thus, if the distribution function of the products over the energy levels is nonequilibrium both during the reaction and after its completion, or if in the course of the chemical reaction the rate of formation of products in the higher energy states exceeds the formation rate of products at lower levels, *population inversion* of the energy levels takes place. The same can occur also in redistribution of the energy over various degrees of freedom of the molecular system.

Reaction products can be excited into electronic, rotational, and vibrational states in reactions of the following types:

photodissociation

$$ABC + h\nu \rightarrow AB^* + C; \tag{1.100}$$

exothermic exchange

$$A + BC \rightarrow AB^* + C,\ A + BC \rightarrow AB + C^*; \tag{1.101}$$

dissociative energy transfer

$$AB + M^* \rightarrow A^* + B + M; \tag{1.102}$$

and recombination, the inverse of dissociation

$$A + B + M \rightarrow AB^* + M,\ A + B + M \rightarrow AB + M^*. \tag{1.103}$$

The excitation of the products in a number of such nonequilibrium chemical reactions is the subject of the next chapter.

In the present section we dwell quite briefly on the essentially nonequilibrium processes in the chemical reactions that take place in the plasma of an electric discharge.

The electromagnetic gas dynamics of plasma flow in external electric and magnetic fields is considered, e.g., in [64]. The quantitative picture of the distribution of these fields in the discharge region can be obtained by numerical methods, as, e.g., in [65, 66]. A still more difficult problem is the treatment of a chemical reaction in an essentially nonequilibrium electric-discharge plasma.

In reactions, particularly pulsed ones, the electron distribution in energy is nonequilibrium, whereas the energy of the translational motion of the heavy particles has a quasiequilibrium distribution.

An approximate method of numerically calculating the kinetic characteristics of nonequilibrium reactions in electric discharges without allowance for hydrodynamic processes (see, e.g., [67]) consists of simultaneous consideration of:

the equations of chemical kinetics

$$\frac{\partial n_i}{\partial t} = \sum_j k_{ij} n_j + \sum_{j,\,k} k_{ijk} n_j n_k \tag{1.104}$$

(n_j are the concentrations of the components that participate in the reactions, namely electrons, ions, neutral and excited particles; k_{ij}, k_{ijk} are the rate constants of ionization, recombination, dissociation, and other processes);

and Maxwell's equations

$$\left.\begin{aligned} &\operatorname{rot}\mathbf{H} = \frac{\partial \mathbf{D}}{\partial t} + \mathbf{j};\\ &\operatorname{div}\mathbf{D} = \rho_e;\\ &\operatorname{rot}\mathbf{E} = -\frac{\partial \mathbf{B}}{\partial t};\\ &\operatorname{div}\mathbf{B} = 0;\\ &\mathbf{D} = \varepsilon'\mathbf{E}, \end{aligned}\right\} \tag{1.105}$$

where **E** and **D** are, respectively, the strength and induction of the electric field; **H**, **B**, strength and induction of the magnetic field; and **j**, ρ_e, current and charge densities of the external sources.

In this system of equations the properties of the medium are expressed in terms of the complex dielectric constant ε', which depends on the electric conductivity of the plasma and on the frequency of the electromagnetic field.

From (1.105), subject to the inequalities [68]

$$\left|\frac{\partial \varepsilon'}{\partial t}\frac{\partial \mathbf{E}}{\partial t}\right| \ll \left|\varepsilon'\frac{\partial^2 \mathbf{E}}{\partial t^2}\right|,\quad \left|\frac{\partial^2 \varepsilon'}{\partial t^2}\mathbf{E}\right| \ll \left|\varepsilon\frac{\partial^2 \mathbf{E}}{\partial t^2}\right| \tag{1.106}$$

we obtain the stationary wave equation, which forms together with (1.104) a nonlinear system. In this system the reaction rate constants k_{ij}, k_{ijk} depend on the electric field strength $\mathbf{E}(\mathbf{r})$, and ε' depends on the time-dependent electron concentration n_e, which is obtained from the solution of Eq. (1.104), and on the effective frequency of the collisions of these electrons with the heavy particles, which depends in turn on $\mathbf{E}(\mathbf{r})$ and on n_e.

The nonstationary equation (1.104) and the wave equation, with boundary conditions determined in the course of the numerical calculation by the iteration method, were integrated [68] for reactions in an essentially nonequilibrium nitrogen plasma produced in a pulsed microwave discharge.

As an example of the study of a chemical reaction in an electric field we can also cite the analysis, in [69, 70], of the decomposition of carbon dioxide in a low-pressure discharge.

LITERATURE CITED

1. N. M. Émanuél' and D. G. Knorre, Course of Chemical Kinetics [in Russian], Vysshaya Shkola, Moscow (1962).
2. V. N. Kondrat'ev and E. E. Nikitin, Kinetics and Mechanism of Gas-Phase Reactions [in Russian], Nauka, Moscow (1974).
3. F. A. Williams, Combustion Theory, Addison-Wesley (1964).
4. F. A. Lindemann, "Discussion on 'The radiation theory of chemical actions,'" Trans. Faraday Soc., 17, 598-606 (1922).
5. J. G. Van't Hoff, Outlines of Chemical Dynamics [Russian translation], ONTI, Leningrad (1936).
6. S. Arrhenius, "Über die Reaktionsgeschwindigkeit bei der Inversion von Rohrzucker durch Säuren," Zh. Phys. Chem., 4, 226-248 (1889).
7. V. I. Vedeneev and A. A. Kibalko, Rate Constants of Gas-Phase Monomolecular Reactions [in Russian], Nauka, Moscow (1972).
8. H. Eyring, "Activated complex in chemical reactions," J. Chem. Phys., 3, 107-115 (1935).
9. E. P. Wigner, "The transition-state method," Trans. Faraday Soc., 34, 29-41 (1938).
10. H. Pelzer and E. Wigner, "Velocity coefficient of interchange reactions," Z. Phys. Chem., 15, 445-471 (1932).
11. N. N. Semenov, "Mechanism of chain decay of halide derivatives of paraffins," Usp. Khim., 21, 641-713 (1952).
12. L. N. Khitrin, Physics of Combustion and Explosion [in Russian], Moscow State Univ. (1957).
13. S. Glasstone, K. J. Laidler, and H. Eyring, The Theory of Rate Processes, McGraw-Hill (1941).
14. V. N. Kondrat'ev, Kinetics of Chemical Gas Reactions [in Russian], Izd. Akad. Nauk SSSR (1958).
15. E. I. Kondrat'eva and V. N. Kondrat'ev, "Active centers in the combustion reaction of carbon monoxide," Zh. Fiz. Khim., 21, 769-776 (1947).
16. W. Ostwald, "Über Oxydationen mittels freien Sauerstoffs," Z. Phys. Chem., 34, 248-252 (1900).
17. N. M. Émanuél', "Kinetics of the slow reaction of hydrogen sulfide oxidation," Zh. Fiz. Khim., 14, 863-876 (1940).
18. W. Ostwald, "Studien zur chemischen Dynamik," Z. Prakt. Chem., 28, 449-495 (1983).
19. W. Ostwald, (1944). Lehrbuch der allegemeinen Chemie. Vol. II, Leipzig, (1887).
20. N. N. Semenov, "On types of kinetic curves of chain reactions," Dokl. Akad. Nauk SSSR, 43, 360-366 (1944).
21. N. N. Semenov, Chain Reactions [in Russian], GKhTI, Leningrad (1934).
22. D. A. Frank-Kamenetskii, Diffusion and Heat Transfer in Chemical Kinetics, Plenum Publ. (1969).
23. Yu. B. Khariton and Z. F. Walta, "Oxydation von phosphordämpfen bei niedrigen drucken," Z. Phys., 39, 547-556 (1926).
24. N. N. Semenov, "Die oxydation des phosphordampfes bei niedrigen drucken," Z. Phys., 46, 109-131 (1927).
25. A. A. Kovalskii, "Kindling of phosphorus vapor in oxygen," Z. Phys. Chem. 4, 288-298 (1929).
26. A. V. Zagulin et al., "Limits of ignition of $2H_2 + O_2$ and $2CO + O_2$ mixtures," Zh. Fiz. Khim., 1, 263-280 (1930); "Entzündungsgrenze des Gemisches $2H_2 + O_2$ und $2CO + O_2$," Z. Phys. Chem., 6, 307-329 (1930).
27. A. V. Zagulin, "Explosion temperatures of gaseous mixtures at different pressures," Zh. Phys. Chem. 1, 275-291 (1928).
28. H. W. Thompson and C. N. Hinshelwood, "The mechanism of the homogeneous combination of hydrogen and oxygen," Proc. R. Soc., A122, 610 (1929).
29. N. N. Semenov, Some Problems in Chemical Kinetics and Reactivity [in Russian], Izd. Akad. Nauk SSSR, Moscow (1958).
30. P. M. Morse, "Diatomic molecules according to the wave mechanics. II. Vibrational levels," Phys. Rev., 34, 57-64 (1929).

31. M. S. Dzhidzhoev, V. T. Platonenko, and R. V. Khokhlov, "Chemical lasers," Usp. Fiz. Nauk, 100, No. 4, 641-679 (1970).
32. V. N. Kondrat'ev, E. E. Nikitin, A. I. Reznikov, et al., Thermal Bimolecular Reactions in Gases [in Russian], Nauka, Moscow (1976).
33. T. Carrington and D. Garvin, "Formation of excited particles in chemical reactions," in: Excited Particles in Chemical Kinetics [Russian translation], A. A. Borisov (ed.), Mir, (1973), pp. 123-213.
34. V. N. Kondrat'ev, "Emission of low-temperature carbon disulfide flame," Zh. Fiz. Khim., 14, 281-286 (1940).
35. A. G. Gaydon and H. G. Wolfhard, Flames, Barnes & Noble (1960).
36. A. G. Gaydon, Spectroscopy of Flames, Barnes & Noble (1957).
37. F. London, Probleme der modernen Physik, Berlin, Sommerfeld Festschrift (1928), p. 104; "Quantenmechanische Deutung des Vorgangs der Aktivierung," Z. Elektrochem., 35, 552-555 (1929).
38. D. L. Bunker and N. C. Blais, "Monte Carlo calculations. V. Three-dimensional study of a general bimolecular interaction potential," J. Chem. Phys., 41, 2377-2386 (1964).
39. J. C. Polanyi, "Dynamics of chemical reactions," Discuss. Faraday Soc., 44, 293-307 (1967).
40. J. R. Airey et al., "Absolute efficiency of conversion of heat of the reaction H + Cl into vibration," J. Chem. Phys., 41, 3255-3256 (1964).
41. P. J. Kuntz, E. M. Nemeth, J. C. Polanyi, et al., "Energy distribution among products of exothermic reactions, II. Repulsive mixed and attractive energy release," J. Chem. Phys., 44, 1168-1184 (1965).
42. K. J. Anlauf et al., "Vibrational population inversion and stimulated emission from the continuous mixing of chemical reagents," Phys. Lett., 24A, 208-210 (1967).
43. C. C. Rankin nd J. C. Light, "Quantum solution of collinear reactive systems: H + $Cl_2 \rightarrow$ HCl + Cl*," J. Chem. Phys., 51, 1701-1719 (1969).
44. D. Russell and J. C. Light, "Classical calculations of linear reactive systems: H + $Cl_2 \rightarrow$ HCl + Cl*," J. Chem. Phys., 51, 1720-1723 (1969).
45. R. F. Gilmore, E. Bauer, and J. W. McGowan, "A review of atomic and molecular mechanisms in nonequilibrium gases to 20,000°K," J. Quant. Spectrosc. Radiat. Transfer, 9, No. 2, 157-183 (1969).
46. D. R. Herschbach, Molecular Beams, J. Ross (ed.), Wiley-Interscience, New York (1966), Chap. 9.
47. G. Karl, P. Kruus, and J. C. Polanyi, "Infrared-emission studies of electronic-to-vibrational energy transfer. II. Hg* + CO," J. Chem. Phys., 46, 224-243 (1967).
48. G. Karl et al., "Infrared-emission studies of electronic-to-vibrational energy transfer. III. Hg* + NO," J. Chem. Phys., 46, 244-253 (1967).
49. M. V. Vol'kenshtein, Structure and Physical Properties of Molecules [in Russian], Izd. Akad. Nauk SSSR, Moscow–Leningrad (1955).
50. R. W. Nicholls, "Transition probabilities of aeronomically important spectra," Ann. Geophys., 29, 144-181 (1964).
51. D. O. Ham and H. W. Chang, "Chemiluminescence spectra of the new molecules NaF_2 and $NaCl_2$ and their implications for reaction dynamics," Chem. Phys. Lett., 24, No. 4, 579-583 (1974).
52. A. A. Kovalskii, "Die Verbrennungskinetik Wasserstoff," Phys. Z. Sow., 4, 723-734 (1933).
53. N. N. Semenov, "Zur theorie des verbrennungsprozesses," Z. Phys., 48, 571-582 (1928).
54. S. A. Losev, Gasdynamic Lasers [in Russian], Nauka (1977).
55. V. S. Avduevskii, Yu. I. Danilov, V. K. Koshkin, et al., Principles of Heat Transfer in Aviation and Rocket Engineering [in Russian], Oborongiz, Moscow (1960); Yu. V. Lapin, Turbulent Boundary Layer in Supersonic Gas Flow [in Russian], Nauka, Moscow (1970).
56. G. K. Vasil'ev, V. V. Vizhin, et al., "Pulsed photolysis of $F_2 + D_2 + O_2 + He$ mixtures," Khim. Vys. Energ., 9, No. 2, 154-159 (1975); G. K. Vasil'ev, E. F. Makarov, and Yu. A. Chernyshev, Kinet. Katal., 16, No. 2, 320-324 (1975).
57. G. K. Vasil'ev, E. F. Makarov, and Yu. A. Chernyshev, "Chain-reaction regimes in pulsed photoinitiation," Fiz. Goreniya Vzryva, 12, No. 6, 896-906 (1976).
58. E. E. Nikitin, Theory of Elementary Atom–Molecular Processes in Gases [in Russian], Khimiya, Moscow (1970).
59. N. A. Generalov et al., "Joint analysis of vibrational relaxation and thermal dissociation of diatomic molecules," Teor. Eksp. Khim., 4, 311-315 (1968).

60. N. M. Kuznetsov, "On the kinetics of dissociation of polyatomic molecules under nonequilibrium vibrational-energy distribution," Dokl. Akad. Nauk SSSR, 202, 1367-1370 (1972); "Kinetics of dissociation of molecules in a molecular gas," Teor. Eksp. Khim., 7, 22-33 (1971).
61. B. V. Kuksenko and S. A. Losev, "Kinetics of excitation of vibration and of dissociation of diatomic molecules in atom–molecule collisions in a gas at high temperature," Teor. Eksp. Khim., 5, 475-483 (1969).
62. A. I. Osipov, "Relaxation processes in gases: I. Nonequilibrium energy distribution over the translational degrees of freedom," Fiz. Goreniya Vzryva, 4, 42-61 (1966).
63. L. S. Polak and A. V. Khatchoian, "Rate coefficient (constant) of nonequilibrium chemical reactions," Trans. Faraday Soc., 67, 1980-1994 (1971).
64. Pai Shih-I, Magnetohydrodynamics and Plasma Dynamics, Springer-Verlag (1962).
65. R. L. Coleman, H. A. Hudson, and B. Garcia, "Distribution of potential and current in plasma MHD arcs," Raket. Tekh. Kosmon., 5, No. 12, 144-148 (1967).
66. Yu. N. Denisov, N. I. Kirelenko, V. S. Kirilkin, et al., "Distribution of potential and current in MHD channel with external azimuthal magnetic field," Magn. Gidrodin., No. 3, 75-79 (1975).
67. L. S. Polak, "Plasmochemical kinetics," in: Outlines of Physics and Chemistry of Low-Temperature Plasma [in Russian], Nauka, Moscow (1971), pp. 302-380.
68. F. B. Vurzel', G. V. Lysov, L. S. Polak, et al., "Kinetics of nonequilibrium chemical reactions in a pulsed microwave discharge. I. Computer calculation of kinetic characteristics of nonequilibrium chemical reactions in a pulsed microwave discharge," Khim. Vys. Energ., 5, 105-111 (1971).
69. K. K. Corvin and S. J. R. Corrigan, "Dissociation of carbon dioxide in the positive column of a glow discharge," J. Chem. Phys., 50, 2570 (1969).
70. Yu. A. Ivanov, L. S. Polak, and D. I. Slovetskii, "On the kinetics of decomposition of carbon monoxide in a glow discharge," Khim. Vys. Energ., 5, 382-387 (1971).

CHAPTER 2

FORMATION OF EXCITED PARTICLES IN THE COURSE OF A NONEQUILIBRIUM CHEMICAL REACTION

2.1. Recombination Mechanism of Excitation

Excitation of Electronic States of Atoms and Molecules. A theoretical analysis of the distributions over the quantum states, resulting from chemical reactions, is as a rule quite complicated even if simple models are used, and predicts the energy distribution only in simple cases [1, 2].

The kinetics of the populations is strongly influenced by energy exchange between the reagents and the reaction products, including the intermediate ones. Six different forms of energy can be distinguished in excitation and energy exchange reactions: T — translational; Te — translational for the electron; R — rotational; V — vibrational; E — electronic; X — chemical. Accordingly, there are 36 different energy-transfer methods: T—R, T—V, V—R, ...[3]. The basic experimental results on energy distribution in chemical-reaction products were obtained using pulsed photolysis and by investigating the emission in discharge tubes and in crossed molecular beams [2, 4-8].

It can also be expected from general theoretical considerations that electronic population inversion, on the basis of which a chemical laser in visible light should operate, occurs rarely in chemical reactions, since the E transitions require larger excitation energies. In addition, the relation between the reagents and the reaction products is limited by symmetry hindrances [9]. In the last decade, however, an increase took place in the number of observations of electronic-state population inversion in the products of chemical reactions and in the number of E-transition chemical lasers [10-12].

Electronic Excitation in Radiative Recombination of Atoms. At a particle thermal velocity on the order of $v_T = 10^5$ cm/sec and at a particle size on the order of $d = 10^{-8}$ cm the collision duration is $\tau \sim d/v_T = 10^{-13}$ sec. The radiative lifetime of the excited particle produced in the collision is about 10^{-7} sec, so that the radiative-recombination probability is of the order of 10^{-6}. This probability becomes even lower when the moment of the radiative transition becomes smaller because of the increase in the distance between nuclei, as is typical of recombining atoms that are in the ground or a metastable state. Radiative recombination in a direct collision between two reacting atoms therefore has low probability, which increases, however, when a third particle takes part. Thus, radiative recombination of oxygen atoms is due to the reactions [13]

$$\left.\begin{aligned} O + O + M \rightarrow O_2(b^1\Sigma_g^+) + M, \\ O + O + M \rightarrow O_2(A^3\Sigma_u^+) + M. \end{aligned}\right\} \qquad (2.1)$$

Both excited states of O_2 correlate with the atoms in the ground state (Fig. 2.1) and are stabilized upon collision with a third particle or on the surface of metallic nickel [14]. In the case of radiative recombination of atoms, e.g., behind a shock wave (T = 2500-3800°K, λ = 230-451.1 nm), the produced O_2 molecules go over from the initial repulsion potential-energy curve into the state $B^3\Sigma_u^-$ and then radiate and go to the ground state [15].

In the reaction

$$N + NO \rightarrow N_2 + O \qquad (2.2)$$

the afterglow radiation intensity decreases sharply at $\lambda < 191.5$ nm, owing to the NO dissociation energy (6.49 eV) [16].

Many data are available on the recombination of nitrogen atoms. The principal radiation from a mixture containing about 1% N_2 is due to the state B, and the remaining radiation is due to the states b^1 and a [17].

Transfer of Electronic Recombination Excitation to Third Particles. Possible mechanisms of electronic excitation of an atom C upon recombination of atoms A and B are:

$$A + B + C \rightarrow AB + C^e; \quad (2.3)$$

$$A + C + C \rightarrow AC + C^e; \quad (2.3a)$$

$$A + B + M \rightarrow AB + M^*; \quad (2.3b)$$

$$M^* + C \rightarrow M + C^e, \quad (2.3c)$$

where M is the third particle.

If Eq. (2.3) is regarded as a collision between particle C and the complex A–B, it can be concluded that the reaction (2.3b) is preferable from the point of view of the excitation rate if M* has a longer lifetime than the complex A–B. In addition, the excited particles C_e can have in this reaction a wider energy spectrum than particles produced in the reaction (2.3) if M* is vibrationally excited and relaxes in multistep collisions. These reactions can be interpreted either as ternary-collision reactions or as formation, as a result of binary collisions, of intermediate complexes that interact subsequently with a third body.

Alkali metals having low-lying electronic states are excited with consumption of only part of the reaction heat. To explain the radiation of flames when alkali-metal salts are added to the initial medium in the presence of hydrogen, the following reaction was proposed [18]:

$$H + H + Na \rightarrow H_2 + Na^e\ (^2p). \quad (2.4)$$

Calculations of the PES for a linear arrangement of the atoms H + H + Na [19] show that the products of the reaction H + H + Na (2s) are H_2 + Na in the ground or in the excited ^2p state. This makes it possible for the reaction (2.4) to proceed adiabatically. Chemiluminescence of a number of metals takes place in the recombination reactions H + H or H + OH [20]. For example, thallium atoms in the ground state are excited in the reaction H + H; and lead atoms, in the reaction H + OH.

Oxygen can be excited as a result of the reactions [21]

$$O + O + O \rightarrow O_2 + O\ (^1s); \quad (2.5)$$

$$O + N + N \rightarrow N_2 + O\ (^1s). \quad (2.5a)$$

The following reactions were proposed [22] for above-equilibrium radiation of OH:

$$H + OH + OH \rightarrow H_2O + OH\ (^2\Sigma^+) \quad (2.6)$$

and

$$H + O_2 + H_2 \rightarrow H_2O + OH\ (^2\Sigma^+). \quad (2.6a)$$

The principal long-lived particles in active nitrogen are N, $N_2(A^3\Sigma_u^+)$, N_2^V, and $N_2(^5\Sigma_g^+)$. The energy of just these particles leads to excitation of such additives as C_2N_2, ClCN, $CHCl_3$, C_2H_2, C_3O_2, $Ni(CO)_4$, $(C_2H_5)_2Zn$, I_2, PbI_2, SF_6 and $SeCl_4$.

Radiation of CN can be produced by vitrational and rotational, as well as electronic, excitation of CN followed by the transitions $B^2\Sigma^+ \rightarrow X^2\Sigma^+$, $A^2\Pi \rightarrow X^2\Sigma^+$ for the violet and red bands, respectively [23].

Excitation of Electronic States in Recombination of an Atom with a Diatomic Molecule. The most investigated reaction of radiative recombination of an atom with a diatomic molecule is

$$O + NO \rightarrow NO_2^e. \quad (2.7)$$

In analogy with many other recombination reactions, the temperature coefficient k(T + 10K)/k(T) of the rate of this reaction is negative, and the rate constant of the reaction at T = 270°K accompanied by radiation in the region λ = 0.4–1.4 μm, is $3.9 \cdot 10^7$ cm^3/(mole•sec), i.e., approximately one out of 10^6 collisions leads to radiation [24]:

$$NO\ (X^2\Pi) + O\ (^3p) + M \rightarrow NO_2^*\ (C) + M; \quad (2.8)$$

$$NO_2^*(C) \rightarrow NO_2^* \ (B) \ \text{(nonradiative transition)}; \tag{2.9}$$

$$NO_2^* (B) \rightarrow NO_2 (A) + h\nu. \tag{2.10}$$

Here A is the ground state and B and C are the excited intersecting states.

Less investigated is radiative recombination in the reaction

$$O + CO \rightarrow CO_2^e. \tag{2.11}$$

The emission spectrum of CO_2 in flames and arcs consists of diffuse bands superimposed on a continuous spectrum. In atomic flames at low pressures and at room temperature the spectrum is only discrete in the wavelength range 0.3-0.6 μm. What is important here is that the ground state of CO_2 correlates with the ground state of CO and with the excited atom $O(^1D)$[25], and in contrast to the reaction O + NO, the correlation with the ground states CO $(^1\Sigma^+)$ + O (^3p) is forbidden by the spin conservation law. Consequently, the reaction CO + O (^3p) cannot produce the ground state directly, and high-intensity radiation is produced.

According to the results of [26], the chemiluminescence reaction

$$O + SO = SO_2^e \tag{2.12}$$

is of second order in pressure, and the temperature dependence of the reaction rate constant can be represented in the form

$$k = 1{,}5 \cdot 10^8 \left(\frac{T}{298}\right)^{-1} \text{ cm}^3/(\text{mole} \cdot \text{sec}). \tag{2.12a}$$

The emission spectrum is bounded by the value λ_{min} = 224 nm and does not reach the value λ = 218.3 nm determined by the reaction heat.

A characteristic chemiluminescent reaction [27] obtained as a result of ternary collisions is

$$H + NO + M \rightarrow HNO^v + M, \ v > 0. \tag{2.13}$$

Luminescence is the result of the following transition mechanism:

$$H\,(^2s) + NO\,(X^2\Pi) + M \rightarrow HNO^e\,(X^1A^1, {}^3A'', {}^1A', {}^3A') + M; \tag{2.13a}$$

$$HNO\,(^3A'') \rightarrow HNO\,(^1A'') \ \text{(nonradiative transition)}; \tag{2.13b}$$

$$HNO\,(^1A'') \rightarrow HNO\,(X^1A^1) + h\nu. \tag{2.13c}$$

Excitation of Vibrational Degrees of Freedom in Recombination of Atoms and Molecules. Recombination reactions due to ternary collisions can lead to vibrational excitation of reaction products that are in the electronic ground state. The reaction rate depends on the partial pressure of the third particles, since the newly produced particle must decay if its energy is not lowered to an excitation energy below the dissociation energy upon collision with the third particle. The vibrational–vibrational V–V relaxation on the reaction products accelerates the energy redistribution appreciably.

A molecule that participates effectively in recombination reactions with formation of vibrationally excited molecules is, e.g., methylene H_2C. Vibrationally excited reaction products are formed when hydrogen atoms (H) combine with olefins. For propylene this reaction can be written in the form [28]

$$H + C_3H_6 \rightleftarrows C_3H_7^v \begin{cases} \xrightarrow{M} C_3H_7 \\ \rightarrow CH_3 + C_2H_4 \end{cases}. \tag{2.14}$$

The vibrationally excited intermediate product $C_3H_7^V$ can dissociate into H and C_3H_6 or into CH_3 and C_2H_4, as well as become stabilized in collisions with an intermediate particle.

From the point of view of chemical excitation, interest attaches to reactions in which the excited product participates in processes other than deactivation or decay into the initial products. These reactions include the formation of polyatomic molecules that have a much weaker bond than produced in recombination, e.g.,

$$CH_3 + CH_2F \rightarrow C_2H_5F^v \qquad (2.15)$$

with release of an excess energy −380 J/mole [5].

Rotational Excitation. Excitation of rotational degrees of freedom is restricted not only by energy conservation, as is the case with excitation of vibrational and electronic states, but also by conservation of the total angular momentum. The total angular momentum of an intermediate complex consists of the orbital angular momentum of the two reagents due to their translational motion relative to the common mass center, and of the internal angular momenta of the reagents. When the complex decays, the total angular momentum is divided into an orbital and a rotational component, and the relation between them is governed by the characteristics of the PES. In second-order radiative-recombination reactions the angular momentum consists of the total angular momentum of the reagents, which includes the rotational and orbital components.

In collisions with participation of a third particle, the excess energy or excess angular momentum of the reaction products is transferred to the third neutral particle, and in this case an excess rotational excitation is unlikely. When intermediate complexes are produced in the reaction

$$A + BC \rightarrow (A - B - C)^* \rightarrow AB + C$$

the rotational angular momentum of the product AB can considerably exceed the total momentum of the complex, since the particle C carries away a large orbital angular momentum, approximately equal in magnitude and opposite in sign to the momentum of particle AB. The maximum momentum is then approximately equal to the orbital angular momentum of the outgoing particle C and is determined by the product of the momentum of the motion and the dissociaton impact parameter, which is equal to the effective radius of the forces between C and AB. For example, in the photodissociation of H_2O [29] the initial complex H_2O^e has a small angular momentum $3\hbar$, whereas the angular momentum of the dissociation product OH^e exceeds $20\hbar$.

2.2. Nonequilibrium Excitation of Particles in Exchange Reactions

Excitation of Electronic Transitions. Exchange reactions of the type

$$A + BC \rightarrow \begin{cases} AB^e + C \\ AB + C^e \end{cases}$$

are not realized in practice in pure form and can be regarded as elementary stages of a complex chemical reaction with formation of an intermediate product A—B—C; this calls for the AB binding energy to be much higher than that of BC. The excitation probability increases in the presence of a low-lying electronic state of AB if the formation of AB in the ground state is forbidden by the spin conservation law. A rather probable reaction is assumed to be

$$H + HI \rightarrow H_2 + I\ (^2P_{1/2}). \qquad (2.16)$$

In this reaction only a few percent of I atoms are produced in the excited state [30].

An example of an exchange reaction with participation of more than three atoms is

$$Br + ClO_2 \rightarrow BrCl^e + O_2, \qquad (2.17)$$

although in fact it proceeds in a more complicated manner than a simple exchange with a Cl atom.

In the reaction

$$O_3 + NO \rightarrow O_2 + NO_2^e\ (-217.7\ \text{kJ/mole}), \qquad (2.18)$$

approximately 10% of the collisions lead to formation of NO_2 ($^2B_1$), and only a few lower V levels of this state are populated [31]. The reaction

$$O_3 + SO \rightarrow O_2 + SO_2 \qquad (2.19)$$

is much more exothermic (−446.3 kJ/mole). The rate constants of the formation of the three possible E states are [32] [in $cm^3/(mole \cdot sec)$]:

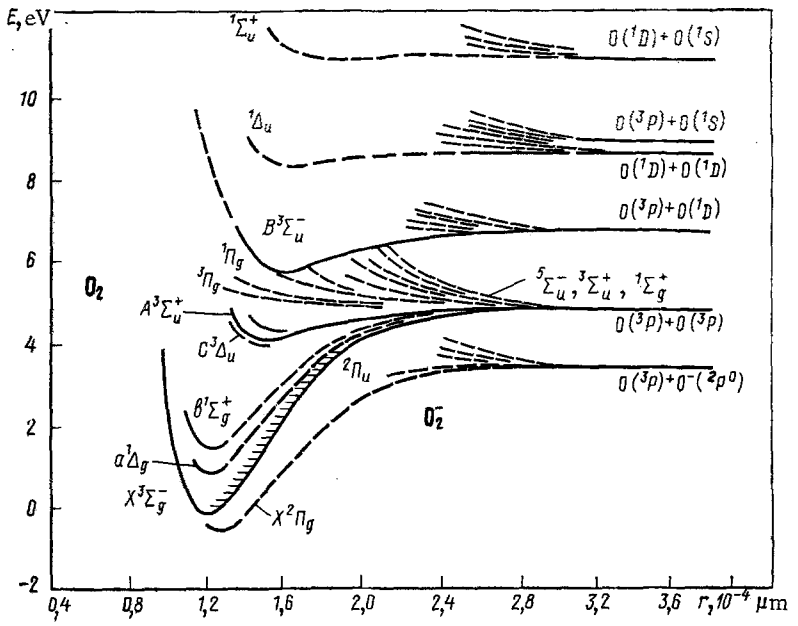

Fig. 2.1. Potential-energy diagram of O_2.

$$\left.\begin{aligned} k(\tilde{X}\,^1A_1) &= 1.5\cdot 10^{12}\exp(-2100/RT);\\ k(\tilde{A}\,^1B_1) &= 10^{11}\exp(-4200/RT);\\ k(\tilde{a}\,^3B_1) &= 3\cdot 10^{10}\exp(-3900/RT). \end{aligned}\right\} \qquad (2.20)$$

Vibrational Excitation in Exchange Reactions. Pulsed photolysis of O_3, NO_2, ClO_2 produces vibrationally excited oxygen molecules. Since the process proceeds in analogous fashion for all three substances, we can confine ourselves to the formation of excited oxygen in the photolysis of O_3. An important role is played here by the following reactions, which proceed with the formation of atomic oxygen [2]:

$$\left.\begin{aligned} &O_3 + h\nu \rightarrow O(^3P) + O_2;\\ &O_3 + h\nu \rightarrow O(^1D) + O_2(^1D);\\ &O(^3P) + O_3 \rightarrow O_2^v + O_2 \quad (-389{,}4 \text{ kJ/mole});\\ &O(^1D) + O_3 \rightarrow O_2^v + O_2 \quad (-745{,}2 \text{ kJ/mole}).\\ &\ldots\ldots\ldots\ldots\ldots\ldots\ldots \end{aligned}\right\} \qquad (2.21)$$

Excited oxygen molecules in the $X^3\Sigma_g^-$ state are observed up to levels $v \leqslant 29$. The maximum in the distribution of the excited molecules takes place at v = 12, 13, and 14, while the populations of the remaining levels decrease monotonically. The O (^{3}P) atoms play a considerable role in the formation of vibrationally excited oxygen molecules. This pertains to thermal decomposition of ozone in a shock wave and to pulsed photolysis of NO_2. The reactions considered above result in the formation of oxygen molecules on high V levels, not accompanied by chemiluminescence, since the vibrational–rotational V–R transitions are forbidden for homonuclear molecules.

The most interesting reactions with hydrogen halides are

$$\begin{aligned} &H + Cl - Cl \rightarrow HCl^v + Cl \quad (-188.4 \text{ kJ/mole}),\\ &Cl + H - I \rightarrow HCl + I \quad (-310 \text{ kJ/mole}), \end{aligned} \qquad (2.22)$$

in which inverted population takes place at low pressures. In the case Cl + H – I the inversion is large and quantum-mechanical generation of radiation is observed. More than half of the reaction heat goes into vibrational excitation. The remainder is converted into rotational energy, so that the translational energy of the products is comparable with the energy of the initial reaction products.

The distributions of the populations of the vibrationally excited oxygen molecules and of the hydrogen-chloride molecules are, in the main, similar. The distribution has a maximum for levels corresponding to half the reaction energy. The distribution of both molecules over the V levels is close to the initial distribution due to the reaction. This distribution may be distorted because of the high rate of R relaxation in the collisions.

Vibrational—translational V—T relaxation has a considerably lower rate than the rotational—translational R—T relaxation, and is substantially different for HCl and O_2, inasmuch as for O_2 the gas-kinetic number of collisions is $Z_0 = 8 \cdot 10^5$, and for HCl $Z_0 = (0.5\text{-}1.5) \cdot 10^3$. Radiative transitions are forbidden for oxygen, and the radiative lifetime of HCl lies in the range 10^{-2}-10^{-4} sec. The initial distribution can thus be expected to be preserved much longer at high pressures in the case of O_2 than in the case of HCl. As a result of V—V energy exchange, however, this distribution can be substantially altered. Thus, in experiments with HCl and OH (the reaction $H + O_3 \rightarrow OH^V + O_2$) at p = 13.33 Pa an almost Maxwell—Boltzmann distribution in the V levels was observed, but the vibrational temperature greatly exceeded the translational and amounted to several thousand degrees. This indicates energy exchange took place as a result of R and V—V relaxation, but the V—T relaxation did not end.

Widely known reactions that lead to effective chemical excitation are those of sodium and potassium atoms with halogens, nitrogen oxides, and alkyl halides. These reactions are rapid, and the activation energy is as a rule less than 21 kJ/mole. The sodium-doublet radiation was found to predominate, since the lifetime of $NaCl^V$ is quite long, the electron-vibrational E—V energy exchange is effective, and the radiative lifetime is only 10^{-8} sec.

The regularities considered are typical of systems containing atoms with low-lying states, in which the transitions are energy-allowed.

The equation for an exchange reaction that proceeds with formation of a four-center complex can be written in the form

$$A - B + C - D \rightarrow A - C + B - D. \tag{2.23}$$

A known reaction of this type, in which formation of vibrationally excited particles has been established, is, e.g., [2]

$$CN + O_2 \rightarrow CO + NO^v.$$

Rotational Excitation in Exchange Reactions. In the reaction

$$K + HBr \rightarrow KBr + H, \tag{2.24}$$

one should expect, according to the conservation law, excitation of the rotational energy of the reaction product. Indeed, the initial rotational momentum of the K atom should be large because of the large mass of K and the appreciable cross section of the reaction ($0.34 \cdot 10^{-14}$ cm^2), whereas the momentum of HBr is small because of the small moment of inertia of this molecule. In the reaction products, KBr has a rather large moment of inertia, so that according to the conservation laws the bulk of the total momentum will go into rotation of the KBr.

For strongly nonequilibrium rotational excitation, e.g., in the reaction

$$Cl + HI \rightarrow HCl\ (v = 2) + I \tag{2.25}$$

almost the entire difference between the reaction heat and the energy needed to excite the v = 2 level goes into rotational excitation.

Strongly nonequilibrium rotational distributions are usually observed in chemiluminescence reactions that lead to formation of electron-excited molecules in ordinary atomic flames and in a discharge. In these cases the R relaxation is hindered by the short lifetime of the E states.

LITERATURE CITED

1. E. E. Nikitin, "Nonequilibrium chemical reactions," in: Problems of Kinetics of Elementary Chemical Reactions [in Russian], Nauka, Moscow (1973), pp. 5-50.
2. T. Carrington and D. Garvin, in: Formation of Excited Particles in Chemical Kinetics [Russian translation], A. A. Borisov (ed.), Mir, Moscow (1973), pp. 123-213.

3. F. R. Gilmore, E. Bauer, and J. W. McCowan, "A review of atomic and molecular excitation mechanism in nonequilibrium gases up to 20,000°K," J. Quant. Spectrosc. Rad. Transfer, 9, No. 2, 157-183 (1969).
4. B. S. Rabinovich and M. S. Flowers, "Chemical activation," in: Chemical Kinetics and Chain Reactions, V. N. Kondrat'ev (ed.), Nauka, Moscow (1966), pp. 61-144.
5. V. N. Kondrat'ev, Kinetics of Chemical Gas Reactions [in Russian], Nauka, Moscow (1974).
6. Physical Chemistry of Fast Reactions [Russian translation], Mir, Moscow (1976).
7. V. N. Kondrat'ev, Rate Constants of Gas-Phase Reactions [in Russian], Nauka, Moscow (1970).
8. Advances in Chemical Physics. V. 28. The Excited State in Chemical Physics , J. W. McCowan (ed.), New York–London, Interscience Publ. (1976).
9. B. A. Thrush, "Gas reactions yielding electronically excited species," Ann. Rev. Phys. Chem., 19, 371-388 (1968).
10. V. S. Zuev, S. B. Kormer, L. D. Mikheev, et al., "Onset of inversion on the $^1\Sigma_g^+ \rightarrow {}^3\Sigma_g^-$ transition of molecular sulfur in the dissociation of COS," Pis'ma Zh. Eksp. Teor. Fiz., 16, No. 4, 222-224 (1972).
11. C. R. Jones and H. P. Broida, "Chemical lasers in the visible," Laser Focus, 10, No. 3, 37-47 (1974).
12. Electronic Transition Lasers, MIT Press, Cambridge, Mass. and London (1976).
13. R. A. Young and J. L. Sharpless, "Chemiluminescent reactions involving atomic oxygen and nitrogen," J. Chem. Phys., 39, No. 4, 1071-1102 (1963).
14. F. R. Gilmore, "Potential energy curves for N_2, NO, O_2 and corresponding ions," J. Quant. Spectr. Rad. Transfer, 5, No. 2, 369-390 (1969).
15. B. F. Mayers and E. R. Bartle, "Shock-tube study of the radioactive combination of oxygen atoms by inverse predissociation," J. Chem. Phys., 48, No. 9, 3935-3944 (1968).
16. Y. Tanaka, "Emission bands of NO in the vacuum ultraviolet region excited in the NO afterglow," J. Chem. Phys., 22, No. 12, 2045-2048 (1954).
17. R. W. F. Gross and N. Cohen, "Temperature dependence of chemiluminescent reactions. II. Nitric oxide afterglow," J. Chem. Phys., 48, No. 6, 2582-2588 (1968).
18. T. M. Sugden, "Excited species in flames," Ann. Rev. Phys. Chem., 13, 369-390 (1963).
19. J. L. Magee and T. Ri, "The mechanism of reaction involving excited electronic states," J. Chem. Phys., 9, No. 8, 638-644 (1941).
20. P. J. Padley and T. M. Sugden, "Chemiluminescence and radical recombination in hydrogen flames," in: 7th Symp. Combustion, Lond., Butterworth, Publ. for the Combustion Institute (1959), pp. 235-244.
21. J. Kaplan, et al., "Atomic reactions in the upper atmosphere," Can. J. Chem., 38, No. 10, 1688-1692 (1960).
22. A. G. Gaydon, The Spectroscopy of Flames, Chapman & Hall (1957).
23. N. H. Kiess and H. P. Broida, "Emission spectra from mixtures of atomic nitrogen and organic substances," in: 7th Symp. Combustion, London, Butterworth, Publ. for the Combustion Institute (1959), pp. 207-214.
24. A. Fontijn, C. B. Meyer, and H. J. Schiff, "Absolute quantum yield measurements of the NO–O reaction and its use as standard for chemiluminescent reaction," J. Chem. Phys., 40, No. 1, 64-70 (1964).
25. K. J. Laidler, The Chemical Kinetics of Excited States, Clarendon, Oxford Univ. Press (1955), p. 180.
26. S. R. Fletcher and B. P. Levitt, "O + SO recombination emission at 3500°K," Trans. Faraday Soc., 65, No. 558, Part 6, 1544-1549 (1969).
27. M. A. A. Clune and B. A. Thrush, "Mechanism of chemiluminescent reactions involving nitric oxide — the H + NO reaction," Discuss. Faraday Soc., 33, 139-148 (1962).
28. B. A. Thrush, "The reactions of hydrogen atoms," Progr. Reaction Kinetics, 3, 65-95 (1965).
29. T. Carrington, "Angular momentum distribution and emission spectrum of $OH(^2\Sigma^+)$ in the photodissociation of H_2O," J. Chem. Phys., 41, No. 7, 2012-2018 (1964).
30. P. Cadman and J. C. Polanyi, "Production of electronically excited atoms. II. $H + HI \rightarrow H_2 + I^*(P_{1/2})$," J. Phys. Chem., 72, No. 11, 3715-3724 (1968).
31. P. N. Clough and B. A. Thrush, "Mechanism of chemiluminescent reaction between nitric oxide and ozone," Trans. Faraday Soc., 63, Part 4, No. 532, 915-925 (1967).
32. C. J. Halstead and B. A. Thrush, "The kinetics of elementary reactions involving the oxide of sulfur. III. The chemiluminescent reaction between sulfur monoxide and ozone," Proc. R. Soc. (London), A295, No. 1443, 380-398 (1966).

CHAPTER 3

BASIC EQUATIONS FOR PROCESSES IN CHEMICAL LASERS

3.1. General Conditions for the Onset of Lasing

The main task in the investigation of the processes in chemical lasers is to study the various reactions at which atoms or molecules can be produced with an energy level such that at least one optical transition satisfies the conditions that lead to synchronization of individual emitters, but for inverted population of the levels and in the case of phase correlation of the emitters. Nonequilibrium excitation of the internal degrees of freedom of the atoms is a necessary but insufficient condition for the emission of coherent radiation in the course of a chemical reaction. It is necessary also to have an inversion reserve to compensate for the losses in the resonant system. These losses determine the maximum population-concentration difference. In lasers whose operation is determined by phase correlation of the emitting particles, the absolute concentration of these particles has a threshold value.

For lasers based on the use of the inversion effect, the critical density of the population inversion of the energy levels is determined by the probability of the given induced optical transition, by the relative emission line width ($\Delta\nu/\nu$), as well as by the properties of the modes excited in the resonator. If the emission line width is the Doppler broadening, as is usually the case at pressures on the order of several torr, the kinetics of the molecules and atoms in the lasing process will differ little. At high pressures in photostimulated chemical reactions, the ratio $\Delta\nu/\nu$ substantially influences both the chemical reaction and the lasing conditions.

Calculations of the emission probabilities are based on the Born-Oppenheimer approximation, which permits a correct estimate of the E-transition probability. The total E-transition probability for an allowed molecular transition is of the same order as for atoms ($\sim 10^7$ $\sec^{-1}$). Allowance for the interaction of the V and R levels, however, makes the probability of an individual allowed E transition smaller by several orders of magnitude than the total probability of all the transitions from a level. This circumstance increases the threshold values of the critical density of the inversion and of the absolute concentrations of the emitting centers.

The critical density of the level population inversion is determined, besides by the vibrational properties of the cavity, also by nonoptical transitions that lead either to further excitation or to relaxation processes that return the system to the equilibrium state. Chemical excitation processes usually lead to an increase of the population in a rather large region of the V and R levels. Owing to the small distance between R levels, they are easily excited or relax on thermal molecules having an energy ~0.1 eV. These relaxation processes essentially determine the kinetics of the energy redistribution among the molecules. This redistribution is attained after only several collisions in weakly bound molecules such as I_2, and after up to $\sim 10^7$ collisions in strongly bound molecules such as N_2.

Within the limits of each degree of freedom, the relaxation processes determine the corresponding temperature whose change gives rise to a particular energy transition. As a rule, the temperature rapidly assumes a steady-state value within one degree of freedom, after which an exchange of energy E takes place between the degrees of freedom. For example, if the system is in an inverted state relative to the V levels, rapid R relaxation can raise the population of the upper lasing level at the expense of neighboring R levels and lower correspondingly the population of the lower lasing level on account of rapid transitions to neighboring R levels in collisions.

In addition, the different relaxation times of the V and R levels make possible inversion of individual V–R levels even when both the vibrational and rotational distribution are normal with temperatures T_V and T_R.

According to Sec. 1.6, the energy of a V–R level of a molecule can be represented in the harmonic-oscillator approximation in the form

$$E(V, J) = E(V) + B(J+1)J, \tag{3.1}$$

where V (v_1, v_2, ... , v_n) is the spectrum of the vibrational quantum numbers.

The following relation holds for the total (vibrational) inversion:

$$n(V_1) - [g(V_1)\, n(V_2)/g(V_2)] > 0. \tag{3.2}$$

Writing down the equilibrium distribution of the V levels

$$\left.\begin{aligned} n(V) &= [g(V)/z_{\text{vib}}] \exp\left[-\sum_l (v_l h\nu_l/k^0 T_l)\right], \\ z_{\text{vib}} &= \prod_l [1 - \exp(-h\nu_l/k^0 T_l)]^{-g_l}, \end{aligned}\right\} \tag{3.3}$$

where v_l are numbers from the set V (v_1, v_2, ..., v_n), v_l, g_l, T_l are the frequency, degree of degeneracy, and temperature of the l-th vibration mode, and g(V) is the statistical weight of the level V, we obtain the condition for the existence of inversion between the levels V_1 (..., v_{i+1}, ..., v_l, ...) and V_2 (..., v_i, ..., v_{l+1}, ...)

$$T_i/T_l > \nu_i/\nu_l > 1. \tag{3.4}$$

Satisfaction of this condition calls for relatively low values of T_i/T_l, so that in the cases of practical importance the ratio ν_i/ν_l is small.

In the case of partial inversion with a Boltzmann distribution over the rotational levels

$$n(V_1, J) - \frac{g(V_1, J)\, n(V_2, J+1)}{g(V_2, J+1)} > 0 \tag{3.5}$$

and for inversion between v + 1, J and v, J + 1 it is necessary to have

$$\frac{n(v+1)}{n(v)} \exp\left[-\frac{E(v+1, J)}{k^0 T} + \frac{E(v, J+1)}{k^0 T}\right] > 1 \tag{3.6}$$

or

$$\frac{T_{\text{vib}}}{T} > h\nu/[2(J+1)B_v + (B_v - B_{v+1})J(J+1)] > 1. \tag{3.7}$$

The last condition makes it possible to estimate the maximum value of the population inversion

$$\Delta n_{\max} = \frac{2(J_m+1)}{z_{\text{vib}}} n(v+1) \exp\left[-\frac{BJ_m(J_m+1)}{k^0 T}\right] \left\{1 - \exp\left[\frac{h\nu}{k^0 T_{\text{vib}}} - \frac{2B(J_m+1) + (B_v - B_{v+1})J_m(J_m+1)}{k^0 T}\right]\right\}, \tag{3.8}$$

where

$$J_m \approx J_0 + \frac{1}{2J_m+3} \frac{k^0 T}{B} \frac{2J_0+1}{2J_m+1},$$

$$J_0 \approx \frac{B}{(B_v - B_{v+1})} \left[\left(1 + \frac{h\nu(B_v - B_{v+1})}{B^2} \frac{T}{T_{\text{vib}}}\right)^{1/2} - 1\right] - 1.$$

The exchange exothermic reaction

$$A + BC \rightarrow \begin{cases} AB^* + C \\ AB + C^* \end{cases}$$

can proceed under light-wave conditions in the following manner with emission of light:

$$A + BC \rightarrow (A - B - C)^* \rightarrow AB + C + h\nu,$$

where (A–B–C)* is a complex containing the chemical energy of the bond.

Chemical lasers based on reactions of this type can convert chemical energy into light at high efficiency and in the shortest way, inasmuch as in a number of such reactions the complex (A – B – C)*, as shown in Sec. 1.6, does not have a conventional lower state, i.e., it is always inversely populated. Furthermore, the concentration of the complexes increases with increasing pressure up to pressures at which ternary collisions assume a substantial role.

With increasing concentration of the emitting particles, the latter can no longer be regarded as isolated emitters. In this case the collective interaction makes the spontaneous emission coherent and substantially more intense [1]. It can be shown that for a number of conditions the rate of a chemical reaction on account of emitter synchronization becomes comparable with the rate of a chemical reaction on account of stimulated transitions. In both cases it is proportional to the square of the concentration of the initial reagents, meaning that the two mechanisms can compete with each other, depending on the absolute values of the radiating transitions and on the phase-correlation volume.

In the case of phase correlation we have for the threshold N_t of the concentrations of the radiating particles the estimate [1]

$$VN_t/4 > 1, \tag{3.9}$$

where $V \cong \lambda^3$ and $\lambda^2 L$, respectively, depending on the manner in which the chemical reaction was produced. Here λ is the radiated wavelength and L is the cavity length.

3.2. Equations of Motion of a Chemically Reacting Gas with Allowance for Nonequilibrium Effects and Radiation

The equations that describe a multicomponent chemically interacting gas mixture in the presence of radiation are quite complicated for use in the solution of practical problems. Taking (1.77)-(1.80) into account, we present here a simplified system of equations based on the use of a phenomenological approach for energy exchange and diffusion of the components.

The continuity equation in the Euler variables (ρ, $\mathbf{u}$) remains valid in the presence of chemical reactions and radiation, and takes the usual form

$$d\rho/dt + \rho \operatorname{div}(\mathbf{u}) = 0. \tag{3.10}$$

In the presence of chemical interaction and diffusion, this equation can be written for the component i in the form

$$\partial\rho_i/\partial t + \operatorname{div}(\rho_i \mathbf{u}) = w_i - \operatorname{div} \mathbf{D}_i, \tag{3.11}$$

where $\mathbf{D}_i = \rho_i (\mathbf{u}_i - \mathbf{u})$ is the diffusion mass flow; w_i is the change of the mass of the i-th component on account of the chemical reaction (or ionization).

The momentum equation, neglecting radiative pressure, is, according to (1.78),

$$\rho d\mathbf{u}/dt + \nabla P = 0. \tag{3.12}$$

The energy equation takes the form

$$\rho dh_e/dt = \operatorname{div}(P\mathbf{u}) - \operatorname{div} \mathbf{q}. \tag{3.13}$$

The conservation equations for the i-th component can be written assuming the component to be a particle in a definite chemical and quantum state. It is convenient to change over to the particle concentrations per unit volume n.

For example, for a molecule of sort m in a vibrational state we can write in lieu of (3.11)

$$dn_v^m/dt = K_v^m. \tag{3.14}$$

Here K_v^m is the change of the number of particles of sort m on the vibrational level v as a result of chemical reactions, collisions with other particles, or radiation.

The equation for the quantum density q_ν is

$$dq/dt = -\alpha I_\nu + w_\nu, \tag{3.15}$$

where I_ν is the intensity of the resonant radiation of frequency ν; w_ν, pumping rate; and α, coefficient of absorption (or amplification) of the light.

3.3. Basic Properties of Chemical Lasers

The basic properties of chemical lasers and the principal quantitative criteria for the onset of lasing can be obtained on the basis of mathematical models [2-5].

We consider the kinetics of chemical pumping and chemical-laser generation on the basis of the simplest two-level model, including chemical pumping of two working levels with populations n_1 and n_2, relaxation, and stimulated emission.

The balance equation for the photon density in the cavity is written in this case in the form

$$dq_\nu/dt = A_{1,2}n_1 + B_{1,2}n_1q_\nu - B_{2,1}n_2q_\nu - q_\nu/\tau_p. \tag{3.16}$$

Here $A_{1,2}$ is the spontaneous-emission coefficient; $B_{1,2}$, $B_{2,1}$, coefficients of induced emission for the respective transitions 1-2, 2-1, n_1, n_2, respective numbers of particles on levels 1 and 2; τ_p, photon lifetime in the cavity.

Recognizing that $A_{1,2} = B_{1,2}\ 8\pi\nu^3/c^3$, $B_{1,2}q_{\nu,1} = q_{\nu,2}B_{2,1}$ and introducing $\sigma = \sigma_{1,2} = B_{1,2}\ q_\nu/\Delta\nu c$, $\Delta n = n_2 - nn_1$, where $\sigma_{1,2}$ is the stimulated-transition cross section, we obtain

$$dq_\nu/dt = A_{1,2}n_1 + \sigma c\Delta n q_\nu - q_\nu/\tau_p. \tag{3.17}$$

For n_1 and n_2 we have analogously

$$dn_1/dt = P_1w + n_2/\tau_r + \sigma c q_\nu \Delta n, \tag{3.18}$$

$$dn_2/dt = P_2w - n_2/\tau_r - \sigma c q_\nu \Delta n, \tag{3.19}$$

where τ_r is the level relaxation time; P_1 and P_2 are the probabilities of formation of the populations n_1 and n_2.

The maximum radiation energy, defined as

$$E_{\max} = \int_0^\infty (h\nu q_\nu/\tau_r)\,dt,$$

is

$$E_{\max} = (1/2)\,h\nu\,(P_2 - P_1)\int_0^\infty w(t)\,dt. \tag{3.20}$$

The maximum efficiency, namely the ratio of the maximum coherent-radiation energy to the thermal effect of the reaction, is called the chemical efficiency η_c and does not depend on the reaction rate [2-5]:

$$\eta_{\max} = \eta_c = \frac{1}{2}\frac{h\nu\,(P_2 - P_1)}{|-\Delta H_e|}. \tag{3.21}$$

Lasing sets in at the initial instant of time if the rate of the chemical reaction satisfies the condition

$$w > w_t = 1/\tau_r\ \sigma c\tau_p = \Delta/\tau_r, \tag{3.22}$$

where $\Delta = (\sigma c\tau_p)^{-1}$ is the threshold inversion density.

In stationary chemical pumping there comes an instant when the lasing stops on account of relaxation at the reaction products. This critical lasing shutoff time equals

$$t_{cr} = (P_2 - P_1)\tau_r. \tag{3.23}$$

When inversion is produced with probability P_3 in molecules by energy transfer from other molecules excited by the chemical reaction, the system of equations is supplemented by an equation for the density n* of the excited particles produced as a result of the chemical reaction:

$$\frac{dn^*}{dt} = w - (P_{r,1} + P_3)n^* \quad \left(P_{r,i} = \frac{1}{\tau_{r,i}},\ i = 1,2\right). \tag{3.24}$$

Taking into account the production of inversion on account of energy transfer from excited particles, we have for n_2

$$dn_2/dt = P_3 n^* - P_{r,2} n_2 - \sigma c q_v (n_2 - n_1). \tag{3.25}$$

Equation (3.17) without the first term is also valid.

Lasing sets in under the condition

$$w > w_t = P_{r,2} (n_1^r + \Delta) (P_{r,1} + P_3)/P_3, \tag{3.26}$$

where n_1^r is the equilibrium population of the lower working level.

We now consider the amplification of the radiation under the conditions of a nonstationary three-dimensional medium [4]. In the case of partial inversion in nonstationary chemical pumping of the vibrational levels of a diatomic molecule, the gain on the R–V transition $(v + 1, J-1) \to (v, J)$ for the $\mathcal{P}$-branch, under equilibrium distribution over the rotational level, takes the form

$$\alpha_v = \alpha_{v,J}^{v+1,J-1} = \sigma_{v,J}^{v+1,J-1} \left(n_{v+1} - n_v \exp\left(-\frac{2\theta_r J}{T} \right) \right). \tag{3.27}$$

Here θ_r is the characteristic rotational temperature; $\sigma_{v,J}^{v+1,J-1}$ is the cross section of the induced transitions.

In the harmonic approximation we have

$$\sigma_{v,J}^{v+1,J-1} = (v+1)\, \sigma_{0,J}^{1,J-1}, \tag{3.28}$$

$$\sigma_{0,J}^{1,J-1} = \frac{c^2}{8\pi (\nu_{0,J}^{1,J-1})^2} A_{0,J}^{1,J-1} (2J-1) \frac{\theta_r}{T} g(0) \exp\left(-\frac{\theta_r}{T} J(J-1) \right), \tag{3.28a}$$

where $\nu_{0,J}^{1,J-1}$ is the transition frequency; g(0), form factor; and $A_{0,J}^{1,J-1}$, Einstein coefficient. From (3.27), (3.28), and (3.28a) it follows that

$$\alpha = \sum_v \alpha_v = \sigma [q_v - \varepsilon_J N], \tag{3.29}$$

where $\varepsilon_J = (\exp(2\theta_r J/T) - 1)^{-1}$; $N = \Sigma n_v$;

$$\sigma = \sigma_{0,J}^{1,J-1} (1 - \exp(-2\theta_r J/T)); \quad q_v = \sum_v v n_v.$$

Using (3.15) as the equation for the medium, we have

$$\frac{dq_v}{dt} = -\alpha I_v + \sum_{i=1}^{p} \beta_i w_i (x, t), \tag{3.30}$$

where β_i and $w_i(x, t)$ are, respectively, the average number of excitation quanta and the rate of excitation on account of the i-th chemical-reaction channel. For example, in the case of pumping by a chemical chain reaction

$$A + B_2 \xrightarrow{P_{1v} k_1} AB(v) + B, \quad B + A_2 \xrightarrow{P_{2v} k_2} AB(v) + A$$

with probabilities of formation of the reaction products on the v-th vibrational level P_{1v} and P_{2v}, we have at p = 2:

$$\beta_1 = \sum_v v P_{1v}; \quad \beta_2 = \sum_v v P_{2v}; \quad w_1 = k_1 [A][B_2]; \quad w_2 = k_2 [B][A_2].$$

With the aid of (3.29) we obtain from (3.30) the equation of the medium:

$$\partial\alpha/\partial t = -\sigma\alpha I_v + K(x, t), \tag{3.31}$$

where $K(x, t) = \sigma[w(x, t) - \partial/\partial t\, (\varepsilon_J N)]$.

At total inversion, for molecules whose upper and lower laser levels belong to different modes (ν_3, ν_1), the expression for the gain on the transition $00^\circ 1 \to 10^\circ 0$ can be written in the form

$$\alpha = \sigma(q_{v,3} - q_{v,1});$$

$$\sigma = f\sigma_{10}^{00^\circ 1}; \quad f = (1 + q_{v,1}/N)^{-2}(1 + q_{v,2}/N)^{-2}(1 + q_{v,3}/N)^{-2}. \tag{3.32}$$

Here $q_{v,i}$ is the density of the vibrational quanta of the i-th mode (i = 1, 2, 3).

3.4. Kinetics of Chemical Pumping and of Lasing in the Pulsed Regime

Inasmuch as in the pulsed regime it is easy to attain high pump powers and lower energy losses, pulsed lasing can be obtained in a considerably larger number of active media and transitions, and in a larger spectral range than in the continuous regime [6].

Reactions with branched chains are the fastest. These include oxidation of H_2, PH_3, SiH_4, CS_2, CO, P, decomposition of NCl_3, a number of reactions of molecular fluorine with H_2, CH_3, I, HI and some others. We expound, following the review [7], the laws governing branched chain reactions with inverse excitation of the products for the well-investigated hydrogen-oxidation reaction [8], e.g., in the reaction of hydrogen with fluorine.

It is shown in [9-11] that this reaction is a branched chain reaction with energy branching, and follows the scheme:

initation of the chains $F_2 \to F + F$ (3.33a)

continuation of the chains $F + H_2 \to HF\ (v \leqslant 3) + H$ (3.33b)

continuation of the chains $H + F_2 \to HF\ (v \leqslant 6) + F$ (3.33c)

branching of the chains $HF\ (v \geqslant 4) + F_2 \to HF\ (v' \leqslant 4) + F + F$ (3.33d)

annihilation of the chains $H + O_2 + M \to HO_2 + M$, $HO_2 \to$ wall (3.33e)

annihilation of the chains $H \to$ wall and $F \to$ wall (3.33f)

V–V relaxation and deactivation of the HF vibrations. (3.33g)

At low pressures the collisions are infrequent and the continuation and branching of the chains takes place at low rates, whereas the probability of annihilation of the active centers H, F, HF ($v \geqslant 4$) on the walls is high. Thus, at low pressures the mixture is stable and does not ignite spontaneously. The mixture is also stable at high pressures, since the probability of the annihilation of the active H atoms in ternary collisions (3.33e) increases considerably. Spontaneous ignition of the mixture takes place when the processes (3.33b), (3.33c), and (3.33d) develop progressively and prevail in a certain intermediate pressure range that is a function of the mixture temperature.

This behavior of a chemical reaction is described in terms of the coordinates T and p, as is well known, by the plot of the ignition peninsula region (Fig. 3.1), which is typical of the branched chain reactions described in Sec. 1.5. The boundaries of this peninsula (solid line) are the lower and upper ignition limits, or, in other words, the first and second ignition limits. For the reactions $HO_2 + F_2 \to HF + O_2 + F$ there also exists a third ignition limit (shown dashed in Fig. 3.1).

The equations for the changes in the particle concentrations n_H, n_F, and $n_{HF(v)}$ are

$$dn_H/dt = -(k_3 n_{F_2} + k_5 n_{O_2} n_M + k_6) n_H + k_2 n_{H_2} n_F; \tag{3.34}$$

$$dn_F/dt = k_3 n_{F_2} n_H - (k_2 n_{H_2} + k_7) n_F + n_{F_2} \sum_{v \geqslant 4} k_{4,v} n_{HF(v)} + w(t); \tag{3.35}$$

$$dn_{HF(v)}/dt = k_3 k_v n_{F_2} n_H - k_{4,v} n_{F_2} n_{HF(v)} + \Omega(t), \tag{3.36}$$

where $\Omega(t)$ is the term describing the relaxation and annihilation on the walls; k_2, k_3, $k_{4,v}$, and k_5, rate constants of the corresponding processes ($k_{4,v>4} = 0$); w(t), rate of the chain-initiation reaction (3.33a); k_6, k_7, certain averaged constants that take into account the size, configuration, and material of the reaction-volume walls in the case when Eqs. (3.34)-(3.36) are linear.

We consider the initial period of the reaction, assuming that w(t) is a delta-like function. In this case the solution of the system (3.34)-(3.36) is a sum of exponential terms

$$n_{HF} = n_0 \exp(st),$$

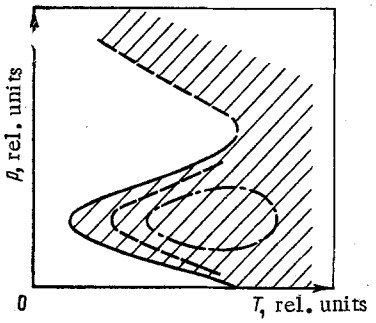

Fig. 3.1. Lasing limits for branched chain reactions.

where s is the largest root of the determinant of the system (3.34)-(3.36) [2, 12].

The ignition peninsula is defined by the condition $s \geqslant 0$. Typical of the initial stage of the reaction is an exponential growth of the reaction products and of the reaction rate.

For an exponential growth of the concentration without V–V relaxation the distribution of n_v is constant at large st and is given by $\bar{n} = s\bar{k}/(s + \tilde{b})$. Corresponding to given values of $\tilde{b}$ and k_v is a minimum s_{min} at which inversion still exists in the system of vibrational levels. Let $k \approx 1$, $k_{v+1} \approx 0$, and $\tilde{b}$ be specified in the form of a harmonic approximation. It follows then for large st that

$$n_1/n_0 \approx s\tau_T\,(1 - \exp(-h\nu/kT))^{-1} \approx s\tau_T. \qquad (3.37)$$

The condition for the existence of inversion in this case is then $s\tau_T > 1$. This condition is satisfied in a region inside the ignition peninsula (shaded in Fig. 3.1) and can be a peninsula or an island (dash-dot curve in Fig. 3.1); it may also not exist at all.

The initial mixture has a temperature and a pressure that are far from the ignition region. External actions typical of this chemical-laser construction, e.g., rapid action of an electric discharge or photolysis, transfer the mixture into the ignition region, and also into the inversion region if the energy is sufficient [13].

From (3.34)-(3.36) we can qualitatively estimate the influence of the V–V relaxation on the course of the reaction. If the processes (3.33e) are very fast, relaxation causes additional population of the level v = 4 via transitions from the third level. The reaction rate can increase somewhat in this case. If, however, the processes (3.33e) are slow, relaxation leads to establishment of a Boltzmann distribution of n_v and the reaction rate decreases.

A calculation of V–V relaxation, within the framework of the linearized problem, was carried out for radical chains, e.g., in [8, 13] for a two-level model, with estimates of the possible efficiency of a branched chain reaction laser.

3.5. Basic Equations of Continuous-Wave Chemical Laser

The theoretical investigation of the characteristics of a cw chemical laser entails considerable difficulties since it is necessary to simultaneously take into account the influence of the diffusion, the chemical reactions, and the radiation [14].

In theoretical models the disequilibrium of the energy distribution can be taken into account by regarding the gas, in analogy with the gas reactions, as a mixture of several components, with each long-lived V level of the active molecule taken to be a separate component of the gas. It is assumed that the formation of the active molecules in the course of mixing and burning of the fuel and the oxidizer is determined by the diffusion, and that the combustion takes place along the front of the flame [15]. Collisional deactivation of each vibrational level of the active molecule via resonant V–V and V–T energy transfer is taken into account by expansion in powers of the ratio of the axial distance to the characteristic deactivation length.

The flow diagram is shown in Fig. 3.2. Two homogeneous semiinfinite parallel gas streams (one consists of the oxidant and diluent, the other of the fuel and a diluent) begin to be mixed and burn at the point x = y = 0. Here x is the coordinate in the flow direction and y is the coordinate perpendicular to x, with positive y corresponding to the region filled with fuel.

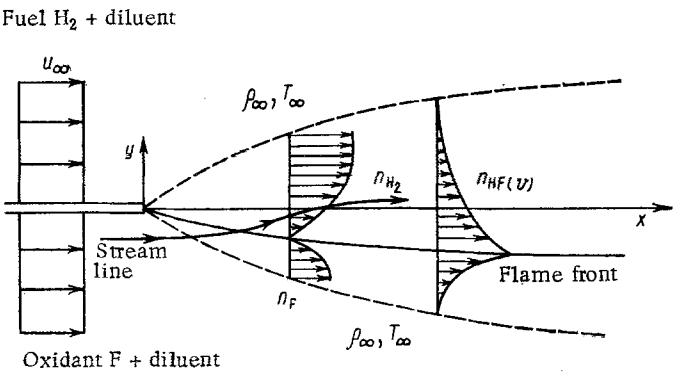

Fig. 3.2. Flow diagram in a diffusion chemical laser.

Such a configuration is an idealization of the stream in the chemical-laser channel and is analogous to boundary-layer flow with velocity components u along the x axis and v along y.

According to boundary-layer theory, it follows from the system (3.10)-(3.14) that [14]

$$\frac{\partial}{\partial x}(\rho u)+\frac{\partial}{\partial y}(\rho v)=0; \tag{3.38}$$

$$\rho\left(u\frac{\partial u}{\partial x}+v\frac{\partial u}{\partial y}\right)=\frac{\partial}{\partial y}\left(\eta\frac{\partial u}{\partial y}\right); \tag{3.39}$$

$$\rho\left(u\frac{\partial h_0}{\partial x}+v\frac{\partial h_0}{\partial y}\right)=\frac{\partial}{\partial y}\left[\frac{\eta}{\mathrm{Pr}}\left(\frac{\partial h_0}{\partial y}+(\mathrm{Pr}-1)\,u\frac{\partial u}{\partial y}\right)\right]-\sum_{v,J}\sum\alpha_{v,J}I_{v,J}; \tag{3.40}$$

$$\rho\left(u\frac{\partial Y_i}{\partial x}+v\frac{\partial Y_i}{\partial y}\right)=\frac{\partial}{\partial y}\left(\rho D_{ij}\frac{\partial Y_i}{\partial y}\right)+w_i+\frac{\mu_{\mathrm{HF}}}{hN_A}\delta_{i,v}\sum_J\left(\frac{\alpha_{v,J}I_{v,J}}{\nu_{v,J}}-\frac{\alpha^{v,J}I^{v,J}}{\nu^{v,J}}\right); \tag{3.41}$$

$$\frac{\partial I_{v,J}}{\partial y}=\alpha_{v,J}I_{v,J}, \tag{3.42}$$

where $\mathrm{Pr}=\eta c_p/\lambda_Q$; η is the viscosity coefficient; $c_p=\Sigma c_{p,i}Y_i$;

$$p=\rho RT\Sigma(Y_i/\mu_i);\quad h_0=h_e+1/2u^2;$$

$$h_e=\sum_i Y_i\left(\int_0^T c_{p,i}\,dT+h_{f,i}\right).$$

The superscript v, J denotes transitions of the $\mathcal{P}$-branch from the level v, J to the level v − 1, J + 1, and the subscript denotes transitions from the level v + 1, J − 1 to the level v, J.

The last term in the right-hand side of (3.40) is the energy loss per unit volume due to stimulated emission and absorption. The last term in the right-hand side of (3.41) describes the onset of the i-th component in a unit volume as a result of stimulated emission and absorption. It is equal to zero for all $i \neq v$. The term w_i describes the onset of the i-th component as a result of the chemical reaction. The optical gain $\alpha_{v,J}$ corresponds to its value at the line center and is given by

$$\alpha_{v,J}=A\,(Y_{v+1}-\varkappa Y_v), \tag{3.43}$$

where

$$A=\frac{8\pi^{5/2}N_A}{3(2k\mu_{\mathrm{HF}})^{1/2}}\,\frac{|H_v^{v+1}|^2JF_{v,J}\rho}{R_J(v+1,\,J-1)\,T^{1/2}}\exp[-E(v+1,\,J-1)/k^0T];$$

$$R_J(v,J)=\sum_{J=0}^{\infty}(2J+1)\exp[-E(v,\,J)/k^0T];$$

$$\varkappa = \frac{R_J(v+1,\ J-1)}{R_J(v,\ J)} \exp\{-[E(v,\ J)-E(v+1,\ J-1)]/k^0 T\}.$$

Here Y_V is the mass fraction of the excited molecules; N_A, Avogadro's number; and R_J, internal energy for the rotational degrees of freedom. The term $|H_V^{V+1}|^2$ takes into account the contribution of the vibrational degrees of freedom to the electric dipole moment, and $F_{V,J}$ is a parameter of the interaction of the vibrational and rotational degrees of freedom.

The enhancement of the radiation in a premixed moving gas flow in the cw regime is described by the system of equations [4]

$$\partial I_\nu/\partial x = \alpha I_\nu;\ v\partial\alpha/\partial y = -\sigma\alpha I_\nu + K(x,\ y), \tag{3.44}$$

where v is the gas-flow velocity along the y axis.

The cross section y = 0 is the boundary of the reference signal propagating along the x axis. The boundary conditions are written in the form

$$I_\nu(0,\ y) = I_{\nu,0} = \begin{cases} 0, & 0 \leqslant y \leqslant y_0, \\ I_{\nu,0}(y), & y > y_0; \end{cases} \tag{3.45}$$

$$\alpha(x,\ y_0) = \tilde{\alpha}(x,\ 0) + \frac{1}{v}\int_0^{y_0} K(x,\ y')\,dy'. \tag{3.45a}$$

In terms of the variables $\zeta = x$, $\vartheta = y/v$ the system of equations and the boundary conditions are:

$$\left.\begin{aligned} &\partial I_\nu/\partial\zeta = \alpha I_\nu; \\ &\partial\alpha/\partial\vartheta = -\sigma\alpha I_\nu + K(\zeta,\ \vartheta); \\ &\zeta = 0;\ I_\nu = I_{\nu,0}(\vartheta) = \begin{cases} 0, & 0 < \vartheta < \vartheta_0 = y_0/u; \\ I_{\nu,0}(\vartheta), & \vartheta > \vartheta_0; \end{cases} \\ &\vartheta = \vartheta_0;\quad \alpha = \tilde{\alpha}(\zeta) = \alpha(\zeta,\ 0) + \int_0^{\vartheta_0} K(\zeta,\ \vartheta')\,d\vartheta'. \end{aligned}\right\} \tag{3.46}$$

The solution of this problem is:

$$I_\nu(\zeta,\ \vartheta) = I_{\nu,0}\frac{1}{z}\exp\left[\int_{\vartheta_0}^{\vartheta}\left(\sigma I_{\nu,0} + \int_0^{\zeta} K\,d\zeta'\right)d\vartheta'\right]; \tag{3.47}$$

$$\left.\begin{aligned} \alpha(\zeta,\ \vartheta) = &\int_{\vartheta_0}^{\vartheta} K\,d\vartheta' - \frac{1}{z}\left\{\int_{\vartheta_0}^{\vartheta}\sigma I_{\nu,0}\times\right. \\ \times\exp&\left[\int_{\vartheta_0}^{\vartheta'}\left(\sigma I_{\nu,0} + \int_0^{\zeta} K\,d\zeta'\right)d\vartheta''\right]\left(\int_{\vartheta_0}^{\vartheta'} K\,d\vartheta''\right)d\vartheta' - \\ &\left.-\tilde{\alpha}\exp\left(-\int_0^{\zeta}\tilde{\alpha}\,d\zeta'\right)\right\}; \\ z = &\int_{\vartheta_0}^{\vartheta}\sigma I_{\nu,0}\exp\left[\int_{\vartheta_0}^{\vartheta'}\left(\sigma I_{\nu,0} + \int_0^{\zeta} K\,d\zeta'\right)d\vartheta''\right]d\vartheta' + \\ &+\exp\left(-\int_0^{\zeta}\tilde{\alpha}\,d\zeta'\right). \end{aligned}\right\} \tag{3.48}$$

In the case of a homogeneous reference signal ($I_{\nu,0}$ = const) and a pump that depends only on the coordinate ϑ, relations (3.47) and (3.48) are greatly simplified. For enhancement of a narrow signal we have

$$I_{\nu,0}=\begin{cases} I_{\nu,0}=\text{const}, & \vartheta_0<\vartheta<\vartheta_1, \\ 0, & \vartheta>\vartheta_1. \end{cases} \tag{3.49}$$

For the condition

$$\vartheta_1-\vartheta_0 \ll \frac{2K(\vartheta_0)}{(\partial K/\partial\vartheta)|_{\vartheta=\vartheta_0}}=\tilde{\vartheta}$$

it can be assumed that K ≈ const in the absence of radiation, and then

$$\frac{I_\nu}{I_{\nu,0}}=\left[\frac{1}{\bar{G}_c}+\left(\frac{1}{\bar{G}}-\frac{1}{\bar{G}_c}\right)\exp\left(-\frac{\vartheta-\vartheta_0}{\vartheta_y}\right)\right]^{-1}, \tag{3.50}$$

$$\alpha=\alpha_c\frac{\vartheta-\vartheta_0}{\vartheta_y}+\frac{\tilde{\alpha}-\alpha_c\dfrac{\bar{G}}{\bar{G}_c}\left[1+\exp\left(\dfrac{\vartheta-\vartheta_0}{\vartheta_y}\right)\left(\dfrac{\vartheta-\vartheta_0}{\vartheta_y}-1\right)\right]}{1+\dfrac{\bar{G}}{\bar{G}_c}\left(\exp\left(\dfrac{\vartheta-\vartheta_0}{\vartheta_y}\right)-1\right)}, \tag{3.51}$$

where

$$\left.\begin{aligned} &\bar{G}=\exp(\tilde{\zeta}\tilde{\alpha});\ \bar{G}_c=1+K\zeta/(\sigma I_{\nu,0});\ \tilde{\alpha}=\alpha(0)+K\vartheta_0; \\ &\alpha_c=K/(\sigma I_{\nu,0}+K\zeta);\ \vartheta_y=(\sigma I_{\nu,0}+K\zeta)^{-1}. \end{aligned}\right\} \tag{3.52}$$

It follows from the solution that when the amplifier length is increased, the output radiation pulse becomes "sharper".

We present here, using (1.104), the general form of the vibrational-relaxation equation:

$$\frac{dn_{m,i}}{dt}=\sum_{s,p,q,j}k^{ij}_{s\to m,\ p\to q}n_{s,i}n_{p,j}-\Sigma k^{ij}_{m\to s,\ q\to p}n_{m,i}n_{q,j}, \tag{3.53}$$

where $n_{m,i}$ is the concentration of the molecules of sort i on the level m; $k^{ij}_{s\to m;\ p\to q}$ is the rate constant of the transition of molecule i from level s to level m and of molecule j from level p to level q. For a polyatomic molecule each of the indices s, m, p, and q is described by a set of vibrational quantum numbers $(v_1, v_2, \ldots, v_n)$.

A direct solution of the system (3.53) is practically impossible without simplifving assumptions. The most significant of these assumptions are the following: the influence of the electronic excitation is negligibly small; the translational and rotational degrees of freedom are in equilibrium; only transition between nearest levels are taken into account; the simplest model, that of a harmonic oscillator, is used.

Naturally, the solutions obtained using these simplifications are not universal and are applicable in certain regions. In particular, e.g., the use of the harmonic-oscillator model is valid at sufficiently small deviations from equilibrium and for low vibrational levels.

3.6. Laser Kinetics under Conditions of Cooperative Spontaneous Emission

Coherence in Spontaneous Emission. Spontaneous emission is usually considered under the assumption that all the gas molecules are independent. In this case the radiation intensity is equal to the sum of the emission intensities of the individual molecules, and the line width and shape of the gas emission are determined by the properties of the isolated molecule. This is valid only when the distance between individual molecules is much larger than the radiated wavelength.

At high pressures, however, many radiating particles are located at distances comparable with the radiation wavelength, and they emit as a single quantum-mechanical system, with a spontaneous-emission intensity proportional to the square of the number of these particles [1]. It must be emphasized that the collective properties of the system of particles exert a direct influence only on the spontaneous and nonradiative processes in the system. With respect to stimulated transitions, the system atoms behave as if they were independent. The reason is that collective effects cancel out in absorption or stimulated emission, whereas for spontaneous and nonradiative processes there is no such cancellation.

Collective interaction of the emitting particles substantially alters the characteristics of chemical lasers operating at high mixture pressures. The condition for the onset of coherent emission from the entire volume of the emitting particles in such a synchronization is not a difference of the level-population concentration, but a difference of the absolute concentration of the emitters (chemical complexes, excited products of chemical reactions, etc.). Superradiance is described in [1] for a system smaller in size than the radiation wavelength. It is assumed for simplicity that the gas molecules have only two nondegenerate energy levels, E_2 and E_1 ($E_2 > E_1$). The molecule radiation is considered in the dipole approximation. The Hamiltonian of the system of molecules, without allowance for the radiation field, is written in the form

$$H = H_0 + E \sum_{j=1}^{n} R_{j3}, \tag{3.54}$$

where $E = h\nu_e = E_2 - E_1$; H_0 and R_{j3} represent, respectively, the energy of the translational motion of the molecules in the intermolecular interaction and the internal energy of the j-th molecule with eigenvalues $\pm^1/_2 E$.

The eigenfunctions are of the form

$$\psi_{gm} = U_g(\bar{r}_k)[R_k], \tag{3.55}$$

where $\bar{r}_k$ are the mass-center coordinates.

If the numbers of molecules in the upper and lower states are designated n_2 and n_1, respectively, then

$$m = (n_2 - n_1)/2. \tag{3.56}$$

Obviously, $n = n_+ + n_-$ is the total number of molecules. The total gas energy is

$$E_{gm} = E_g + E_m, \tag{3.57}$$

where E_g is the energy of the translation motion and of the interaction of the molecules.

The energy E_{gm} has degenerate multiplicities

$$\frac{n!}{n_+!\,n_-!} = \frac{n!}{(n/2+m)!\,(n/2-m)!}. \tag{3.58}$$

We introduce a quantum number r, called the cooperation number of the gas, which satisfies the inequality

$$|m| \leqslant r \leqslant n/2. \tag{3.59}$$

As a result we obtain for the intensity of the spontaneous emission of a gas in the state (r, m) the expression

$$I = (r + m)(r - m + 1) I_0, \tag{3.60}$$

where I_0 is the intensity of the spontaneous emission of the isolated molecule.

The gas can thus have special bound states in which the spontaneous-emission intensity is proportional to the square of the number of molecules. Such, e.g., is the state $r = n/2$, $m = 0$. The emission intensity of a gas in such a state is

$$I = (n/2)(n/2 + 1) I_0 \cong n^2 I_0/4. \tag{3.61}$$

The gas can have states that do not emit energy at all, e.g., $r = m = 0$.

It must be noted that in all system transitions accompanied by emission, the quantum cooperation number r remains unchanged.

In the general case when the state of the gas is a superposition of states with different r and m, or for a mixture with different r and m states, the intensity is

$$I = I_0 \sum_{r,n} P_{r,m}(r+m)(r-m+1), \tag{3.62}$$

where $P_{r,m}$ is the probability that the system is in the state (r, m) at the instant of emission.

In the thermal-equilibrium state, when

$$n_2/n_1 = \exp(-E/k^0T), \tag{3.63}$$

the mean value is

$$\bar{m} = (n_2 - n_1)/2 = [n \operatorname{th}(E/k^0T)]/2 \cong -nE/(4k^0T). \tag{3.64}$$

The superior bar denotes here averaging over an ensemble with a Boltzmann distribution. The mean value of r coincides with $|\bar{m}|$.

If r coincides exactly with (-m), the emission intensity is zero. If, however, r differs from (-m) by unity, then

$$I = -2mI_0 = (E/2kT)\, nI_0. \tag{3.65}$$

While the spontaneous-emission intensity depends on the state (r, m) of the gas, the total emission or absorption intensity in the presence of an an external field is always proportional to the number of active molecules.

If the system dimensions are comparable and are much larger than the wavelength, but the distances between individual molecules are much shorter than or comparable with the wavelength, coherent emission is possible, but the gas can emit coherently only in one direction.

A classical system of simple harmonic oscillators distributed over a large region can be relatively phased in such a way that coherent emission in a definite direction is obtained.

Effect of Collective Phenomena on a Radiative Chemical Reaction. Among the chemical reactions, particular interest for laser development attaches, from the viewpoint of significant increase of the radiation intensity when the emitters are phase-correlated, to the reactions whose rates depend on the presence of electromagnetic radiation. These reactions include, e.g., photorecombination, where a mechanism is possible for the enhancement of the light-stimulated rate of the chemical reaction [16]. In such reactions the phototransition takes place during the elementary chemical reaction itself. In this radiative reaction mechanism the energy of the chemical bond is emitted by the phototransition, whereas in an ordinary chemical reaction the energy is given to a third molecule or is carried away by the chemical-reaction products. If conditions are produced for the realization of the mechanism of phase correlation of the spontaneously emitting particles, when the collective interaction of the particles via the common electromagnetic field strongly decreases the emission time of the excited particles, it becomes possible to substantially accelerate the photostimulated chemical reaction [17]. If the rate of formation of the energetically excited particles exceeds the rate of their deactivation by superradiance, a growing process results.

The inverse process contains a number of pulses of damped amplitude and increasing duration. In this case the cooperative phenomena in the spontaneous emission lead, naturally, to a considerable increase of the lasing power in the individual pulses. In stationary lasing, when the rate of the process is determined by the rate of excited-particle formation, the contribution of the cooperative phenomena can, in principle, be of the same order as that of other deactivation and emission processes. Nevertheless, the need for creating conditions for the onset of cooperative effects is compensated by a number of obvious advantages of the reaction. For example, it is possible to use for chemical lasers a larger class of reactions, since the working molecules that produce the coherent emission are not only the products of a reaction with inverted population, but also directly excited particles. In addition, when the emitters are phase-correlated the threshold of the required equilibrium density of the excited reaction products (n*) will be less than the threshold of the concentration of the inversely populated particles (n^*_{ind}) in the mechanism of a chemical reaction stimulated by induced phototransitions.

In fact, the rate of a chemical reaction with phase correlation can be represented in the form

$$w_\varphi \approx w_{sp}\,(V/4)\, n^*_\varphi, \tag{3.66}$$

where $w_{sp} = Pn^*_\varphi$ is the rate of the spontaneous emission of n^*_φ independently emitting parti-

cles; P, probability of spontaneous emission of the excited reaction products; and V, phase-correlation volume.

$$w = w_{\varphi} = w_{\text{ind}} = k_1 n^2, \tag{3.67}$$

where k_1 is the rate constant of formation of the excited reaction products; n is the concentration of the initial reagents.

For w_{ind} we have [16]

$$w_{\text{ind}} \approx 10^{-12} P (n^*_{\text{ind}})^2. \tag{3.68}$$

Hence

$$n^*_{\varphi}/n^*_{\text{ind}} = \sqrt{4b^2/pV\, k(T_0)}, \tag{3.69}$$

where $b = P\pi^2 c^3/\omega_m^2 \Delta\omega_m$, and ω_m, $\Delta\omega_m$ are the cylic frequency and the effective bandwidth of the spontaneous emission at the maximum of the emission intensity. Substituting $P = 10^6$ sec^{-1}, $b = 10^{-6}$ cm^3/sec, $k(T_0) = 2 \cdot 10^{-15}$ cm^3/sec, $V = 1$ cm^3, we obtain $n^*_{\varphi}/n^*_{\text{ind}} \sim 0.05$.

Thus, the use of a photostimulated chemical reaction with phase correlation of the reaction products that are in an excited (not necessarily inverted-population) state makes it possible to use a larger range of initial reagents. The reaction is realized by choosing the concentration of the initial reagents and the mixture temperature (T_0) such that the following inequality is satisfied for the two components:

$$\sqrt{(V/4)(k(T_0)/P)\, n_1 n_2} > 1. \tag{3.70}$$

3.7. Optical Cavity

The cavity is one of the principal parts of any laser and shapes the directivity pattern of the radiation. A cavity made up of two plane-parallel mirrors [18] made it possible to obtain, for the first time ever, coherent radiation in the optical band. Extensive use is made of cavities based on interferometers with spherical, parabolic, and other surfaces. The modes in such cavities are characterized by small apertures [19]. Unstable cavities solve to some degree the problem of greatly filling the active medium with the radiation [20], but in their case the ratio of the aperture to the cavity length does not make compact lasers possible. Owing to the development of a theory of open cavities by using the concepts of the theory of nonlinear systems, cavities with periodic modes were developed [21]. Various types of cavities and their theory are given, e.g., in [22], and their features when used in chemical lasers are described in detail in [23]. We consider, as an example of a periodic-mode cavity, a system with mirrors whose surfaces of curvature have radii R_1 and R_2. The space-frequency characteristic of such a system is of the form

$$H_0(\xi) = [1 - H_1(\xi)]^{-1}, \tag{3.71}$$

where ξ is a variable describing the excitation of the electromagnetic field in the cavity; $H_1(\xi)$ is the space-frequency characteristic corresponding to one pass of the electromagnetic excitation in the cavity. $H_1(\xi)$ can be expressed in terms of the space-frequency characteristics H_{11} and H_{12} of the first and second mirror, respectively, in the form

$$H_1(\xi) = H_{11}(\xi)\, H_{12}(\xi); \tag{3.72}$$

$$H_{11}(\xi, x) = \exp i\left[\frac{-\xi^2}{4(2\alpha - \beta_1)}\right] \exp(-i\beta_1 x^2); \tag{3.73}$$

$$H_{12}(\xi, x) = \exp i\left[\frac{-\xi^2}{4(2\alpha - \beta_2)}\right] \exp(-i\beta_2 x^2), \tag{3.74}$$

where $\alpha = k/2L$; $\beta_1 = k/2f_1$; $\beta_2 = k/2f_2$; f_1 and f_2 are, respectively, the focal lengths of the first and second mirrors; L, distance between mirrors; and $k = 2\pi/\lambda$, wave number.

The inverse Fourier transform of the space-frequency characteristic $H_1(\xi, x)$ as a linear system with feedback, obtained from Eqs. (3.71)-(3.74), yields the pulsed response of the system or the Green's function of the given problem:

$$h_0(x) = \frac{1}{2\pi}\int_{-\infty}^{\infty} H_0(\xi, x)\exp(i\xi x)\,d\xi, \tag{3.75}$$

expressed by means of the sum of the eigenfunctions or modes of the optical cavity.

The residues of the integrand $H_0(\xi, x)$ exp (i ξ x) yield eigenfunctions of the form

$$\exp(i\,\xi_m x), \tag{3.76}$$

where the values of ξ_m are determined from the relation

$$\left|\left(\frac{1}{4(2\alpha-\beta_1)}+\frac{1}{4(2\alpha-\beta_2)}\right)\xi_m^2+(\beta_1+\beta_2)x^2\right| = 2\pi m,\ m=0,1,2,\ldots. \tag{3.77}$$

It follows therefore that

$$\xi_m = \sqrt{-\frac{4(\beta_1+\beta_2)(2\alpha-\beta_1)(2\alpha-\beta_2)}{4\alpha-(\beta_1+\beta_2)}x^2+2\pi m\frac{2(2\alpha-\beta_1)(2\alpha-\beta_2)}{4\alpha-(\beta_1+\beta_2)}}. \tag{3.78}$$

This formula gives the field distribution on the cavity mirror for arbitrary distances and curvature radii of the mirrors, and is the most general formula. For cavities with identical mirrors $R_1 = R_2 = R$ and m = 0, we have

$$\xi_0 = i2\alpha x\sqrt{2\bar{l}-\bar{l}^2} = i\frac{2\pi}{\lambda L}\sqrt{2\bar{l}-\bar{l}^2}\,x,$$

(here $\bar{l} = \beta/\alpha = L/R$), whence

$$\psi_0(x) = \exp(i\xi_0 x) = \exp\left(-\frac{2\pi}{\lambda L}\sqrt{2\bar{l}-\bar{l}^2}\,x^2\right). \tag{3.79}$$

Owing to the linearity of the entire system and to the differentiation operation, the n-th derivative of the function (3.79) is the solution and the eigenfunction of the cavity equation. The following relation holds for Hermite polynomials $H_n(x)$:

$$(-1)^n\frac{d^n}{dx^n}\exp(-x^2/2) = \exp(-x^2/2)\,H_n(x). \tag{3.80}$$

Differentiating (3.79) n times we obtain an expression for the n-th eigenfunction

$$\psi_n(x) = H_n(\sqrt{2}\,x/r)\exp(-x^2/r^2) \tag{3.81}$$

(r is the mirror radius).

In the case of infinite plane-parallel mirrors, the cavity can be regarded as a spatially invariant system with a general space-frequency characteristic

$$H_0(\xi) = [1 - \exp i\,(-L\xi^2/k)]^{-1}. \tag{3.82}$$

The pulsed response of such a system has first-order poles at the points

$$\xi_m = \pm\sqrt{2\pi m L/k} \tag{3.83}$$

and a second-order pole at the point $\xi = 0$. The residue at the point $\xi = 0$ is zero. The residue at the point $\xi = \xi_m$ equals k $(2L\xi_m)^{-1}$ exp (i ξ_m x). Consequently, the pulsed response of the cavity takes the form of the sum

$$h_0(x) = \sum_m \frac{\cos\xi_m x}{L\xi_m/k}, \tag{3.84}$$

each term of which is an eigenfunction and constitutes a periodic distribution, dependent on the cavity length, of the field at the mirror. From this analysis follow the condition

$$L_N = Nx_0^2/\lambda \tag{3.85}$$

for optimal mode locking for a cavity with plane-parallel mirrors, one of which has a periodic structure, e.g., in the form of alternating reflecting and transparent strips of equal width $x_0/2$ or openings. For the general case with mirror curvature radii R_1 and R_2

$$[\lambda L - \lambda L^2 (1/R_1 + 1/R_2)] = Nx_0^2, \; N = 1,2,... \qquad (3.86)$$

Periodic modes ensure complete filling of the working medium and make it possible to produce cavities with the aperture and length ratios required by the design. Experimental investigations with a grating in the cavity [24] have shown that at a cavity length different from L_N (3.85) alternating-sign fields are excited, and at length L_N the fields excited are in phase with a large energy contribution in the central lobe of the directivity pattern.

LITERATURE CITED

1. R. H. Dicke, "Coherence in spontaneous radiation processes," Phys. Rev., 93, No. 1, 99-111 (1954); "Swept-gain superradiance theory draws wide acclaim," Army Res. Dev. and Acquis. Mag., 19, No. 5, 28 (1978).
2. A. S. Bashkin et al., "Chemical lasers," in: Science and Engineering Summaries: Radio Engineering [in Russian], Vol. 8, VINITI, Moscow (1975).
3. K. L. Kompa, Chemical Lasers, Springer-Verlag (1973), p. 92.
4. V. P. Pimenov and V. A. Shcheglov, "Amplification of monochromatic radiation under conditions of nonstationary and spatially inhomogeneous excitation of a gas medium," Kvantovaya Elektron. (Moscow), 3, No. 5, 1041-1050 (1976).
5. N. G. Basov et al., "Dynamics of chemical lasers," Kvantovaya Elektron. (Moscow), No. 2, 3-24 (1971).
6. G. G. Petrash, "Pulsed gas-discharge lasers," Usp. Fiz. Nauk, 105, No. 4, 645-676 (1971).
7. M. S. Dzhidzhoev, V. T. Platonenko, and R. V. Khokhlov, "Chemical lasers," Usp. Fiz. Nauk, 100, No. 4, 642-679 (1970).
8. A. N. Oraevskii, "Chemical lasers based on branched reactions," Zh. Eksp. Teor. Fiz., 55, No. 4(10), 1423-1429 (1968); V. I. Igoshin and A. N. Oraevskii, "Kinetic phenomena in thermal ignition with inverse excitation of the products," Zh. Eksp. Teor. Fiz., 59, No. 10, 1240-1250 (1970).
9. N. N. Semenov and A. E. Shilov, "Role of excited particles in branched chain reactions," Kinet. Katal., 6, No. 1, 3-6 (1965).
10. G. A. Kapralova, T. M. Trofimova, and A. E. Shilov, "Upper limit of ignition in the reaction of fluorine with hydrogen," Kinet. Katal., 6, No. 6, 977-983 (1965).
11. G. A. Kapralova, T. M. Trofimova, L. Yu. Rusin, et al., "Experimental proofs of branching in chain reactions of molecular fluorine," Kinet. Katal., 4, No. 4, 653-654 (1963).
12. N. G. Basov, L. V. Kulakov, E. P. Markin, et al., "Emission spectrum of $H_2 + F_2$ chemical laser," Pis'ma Zh. Eksp. Teor. Fiz., 9, No. 11, 613-617 (1969).
13. O. M. Batovskii et al., "Chemical laser on branched chain reaction of fluorine with hydrogen," Pis'ma Zh. Eksp. Teor. Fiz., 9, No. 6, 341-343 (1969).
14. R. Hofland and H. Mirels, "Flame-sheet analysis of CW diffusion type chemical laser. I. v_n coupled radiation," AIAA J., 10, No. 4, 420-428 (1972); W. S. King and H. Mirels, "Numerical study of a diffusion-type chemical laser," AIAA J., 10, No. 12, 1647-1654 (1972).
15. F. A. Williams, Combustion Theory: The Fundamental Theory of Chemically Reacting Flow Systems, Addison-Wesley (1965), p. 447.
16. S. I. Pekar, "High-pressure chemical lasers and optically stimulated chemical reactions," Dokl. Akad. Nauk SSSR, 187, No. 3, 555-557 (1969).
17. V. K. Ablekov, Yu. N. Babaev, and V. V. Proshkin, "Optically stimulated chemical reactions in the phase-correlation regime," Dokl. Akad. Nauk SSSR, 246, No. 4, 899 (1979).
18. A. M. Prokhorov, "Submillimeter-wave molecular amplifier and generator," Zh. Eksp. Teor. Fiz., 34, No. 6, 1658-1659 (1958); A. L. Schawlow and C. H. Townes, "Infrared and optical masers," Phys. Rev., 112, No. 6, 1940-1949 (1958).
19. A. L. Mikaélyan, Yu. G. Turkov, and V. G. Savel'ev, "High-energy ruby laser with diffractive divergence," Pis'ma Zh. Eksp. Teor. Fiz., 6, No. 6, 675-677 (1967).
20. Yu. A. Anan'ev, N. A. Sventsitskaya, and V. E. Sherstobitov, "Properties of a laser with an unstable cavity," Zh. Eksp. Teor. Fiz., 55, No. 1(7), 130-140 (1968).
21. V. K. Ablekov and V. S. Belyaev, "System approach to the optical-cavity problem," Zh. Prikl. Spektrosk., 23, No. 6, 1110-1112 (1975); "Optical cavity as a linear system," in: System Research [in Russian], No. 2, Izd. DVNTs (Far-East Sci. Center) AN SSSR (1973), Vladivostok, pp. 32-54; V. K. Ablekov, P. I. Zubkov, and A. V. Frolov, Optical and Optoelectronic Information Processing [in Russian], Mashinostroenie, Moscow (1976); V. K. Ablekov, V. S. Belyaev, V. M. Marchenko, et al., "Diffraction properties of per-

iodic modes of optical cavities," Dokl. Akad. Nauk SSSR, 230, No. 5, 1066-1068 (1976); V. K. Ablekov, V. S. Belyaev, V. P. Vasil'ev, et al., "Periodic modes of optical cavity, Zh. Prikl. Spektrosk., 28, No. 1, 57-59 (1978); V. K. Ablekov, V. I. Vinogradov, V. G. Marchenko, et al.,"Radiation field of neodymium laser with grating mirror," Opt. Spektrosk., 44, No. 6, 1208-1210 (1978).

22. A. Maitland and M. H. Dunn, Laser Physics, Elsevier (1970); Yu. A. Anan'ev, Optical Cavity and the Problem of Laser Beam Divergence [in Russian], Nauka, Moscow (1979).
23. R. A. Chodzko and A. N. Chester, "Optical aspects of chemical lasers," in: Handbook of Chemical Lasers, Wiley—Interscience, New York (1976), pp. 95-201.
24. V. K. Ablekov and V. G. Marchenko, "Angular spectrum of the emission of a laser with a grating in the cavity, and distribution of the fields of the periodic modes on the grating," Zh. Prikl. Spektrosk., 29, No. 4, 607-613 (1978).

CHAPTER 4

STATIC GAS CHEMICAL LASERS

4.1. Photochemical Static Gas Lasers

Chemical lasers with a working medium in a constant volume, in other words static-gas lasers, have the simplest construction. Their basic elements are systems for preparation of the working mixture and for the extraction and removal of the generated radiation. Such lasers are pulsed — they generate coherent emission of energy in a short time interval: $h\nu = f(t)$. A mixture of the initial gases is fed into the working volume (reactor) from a separate vessel. An external source then initiates a chemical reaction practically simultaneously over the entire working volume. Part of the energy of the excited reaction products is extracted through windows in the reactor in the form of radiation generated in a system (cavity) for selective extraction and removal of this energy. The spent gas mixture is then taken out of the reactor and the system is returned to the initial state by filling the reactor with a fresh working mixture.

Photodissociation Static Gas Chemical Lasers. Operating Principle and Principal Characteristics. This type includes the iodine chemical laser, the processes in which are shown in Fig. 4.1. It is optically pumped at a wavelength 0.28 μm [1]. The following reactions that take place in the pumping-pulse stage prior to the start of the pyrolysis are worthy of attention:

$$\left.\begin{array}{ll}
1)\ I^* + CF_3 \xrightarrow{k_1} CF_3I; & 7)\ I_2 + \widetilde{CF_3} \xrightarrow{k_7} CF_3I + I;\\
2)\ I^* + CF_3I \xrightarrow{k_2} I + CF_3; & 8)\ I_2 + h\nu \xrightarrow{k_8} 2I;\\
3)\ I + CF_3 \xrightarrow{k_3} CF_3I; & 9)\ \widetilde{CF_3} + CF_3I \xrightarrow{k_9} C_2F_6 + I^*;\\
4)\ 2I + CF_3I \xrightarrow{k_4} I_2 + CF_3I; & 10)\ CF_3 + CF_3I \xrightarrow{k_{10}} C_2F_6 + I^*;\\
5)\ 2CF_3 \xrightarrow{k_5} C_2F_6; & 11)\ CF_3 + CF_3I \xrightarrow{k_{11}} C_2F_6 + I;\\
6)\ I^* + I_2 \xrightarrow{k_6} I + I_2; & 12)\ \widetilde{CF_3} + CF_3I \xrightarrow{k_{12}} CF_3 + CF_3I.
\end{array}\right\} \quad (4.1)$$

Here I* is the iodine atom in the 5 $^2P_{1/2}$ state, $\widetilde{CF_3}$ is the "hot" radical. The transition $^2P_{1/2} \rightarrow {}^2P_{3/2}$ (λ = 1.315 μm) ensures generation of stimulated emission up to the kilowatt range, with duration of several microseconds. Photodissociation static gas iodine chemical lasers were constructed with an energy of several dozen joules [2] and lasing duration of several nanoseconds [3] at approxiately 0.5% efficiency. The lasing energy E was raised in [4] to 1000 J at an efficiency 1.4%. The efficiency of a photodissociation static gas chemical laser is increased by broadening the absorption spectrum of the working substances, as well as by using various chemical reactions that accompany the photolysis [5, 6]. The working substancesused in photodissociation static gas iodine chemical lasers contain the atom bond C-I in molecules of the type RI, where R= CF_3, C_2F_5, C_3F_7,..., etc. The use of other promising working substances for such a chemical laser is restricted by the requirement that this substance have the sufficiently high vapor tension needed to obtain high concentrations of the excited molecules in the gas phase, and hence large values of the specific energy delivery ε_V from a unit volume of the working chamber.

The excitation of chemical lasers in the course of photodissociation was investigated in [7]. Studies were made of the photodissociation of a large number of compounds containing an iodine atom bound to an element of group V, namely P, As, Sb, and N. It was experimentally demonstrated that about 66% of the stored energy can be released in the form of radiation. The stimulated-emission cross section is regulated by adding to the working medium a buffer gas. A typical schematic diagram of an experimental photodissociation static gas iodine chemical laser is shown in Fig. 4.2 [5].

The working tube, 1 m long with inside diameter 10 mm, is equipped with quartz Brewster windows. The cavity consists of two spherical confocal gold-coated mirrors. Pumping is with a straight xenon flash lamp with average pulse growth time 20 μsec and duration 150 μsec. The

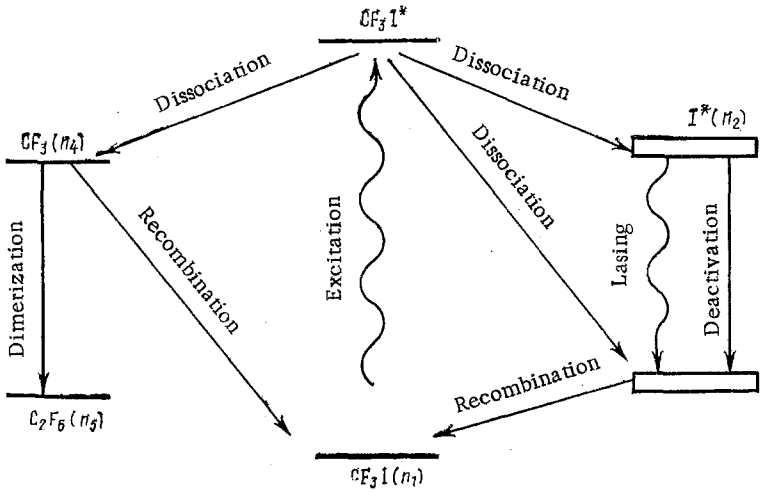

Fig. 4.1. Scheme of processes in an iodine photochemical laser.

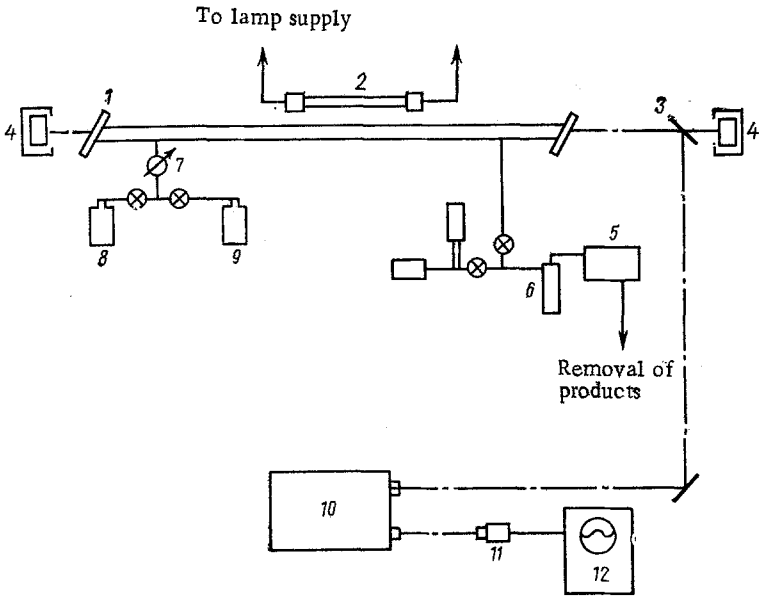

Fig. 4.2. Schematic diagram of photodissociation static gas iodine chemical lasers: 1) Brewster window; 2) flash lamp; 3) beam-splitting plate; 4) mirror; 5) vacuum pump; 6) cooled trap; 7) manometer; 8) cylinder with inert gas; 9) cylinder with working gas; 10) spectrometer; 11) infrared detector; 12) oscilloscope.

flash lamp and the working tube are located at the conjugate foci of a polished elliptic reflector.

The flash lamp was fed from an 18-μF capacitor charged to 15 kV with energy up to 1760 J. The minimum energy applied to the system was 225 J. Premature discharging was prevented by adjusting the discharge gap. Two 30-kV triggering blocks simultaneously ionized the lamp and the discharge gap, and triggered the oscilloscope sweep.

Up to 4% of the generated beam was deflected with a quartz plate to a spectrometer and to a detector connected with the oscilloscope. The detector was either a germanium diode or an InSb photoresistor. The system was evacuated with a two-stage vacuum pump. A freeze-out trap removed the condensation products. The operation of such a chemical laser depends mainly on the pressure of the reagents and on the energy of the flash lamp. Since only part of the reagent dissociates during one flash, multiple pulsed exposures permit a more effective use of the reagent. The duration of the generated pulse could be increased by adding inert gas.

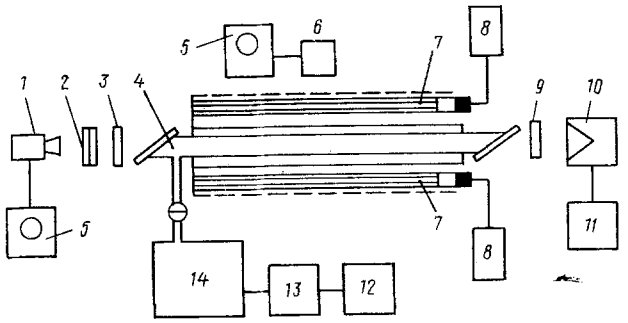

Fig. 4.3. Diagram of experimental setup: 1) photodiode; 2) scatterers and neutral filters; 3) mirror; 4) working chamber of laser; 5) oscilloscope; 6) photomultiplier; 7) IFP-5000 xenon flash lamps; 8) capacitor bank; 9) output mirror; 10) calorimeter; 11) microammeter; 12) forevacuum pump; 13) oil-vapor pump; 14) vacuum receiver.

The customarily employed active media (CF_3I or $n\text{-}C_3F_7I$) must still be changed after each flash pulse, for otherwise the lasing power decreases strongly. Experimental data on the repeated use of one and the same medium $(CF_3)_2AsI$ were obtained in [8]. The experiments were performed with the setup illustrated in Fig. 4.3.

The cavity comprised two flat dielectric mirrors spaced approximately 1 m apart. The transmissivity of the first mirror was 0.2% and of the second 0.6 to 50% at $\lambda = 1.315$ μm. The working chamber was a quartz tube of 10-20 mm outside diameter with its ends covered with glass windows placed at the Brewster angle ($\alpha_B \approx 57°$). A quartz jacket filled with distilled water was placed over the illuminated part of the working chamber ($l_{ef} \approx 25$ cm). The pump light sources were two IFP-5000 lamps fed from separate capacitor banks with C = 47 μF, each at a maximum voltage 7 kV. Both lamps and the working chamber were wrapped on the outside with polished aluminum foil that served as a reflector. To obtain a short pulse ($\tau_{1/2} \approx 3$ μsec) a capacitor with C = 5 μF charged to 25 kV was connected to the lamp through a vacuum discharge gap. The energy E of the generated radiation was measured with a KIM-1 calorimeter. The waveform of the lasing pulse was recorded with an FD9E11 photodiode and with an S1-37 oscilloscope. The pump-lamp radiation was monitored with an FEU-18 photomultiplier equipped with a filter corresponding to the absorption band of the medium. The gas phase of the $(CF_3)_2AsI$ compound has, in the ultraviolet, two absorption regions: longwave ($\sigma_{max} = 3.3 \cdot 10^{-18}$ cm^2 at $\lambda_{max} = 290$ nm) and shortwave ($\sigma_{max} = 10^{-17}$ cm^2 at $\lambda_{max} = 217$ nm). At the same time, substances with C-I bonds (e.g., CF_3I, C_3F_7I) have in the "quartz" ultraviolet region a maximum absorption cross section smaller by a factor of four or five than in the longwave band of $(CF_3)_2AsI$.

To limit the spectral composition of the pump light source, a liquid filter was used, consisting of a 0.003% solution of $NaNO_2$ in distilled water. This filter does not change its properties in the course of time, does not transmit radiation in the shortwave band of $(CF_3)_2$-AsI, and does not block the longwave bands of CF_3I and C_3F_7I.

Investigation of the lasing in the $(CF_3)_2AsI/CF_3I$ and $(CF_3)_2AsI/C_3F_7I$ mixtures shows that at low mixture pressures p the energy E of the generated radiation is determined by the energy characteristics of the mixture components. From the dependence of E on the number of flashes produced without changing the working medium at low pump energies, it was found that for $n\text{-}C_3F_7I$ the value of E is decreased by approximately a factor of four after the first flash, whereas $(CF_3)_2AsI$ withstands more than 50 flashes without a noticeable lowering of E.

Photodissociation of other substances, such as cyanides, have also been tested for use in static gas chemical lasers.

Other Photochemical Static Gas Lasers. The first produced photochemical static gas laser was based on the reaction of chlorine with hydrogen [10]. To rapidly initiate the reaction in the Cl_2/H_2 mixture, a flash lamp that caused partial dissociation of Cl_2 was used. The mechanism of the photochemical chain reaction $H_2 + Cl_2$, which proceeds with the formation of vibrationally excited HCl, can be described as follows:

$$\left.\begin{aligned}
&1)\ Cl_2 + h\nu \xrightarrow{k_i} 2\,Cl \quad \text{(initiation);}\\
&2)\ Cl + H_2 \xrightarrow{k_1} HCl\,(v=0) + H \quad \text{(growth of chain);}\\
&3)\ H + Cl_2 \xrightarrow{k_2^n} HCl^*\,(v=n) + Cl;\\
&4)\ H + HCl^*\,(v=n) \xrightarrow{k_3^n} H_2 + Cl \quad \text{(inhibition);}\\
&5)\ Cl + Cl + M \xrightarrow{k_t} Cl_2 + M \quad \text{(breaking of chain).}
\end{aligned}\right\} \qquad (4.2)$$

To maximize the number of parallel chains in (4.2) the concentration of the chlorine atoms must be high. Consequently, to increase the generated energy E it is necessary to increase the Cl_2 pressure, the energy, and the light-flash power. To prevent the slow link 2) of the chain from limiting the overall growth rate of the chain, a high hydrogen concentration must be ensured.

Another method of increasing the chain growth in reaction 2) is to raise the mixture temperture. These conclusions were confirmed by experiment. For example, it was impossible to obtain lasing on DCl molecules at room temperature in a wide range of the reagent pressure and of the light-flash energies, whereas at increased temperatures lasing on DCl molecules entails no difficulty [11]. Lowering the temperature of a mixture, with partial pressures 2.4 kPa of Cl_2 and 23.3 kPa of D_2, from 510 to 450°K, decreased the lasing intensity by a factor of five.

The sequence of the onset of lasing on various V–R transitions within a single band follows a law common to both H_2/Cl_2 and D_2/Cl_2 chemical lasers: lasing appears first on a transition with a small J, followed by transitions with large J. The apparent reason is the rise of the gas temperature on account of the energy released in the chemical reaction, followed by a change in the gains of the various V–R transitions. In addition, successive lasing on transitions with different J is possible also at constant temperature if the emission changes the ratio of the populations of the different vibrational levels.

The need for raising the mixture temperature and the hydrogen concentration leads in the final analysis to a limitation on the chemical laser, since the rate of relaxation of the excited HCl molecules increases. More profitable from the viewpoint of energy is the reaction described in Sec. 2.2,

$$Cl + HI \rightarrow HCl^*\ (v \leqslant 4) + I\ (-134\ \text{kJ/mole}), \qquad (4.3)$$

in which up to 70% of the chemical reaction goes over into vibrational energy of the HCl molecules, and inversion can be produced between upper vibrational levels [12]. In a chemical laser based on this reaction [13] the gas mixture was drawn through the tube (length 60 cm, inside diameter 14 mm) to decrease the influence of the spontaneous reaction that takes place in the Cl_2/HI mixture at a relatively high velocity. Lasing was observed in the pressure range p = 0.8–5.33 kPa with an emission spectrum on the transitions $\mathcal{P}_{3-2}$ (4)–$\mathcal{P}_{3-2}$ (5), $\mathcal{P}_{2-1}$ (5)–$\mathcal{P}_{2-1}$ (7), $\mathcal{P}_{1-0}$ (9)–$\mathcal{P}_{1-0}$ (13) (i.e., on the processes v = 3 → v = 2 of the $\mathcal{P}$ branch from J = 4 to J = 5, etc.).

It should be noted that operation of a Cl_2/HI chemical laser involves considerable difficulties, the most serious of which is the condensation of iodine on the cold part of the system. Free of this shortcoming is a chemical laser using the mixture Cl_2/HBr [14] in which the reaction

$$Cl + HBr \rightarrow HCl^* + Br\ (-65\ \text{kJ/mole})$$

takes place with a maximum radiation power W = 12 kW and E = 0.12 J, p = 0.87 kPa, and initiating-flash energy E_I = 1350 J. The limitation on the generated-radiation energy is due to the large relaxation rate as a result of the collisions

$$HCl\ (v=1) + HBr\ (v=0) \rightarrow HCl\ (v=0) + HBr\ (v=1) \qquad (4.4)$$

At a working-medium pressure p ≈ 1.33 kPa the relaxation time is of the order of several microseconds. Raising p to several kilopascals with simultaneous increase of the pump power can yield values of W up to 30 kW and E ~ 0.2–0.3 J.

Chemical lasers are also possible using Br atoms produced in the photolytic reaction

$$I^* + Br_2 \rightarrow IBr + Br^*,$$

with lasing on the electronic transition $4^2P_{1/2} \rightarrow 4^2P_{3/2}$ at $\lambda = 2.714$ μm [15].

The high rate of the F + H_2 reaction, the high energy release, and the fact that a considerable fraction of the energy (about 65%) goes over into vibrational energy of the produced molecules [16, 17] makes this reaction attractive for use in static gas chemical lasers. At room temperature, the rate constant of the reaction F + H_2 is $2.5 \cdot 10^{-11}$ cm^3/sec, much larger than the rate constant $1.7 \cdot 10^{-12}$ cm^3/sec of the main pumping reaction in the H_2/Cl_2 laser [18].

Lasing on HF molecules was first obtained by photoinitiation of the mixture UF_6/H_2 [19, 20]. In this case the following reactions are possible:

$$\left.\begin{array}{l} 1)\ UF_6 + h\nu \rightarrow UF_5 + F; \\ 2)\ F + H_2 \rightarrow HF^* + H \quad (-134\ \text{kJ/mole}); \\ 3)\ H + UF_6 \rightarrow HF^* + UF_5 \quad (-192{,}6\ \text{kJ/mole}); \\ 4)\ UF_6 + UF_5 \rightarrow UF_4 + UF_6; \\ 5)\ H + UF_5 \rightarrow HF^* + UF_4. \end{array}\right\} \qquad (4.5)$$

The HF molecules emit on the transitions $\mathcal{P}_{2-1}(3)$-$\mathcal{P}_{2-1}(9)$. When H_2 is replaced by D_2, the DF molecules emit on the transitions $\mathcal{P}_{3-2}(4)$-$\mathcal{P}_{3-2}(9)$ and $\mathcal{P}_{2-1}(3)$-$\mathcal{P}_{2-1}(8)$.

The presence of transitions between high-lying vibrational levels of the HF molecule is typical of the reaction

$$H + F_2 \rightarrow HF^*\ (v \leqslant 9) + H \quad (-410\ \text{kJ/mole}); \qquad (4.6)$$

in which enough energy is released to populate the high vibrational levels. Among the processes that determine the formation of the emission spectrum of photochemical lasers are also:

population of vibrational levels

$$F + H_2 \rightarrow HF^*\ (v \leqslant 3) + H\ (-134\ \text{kJ/mole}); \qquad (4.7)$$

V–V and V–T exchange

$$\left.\begin{array}{l} HF(v) + HF(v) \rightarrow HF(v+1) + HF(v-1); \\ HF + M \rightarrow HF(v-1) + M; \\ (M = HF, H_2, F_2, H, F, He, O_2); \end{array}\right\} \qquad (4.8)$$

stimulated emission

$$HF(v) \rightarrow HF(v-1) + h\nu. \qquad (4.9)$$

As a result of the reaction (4.6), the level with v = 5 ($k_1:k_2:k_3:k_4:k_5:k_6$ = 0.2:0.75:0.6:0.7:1.0:0.95) is populated at a maximum rate. The reaction (4.7) populates most intensivelythe level with v = 2 ($k_1:k_2:k_3$ = 0.29:1.0:0.47) [16]. The dependence of the level populations of the HF molecule on the quantum number v as a result of reactions (4.6) and (4.7) is a smooth curve with two maxima, the principal one at the v = 2 level and the supplementary at v = 5.

The experimental results unequivocally confirm the chain character of this chemical reaction. Indeed, the radiation intensity remains constant or increases after the end of the pumping. The principal influence on the HF production is exerted by the vanishing of the F atoms via the reaction with H_2, the damping constant of which is $\tau_F \leqslant 3$ μsec, and the formation of H with $\tau_H \leqslant 8$ μsec. The influence of other reactions, such as recombination of the atoms or the thermal dissociation of F_2 and H_2 at T < 1200 K, is smaller by several orders. The existence of lasing during several dozen microseconds after the end of the pumping in hydrogen-rich mixtures suggests the existence of a chain mechanism of the reaction. In this case it is also easy to explain the presence of lasing when the pump power is decreased (or even turned off), since the rate of the chain reaction can increase with time because of self-

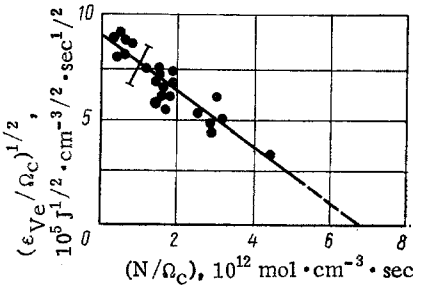

Fig. 4.4. Parametric dependence.

heating of the mixture by the release of chemical energy. When the possibility of a chain reaction was excluded, e.g., by replacing F_2 with MoF_6, the lasing duration did not exceed the length of the pump pulse.

A parametric analysis of a photochemical laser based on the reaction $H_2 + F_2$ [21] yielded, for the specific energy output per unit volume, the expression

$$\varepsilon_V = h\nu \frac{\Omega}{\bar{k}_n}\left(1 - \frac{\bar{k}_N N}{\Omega}\right)^2, \tag{4.10}$$

where $h\nu$ is the energy of the lasing quantum; $\bar{k}_n = 2k_n\psi\chi^{-2}$ and $\bar{k}_N = k_n\psi\chi^{-1}$ are the effective model constants for the relaxation of vibrationally excited HF molecules on the molecules HF and F_2, respectively; $\chi = (w_2 - w_1)/(2\Omega n)$; $\psi = (n_1^0 - n_2^0)/2n$; $\Omega = (1/n)\, dn/dt$; and n_2 and n_1 are the populations of the upper and lower lasing levels, respectively.

To find the effective model constants a curve was plotted (Fig. 4.4) in the coordinates $(\varepsilon_{Ve}\Omega_c^{-1})^{1/2}$ and $N\Omega_c^{-1}$, where the subscripts "e" and "c" label, respectively, the experimental and calculated quantities. It can be seen that the aggregate of the results is described by a linear plot. Hence $h\nu k_n^{-1} = 0.8\cdot10^{-8}$ J/(cm^3·sec), $\bar{k}_N = 1.5\cdot10^{-13}$ cm^3/sec and $\varepsilon_V = 0.8\cdot10^{-8}\cdot\Omega(1 - 1.5\cdot10^{-13}\, N/\Omega)$ J/cm^3.

A comparative analysis of the effectiveness of using various photolytic fluorine-atom sources shows that the largest gain on HF molecules is realized for the mixture WF_6/H_2 [22]. However, work with WF_6 is made difficult by the poor reproducibility of the results and by the difficulty of obtaining pure WF_6.

The CO molecule is of interest as a working molecule for a photochemical static gas laser. Many reactions that lead to formation of CO are highly exothermic, so that the CO can be easily excited to high vibrational levels ($v \leqslant 17$). This leads to low relaxation rates of the CO molecules when they collide with unexcited particles.

The first photochemical static CO gas laser was based on the oxidation of carbon disulfide [23]. The working chamber was a quartz tube with KCl Brewster windows, of 7 mm diameter, placed in a cavity 1 m long. The CS_2/O_2/He mixtures were pumped with a xenon lamp 50 cm long. The radiation power increased with increasing He pressure, and the excitation energy at the optimal He pressure p = 20 kPa reached about 0.5 W.

Lasing was observed on transition 31 of the $\mathcal{P}$ branch. Some 270 more transitions were observed on the $\mathcal{P}$ and $\mathcal{R}$ branches of the CO molecule. A common regularity is that lasing on transitions with low values of J appear earlier than on transitions with high values of J.

Lasing with λ = 4.7-5.7 μm was observed in wide ranges of mixture compositions, of initiation energies (from 0.5 to 4 kJ), and of pressures (from 0.066 to 13.3 kPa) [25]. The pressure corresponding to the maximum power increases approximately as $\sqrt{E_I}$, where E_I is the initiation energy, and the maximum power first increases very rapidly, and then in proportion to $E_I^{1,5-2}$.

The lasing process is not affected by vibrational relaxation of the CO molecules, and the characteristics of this process are determined only by the chemical reactions [26]. The most important among them are the following:

$$
\left.\begin{aligned}
&0)\ CS_2 + h\nu\,(\lambda < 220\text{nm}) \rightarrow CS + S;\\
&1)\ S + O_2 \xrightarrow{k_1} SO + O \quad (-27{,}1\ \text{kJ/mole});\\
&2)\ O + CS_2 \xrightarrow{k_2} CS + O \quad (-96\ \text{kJ/mole});\\
&3)\ O + CS \xrightarrow{k_3} CO^* + S \quad (-313\ \text{kJ/mole});\\
&4)\ S + CS_2 \xrightarrow{k_4} CS_3 + M.
\end{aligned}\right\} \qquad (4.11)
$$

According to the data of [27, 28], $k_1 = 2 \cdot 10^{-12}$ cm^3/sec, which is larger by three orders of magnitude than the value assumed in [25] (at T = 300°K). In this case not only the reaction 4), but any trimolecular reaction in which the active particles vanish (e.g., SO + O + M → SO_2 + M), cannot be comparable in rate with the bimolecular reactions 1)-3) at low pressures of CS_2 (p_{CS_2} ~ 0.1 kPa), at which the lasing energy and power decrease. To analyze the observed contradiction between the decisive role of the trimolecular shutoff and the low calculated rate of this reaction compared with the rates of the bimolecular reactions, special experiments were performed [29]. The optical-quartz working tube of the chemical laser (with transmission up to 200 nm), 50 cm long and with inside diameter 20 mm, was closed on both ends by calcium fluoride (or barium fluoride) windows. The cavity length was 120 cm. The initiation was produced by two series-connected xenon lamps (p_{Xe} = 0.266 kPa). The lamps and the tube were placed inside a cylindrical reflector of aluminum foil. The dependence of the energy E of the generated radiation on the partial pressure of CS_2 diluted with He, Ar, or Xe gas was investigated. The influence of the dilution at high CS_2 pressures is evidence in favor of the assumption that the chemical process that limits the lasing energy and power is trimolecular.

The dependence of E and W on the pressure of the components CO_2, N_2O, OCS is qualitatively the same as in dilution with inert gases. The CO_2 effectiveness is close to that of helium ($k_{CO\text{-}CO_2} \approx 10^{-14}$ cm^3/sec), and the relaxation on N_2O is more effective ($k_{CO\text{-}N_2O} \approx 10^{-13}$ cm^3/sec). The strongest resonant exchange with CO vibrational levels ($4 \leqslant v \leqslant 13$) is observed for the molecule OCS ($k_{CO\text{-}OCS} \approx 10^{-12}$ cm^3/sec).

Thus, the aforementioned contradiction still remains, and to resolve it, it is necessary to include in the scheme of the process new fast channels for active-particle formation. It is proposed, e.g., to use the reaction SO + CS → OCS + S + 125 kJ/mole it its constant is larger than or of the order of 10^{-11} cm^3/sec.

Photochemical Static Gas Lasers Pumped by Particles Excited in the Course of Chemical Reactions. To raise the chemical efficiency of lasers, polyatomic working molecules, such as CO_2, are pumped by energy transfer from molecules such as the type HX, excited by chemical reactions (here X = F, Cl, Br, etc.). To obtain lasing in this case there is no need for population inversion of the chemical-reaction products. It suffices only that they be in an excited state. The use of polyatomic molecules pumped by chemical-reaction products makes it possible, in addition, to lengthen the period of the chemical pumping of the working molecules and to carry out selective pumping of individual levels, thereby likewise increasing the efficiency.

In the first photochemical static gas laser with energy transfer to CO_2 and N_2O molecules, the pumping was by excited molecules DCl (HCl) and HI. The largest value E = 95 mJ at a wavelength λ = 10.6 μm was obtained in a mixture with partial pressures p_{Cl_2} = 1.333 kPa, p_{HI} = 0.266 kPa, p_{CO_2} = 2 kPa. For the N_2O molecules, E_{max} amounted to only one-third the value obtained with the CO_2 molecules. By pumping CO_2 molecules with DF (HF) molecules excited in the reaction F_2O + D_2 (H_2), it is possible to obtain an approximate peak power 10 kW and to extract about double the reaction energy obtained with the DF molecules themselves [30, 31]. In the range of low partial pressures of the CO_2, an increase of this pressure enhances the energy transfer from DF to CO_2 and leads to a linear dependence of the energy on P_{CO_2}. At high CO_2 concentrations an increase of the pressure leads to an increase of the population of the lower level (0°0) and hence to a decrease of the energy of the generated radiation.

The theoretical model of a photochemical laser based on energy transfer by the CO_2 molecules from excited DF molecules includes the following elementary processes:

$$
\left.\begin{aligned}
&0)\ F_2 + h\nu \xrightarrow{k_0(t)} 2F;\\
&1)\ F + D_2 \xrightarrow{k_1} DF + D;\\
&2)\ D + F_2 \xrightarrow{k_2} DF + F;\\
&3)\ F + F + M \xrightarrow{k_3} F_2 + M;\\
&4)\ D + D + M \xrightarrow{k_4} D_2 + M;\\
&5)\ D + F + M \xrightarrow{k_5} DF + M;\\
&6)\ D + O_2 + M \xrightarrow{k_6} DO_2 + M;\\
&7)\ DF(v) + CO_2(v_1, v_2, v_3) \xrightarrow{k_7(v)} DF(v-1) + \\
&\quad + CO_2(v_1, v_2, v_3 + 1);\\
&8)\ \text{relaxation of asymmetric } CO_2 \text{ mode;}\\
&9)\ \text{relaxation of symmetric } CO_2 \text{ mode;}\\
&10)\ DF(v) + M \xrightarrow{k_{10}^M} DF(v-1) + M;\\
&11)\ CO_2(00^0\,1) \xrightarrow{A} h\nu + CO_2(10^0\,0);\\
&12)\ CO_2(00^0\,1) + h\nu \xrightarrow{B} CO_2(10^0\,0) + 2h\nu.
\end{aligned}\right\} \qquad (4.12)
$$

Calculations based on such a model are in satisfactory agreement with the experimental data [32, 33].

The energy E_{max} in the pulse, obtained in the experiments, is 2.5 J. It corresponds to $\varepsilon_V = 0.025$ J/cm³ determined over a total active-medium volume 100 cm³ and to $\eta_c = 2\%$. Introduction of He (up to $p_{He} \approx 8$ kPa) makes it possible to more than triple η_c (to 6.4%).

The characteristics of a chemical DF/CO_2 laser amplifier with higher parameters were investigated when initiated with a light pulse of duration shorter than the inversion lifetime [32, 34]. The $D_2/F_2/CO_2/He$ working mixture was prepared by dynamic mixing. Chemically compatible gases were mixed at the proper proportions at equal total pressures in two identical stainless-steel mixers, after which they were fed through a common pipe into the working chamber. The dark reaction was slowed down by adding to the mixture oxygen at a pressure equal to 6% of the fluorine pressure.

The use of a high-power light source of duration much shorter than the inversion lifetime has made it possible to obtain at atmospheric pressure $\varepsilon_{V max} = 0.15$ J/cm³ on the $\mathcal{P}(20)$ and $\mathcal{P}(22)$ lines for a mixture $D_2/F_2/CO_2/He = 1/1/4/5$, $\eta_c = 7\%$. The dependences of ε_V on the partial pressure of the fluorine and on the energy stored in the light-source bank exhibited no tendency to saturate under the experimental conditions.

In photochemical static gas lasers based on energy transfer from DF to CO_2 molecules, one of the shortcominings that hinder the increase of the power and of ε_V is the low rate of energy transfer from the DF to the CO_2. In the TF/CO_2 system the energy transfer is faster by almost one order of magnitude than in the DF/CO_2 system. However, comparison of the processes in the mixtures $T_2/F_2/CO_2$ and $D_2/F_2/CO_2$ has shown that the energy emitted by the TF/CO_2 laser is lower than that of the DF/CO_2 chemical laser at all CO_2 pressures.

The lasing energy also decreases monotonically with increasing mixture-storage time. This is attributed to the increased rate of the relaxation of the CO_2 molecules on the DF (TF) molecules produced in the mixture during its preliminary storage. The increase of the spontaneous chain initiation because of the radioactivity of the tritium did not make it possible to raise its partial pressure above several kPa, so that no large value of ε_V could be obtained. In addition, the increase of the rate of chain initiation reduces the time of preliminary storage of the working mixture to a minimum.

Experiments [35] yielded W = 200 kW and E = 5 J at normal pressure of the $D_2/F_2/CO_2/He$ mixture. The radiation energy increases weakly when p is increased from 1.33 kPa to 0.1 MPa. The pulse duration changed from 1.2 msec at p = 2 kPa to 100 μsec at high pressure, owing to the lasing shutoff due to thermal heating of the mixture. At optimal pressure, the gain is $\alpha = 0.03$ cm^{-1}, and E ≈ 5 J. The value of η_c determined for the entire volume is 3.2%, and if only the radiating part of the volume is considered it amounts to about 20%.

The peculiarities of the DF → CO_2 energy transfer were analyzed in [36] on the basis of experimental investigations of the output parameters of a photochemical laser using CO_2 mixtures with chlorine fluorides and deuterium and with fluorine and deuterium. It was shown that the most effective DF → CO_2 energy transfer took place in the mixture $F_2/D_2/CO_2$.

4.2. Electric-Discharge Static Gas Chemical Lasers

More advantageous from the energy point of view is initiation of a chemical reaction directly with an electric discharge. However, a uniform excitation of the working volume by an electric discharge that is longitudional relative to the cavity axis can be realized only at mixture pressures p not exceeding several hundred Pa. At higher p the discharge contracts, so that the time of propagation of the reaction over the entire volume is lengthened, and this leads to vanishing of the particle population inversion at the sites of the chemical reaction. Excitation with a transverse electric discharge makes it possible to raise the working pressure to several dozen kPa. Even this scheme, however, is deficient in that it is difficult to excite the entire working volume uniformly.

Figure 4.5 shows two typical supply circuits for the initiation of a static gas chemical laser with a transverse electric discharge.

In the discharge circuit with the needle electrodes 8 the capacitance C_D of the discharge capacitor is 0.005-0.05 μF, and it is discharged through the working chamber 4 when the spark discharge gap 2 is shorted. The grounded electrode in the system with flat electrodes 6 and 7 and with preionization of the discharge gap by an auxiliary electrode is an aluminum rod on which a copper wire is wound. The optimum distance between the electrodes is 3.8 cm. A uniform discharge in the interelectrode gap is ensured by an additional discharge between the high-voltage 6 and grid 7 electrodes. The discharge capacitor is usually C_D = 0.05 μF, and the ratings of the capacitors C_{T_1} and C_{T_2} in the triggering circuit are of the order of 0.005 μF.

Homogeneity of the discharge can be ensured also by preionization of the gas mixture by ultraviolet radiation or by a beam of fast electrons. For strongly negative molecules of the fluorine type, the electroionization method of initiating a chemical reaction may not be effective enough because of the high probability of electron loss by sticking to molecules and because of the decrease of the electron mobility.

Emission in hydrogen and deuterium halides under the influence of a pulsed electric discharge was investigated in [37, 38]. HF and DF are produced when H_2 reacts chemically with the freons CF_4, $CBrF_3$, $CClF_3$, CCl_2F_2. Other halides are produced by reaction of gaseous chlorine or bromine with hydrogen or deuterium. Ten lines were observed in the emission of HCl between 3.7 and 4.0 μm, and 24 lines of DCl between 5.2 and 5.6 μm. Transitions up to v = 5 were observed for DCl and DBr. Electric-discharge initiation produced chemical reactions in hydrogen–oxygen and hydrogen–methane mixtures, and the lasing took place at λ = 28.27, 27.97, and 23.36 μm.

Lasing was obtained also on transitions of fluorine atoms, which emit in the visible band [39]. Large gains were observed on the lines λ = 0.7037 and 0.7127 μm, as attested to by the presence of superradiance when the mirrors were misaligned. Lasing was preserved even in the case of strong scattering from the mirror surfaces.

Helium is used as an additional component of the working medium in such processes. An attempt to replace He by other gases (Ar, N_2, O_2, H_2, CO_2) was unsuccessful. The reason is that the pumping mechanism is due to excitation of F in dissociative collisions between He and HF. Other dissociative collisions, however, e.g., Ar–HF, do not lead to lasing, so that even though metastable argon $Ar(^1S)$ has more than enough energy to dissociate the HF, the energy is still insufficient to simultaneously excite an electronic state of F. The production of H upon dissociation of HF, a process that is almost resonant (its cross section is $\sigma = 10^{-13}$-10^{-14} cm^2), and the subsequent deactivation cause depletion of the lower levels. This process determines the lifetime of the excited F atoms, equal to 10^{-7}-10^{-8} sec at p ~ 1 Pa.

An investigation of an electric-discharge static gas chemical laser using an H_2/Br_2 mixture with SF_6 added was carried out in [40]. The reaction was initiated by pulsed discharge of a capacitor (0.03 μF, 25 kV) in the gas mixture introduced into the working chamber of the chemical laser, and the gas was pumped out and a fresh mixture added after two pulses. The SF_6 was added to the H_2/Br_2 mixture with p = 4 kPa and with an optimal molar-concentration

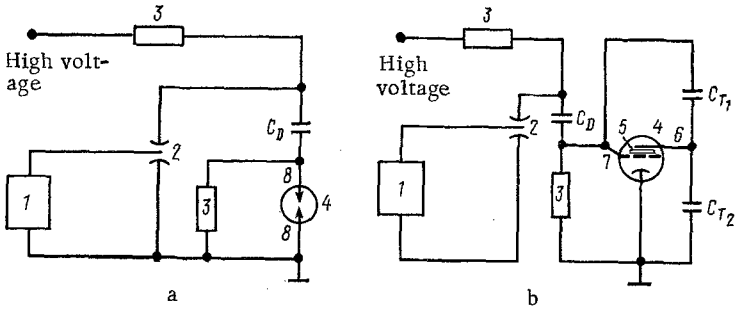

Fig. 4.5. Typical discharge devices for electrochemical lasers with needle-shaped electrodes (a) and with flat electrodes and preionization of the discharge gap by an auxiliary discharge (b): 1) triggering-pulse generator; 2) spark discharge gap; 3) resistors; 4) chemical-laser working chamber; 5) insulator; 6, 7) high-voltage and grid electrodes, respectively; 8) needle electrodes.

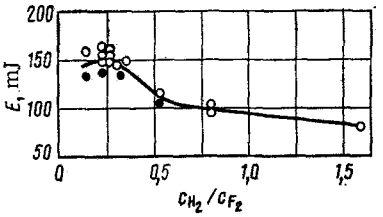

Fig. 4.6. Radiation energy E vs the H_2/F_2 molar ratio for the mixture $F_2/H_2/O_2/He$ = 1/x/0.08/15 at a total pressure 32 kPa: ○) C = 250 pF, V = 35 kV; ●) C = 333 pF, V = 25 kV.

ratio H_2/Br_2 = 29/1. The total energy of the lasing on the molecules of HBr (and HF) increases monotonically when the SF_6 pressure is increased to p = 5.33 kPa, and decreases at higher pressure. Selectively vibrationally excited HBr particles (v = 3, 4) are produced in the reaction

$$H + Br_2 \rightarrow HBr^* + Br \quad (-172 \text{ kJ/mole}). \tag{4.13}$$

The use of an inductive energy storage unit in the supply circuit of an electric-discharge HF chemical gas laser [41] makes it possible to shape a uniform longitudional electric discharge in cells of appreciable volume at SF_6/H_2 pressures of several kPa, and to obtain high-power lasing pulses of ~0.1 μsec duration. A value ε_V = 6.2 mJ/cm^3 was obtained in this manner from a volume 290 cm^3 from a SF_6/H_2 = 3/1 mixture at 9 kPa pressure.

An energy of 270 kJ/mole is released in the reaction F + HI → HF + I, whereas excitation of the vibrational level of HF (v = 6) requires only 242 kJ/mole. In this connection, the energies of the generated radiation were compared [42] with the energies obtained in the reactions $H_2 + F_2$ and F_2 + HI under similar experimental conditions, in a setup with a transverse pulsed discharge. It was found that the energy of the generated radiation is twice as high when HI is used as the source of the hydrogen atoms.

The hydrogen-atom sources investigated [43] were CH_4, C_3H_8; SiH, GeH, and AsH_3. The fluorine atom sources were SF_6, NF_3, N_2F_4, IF_7, OF_2, BrF_5, ClF_3, ClF_5, XeF_5. The mixtures were at room temperature, the relative concentration c_F/c_H ranged from 0.5 to 5, and the pressure ranged from 1.33 to 8 kPa. Some of these mixtures were stable, while others exploded spontaneously and inhibitors had to be used for them.

The mechanism whereby the HBr molecules are excited by initiating a reaction in the H_2/Br_2 by a transverse discharge in a working chamber 115 cm long and with inside diameter 4 cm was investigated in [44]. The voltage was applied to the electrodes from a 20-pF bank of 20 capacitors charged to 20 kV. It was found that for a mixture with p_{H_2} = 13.3 kPa and p_{Br} = 4 kPa the energy of the generated radiation increases successively on the transitions 1–0, 2–1, and 3–2. When p_{Br_2} is decreased to 1.33 kPa (at the same p_{H_2}) this sequence is reversed.

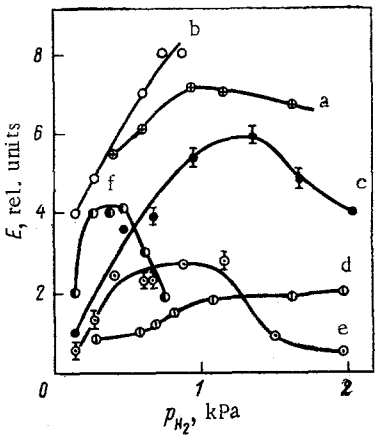

Fig. 4.7. Effect of hydrogen pressure on the total radiated energy when various substances are used: a) hydrogen, b) xylene, c) toluene, d) gasoline, e) acetone, f) methanol.

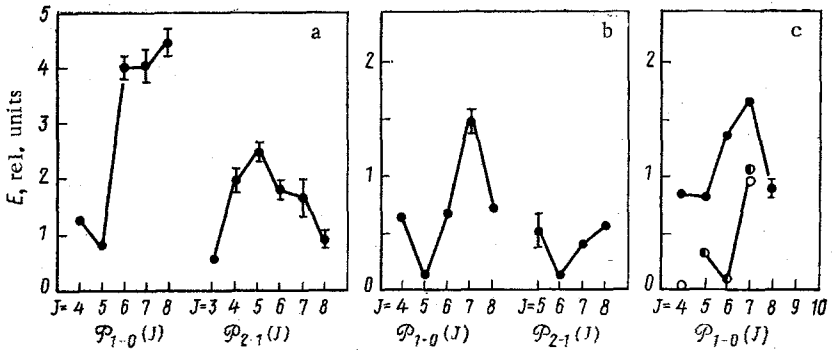

Fig. 4.8. Partition of the generated energy at p = 4.4 kPa among the individual lines: a) SF_6/xylene = 30/3; b) SF_6/toluene = 30/3; c) ●) SF_6/C_6H_6 = 30/3; ◐) SF_6/CH_3OH = 30/3; o) $SF_6/(CH_3)_2CO$ = 30/3.

The output characteristics of an HF chemical laser were considered in [45] in a wide range of pressures and gas-mixture compositions. The mixture was stabilized by adding O_2 and He to the F_2, followed by cooling to 84°K prior to mixing with the H_2. A value E_{max} = 0.15 J was observed (Fig. 4.6) at a mixture pressure 32 kPa and at partial component ratios $F_2/H_2/O_2/He$ = 1/0/23/0.08/12. The *electric efficiency* η_{el}, defined as the ratio of the energy of the generated radiation to the electric energy consumed in the initiation of the reaction, reached 140%.

The effect of the employed hydrogen sources C_6H_6, $C_6H_5CH_3$, $C_6H_4(CH_3)_2$, CH_3OH, $(CH_3)_2CO$ on the lasing when the reaction is initiated with a transverse electric discharge (21 kV, 30 pF) is illustrated by the plots of Figs. 4.7, 4.8 [46].

4.3. Static Gas Chemical Lasers with Reaction Initiation by an Electron Beam

The method of initiating static gas chemical lasers by an electron beam is attracting much attention at present. Electron-beam initiation offers a number of advantages over other methods of initiating a reaction in a chemical laser: volume homogeneity of the pumping, high efficiency, possibility of high energy input in a short time, and appreciable volumes of active medium at sufficiently high working pressures. In addition, dissociation of the molecules that supply initial active atoms whose spectra lie in the far ultraviolet, which cannot be gotten by ordinary standard light sources, is possible.

The characteristics of a static gas chemical laser initiated by an electron pulse, as a function of the pressure and of the ratio of the components IF_7 and H_2, were investigated in [47]. A diagram of the experimental setup is shown in Fig. 4.9.

A pulsed monoenergetic electron beam of energy E_e = 12 J (500 keV) and duration τ_e = 3 nsec was injected by a cathode-ray tube of 4.5 cm diameter. The laser output radiation at

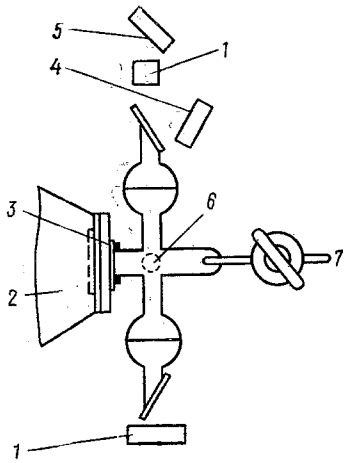

Fig. 4.9. Diagram of experimental setup with the chemical reaction initiated by an electron beam: 1) mirrors; 2) cathode-ray tube; 3) aluminum foil; 4) detector; 5) thermopile; 6) active zone; 7) gas inlet and outlet.

λ = 2.7-3 μm was recorded with a Ge—Au detector cooled to liquid-nitrogen temperature. The generated radiation energy E was measured with a ballistic thermopile.

The waveform of the generated radiation pulse depends on the variation of the mixture pressure p. The experiments were performed with a glass chamber of up to 2.5 cm diameter, and with a chamber with a 4-cm spherical central section. It was found that the electron-beam energy loss dE_e/dx was small in both cases, and that the energy absorbed per unit mass of gas was constant for p > 3.33 kPa. The maximum generated radiation energy E_{max} was reached at p = 20 kPa and at a mixture component ratio IF_7/H_2 = 6/1, which differed greatly from the stoichiometric ratio 2/7. This is evidence that less than 5% of the fluorine atoms contribute to the lasing.

A diagram of an $SF_3/F_2/H_2(D_2)$ static gas chemical laser pumped by an electron beam with maximum accelerating voltage 50 kV and E_e = 900 J is shown in Fig. 4.10 [48]. A beam of electrons from a cathode measuring 3.8 × 20.3 cm passed through an aluminum foil 1 mm thick into a working chamber with variable dimensions 3 × 4 × 20.3 and 10.2 × 10.2 × 40.6 cm. The D_2 was obtained by electrolysis of D_2O. The total lasing power was directly proportional to the pressures of H_2 and F_2, in accordance with the theory. It was observed that the power is not linearly dependent on the working volume. This is due mainly to the enhancement of the inhomogeneities in the working medium when the volume is increased. An electric efficiency η_{el} = 6% was obtained. The kinetic model of the lasing was refined on the basis of the experimental data. Calculations in accordance with this model yielded, for the specific energy output, a value larger by one order than in experiment. This is attributed to parasitic oscillations in the volume and to the low initial fluorine concentrations.

The efficiency of electron-beam initiation of an $H_2/F_2/He/O_2$ static gas chemical laser at relatively low current density j_e in the electron beam was investigated in [49]. To lower the excitation level, a mixture with increased partial pressure of the fluorine was used. To raise the total pressure p to atmospheric at relatively low partial pressures of H_2 and F_2, helium was used as ballast. Oxygen was added in the course of mixing to prevent a reaction. The mixtures H_2/He and $F_2/He/O_2$ entered through fast-acting valves into a mixer, from which the working mixture flowed over slowly into the working volume. The initiating electron beam, with j_e = 20 A/cm^2, an accelerating voltage 140 kV, τ_e = 200 nsec, and cross section 1 × 25 cm, was introduced through an aluminized tantalum foil 50.8 μm thick secured on a stainless-steel mounting.

The efficiency of conversion of the electric energy into electron-beam energy was 60%. A cavity 75 cm long with an active volume of 100 cm^3 was made up of a spherical copper mirror and a sapphire plate that reflected 10% of the light in the lasing range λ = 21.7-3.1 μm. The lasing energy E at fixed concentrations c_{H_2} and $C_{O_2} = 0.04c_{F_2}$ increased with increasing c_{F_2} until the latter exceeded c_{H_2} by 2-4 times.

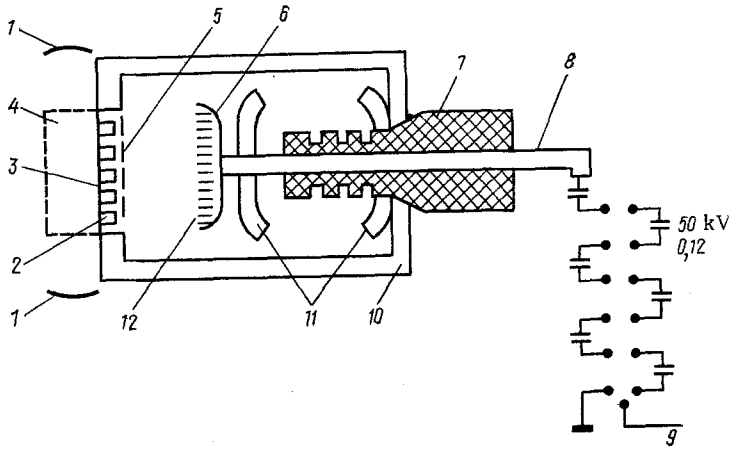

Fig. 4.10. Diagram of experimental setup of $SF_3/F_2/H_2(D_2)$ static gas chemical laser: 1) cavity; 2) foil mounting; 3) foil; 4) lasing zone; 5) grounded grid; 6) holder for cold cathode; 7) high-voltage insulator; 8) low-inductance lead-in; 9) trigger; 10) vacuum chamber; 11) corona-discharge ring; 12) thermionic cathode.

At $c_{F_2} = 30\%$ and $c_{H_2} = 8\%$, a value $\varepsilon_{V\,max} = 0.051$ J/cm^3 referred to atmospheric pressure and a value $\eta_{el} = 875\%$ were obtained. The value of η_c, defined as the ratio of the lasing energy to the chemical energy released in the active volume, under the assumption that all the H_2 molecules participate in the reaction and release 130 kcal/mole of H_2, was 0.75-2.8%. In an H_2/F_2 chemical laser the energy per lasing pulse [50] exceeds the value obtained in chemical lasers on mixtures using SF_6 and C_2H_6 [48].

For the H_2/F_2 mixture, $\varepsilon_V \approx 0.13$ J/cm^3, while η_{el} and η_c are, respectively, 180 and 11.4%. If it is assumed that $j_e \approx 80$ A/cm^2, these figures are in satisfactory agreement with calculations by the simplified model of the kinetic processes in an H_2/F_2 chemical laser initiated by an electron beam.

The lasing energy E in the mixture $F_2/O_2/H_2 = 1/0.3/0.25$ increases approximately linearly with the pressure p_{F_2}. Similarly, a linear dependence is observed for the electron energy lost in the working mixture. With increasing p_{SF_6} the value of E and the electron-beam energy lost in the gas increase nonmonotonically, while addition of SF_6 up to p = 13.3 kPa increases the energy input to the gas from the electrons by more than 1.8 times compared with the case when there is no SF_6.

For the mixture $F_2/O_2/SF_6/H_2 = 3.6/1.4/1.0/1.0$ initiated by an electron beam ($E_e = 150$ J, $\tau_e = 30$ nsec) the lasing energy obtained in [51] was E = 67 J with a duration 100 nsec, $\eta_{el} \approx 45\%$, and a beam divergence $5 \cdot 10^{-2}$ rad.

Initiation of the reaction in $F_2/H_2/He/Ar = 6/3/54/37$ at atmospheric pressure by an electron beam of short duration [52] yields $\varepsilon_V = 0.042$ J/cm^3 at an energy input 0.028 J/cm^3. In this case η_c and η_{el} are, respectively, 6.3 and 150%. A pulse energy E = 2.52 J was obtained in a mixture of H_2 with 6% F_2 at an electric field intensity 11 kV/cm.

By increasing the mixture pressure to several MPa it was possible to appreciably decrease the chamber volume and to increase the specific characteristic of a static gas laser [50].

A diagram of the experimental setup is shown in Fig. 4.11. The working chamber (anode) 18.5 cm long was part of a coaxial high-voltage field-emission diode placed inside the accelerating tube. To increase the strength, the chamber was made up of separate sections 5 cm long, capable of withstanding p = 11 MPa. The amplitude of the current pulse of duration $4 \cdot 10^{-8}$ sec was 5.7 kA, the maximum electron energy 2.9 MeV, and $E_e = 420$ J. The cavity was made up of a flat gold-coated total-reflection mirror on a metallic substrate and a semitransparent interference mirror with transmissivity 20 or 40% in the range $\lambda = 2.5$-3.5 μm; plates of polished germanium and of barium fluoride were also used.

A value $E_{max} = 0.79$ J was obtained for a mixture $SF_6/H_2 = 70/1$ at p = 0.27 MPa and at $\varepsilon_V = 21$ mJ/cm^3.

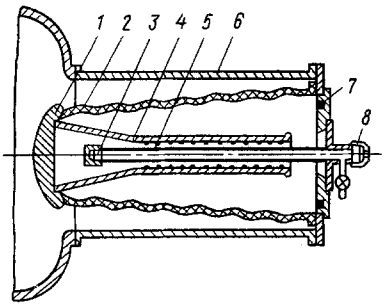

Fig. 4.11. Diagram of accelerating tube with coaxial diode: 1) accelerating-tube electrode; 2) insulator; 3) mirror; 4) cylindrical cathode; 5) working chamber of chemical laser (anode); 6) accelerating-tube housing; 7) Rogowski loop; 8) semitransparent mirror.

The main obstacle to improvement of the characteristics of a chemical laser with the reaction initiated in an SF_6/H_2 mixture at $p \gtrsim 1$ MPa is apparently the collisional deactivation of the active HF (v) molecules by H_2 molecules [53]. The influence of collisional deactivation can be decreased to some degree by shortening the duration of the initiating pulse [50]. This, as well as raising the pressure of the $D_2/F_2/CO_2/He$ mixture to several hundred kPa and optimization of the mixture composition, should substantially increase the specific energy output and the lasing quantum yield in an electron-beam-initiated chemical laser [54]. In [55], for a mixture $H_2/F_2/O_2/He = 30/75/6/250$ at a pressure 96.3 kPa the authors obtained $\varepsilon_V = 91$ mJ/cm^3 at efficiencies relative to the energy input $\eta_{el} = 936\%$, $\eta_c = 4.7\%$ and at an electron-beam-energy utilization efficiency 250%. HCl chemical lasers (working mixture ClF/H_2) initiated by an electron beam also had parameters that are high for lasers of this type, namely $\varepsilon_V = 5$ mJ/cm^3 and W = 0.4 MW.

The parameters of chemical lasers can also be increased by using a master oscillator + amplifier combination [56]. The master oscillator can be, e.g., a $F_2/H_2/He/O_2$ photochemical static gas laser, and the amplifier can be a tube with the same mixture components, placed in a solenoid that contains and rotates the initiating electron beam. The use of such a combination for high-energy chemical sources of coherent radiation can solve the problem of the optical strength of the reflectors for optical cavities, obviate the need for large-size optics, and decrease the beam divergence.

4.4. Static Gas Excimer Lasers

One of the promising trends in the search for a new working medium for lasing in the visible and in the ultraviolet is the use of excimers, which are unstable molecules made up of radicals, one of which is in an excited state. Included among these molecules are, e.g., the halides XeF, XeCl, XeBr, KrF, XeO, KrO, ArO [57]. Lasing on inert-gas halides in excimer chemical lasers is based on populating the upper working state via a chemical reaction between the excited inert-gas atoms and molecules that include halogen atoms. The molecules are produced in the reaction mainly in the electron-excited state $^2\Sigma$ and relax via collisions to lower vibrational levels, after which they go over to the molecule ground state. Rapid decay of this molecule leads to inverted population.

Such chemical lasers are pumped by the following: high-current electron beam, flash lamp, electric discharge, as well as a number of combined systems. Excimer chemical lasers are compact and simple, and can deliver a sufficiently high power at an efficiency ~1-10% in the ultraviolet. For example, the peak power of a KrF chemical laser at $\lambda = 0.2484$ μm is $W = 1.9 \cdot 10^9$ W at a pulse energy E = 108 J with $\eta \approx 3\%$. The sources of the halogen-donor atoms were Cl_2, CH_2Cl_2, F_2, HBr, SF_6, etc.

To improve the homogeneity of the energy release, the UV pump source used [58] was a special chamber filled with Ar at p = 1.3 MPa, excited by a beam of relativistic electrons. Radiation of 1 J energy passed through a number of MgF_2 windows into another working chamber filled with an active medium consisting of Ar (4.35 MPa) and N_2O (266.6 Pa). At 0.25 μsec after the pump pulse, absorption of a probing-radiation pulse was observed in the active medium, followed by amplification of the signal for a time equal to the lifetime of the excited level. Lasing took place on the $^1S_0 - {}^1D_2$ transition of atomic oxygen. The profile of the

emission spectrum corresponded not to the collisional complex Ar—O*, but to the ArO* molecule in the excited $2^1\Sigma^+$ state, which includes the excited state of the O atom and the ground state of Ar. The concentration of the excited O* atoms is given by

$$n(\mathrm{O}^*) = n_0(\mathrm{O}^*)\exp(-t/\tau') \tag{4.14}$$

with a characteristic time $\tau' = 10^{-3}$ sec of emission of the energy stored in the medium. The luminescence intensity increases linearly with increasing p_{Ar}. Owing to relaxation on N_2O at p_{N_2O} = 33 Pa, the excited-state lifetime is $\tau \sim 2.6$ μsec, less than the calculated $\tau \sim 12$ μsec, and remains at this value all the way to $p \sim 3$ MPa.

High efficiency and output power were obtained with the excimers KrF and XeF excited by an electron beam [59]. The emission of these excimers is due to a transition from a bound upper state to a dissociative or a weakly bound ground state, made up of a combination of an inert gas in a $^1S_0$ state and a halogen atom in the state $^2P_{3/2}$ or $^2P_{1/2}$.

The energy of KrF and XeF excimer lasers with the electron beam entering perpendicular to the tube (transverse pumping) had a maximum when small concentrations of Xe (4 kPa) or Kr (20 kPa) and halogen donors (1.33 kPa) were added to the argon. The beam energy was transferred to the argon, and then redistributed to the Kr or Xe by collision.

The most important processes in XeF chemical lasers are [60]:

$$\left.\begin{array}{l}
1)\ \mathrm{Ar}+e\rightarrow \mathrm{Ar}^*+\mathrm{Ar}^+ +e;\\
2)\ \mathrm{Ar}^+ +2\,\mathrm{Ar}\rightarrow \mathrm{Ar}_2^*+\mathrm{Ar};\\
3)\ \mathrm{Ar}_2+e\rightarrow \mathrm{Ar}^*+\mathrm{Ar};\\
4)\ \mathrm{Ar}^*+2\,\mathrm{Ar}\rightarrow \mathrm{Ar}_2^*+\mathrm{Ar};\\
5)\ \mathrm{Ar}^*+\mathrm{NF}_3\rightarrow \mathrm{ArF}^*+\mathrm{NF}_2;\\
6)\ \mathrm{Ar}^*+\mathrm{Xe}\rightarrow \mathrm{Ar}+\mathrm{Xe}^*;\\
7)\ \mathrm{Xe}^*+\mathrm{Xe}+\mathrm{Ar}\rightarrow \mathrm{Xe}_2^*+\mathrm{Ar};\\
8)\ \mathrm{Xe}^*+\mathrm{NF}_3\rightarrow \mathrm{XeF}^*+\mathrm{NF}_2;\\
9)\ \mathrm{XeF}^*+\mathrm{NF}_3(\mathrm{NF}_2)\rightarrow \mathrm{Xe}+\mathrm{F}+\mathrm{NF}_3(\mathrm{NF}_2);\\
10)\ \mathrm{XeF}^*\rightarrow \mathrm{Xe}+\mathrm{F}+h\nu.
\end{array}\right\} \tag{4.15}$$

The lasing energy increases here linearly with pressure, up to 0.3-0.4 MPa. The decrease of the output power can be attributed to an increase in the deexcitation rate, e.g., as a result of collision of the excited particles with argon, atomic fluorine, and xenon, as well as to formation of Xe_2^* as a result of the competing process [61]

$$\mathrm{Xe}^*(\mathrm{Kr}^*) + \mathrm{Xe}(\mathrm{Kr}) + \mathrm{Ar} \rightarrow \mathrm{Xe}_2^*(\mathrm{Kr}_2^*) + \mathrm{Ar}.$$

The maximum values $W = 1.1\cdot10^8$ W and E = 5.6 J were obtained at η = 3%.

Transverse pumping, however, is not effective, since only a small fraction of the electron-beam energy is transferred to the gas. To increase the efficiency of energy input, other beam-entry configurations are used. Thus, if the beam enters axially, the pulse energy increases to 200 J and the peak power to $5\cdot10^9$ W. It is precisely with such an entry of the beam into the working medium that appreciable lasing powers and energies were obtained with KrF and ArF [57].

The *quantum efficiency* of a KrF chemical laser pumped by an electron beam with Ar used as the buffer gas depends on the energy E(Ar) consumed in the excitation of the argon, and is defined as $\varphi \approx h\nu\,(\mathrm{KrF})/E\,(\mathrm{Ar}) \approx 24\%$, whereas the maximum attainable efficiency, with account taken of the reactions $Kr^* + F_2 \rightarrow KrF^* + F$, $Kr^+ + F^- + M \rightarrow KrF^* + M$, is 8%. The maximum efficiency of an electric-discharge chemical laser is limited by the energy E* needed to form lowest-energy metastable rare-gas atoms. In the case of a KrF electric-discharge chemical laser the efficiency is connected with the Kr and equals $\varphi = h\nu\,(\mathrm{KrF})/E^*\,(\mathrm{Kr}) = 50\%$. The maximum attainable efficiency determined by the indicated reactions, however, is ≤25%.

Electron beams are successfully used to pump chemical lasers on the mixture Ar/I_2 [62], on the dimers Xe_2^*, Kr_2^*, Ar_2^* [63], and on XeBr [64], XeO and KrO [65].

When an electron beam is used for pumping, the power attainable is limited by the strength of the thin foil used to admit the beam and to separate the vacuum chamber of the electron gun from the chemical-laser chamber with the high-pressure working mixture, as well

as by the loss of beam energy in this foil. The temperature rise of the foil also limits the repetition frequency of the lasing pulses.

Pumping by electric discharge is free of these shortcomings and leads, in principle, to high lasing power with high repetition frequency using relatively simple power sources. Pumping of an XeF chemical laser with a pulsed electric discharge is effective because the lower electronic state of the XeF molecule is weakly bound, and the lifetime of the upper electronic state is high enough — 50 nsec.

The efficiency and lasing intensity of the mixture $He/Xe/NF_3 = 100/3/1$ at relatively low pressures, p = 27-53 kPa, were investigated in [66] using a pulsed electric discharge as the pump. The XeF* molecules are produced here in an excited electronic state as well as in high vibrational states. Collisions with the buffer gas (He, Ar) transfer them to lower vibrational levels. The investigations were made using a power supply with discharge duration t_d = 10 nsec and with a discharge volume 1 × 0.33 × 50 cm. The discharge voltage U_d was varied from 5 to 20 kV, and the pressure p from 2.66 to 66.5 kPa. The pulse repetition frequency was several hundred Hz. No lasing was observed below p = 26.6 kPa, after which the lasing increased continuously with increasing p. The maximum lasing Energy E was obtained at p = 53.3 kPa. Further increase of p led to contraction of the discharge and to a decrease of E. The output pulse energy was E = 1 mJ at p = 46.6 kPa, and $\varepsilon_V = 0.07$ mJ/cm³. In this case η_{el} = 0.2%, and relative to the energy input to the gas — 1.2%. The lasing lines were the same as when pumped with an electron beam (351 and 353 nm). In addition, a weak line was observed at λ = 349 nm. The value of W_{max} was ≈25 kW. Owing to the relatively low pressure, the Xe_2^* concentration was low, so that three-particle recombination (Xe^+, F, He) played a negligible role in the formation of the XeF*.

The use of a simplified kinetic model leads to the following expressions for the concentration:

$$\left.\begin{aligned} n_{XeF^*} &= N\left\{\frac{T}{\tau}\left[1-\exp\left(-\frac{t}{T}\right)\right]+\left[\frac{T}{(T-\tau)}\right]\times\right. \\ &\left.\times\left[\exp\left(-\frac{t}{\tau}\right)-\exp\left(-\frac{t}{T}\right)\right]\right\}; \\ n_{Xe} &= N\left[1-\exp\left(-\frac{t}{\tau}\right)\right], \end{aligned}\right\} \qquad (4.16)$$

where $N = \langle\sigma v\rangle n_e n_{Xe}/kn_{NF_3}$; $\tau = (kn_{NF_3})^{-1}$; is the lifetime of XeF*; and σ is the excitation cross section.

Under actual conditions; $He/Xe/NF_3 = 100/3/1$, p = 46.6 kPa, U_d = 8 kV, j_e = 100 A/cm², discharge duration t = 10 nsec, E_e = 4 eV: at $k = 10^{-9}$ cm³/sec, one obtains $\tau \approx 10$ nsec $\approx t$, which is less than T = 50 nsec. As a result $n_{Xe^*} \approx N = 10^{14}$ cm^{-3} $\ll n_{Xe} = 3.6\cdot10^{17}$ cm^{-3}. From (4.16) we then get, at $\tau/T \ll 1$, $t/\tau \sim 1$, $n^* \approx Nt/\tau = 10^{14}$ cm^{-3}, which corresponds to an energy $E = h\nu n^* V \approx 10^{-3}$ J, and the gain is estimated at $\alpha_0 = \sigma n^* \approx 10^{-2}$ cm^{-1}. This value agrees with the experimental data.

An electric-discharge XeCl chemical laser was produced [67] with CF_2Cl_2, C_2F_3Cl, CCl_4, BCl_3 as donors, with He predominating in the mixture. The excited halide molecules were produced here by chemical reaction of the excited inert-gas atoms with the halogen donors. With NF_3 used as the donor, the detailed structure of the lasing of an XeF chemical laser at λ = 353.54; 353.05; 351.14; 350.97; 350.91, 348.75 nm was observed. Lasing on XeCl molecules was observed only at high pressures (>0.12 MPa). The maximum pulse energies obtained in [67] were 2, 1, and 0.5 mJ for XeF, XeCl, and KrF, respectively. With another mixture $He/Kr/NF_3$ = 500/50/1, which turned out to be optimal, and with a total pressure 93.3 kPa [68], lasing was obtained at λ = 248.5 and 249.5 nm with E = 0.8 mJ, τ = 25 nsec, W = 32 kW, and ε_V = 0.08 kJ/cm³. Practically no decrease in power was observed at a repetition frequency ≤20 Hz.

Great possibilities for developing and investigating excimer chemical lasers are offered by combined pumping schemes. Thus, it was demonstrated in [69] that it is possible to pump the molecules ArF, KrF, and XeF by a transverse discharge following preliminary photoionization by an additional spark discharge. The spark discharge was fed from a separate source, so as to be able to control the delay of the preionization and main-discharge pulses in an interval 0.1-25 μsec. The preionization light-pulse duration was 400 nsec, and that of the main discharge current 40 nsec. The main-discharge stored energy was about 10 J.

The discharge was produced in a He/F_2 (NF_3)/Xe (Kr, Ar) mixture prepared in a stainless-steel fluorine-passivated mixing system. The chemical-laser working chamber was first evacuated to p = 13.3 Pa, then scrubbed with helium and filled with the mixture up to p = 0.2 MPa.

XeF molecule lasing was observed on the lines 351.1, 353.2, and 348.8 nm. E_{max} = 65 mJ was reached in a mixture $He/Xe/NF_3$ = 100/1/0.3 at p = 0.2 MPa. The XeF chemical laser cavity consisted of a total-reflection mirror and a mirror with 70% transparency. When KrF was used, the maximum energy obtained was 130 mJ. With an exit mirror having 50% transparency, the emission spectrum revealed a maximum of approximate width 0.3 nm in the vicinity of λ = 248.4 nm. When a high-Q cavity was used, lasing was observed also at λ = 248.1 nm. Replacement of F_2 with NF_3 decreased the pulse energy by two or three times.

A maximum lasing energy 60 mJ was reached in an ArF chemical laser at λ = 193.3 nm. The spectrum profile was approximately the same as with electron-beam pumping, but with better definition.

The lasing-pulse duration in all these three types of chemical laser was 20-25 nsec, and the pulse profiles were similar. The maximum emission power was 2-4 MW. It was found that the rate of decrease of the lasing energy was very small compared with the preionization rate, owing to the dissociative attachment, characterized by a value on the order of 10^9 sec^{-1}, of the electrons to the fluorine molecule. This means that the negative F^- ions are effective sources of negative charges.

Excimer chemical lasers on rare-gas halides are being steadily improved — lasing was obtained at increased pressures, in a quasicontinuous regime, in a closed-cycle system with photodissociation of molecules, in the so-called double discharge with stabilization by a beam of fast electrons, etc. Many properties of such chemical lasers, with references to the literature, were systematized in [70].

LITERATURE CITED

1. S. Solimeno, "Chemical lasers," Phys. Bull., Nov., 517-520 (1974).
2. N. G. Basov, L. E. Golubev, V. S. Zuev, et al., "Short-pulse iodine laser with 50-J energy and 5-msec duration," Kvantovaya Elektron. (Moscow), No. 6(18), 116 (1973).
3. G. Brederlow, W. Fuss, K. L. Kompa, et al., "60-J 1-nsec iodine laser," J. Appl. Phys., 46, No. 2, 808-809 (1975).
4. A. S. Antonov, I. M. Belousova, V. A. Gerasimov, et al., "Flashlamp-excited photodissociation laser," Pis'ma Zh. Tekh. Fiz., 4, No. 19, 1143-1145 (1978).
5. D. E. O'Brien and J. Bowen, "Parametric studies of the iodine photodissociation laser," J. Appl. Phys., 42, No. 3, 1010-1015 (1971).
6. J. V. V. Kasper, J. H. Parker, and G. C. Pimentel, "Iodine-atom laser emission in alkyl iodine photolysis," J. Chem. Phys., 43, No. 5, 1827-1828 (1965).
7. T. L. Andreeva, V. A. Dudkin, V. I. Malyshev, et al., "Gas laser excited by photodissociation," Zh. Eksp. Teor. Fiz., 49, 1408 (1965).
8. T. L. Andreeva et al., "Investigations of photodissociation iodine lasers containing bonds of the iodine atom with group-V elements. I. Experiments on the $(CF_3)_2AsI$ molecule," Kvantovaya Elektron. (Moscow), 3, No. 7(49), 1442-1456 (1976).
9. J. T. Knudtson and M. J. Berry, "Methyl isocyanide photodissociation chemical laser, determination of energy partitioning into the cyanide radical photochemical product," J. Chem. Phys., 68, No. 10, 4419-4430 (1978); G. A. West and M. J. Berry, "ICN photodissociation and predissociation: $CN^*(A^2\Pi_j)$ fluorescence excitation spectrum and CN^+-$(X^2\Sigma^+)$ chemical laser emission," Chem. Phys. Lett., 50, No. 3, 423-428 (1978).
10. J. V. V. Kasper and G. C. Pimentel, "HCl chemical lasers," Phys. Rev. Lett., 14, 352 (1965); V. I. Igoshin and A. N. Oraevskii, "Kinetics of hydrogen chloride chemical laser," Khim. Vys. Energ., 5, 397 (1971).
11. P. H. Corneil and G. C. Pimentel, "Hydrogen-chlorine explosion laser. II. DCl," J. Chem. Phys., 49, No. 3, 1379-1386 (1968).
12. J. C. Polanyi, "Vibrational—rotational population inversion," Appl. Opt. Suppl. 2, 109-127 (1965).
13. J. R. Airey, "A new pulsed IR chemical laser," IEEE J. Quantum Electron., QE-3, No. 5, 208 (1967).
14. J. R. Airey, "Cl + HBr pulsed chemical laser: a theoretical and experimental study," J. Chem. Phys., 52, No. 1, 156-157 (1970).
15. D. J. Spencer and C. Wittig, "Atomic bromine chemical laser," J. Opt. Soc. Am., 68, No. 5, 652 (1978).

16. J. C. Polanyi and D. C. Tardy, "Energy distribution in the exothermic reaction F + H_2 and the endothermic reaction HF + H*," J. Chem. Phys., 51, No. 12, 5717-5719 (1969).
17. J. N. Jonathan, C. M. Melliar-Smith and D. H. Slater, "Initial vibrational energy level populations resulting from the reaction H + F_2 as studied by infrared chemiluminescence," J. Chem. Phys., 53, No. 11, 4396-4397 (1970); J. C. Polanyi and K. B. Woodal, "Energy distribution among reaction products. VI. F + H_2, D_2," J. Chem. Phys., 57, No. 4, 1574-1586 (1972).
18. V. N. Kondrat'ev, Rate Constants of Gas-Phase Reactions [in Russian], Moscow, Nauka (1970).
19. K. L. Kompa and G. C.Pimentel, "Hydrofluoric acid chemical laser," J. Chem. Phys., 47, No. 2, 857-858 (1967).
20. K. L. Kompa, J. H. Parker, and G. C. Pimentel,, "UF_6—H_2 hydrogen fluoride chemical laser: Operation and chemistry," J. Chem. Phys., 49, No. 10, 4257-4264 (1968).
21. V. Ya. Agroskin et al., "Parametric analysis of pulsed H_2—F_2 laser," Kvantovaya Elektron. (Moscow), 3, No. 9, 1932-1939 (1976).
22. M. J. Berry, "A comparison of photolytic fluorine-atom sources for chemical laser studies," Chem. Phys. Lett., 15, No. 2, 269-273 (1972).
23. M. A. Pollak, "Laser oscillation in chemically formed CO," Appl. Phys. Lett., 8, No. 9, 237-238 (1966).
24. D. W. Gregg and S. J. Thomas, "Analysis of the CS_2—O_2 chemical laser showing new lines and selective excitation," J. Appl. Phys., 39, No. 9, 4399-4404 (1968).
25. C. K. N. Patel, "Vibrational—rotational laser action in carbon monoxide," Phys. Rev., 141, No. 1, 71-83 (1966).
26. E. B. Gordon, V. S. Pavlenko, Yu. L. Moskvin, et al., "Kinetics of chemical CO laser with photodissociation in hydrogen-sulfide oxidation," Zh. Eksp. Teor. Fiz., 63, No. 4, 1159-1172 (1972).
27. D. D. Davis, R. B. Klemm, and M. Pilling, "A flash photolysis—resonance fluorescence kinetics study of ground-state sulfur atoms. I. Absolute rate parameters for reaction of $S(^3P)$ with $O_2(^3\Sigma)$," Int. J. Chem. Kinetics, 4, No. 4, 367-394 (1972).
28. R. J. Donovan and D. J. Little, "The rate of the reaction $S(^3P_j)$ + O_2," Chem. Phys. Lett., 13, No. 5, 488-490 (1972).
29. E. B. Gordon et al., "Character of the effect of mixture pressure on generation of a pulsed carbon monoxide laser," Kvantovaya Elektron. (Moscow), 2, No. 2, 327-331 (1975).
30. R. W. F. Gross, "Chemically pumped CO_2 laser," J. Chem. Phys., 50, No. 7, 1889-1890 (1969).
31. R. W. F. Gross, N. Cohen and T. A. Jacobs, "HF chemical laser produced by flash photolysis of F_2O—H_2 mixtures," J. Chem. Phys., 48, No. 8, 3821-3822 (1968).
32. N. G. Basov, S. I. Zavorotnyi, E. P. Markin, et al., "Pulsed D_2 + F_2 + CO_2 + He chemical laser," Kvantovaya Elektron. (Moscow), 1, No. 3, 560-564 (1974).
33. L. V. Kulakov, A. I. Nikitin, and A. N. Oraevskii, "Investigation of the properties of a chemical laser with transfer of the excess energy from DF molecules to CO_2 molecules," Kvantovaya Elektron. (Moscow), 3, No. 8, 1677-1688 (1976).
34. N. G. Basov, A. S. Bashkin, P. G. Grigor'ev, et al., "Chemical DF—CO_2 quantum amplifier with high specific parameters," Kvantovaya Elektron., 3, No. 9, 2067-2069 (1976).
35. T. O. Pochler, M. Shandor and R. E. Walker, "High-pressure pulsed CO_2 chemical transfer laser," Appl. Phys. Lett., 20, No. 12, 487-499 (1972); T. O. Pochler, J. C. Pirkle Jr., and R. E. Walker, "A high pressure pulsed CO_2 chemical transfer laser," IEEE J. Quantum Electron., QE-9, No. 1, Part 2, 83-93 (1973).
36. N. F. Chebotarev and S. Ya. Pshezhetskii, "Features of DF—CO_2 energy transfer in chemical lasers based on chlorine fluorides," Kvantovaya Elektron. (Moscow), 6, No. 1, 231-235 (1979).
37. T. F. Deutsch, "Molecular laser action in hydrogen and deuterium halides," Appl. Phys. Lett., 10, No. 8, 234-236 (1967).
38. T. F. Deutsch, "New infrared laser transitions in HCl, HBr, DCl, and DBr," IEEE J. Quantum Electron., QE-3, No. 9, 419-421 (1967).
39. M. A. Kovacs and C. J. Ultee, "Visible laser action in fluorine," Appl. Phys. Lett., 17, No. 1, 39-40 (1970); W. Q. Jeffers and C. E. Wiswall, "Laser action in atomic fluorine based on collisional dissociation of HF," Appl. Phys. Lett., 17, No. 10, 444-447 (1970).
40. H. Oodate, M. Obara, and T. Fujioka, "Enhanced HBr chemical laser output with addition of SF_6," Appl. Phys. Lett., 24, No. 6, 272-274 (1974).

41. A. F. Zapol'skii and K. B. Yushko, "Electric-discharge SF_6—H_2 laser pumped from an inductive energy storage," Kvantovaya Elektron. (Moscow), 6, No. 2, 408-411 (1979).
42. S. W. Mayer, D. Taylor, and M. A. Kwok, "HF chemical lasing at higher vibrational levels," Appl. Phys. Lett., 23, No. 8, 434-436 (1973).
43. J. V. Parker and R. R. Stephens, "Pulsed HF chemical lasers with high electrical efficiency," Appl. Phys. Lett., 22, 450-452 (1973).
44. Gen. Inoue and Soji Tsuchiya, "Mechanism of transversely excited chemical HBr laser," Jpn. J. Appl. Phys., 13, No. 9, 1421-1428 (1974).
45. J. S. Whitter andl R. L. Kerber, "Performance of a HF chain-reaction laser with high initiation efficiency," IEEE J. Quantum Electron., QE-10, 844-847 (1974).
46. M. Obara and T. Fujioka, "Pulsed HF chemical laser from reactions of fluorine atoms with benzene, toluene, xylene, methanol and acetone," Jpn. J. Appl. Phys., 14, No. 8, 1183-1187 (1975).
47. V. L. Pan, C. E. Turner, and K. J. Pettipiece, "The characteristics of an electron-beam-initiated pulsed chemical laser," Chem. Phys. Lett., 10, No. 5, 577-579 (1971).
48. R. Aprahamian et al., "Pulsed electron-beam-initiated chemical laser operating on the H_2/F_2 chain reaction," Appl. Phys. Lett., 24, No. 5, 239-242 (1974).
49. J. A. Mangano, et al., "Efficient electrical initiation of an HF chemical laser," Appl. Phys. Lett., 27, No. 5, 293-295 (1975).
50. R. A. Gerber, et al., " Multikilojoule HF laser using intense-electron-beam initiation of H_2—F_2 mixtures," Appl. Phys. Lett., 25, No. 5, 281-283 (1974); R. A. Gerber and E. L. Patterson, "Studies of high-energy HF laser using an electron-beam-excited mixture of high-pressure F_2 and H_2" J. Appl. Phys., 47, No. 8, 3524-3529 (1976).
51. V. K. Baranov, Yu. N. Demidenko, K. F. Zelenskii, et al., "Chemical F_2—H_2 laser initiated by an electron beam," Kvantovaya Elektron. (Moscow), 5, No. 2, 415-417, 475 (1978).
52. R. Hofland et al., "Atmospheric-pressure H_2—F_2 laser initiated by electron-beam-irradiated discharge," J. Appl. Phys., 47, No. 10, 4543-4546 (1976).
53. A. G. Ponomarenko, R. I. Soloukhin, and Yu. I. Khapov, "Energy characteristics of chemical HF laser initiated by an electron beam," in: Gas Lasers [in Russian], Nauka, Novosibirsk (1977), pp. 105-111.
54. V. I. Igoshin, V. Yu. Nikitin, and A. N. Oraevskii, "Possibility of increasing the lasing quantum yield and the specific energy output of a chemical DF/CO_2-laser," Kratk. Soobshch. Fiz., No. 6, 20-25 (1978).
55. A. S. Bashkin, A. F. Konoshenko, A. N. Oraevskii, et al., "Effective chemical e-beam HF laser with high specific energy output," Kvantovaya Elektron. (Moscow), 5, No. 7, 1608-1610 (1978); A. S. Bashkin, A. F. Konoshenko, A. N. Oraevskii, et al., "Investigation of the energy characteristics of a chemical ClF—H_2 laser initiated by an electron beam," Kvantovaya Elektron. (Moscow), 5, No. 12, 2657-2659 (1978).
56. N. G. Basov, A. S. Bashkin, P. G. Grigoriev, et al., "Quantum chemical DF—CO_2 amplifier with high-power photoinitiation," Preprint of P. N. Lebedev Phys. Inst., 62, 1-12 (Moscow, 1976); G. C. Tisone and J. M. Hoffman, "Optical energy extraction from electron-beam-initiated H_2—F_2 mixtures," J. Appl. Phys., 47, No. 8, 3530-3532 (1976); N. G. Basov, A. S. Bashkin, L. E. Golubev, et al., "Investigation of the system HF—master oscillator—amplifier with chain fluorine—hydrogen reaction," Kvantovaya Elektron. (Moscow), 5, No. 4, 910-913 (1978).
57. J. E. Velazco and D. W. Setser, "Bound—free emission spectra of diatomic xenon halides," J. Chem. Phys., 62, No. 5, 1990-1991 (1975); C. A. Brau and J. J. Ewing, "Emission spectra of XeBr, XeCl, XeF, and KrF," J. Chem. Phys., 63, No. 11, 4640-4647 (1975); J. M. Hoffman, A. K. Hays, and G. C. Tisone, "High-power UV noble-gas-halide lasers," Appl. Phys. Lett., 28, No. 9, 538-539 (1976); N. G. Basov, A. N. Brunin, V. A. Danilychev, et al., "High-pressure KrF-molecule UV laser," Kvantovaya Elektron. (Moscow), 4, No. 7, 1595-1597 (1977); M. Rokni et al., "Rare gas fluoride lasers," IEEE J. Quantum Electron., 14, No. 7, 464-481 (1978); W. Shuntaro et al., "Efficient amplification of a discharge-pumped KrF laser," Appl. Phys. Lett. 33, No. 2, 141-143 (1978).
58. W. M. Hughes, N. T. Olson and R. Hunter, "Experiments on 558-nm argon oxide laser system," Appl. Phys. Lett., 28, No. 2, 81-83 (1976).
59. G. C. Tisone, A. K. Hays, and J. M. Hoffman, "Studies of rare-gas/halogen molecular lasers excited by an electron beam," in: Electron Transit. Lasers, Cambridge, Mass., London: MIT Press (1976), pp. 191-194.
60. E. R. Ault, R. S. Bradford, Jr., and M. L. Bhaumik, "High-power xenon fluoride lasers," Appl. Phys. Lett., 27, No. 7, 413-415 (1975).

61. N. G. Basov et al., "High pressure gas lasers on electronic transitions of molecules," Preprint No. 23, FIAN (1977); C. A. Brau and J. J. Ewing, "Spectroscopy, kinetics and performance of rare gas monohalide lasers," in: Electron Transit. Lasers, Cambridge, Mass., London, MIT Press (1976), pp. 195-198.
62. R. S. Bradford, Jr., E. R. Ault and M. L. Bhaumik, "Three efficient e-beam-pumped high-power lasers: XeF, Ar–I_2, and KrF," ibid., pp. 211-213.
63. A. V. Johnson, D. B. Gerardo, and R. E. Palmer, "Vacuum UV lasers on rare-gas dimers," Kvantovaya Elektron. (Moscow), 3, No. 4, 823-829 (1976).
64. S. K. Searles and G. A. Hart, "Stimulated emission at 281.8 nm from XeBr," Appl. Phys. Lett., 27, No. 4, 243-245 (1975).
65. H. T. Powell, J. R. Murray and C. K. Rhodes, "Laser oscillation on the green bands of XeO and KrO," Appl. Phys. Lett., 27, 730-732 (1974) [sic].
66. C. P. Wang, et al., "Fast-discharge-initiated XeF laser," Appl. Phys. Lett., 28, No. 6, 326-328 (1976).
67. Yu. A. Kudryavtsev and I. P. Kuz'mina, "Excimer UV gas-discharge XeF, XeCl, and KrF lasers," Kvantovaya Elektron. (Moscow), 4, No. 1, 220-222 (1977).
68. D. G. Sutton et al., "Fast-discharge-initiated KrF laser," Appl. Phys. Lett., 28, No. 9, 522-523 (1976).
69. R. Burnham and N. Djeu, "Ultraviolet-preionized discharge-pumped lasers in XeF, KrF, and ArF," Appl. Phys. Lett., 29, No. 11, 707-709 (1976).
70. I. N. Knyazev and V. S. Letokhov, "Gas lasers in the UV and far UV regions of the spectrum," in: Laser Handbook [in Russian], A. M. Prokhorov (ed.), Sov. Radio (1978), Vol. 1, 197-220; V. A. Danilychev, O. M. Kerimov, and I. B. Kovsh, "High-pressure molecular gas lasers," in: Science and Electrical Engineering Summaries, Radio Engineering, Vol. 12, VINITI (1979), p. 255; Excimer Lasers (ed. Ch. K. Rhodes), Springer-Verlag (1979).

CHAPTER 5

SUBSONIC CHEMICAL LASERS

5.1. Chemical Lasers with Continuous Flow of Premixed Components

The static gas chemical lasers described in Chap. 4 include units for replacing the spent medium with fresh components. If the replacement of the reagents and of the reaction products is carried out at the necessary rate continuously, a quasistationary or stationary level of generation can be ensured. We consider a laser with subsonic continuous flow and the features of its operation.

To realize the quasicontinuous lasing regime, particularly in HF chemical lasers, it is necessary to rapidly replace the active medium within a time contained in the interval between the pulses. Then the pulse evolves in a medium that does not contain HF, thus decreasing the relaxation rate to a permissibly low level. At an optimal choice of the laser parameters (geometry and flow rate) it is possible to attain a pulse repetition rate up to 100/sec [1]. In a number of papers (e.g., [2, 3]) similar HF chemical lasers are described, but with lower repetition frequencies.

Several reactions result in vibrationally excited HF, e.g., reaction between atomic fluorine and molecular hydrogen. Atomic fluorine is obtained quite simply from SF_6, a stable nontoxic gas. There are also other possibilities: CF_4, freon, and inorganic fluorine containing compounds NF_3 and N_2F_4. However, SF_6 is preferable from safety considerations.

A mixture of SF_6 gas with H_2 is subjected to the action of a discharge that decomposes the SF_6 mainly into SF_4 and F, although free sulfur is also released. The fluorine reacts next with H_2:

$$\left.\begin{aligned} &SF_6 \rightarrow SF_4 + 2F, \\ &F + H_2 \rightarrow HF(v = 2, 1, 0) + H. \end{aligned}\right\} \qquad (5.1)$$

In this reaction HF is initially produced in the state v = 2 [4, 5], so that inversion takes place.

Other reactions, e.g., with participation of H atoms, differ in having a very high activation energy, or require ternary collisions, which makes them too slow for the process considered. The reaction products are small amounts of SF_4 and HF, mixed with a large amount of SF_6 and He, the latter added to increase the heat capacity and to maintain a stable discharge. Usual laboratory pumps can readily cope with pumping the gases that take part in the reaction.

The construction of such a chemical laser is shown schematically in Fig. 5.1, where all the junctions are standard vacuum units, thereby avoiding the need of using glass–metal seals. The dimensions indicated in Fig. 5.1 are the results of optimization with respect to stability, repetition frequency, spectral range, and output power. In particular, the small diameter of the discharge capillary leads to a good reproducibility of the discharge pulses. To realize a single-frequency regime, one of the cavity mirrors was replaced by a diffraction grating. The discharge was produced by a capacitor connected to a transformer. The basic experiments were performed at a pulse energy 0.06 J, and increasing this energy to 0.2 J did not significantly influence the characteristics of the chemical laser. The growth time of a 0.75 A current pulse was approximately 0.1 μsec.

The initial measurements were performed in a multifrequency variant. The output radiation was registered with a spectrometer which measured the averaged output power. The spectrum usually included the lines $\mathcal{P}_{1-0}(2)$-$\mathcal{P}_{1-0}(17)$, $\mathcal{P}_{2-1}(2)$-$\mathcal{P}_{2-1}(9)$ and $\mathcal{P}_{3-2}(4)$-$\mathcal{P}_{3-2}(5)$ (this transition manifests itself weaker than the two preceding ones). The distribution over the spectrum did not change substantially when the composition was varied and the resonator adjusted, so long as $SF_6/H_2/He$ mixtures were used. The average output power under such conditions was approximately 20 mW.

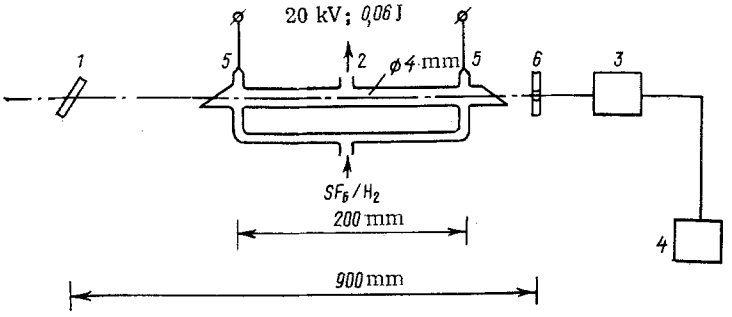

Fig. 5.1. Diagram of simplest continuous-flow chemical laser: 1) diffraction grating; 2) vacuum; 3) receiver; 4) recording apparatus; 5) electrodes; 6) mirror.

In the investigation of chemical lasers in the selective variant, i.e., with a grating in place of a mirror, the total output power turned out to be lower. The lowering of the output power was observed on the 1—0 transition, and was probably due to the absence of pumping from the 2—1 transition.

After a current pulse with delay 0.15-2.0 μsec, 21 transition lines were observed. The transition 0—1 has a delay of 0.4-0.5 μsec. Good reproducibility of the output radiation pulses was observed. Their repetition frequency depends on the rate of replenishment of the gas in the discharge. At a flow rate 0.021 cm^3/min, repetition frequencies of 100 and 40 pulses/sec were obtained for the 2—1 and 0—1 transitions, respectively.

In addition to HF, it was possible to use CO in the described chemical-laser variant, with the less toxic mixture CS_2/O_2. The modifications consisted in this case of replacement of the NaCl Brewster plates by sapphire plates and of the Irtran window by a gold-coated mirror having a curvature radius 10 m and a central opening 1.5 mm. In addition, the oil in the pump was replaced by silicone, which resists oxidation. Since the mixture CS_2/OD_2 is explosive, the experiments were performed at low pressures. The total power obtained was 3.5 mW, distributed among 65 lines of vibrational transitions from $v = 13 \rightarrow 12$ to $v = 5 \rightarrow 4$. The lasing pulses of 0.5 msec duration were delayed relative to the current by 0.1-0.2 msec, apparently as a result of the slower rates of the reaction and of the relaxation of the CO system.

The possibilities of experimental realization of lasers in both the pulsed and continuous regime, using CO molecules obtained in the excited state in the course of various chemical reactions, are noted in a considerable number of papers (see [6-19]).

In [13] is described a CO chemical laser with longitudinal flow and with longitudinal discharge. The construction is shown in Fig. 5.2. The gas was injected from the ends of tube 1 and evacuated from its center with a pump having a delivery 180 m^3/h. The chemical laser operated in regimes with "internal" and "external" discharges. In the former case the continuous discharge was ignited between electrodes 5 and 6 and between the symmetrical electrodes 5' and 6'. The chemical laser operated on a mixture of O_2 with CS_2 [see the reactions (4.11)], with or without He or CO as an additive. Lasing was obtained on R—V transitions from the vibrational levels of CO, which have v from 13 to 7.

Experiments have shown that addition of He greatly increases the power of this chemical laser, from 0.8 to 2.3 W. Besides possibly facilitating the dissociation of the O_2 and preventing recombination of the oxygen atoms, the addition of He increases the rate of exchange of the mixture in the system. Thus, it was noted in [13] that when He is added the pressure in the working tube increases and the flow in the pumped-out system increases. Addition of CO turned out to have an insignificant effect. If this gas was added without helium, the power increased only insignificantly.

In the case of an external discharge, the continuous discharge was produced in the tubes that supplied the O_2 and He. The O_2 and He were not excited by the discharge in this case between the electrodes 5, 7, and 5', 7', so that the instant of formation of the atomic oxygen was delayed somewhat relative to the instant of the mixing with CS_2. The highest chemical-laser power in this case, 0.35 W, was obtained at flow rates (mmole/sec): O_2 — 1.34; He — 36.8; CS_2 — 27.4; CO — 0.9. The construction of another chemical laser with longitudinal

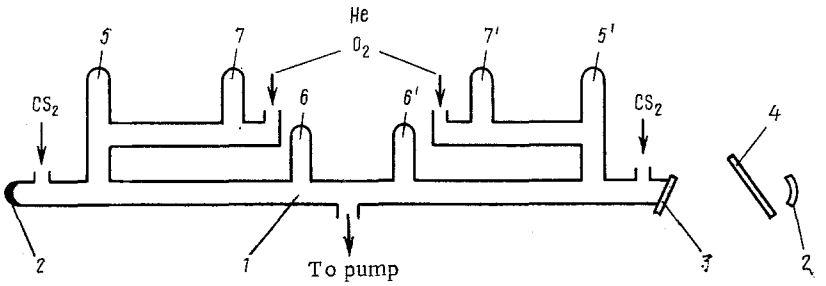

Fig. 5.2. Diagram of CO chemical laser with longitudinal flow and longitudinal discharge: 1) working tube; 2) spherical mirrors of cavity; 3) NaCl Brewster window; 4) plane-parallel NaCl plate; 5, 6, 7 (5', 6', 7') — electrodes.

pumping, but with transverse discharge, is shown in Fig. 5.3 [14], where a cylindrical working tube similar to those shown in Figs. 5.1 and 5.2, with a longitudinal optical cavity and with provision for entry and evacuation of the gas mixture, was equipped with transverse-discharge electrodes. The reactions were initiated by discharging a capacitor of 0.02 μF charged to 20 kV through a chain of resistors (each ~100 Ω). This chemical laser operated both in the gas static regime and with continuous flow of the mixture.

Figure 5.4 shows the data obtained on the dependence of the lasing energy on the mixture pressure. The ordinates represent the lasing pulse energy in relative units, divided by the CS_2 concentration. The maximum pulse energy in the absence of a diluent (curve 1) was reached at a pressure 2.66 kPa. The CS_2/O_2 concentration ratio was 2/25, and it is precisely at this ratio that the highest energy was generated. If He or N_2 was added to such a mixture, starting with a pressure 1.33 kPa, a considerable increase of the generated radiation was observed (curves 3 and 2, respectively). The maximum energy E of the generated radiation, 26 mJ, was reached in a mixture with helium at a pressure 4 kPa. The peak power was determined under the assumption that the laser pulse has a triangular shape. In a mixture with helium, at a pressure 4 kPa, the peak power obtained was 1 kW. Under these conditions, the pulse duration was ~40 μsec and decreased with increasing pressure.

The wavelengths of the lasing transitions lie in the range 4.7-5.7 μm. Spectral measurements were carried out at a constant flow of the $CS_2/O_2/N_2$ = 2/25/50 mixture at a pressure 4 kPa and a pulse repetition frequency 2 Hz. A total of 79 lines were registered and identified as transitions of the $\mathcal{P}$ branch when the vibrational numbers changed from v = 13 → v = 12 to v = 2 → v = 1. A definite sequence in the line emission was observed, and is explained by cascade transitions.

There are two possible mechanisms of producing inverted population when the burning of the mixture is initiated by an electric spark. In the first it is assumed that simultaneous dissociation of both oxygen and carbon disulfide is possible, followed by direct formation of the excited CO molecules, i.e.,

$$CS_2 = CS + S; \tag{5.2}$$

$$O_2 = 2O; \tag{5.3}$$

$$CS + O = CO^* + S\ (-313\ \text{kJ/mole}). \tag{5.4}$$

If the inversion is obtained as a result of a chain reaction of combustion initiated by a spark, another possibility is the following system of reactions:

$$O + CS_2 = CS + SO; \tag{5.5}$$

$$CS + O = CO^* + S\ (-313\ \text{kJ/mole}); \tag{5.4}$$

$$CS + O_2 = CO^* + SO\ (-339\ \text{kJ/mole}); \tag{5.4a}$$

$$S + O_2 = SO + O. \tag{5.6}$$

If photodissociation is used to initiate the reactions, it is possible to obtain the same initial concentration of the oxygen atom as in an electric discharge. In an electric discharge it is possible to obtain sufficiently large concentrations of oxygen atoms and CS radicals so that the principal role is played by the reaction (5.4), whereas in photodissociation the principal role is played by the reaction (5.4a).

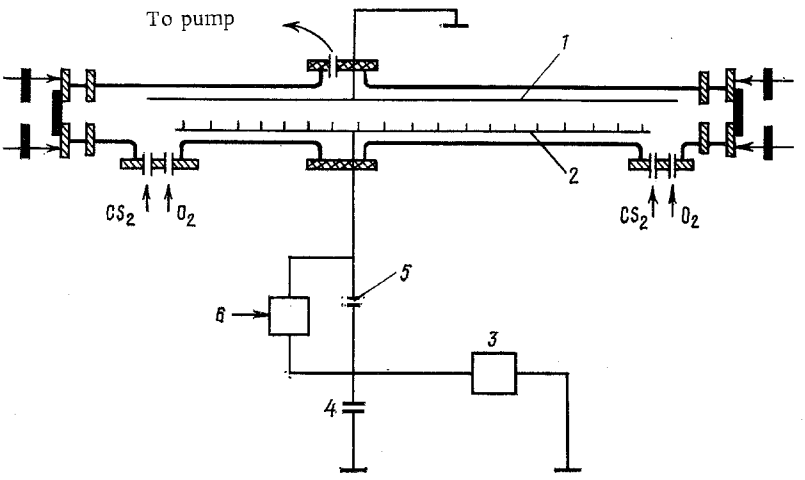

Fig. 5.3. Diagram of chemical laser with longitudinal pumping and transverse discharge: 1) cathode; 2) anode with chain of resistors; 3) supply source; 4) capacitor; 5) electric discharger; 6) trigger.

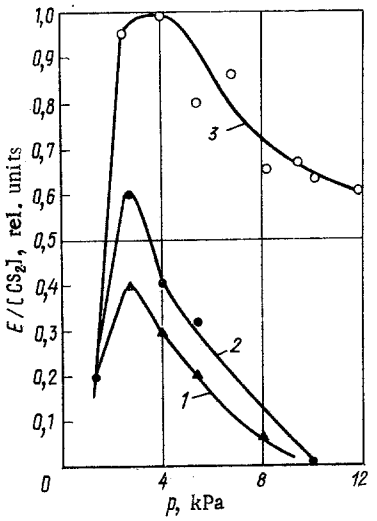

Fig. 5.4. Dependence of the energy of the generated radiation on the mixture pressure (C = 0.2 μF, V = 20 kV, CS_2/O_2 = 2/25): 1) CS_2/O_2; 2) $CS_2/O_2/N_2$; 3) CS_2/O_2/He.

That chain reactions are promising for chemical lasers was indicated in [20, 21], and the kinetic scheme of such reactions is given in [22]. Lasing with components H_2 and F_2 was first obtained in [23], with the chain reaction initiated by electric discharge. Such a reaction was realized in [24] with both a discharge and a photopulse, and was subsequently investigated in [25-28]. The study of the characteristics of HF chemical lasers excited by a pulsed CO_2 laser was carried out, e.g., in [29].

Typical lasers based on a branched chain reaction are possible using the components ClF or ClF_3 with H_2 or CH_4 [30]. Each of these fluorine compounds produces, upon photodissociation, a fluorine atom. The presence of the fluorine atom offers additional advantages. Even more valuable is the fact that it is possible, in principle, to amplify the radiation on the basis of a branched chain reaction in the system with ClF_3.

However, the indicated initial substances react at room temperature with H_2 and CH_4, so that preliminary mixing of the initial substances followed by photoinitiation is impossible under ordinary conditions. This difficulty is eliminated in a continuous-flow system, in which the time of spontaneous development of the reaction after the mixing is reduced to a minimum. To decrease this time, the components are carefully rid of impurities, especially

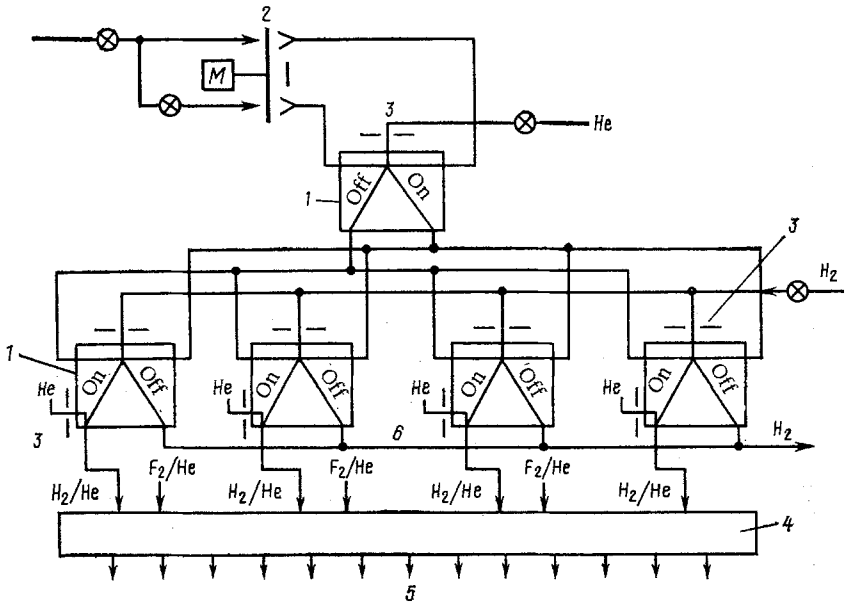

Fig. 5.5. High-speed gas-admission system: 1) two-position liquid regulator; 2) chopper; 3) sonic nozzles; 4) mixing chamber; 5) exit to cavity; 6) exhaust of H_2.

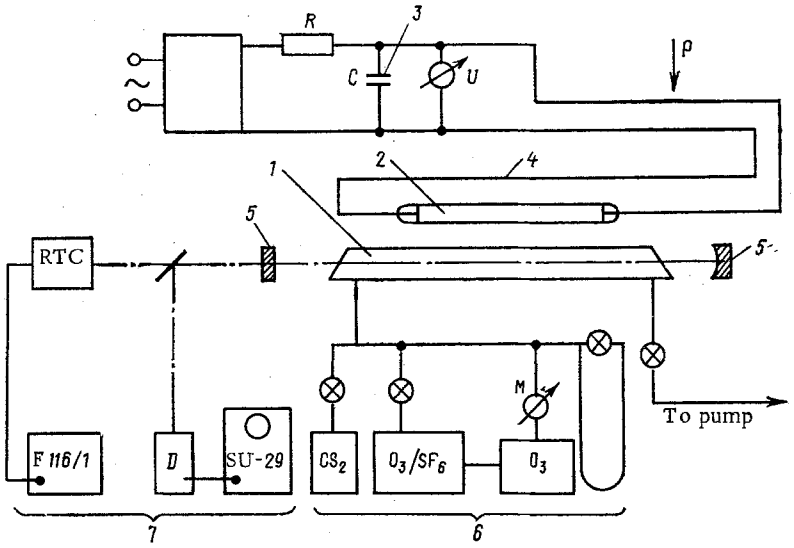

Fig. 5.6. Setup for the investigation of the energy characteristics of chemical lasers: 1) working tube; 2) photoinitiating lamp; 3) electric storage bank; 4) network of oppositely directed wires; 5) mirrors; 6) component supply system; 7) measurement system.

of HF. Contact between the reagent and glass is prevented, and stainless steel, copper, or brass is used in the construction, with prior conditioning at a ClF_3 pressure of 33.3 kPa for several hours. In view of the high chemical activity of ClF and ClF_3, the reacting gases were admitted into the working tube through separate ports, and a continuous flow (about 100 μmole/sec) was maintained.

In addition, both reacting gas mixtures were cooled before the mixing by being passed through stainless-steel cooling coils located directly ahead of the entrance to the tube.

In [30], lasing on HF was obtained in all systems, but stimulated emission with HCl was obtained only for the mixtures ClF/H_2 and ClF_3/H_2.

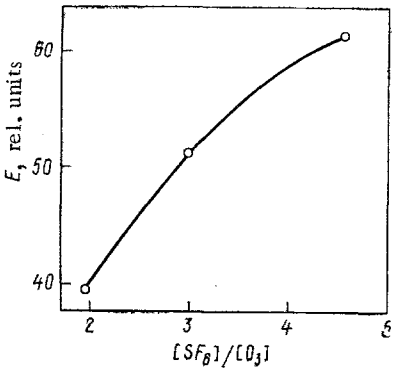

Fig. 5.7

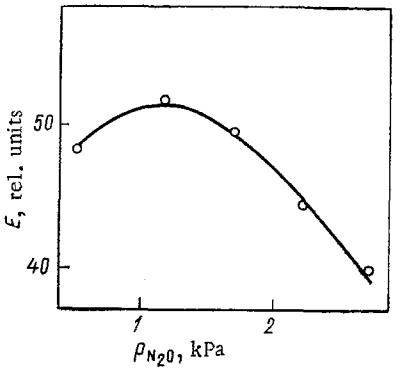

Fig. 5.8

Fig. 5.7. Influence of relative flow rate of sulfur hexafluoride on the lasing energy [pressure: CS_2 — 0.8; O_3 — 1.33; N_2O — 1.6 kPa; pumping; energy 2 kJ].

Fig. 5.8. Dependence of the energy of the generated radiation on the N_2O pressure [pressure: CS_2 — 0.53; O_3 — 0.93; SF_6 — 4.66 kPa].

Quasicontinuous chemical lasers can also operate with premixed components H_2 and F_2 with a rapidly operating system for periodic admission of the gas. Thus, in [31] the initial mixture that enters again into the cavity volume is kept from being ignited by contact with the already reacted volume of gas by the fact that a buffer zone was produced, made up of nonreacting gas between the reacting volume of the gas and the fresh mixture. This was ensured by a supply system in which the flow of the H_2 was interrupted for a short time while the F_2 and He were fed continuously.

The diagram of such a system is shown in Fig. 5.5. It is based on two-position liquid regulators 1, which have no moving parts and operate at a speed of 1 msec, using a jet coming from a chopper in the form of a rotating disk 2.

The gases H_2 and He enter the regulators 1 through sonic nozzles 3. The components enter the mixing chamber 4 and from them into the region of the cavity 5. The chopper controls both the regulators 1 and the turning on of the flash lamp that initiates the reaction. Monitoring the time dependence of the process in the cavity volume with a photomultiplier has demonstrated the reliable operation of such a supply system.

Another chemical laser with flow of the premixed components is one using the mixture CS_2/O_3 [32]. In such a mixture, the reagents are prematurely exhausted in the course of the dark reaction, so that the laser is made to operate in the continuous-flow regime. A diagram of the setup used to study the energy characteristics of the radiation of a CO chemical laser using a CS_2/O_3 mixture is shown in Fig. 5.6. The quartz working tube 1 (length 1 m, inside diameter 12 mm) was equipped with CaF_2 windows oriented at the Brewster angle. Two parallel-connected IFP-20,000 xenon flash lamps 2 (the figure shows only one) with reduced xenon pressure (1.33-2.66 kPa) were fed from a capacitor 3 (15 μF, 25 kV, 4.7 kJ). To lower the inductance of the electric circuit, the power was fed through bus bars and the lamps were connected to two oppositely directed leads 4. This made it possible to increase the maximum power input to lamp 2. Two mirrors, one of which had a curvature radius 5 m and a dense gold coating, made up a cavity of length 2 m. The second flat mirror was interchangeable in order to vary the reflection coefficient. The results were recorded with a photoresistor and a radiation thermocouple in the measurement circuit 7.

When carbon disulfide and pure ozone were used, lasing was observed only at a low pressure of the components. Increasing the pressure caused the mixture to explode in the tube and stopped the lasing. Dilution of the mixture with argon or helium increased the heat capacity of the mixture and slowed down the consumption of the ozone in darkness. Addition of a diluent with higher heat capacity than inert gases, e.g., sulfur hexafluoride, makes it possible to obtain considerably higher output energies (Fig. 5.7), and further increase of the SF_6 pressure improved the lasing. Addition of nitrous oxide increased the output energy by 1.5 times (Fig. 5.8). Addition of CO and OCS led, on the contrary, to a deterioration of the lasing [32].

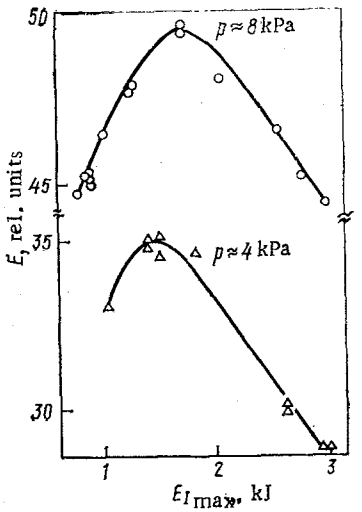

Fig. 5.9. Dependence of the lasing energy on the pump energy. Mixture composition: $CS_2/O_3/N_2O/SF_6$ = 3/5/6/15.

The operating regime of the chemical laser was optimized by using the influence of the initiation energy $E_{I\ max}$ on its output energy E. Figure 5.9 shows plots obtained for two values of the working-mixture pressure. They have a clearly pronounced maximum. The optimal initiation energy increases with increasing pressure.

The investigated CS_2/O_3 mixture chemical laser is not inferior with respect to energy delivery to the electron-ionization lasers using CO, operating at room temperature, and exceed by one order of magnitude the latter in efficiency relative to the input energy [33]. When this mixture is used in a continuous CO chemical laser, the difficulties connected with the metastable character of the CS_2/O_3 mixture are avoided. When proper flow velocity of the reagents is ensured, such a chemical laser can produce an output of power from a transverse cross section of the stream up to 45 W/cm^2. The efficiency of the system is determined in this case only by the efficiency of the pump lamps and can reach 1% [32].

5.2. Chemical Laser with Subsonic Mixing of the Components

Purely Chemical Subsonic Lasers. A laser is called purely chemical if the quantum mechanical excitation and the lasing are produced in it only by chemical reactions without any external energy sources, i.e., even without preliminary external initiation of the reaction. In such a laser the process is so rapid that it competes successfully with the relaxation that quenches the excited molecules produced in the course of the reaction. The production of these molecules is possible in exchange reactions of the atoms or radicals with the molecules. However, to obtain reagents in the atomic state in the course of one act it is necessary to expend additional energy and consequently this is unprofitable energywise. Therefore, a reaction is used with a long chain of the type $H_2 + F_2$, and the atoms or radicals are used as the priming components.

A purely chemical cw laser was first produced in [34, 35] with quasiresonant transfer of vibrational energy from the excited molecules produced at the reaction to the cold working molecules [36], and without external excitation sources [37]. The quantum-mechanical lasing effect is obtained, e.g., in the course of a chain reaction of deuterium and fluorine with transfer of the vibrational quanta from the excited molecules of the deuterium fluoride to the CO_2 molecules [38]; a scheme of this process for the case of photoinitiation of the reaction was considered in Sec. 4.1. It is precisely this reaction which has the advantage that a long optical chain is realized in it. The priming component in this case is NO. The sequence of the reactions in such a chain when the reagents enter for mixing into a subsonic flow is shown in Fig. 5.10.

The actual mechanism of inversion production is determined to a great degree by the exchange of vibrational energy between the molecules and the subsequent redistribution of the energy over the vibrational levels. For example, vibrational excitation of the HF molecules

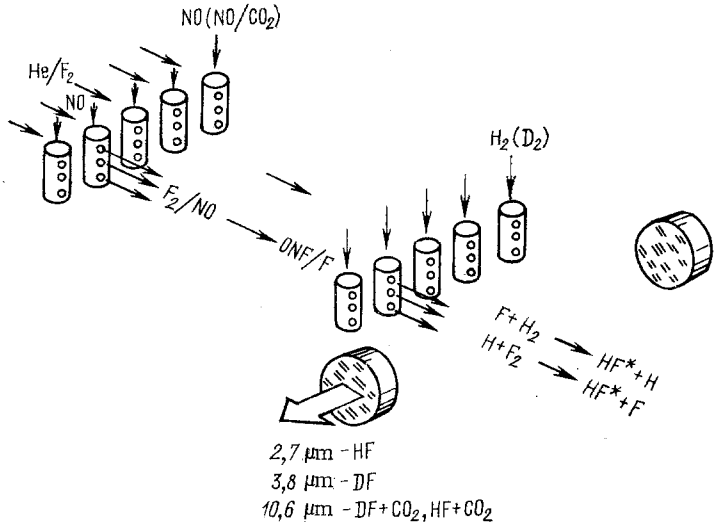

Fig. 5.10. Entry of the reagents in a pure chemical laser with transverse pumping.

produced in the reaction

$$F + H_2 \rightarrow HF\ (v = n) + H, \tag{5.7}$$

where n = 1, 2, or 3, is very rapidly redistributed among many levels by almost resonant vibrational-quantum exchange processes:

$$HF\ (v = n) + HF\ (v = m) \rightarrow HF\ (v = n - 1) + HF\ (v = m + 1). \tag{5.8}$$

The relative rate of the processes (5.7) and (5.8) governs the possibility of lasing on the HF molecules in the 2.7-μm region as a result of total or partial inversion. It also governs the following laser characteristics: the V–R lasing spectrum, the radiation power, the gain, and the chemical efficiency. In addition, the vibrational excitation of the HF molecule by the reaction (5.7) can lead to total inversion of the CO_2 and to onset of lasing at 10.6 μm as a result of the processes

$$\left.\begin{aligned} &HF\,(v=n)+CO_2\,(00^0\,0)\rightarrow HF\,(v=n-1)+CO_2\,(10^0\,1);\\ &CO_2\,(10^0\,1)+CO_2\,(00^0\,0)\rightarrow CO_2\,(10^0\,0)+CO_2\,(00^0\,1). \end{aligned}\right\} \tag{5.9}$$

The principal reactions when deuterium is used are [39]:

$$F_2 + NO \rightarrow ONF + F \quad (-75{,}2 \text{ kJ/mole}); \tag{5.10}$$

$$F + NO \rightarrow ONF\ (-238 \text{ kJ/mole}); \tag{5.11}$$

$$F + D_2 \rightarrow DF\ (v = n) + D\ (-129{,}5 \text{ kJ/mole}); \tag{5.12}$$

$$D + F_2 \rightarrow DF\ (v = n) + F\ (-414 \text{ kJ/mole}); \tag{5.13}$$

$$D + ONF \rightarrow DF\ (v = n) + NO\ (-326 \text{ kJ/mole}); \tag{5.14}$$

$$DF\ (v = n) + DF\ (v = m) \rightleftarrows DF\ (v = n - 1) + DF\ (v = m + 1); \tag{5.15}$$

$$DF\ (v = n) + M \rightleftarrows DF\ (v = n - 1) + M; \tag{5.16}$$

$$DF\ (v = n) + CO_2\ (00^00) \rightleftarrows DF\ (v = n - 1) + CO_2\ (00^0\,1); \tag{5.17}$$

$$CO_2\ (00^01) + M \rightleftarrows CO_2\ (nm^l\,0) + M; \tag{5.18}$$

$$CO_2\ (10^00) + CO_2\ (00^0\,0) \rightleftarrows 2CO_2\ (01^10); \tag{5.19}$$

$$CO_2\ (01^1\,0) + M \rightleftarrows CO_2\ (00^00) + M, \tag{5.20}$$

where M = DF, NO, He, F_2, D_2, ONF, CO_2, F or D. If the deuterium is replaced by hydrogen, Eq. (5.17) should be replaced by (5.9).

To illustrate the manner in which the energy is transferred from the vibrationally excited HCl, HF, DF, HI or HBr to CO_2 ($00^\circ 1$), Fig. 5.11 shows a diagram of the vibrational levels of these molecules. In the left-hand part of the diagram are shown the levels ($00^\circ 0$), ($00^\circ 1$), ($10^\circ 1$) and ($02^\circ 1$) of CO_2. In the right-hand side are shown the energies corresponding to V–R transitions of DF (very close to HCl) and HF in the bands $1 \to 0$, $2 \to 1$, $3 \to 2$, and $4 \to 3$. For the assumed values of the vibrational and rotational temperatures, Fig. 5.11 shows qualitatively the relative distribution of the molecules over the V–R states as a function of the resonance defects, whose values are indicated for the $1 \to 0$ band.

The construction of a chemical laser operating on the reactions (5.10)-(5.20) under transverse flow conditions [38] is illustrated in Fig. 5.12.

Such a laser operates in the following manner. The premixed F_2 with He and NO with CO_2 are fed into the upper part of the flow channel 11 with cross section 1×15 cm through two sets of gas-mixing injector tubes 1, 2. The gases flow into the tubes through lines secured in the upper part of the channel 11. The gases are rapidly mixed (within approximately 50 μsec) and the required initial concentration of the F atoms is subsequently established in the stream as a result of reactions (5.10), (5.11). Deuterium or hydrogen is injected into the flow from tubes 3, which are analogous to the tubes in the first two rows of the injectors, except that the gas from tubes 3 emerges at a right angle to the flow through openings arranged in checkerboard fashion.

A five-pass optical resonator with axis directed across the stream ensures selection and extraction of the energy from a region located at a distance of 0.5–6 cm from the injectors 3. To eliminate the possibility of parasitic lasing directly via the two flat mirrors 6 and 7, these mirrors are slightly misaligned. Streams of dry nitrogen are directed along the side walls of channel 11 to protect the mirrors against contact with the chemically active components of the stream. To employ the outer spherical mirrors, NaCl Brewster angles are used. All the mirrors are cooled with water. The total-reflection mirrors, which are not intended for transmission of radiation, have metal-dielectric coatings with reflection coefficient 99.4%. The output mirrors are made on a Ge substrate 3 mm thick and have a dielectric coating and a reflectivity from 10 to 50%. The optical path between the mirrors of 10 m radius (see Fig. 5.12) is 1.8 m.

The actual construction of the described chemical-laser scheme calls for study of the mutual relations between the various parameters and their optimization. Thus, the choice of the evacuation system is connected with the optimal pressure in the resonator, the chemical efficiency is connected with the per-unit flow of the reagents, and the dimensions of the laser are connected with the optimization of the construction and the composition of the working gas mixture. For example, it is desirable to ensure as high a pressure in the cavity as possible, to simplify the construction of the evacuation system. Increasing the chemical efficiency entails a decrease of the flow of reagents per unit radiation power. Optimization of the composition and of the mixture-flow velocity to reach maximum power makes it possible to decrease the dimensions of the cavity and of the entire chemical laser.

Thus, Fig. 5.13 shows a typical dependence of the output lasing power W on the mixture pressure p_c in the cavity [40]. The change of the output power with changing total pressure of the mixture in the cavity depends here on the molar concentration of the radicals NO introduced into the mixture. It can be seen that the optimal total pressure of the reagents in the resonator, corresponding to the maximum lasing power, depends on the NO concentration. Increasing the mixture pressure leads to a lowering of the molar concentration of NO in inverse proportion to p_c^2. Figure. 5.13 also shows the existence of an optimal mixture pressure (2.26 kPa) and of an optimal flow of NO (7 mmole/sec), which ensure a maximum output power of the generated radiation.

The character of the distribution in the x direction downstream, starting with the injector of H_2 (D_2), of the relative population n_v/n of the upper level of $CO_2(00^\circ 1)$ in the resonator region x_c and behind this region is shown in Fig. 5.14. Increasing the NO flow velocity accelerated the chain reaction and caused an amplification of the intensity of the radiation at 4.3 μm, and caused a decrease of the distance x_p to the peak of the relative population and accordingly of the maximum of the radiation intensity.

We present by way of example certain data on the lasing powers W and chemical efficiencies η_c of subsonic purely chemical lasers with transverse pumping (Table 5.1).

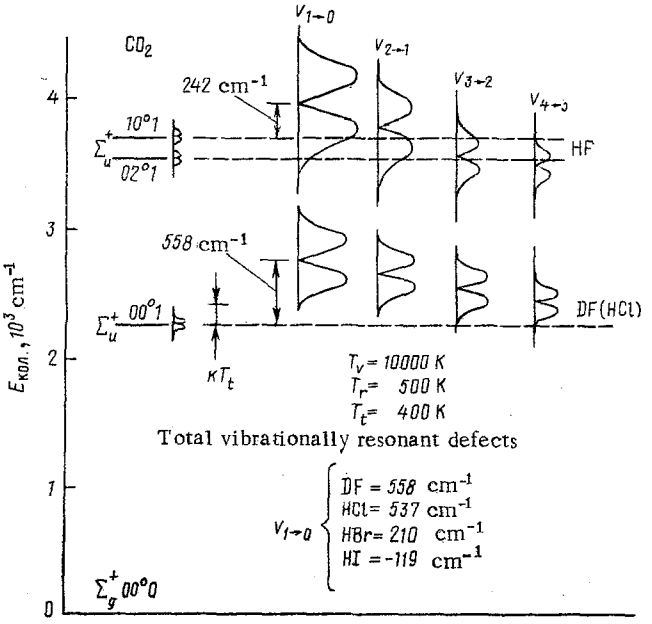

Fig. 5.11. Diagram of vibrational levels of CO_2 in hydrogen halides.

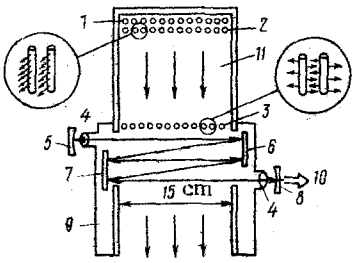

Fig. 5.12. Diagram of subsonic chemical laser with mixing of the reagents and energy transfer: 1) injectors of F_2 in He; 2) CO_2 and NO injectors; 3) D_2 or H_2 injectors; 4) NaCl Brewster windows; 5) spherical mirror (curvature radius 10 m); 6, 7) flat mirrors; 8) semitransparent spherical mirror (curvature radius 10 m); 9) compartment for blowing nitrogen around the mirrors; 10) output radiation of chemical laser; 11) flow channel.

Subsonic purely chemical lasers were also developed with longitudinal pumping [42, 43]. A schematic diagram of such chemical lasers is shown in Fig. 5.15 [43]. The reactions (5.12), (5.13) and (5.17) were produced in a teflon tube 1. Tube length as 150 mm, and the inside diameter 8 mm. The reaction (5.10) took place in a $He/F_2/NO$ stream in a copper supply tube 2 over a section 35 cm long, and the produced gas mixture was fed to the end section of reactor 3. To introduce the gas mixture CO_2/D_2, supply tube 4 was used. This mixture was injected into the reaction volume through a number of openings distributed over the perimeter near the end section 3 of the teflon tube 1. The semiconfocal resonator was made up of gold-coated mirror 5. The generated radiation was extracted from the side of a flat mirror through an opening of 1 mm diameter. The pressure at the entrance to the reaction volume under the experimental conditions was 2-2.66 kPa. To ensure a sufficient flow velocity of the gas mixture through the reaction tube 1, the latter was connected to the ballast volume by a large-diameter tube 6. This ensured an average flow velocity of ~200 m/sec.

The working-component mixture flow rates (mmole/sec) that are optimal from the point of view of the radiation power were found in experiment [43] to be: NO — 0.04; F_2 ~ 0.45; D_2 — 0.37; CO_2 — 1.65; He — 5.07. Figure 5.16 shows the dependences of the power of a cw chemical laser with longitudinal flow on the gas flow rate. Since the output power of a purely chemical cw laser depends significantly on the rate of mixing of the initial reagents, the changes

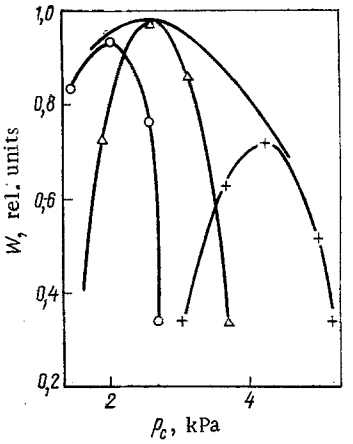

Fig. 5.13. Dependence of the relative output power of a subsonic chemical laser with energy transfer ($DF - CO_2$) on the static pressure in the resonator p_c at different flow rates of NO, mole/sec: ○) 0.011; Δ) 0.007; +) 0.002. The envelope curve shows the change of the lasing power with changing pressure in the cavity at the optimal NO concentration.

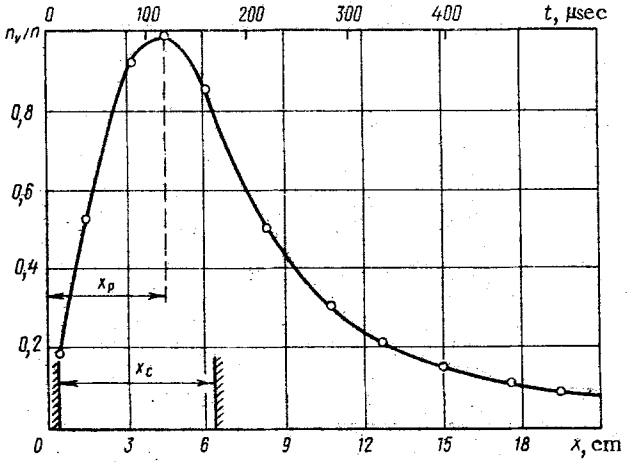

Fig. 5.14. Distribution, along the x axis, of the relative population n_v/n of the upper level of CO_2 (00°1).

TABLE 5.1. Values of W and η_c According to Data from Various Sources

Parameter	Reference		
	[40]	[38]	[41]
W, Watts	560	160	19
η_c, %	4	4,6	4,2

of the reagent-mixing conditions were realized in [43] by decreasing the diameter of the injection openings. Thus, at an opening diameter d = 1 mm the pressure drop between the injected medium and the reaction volume was Δp = 1.33-2 kPa, and at d = 0.35 mm and at the same gas consumption Δp ~ 0.1 MPa. A decrease in the opening diameter increased the velocity of the injected jets, i.e., improved the component-mixing conditions. The improvement of the mixing conditons at d = 0.35 mm increased the cw power by approximately 4 times to 2.1 W.

Electric-Discharge Subsonic Chemical Lasers. The increase in the cw radiation power as a result of chemical reactions excited by electric discharge was first obtained in reactions of the exchange type [44]. The reaction took place in an H_2–halogen mixture, and under low pressures (1.33-0.13 Pa) vibrationally excited molecules of hydrogen halides were generated:

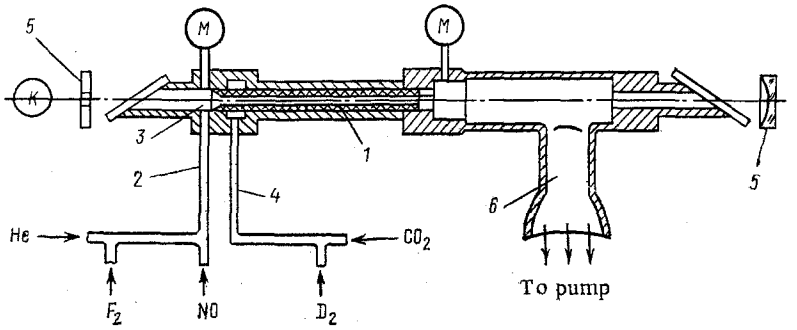

Fig. 5.15. Purely chemical laser with longitudinal flow: 1) working tube (reactor); 2) entrance of $He/F_2/NO$ mixture; 3) end section of reactor; 4) entrance of CO_2/D_2 mixture; 5) mirrors; 6) branch pipe.

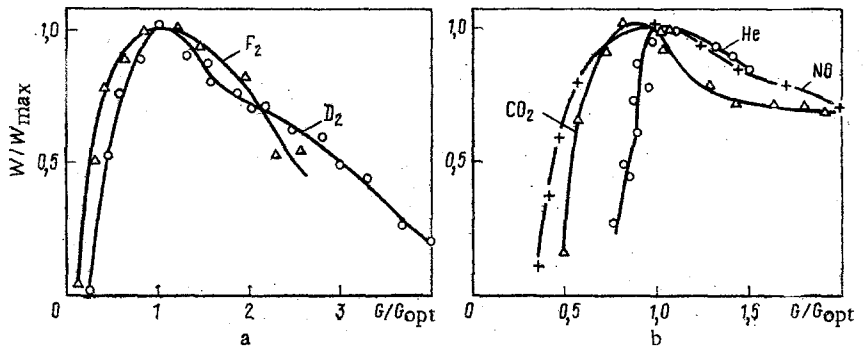

Fig. 5.16. Dependences of the power of a continuous chemical laser on the consumption of the gas reagents: a) reactions (5.12), (5.13); b) reactions (5.11), (5.17), (5.18).

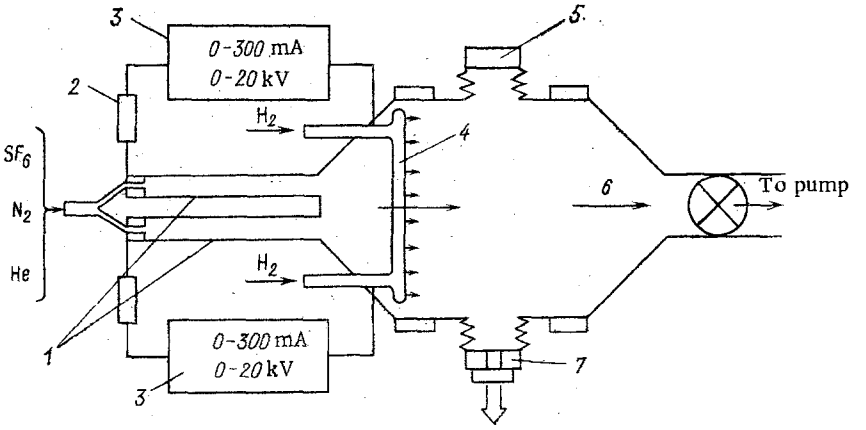

Fig. 5.17. Diagram of cw subsonic electric-discharge HF chemical laser with transverse pumping and mixing of the reagents: 1) pyrex discharge tubes; 2) ballast resistor to stabilize the discharge; 3) discharge supply source; 4) injection tube; 5) total-reflection mirror; 6) gas stream; 7) mirror with opening for the extraction of the radiation.

$$H + Cl_2 \rightarrow HCl^* + Cl; \tag{5.21}$$

$$H + Br_2 \rightarrow HBr^* + Br; \tag{5.22}$$

$$Cl + HI \rightarrow HCl^* + I. \tag{5.23}$$

A cw chemical laser (e.g., [45, 46]) in which F atoms were obtained by electric discharge in a gas mixture of He, O_2, and SF_6, operated at higher pressures, from 0.66 to 2 kPa. The SF_6 was subsequently mixed with hydrogen, which was injected into the flow region upstream relative to the axis of the transverse optical cavity.

Fluorine atoms were also produced with a dc discharge in a mixture of N_2, He, and SF_6 [47] and subsequently reacted in the same manner with H_2 or D_2.

The setup described in [47] is shown schematically in Fig. 5.17. A characteristic feature is that the location of the injection tube could be changed. The mixing of the gases, the chemical reactions, and the lasing take place in a stream with cross section 30 × 1.25 cm. The cavity is made up of mirrors with curvature radii 2 m spaced 45 cm apart. Radiation is extracted from the resonator through an opening 5 mm in diameter in one of the mirrors.

Typical gas flow rate in mmole/sec was 3, 20, and 10 for H_2, N_2, and He, respectively, while the consumption of SF_6 was varied from 3 to 20. Increasing the amount of SF_6 in the mixture led to an increase of the impedance of the discharge and hence to an increase in the power consumption. Addition of N_2 to the mixture also increased the power consumption, since the voltage drop across the discharge increased. Helium was introduced into the mixture to stabilize the discharge and to lower the gas temperature.

At an extraction flow rate 0.236 m^3/sec the pressure in the stream in the mixing region was ~0.7 kPa, and the stream velocity was $\sim 4 \cdot 10^3$ cm/sec (the sound velocity in the mixture was estimated at $7 \cdot 10^4$ cm/sec). Under these conditions a sufficient efficiency of the chemical laser was reached only when the tube through which the H was injected was located 2 ± 0.5 cm upstream from the cavity axis. This makes it possible to estimate the lifetime of the excited gas mixture at ~3.6 msec — the upper limit of the lifetime of the excited HF molecule governed by the actual conditions in the given setup. The HF constitutes a small fraction of the total number of particles, and the mixture temperature is approximately 150°C. The relatively brief stay of the mixture in the cavity is useful because HF molecules in the ground state are carried away from the cavity together with the gas stream, and it therefore becomes possible to obtain lasing on the (1—0) transition, in contrast to systems in which the gas stream is parallel to the cavity axis.

The lasing power of such an HF chemical laser depends linearly on the electric supply power. The maximum lasing power 5.5 W obtained with HF corresponds to a generated emission intensity 700 W/cm^2 at a beam diameter ~1 mm. Under similar conditions, the lasing power using DF is half as large. The ratio of the energy of the generated radiation to the electric energy consumed in the initiation of the reaction, called the electric efficiency of the electric-discharge chemical lasers, was of the order of 0.1%.

A chemical laser using CS_2/O_2 and nitrogen was developed [9, 48] using separate discharge tubes and longitudinal flow of the reagents (Fig. 5.18). When N_2 dissociates in the electric discharge, N atoms are produced in tubes 1 and are subsequently mixed with CS_2/O_2 in teflon injectors 2 into the interior of a cavity that is longitudinal relative to the stream. The cavity is made up of a flat mirror 5 and a spherical mirror 7. The radiation is extracted to an InSb detector 4 through an opening in the flat mirror.

The reaction can be initiated here in two ways. One is by dissociation of N_2 and the other by dissociation of O_2 if the discharge tubes 1 are filled with a mixture of O_2 and He. It was found in [48] that increasing the consumption of O_2 or N_2 increases the output power of the laser. The reactions that take place in such a chemical laser are similar to the reactions in the CO photochemical laser described in [7].

A similar mixture is used in an electric-discharge subsonic chemical laser with transverse flow, a diagram (a) and exterior (b) of which are shown in Fig. 5.19 [49]. The discharge section consists of a pyrex tube 1, in the entrance to which a copper-disk anode 2 with a central opening for the passage of O_2, He, N_2 fed from mixer 3 is placed. From the discharge section 1 (length 90 cm, diameter 2.5 cm) the gas stream goes through a transition piece 4 into the rectangular working channel 5 (50.8 × 30.5 × 1.3 cm) with adjustable placement of injectors 6 for the entry of CS_2 along the stream. The discharge that initiates the reaction is produced between the anode 2 and the cathode 7. The transition junction 4 and the channel 5, made, respectively, of copper and stainless steel, are water-cooled. On channel 5 are mounted transverse cavities 8. The gas is evacuated through port 9. The discharge is stabilized by ballast resistor 10.

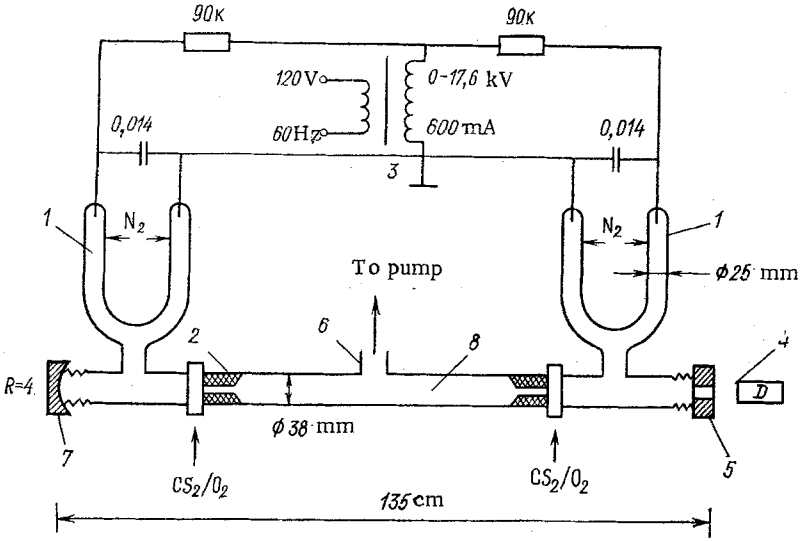

Fig. 5.18. Diagram of electric-discharge chemical laser with longitudinal mixing of the reagents: 1) discharge tubes with entry of N_2; 2) injectors with entry for the CS_2/O_2 mixture; 3) discharge electric-supply block; 4) radiation detector; 5) flat mirror; 6) extraction of gas at a flow rate 5 m^3/min; 7) spherical mirror; 8) working tube (reactor).

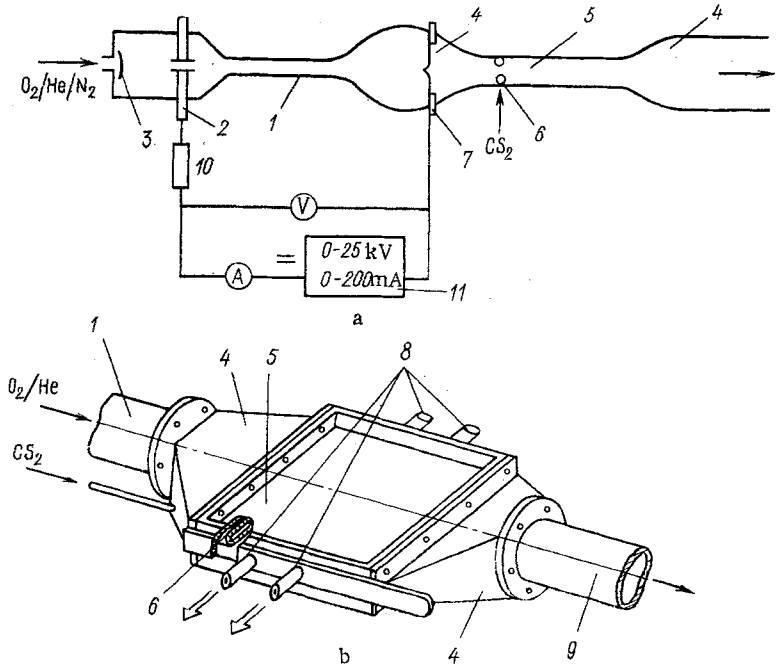

Fig. 5.19. Electric-discharge subsonic chemical laser with transverse flow: 1) discharge section; 2) anode; 3) mixer; 4) transition section; 5) working channel; 6) injectors with CS_2 inlets; 7) cathode; 8) cavities; 9) branch pipe for the extraction of the gas; 10) ballast resistor; 11) discharge-supply source.

A power of 4.5 W was reached in such a chemical laser with He, O_2, and CS_2 consumption of, respectively, 7.7, 33.4, and 2.4 g/min, at a total pressure 0.72 kPa, a discharge power 800 W, and a distance between the CS_2 injector and the optical axis of the cavity 1.5 cm. The electric efficiency was 0.56% and the chemical efficiency 2.7%. The dependences of the output power W_{out} on the input power W_{in} and on the partial pressures p_i of the O_2 and He are shown in Fig. 5.20. (The unstable-discharge region is hatched.)

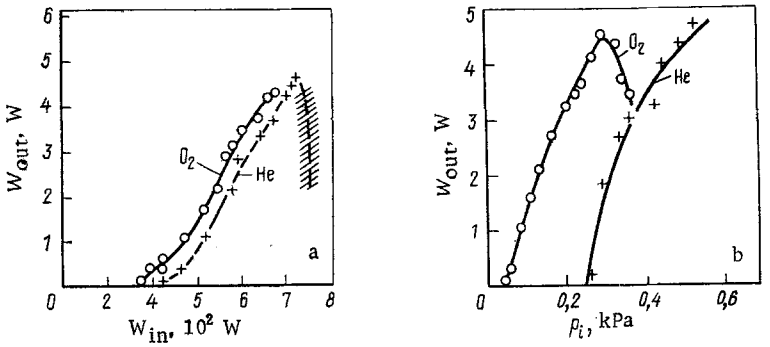

Fig. 5.20. Dependences of the output power of the chemical laser on the input energy (a) and on the partial pressures of O_2 and He (b).

The described chemical laser [49] operates more efficiently than, e.g., the similar chemical laser in [8, 11]. The probable reason is the possibility of optimizing the position of the CS_2 injector in the cavity. Another explanation is the decrease of the rotational temperature of the CO.

Similar in construction to the chemical laser shown in Fig. 5.19 is the small subsonic electric-discharge HF (DF) cw laser (Fig. 5.21), whose parameters were investigated in [50] as functions of the change of the mass flow $\dot{m}$ of the components of the working mixture $SF_6/H_2(D_2)/He/O_2$. The small dimensions of the chemical laser are made possible by the relatively small size of the channel, 20 × 10 × 0.3 cm. On the lateral sides of the channel are mounted the Brewster windows of BaF_2, so that the optical axis passes 1 mm downstream from the openings of the injector for the H_2. The cavity is made up of two mirrors spaced 40 cm apart, one flat and the other interchangeable and spherical, with a radius ranging from 1 to 10 m. Some results of the investigation of such a small-size chemical laser are shown in Figs. 5.21, 5.22.

To obtain active atoms that initiate the reaction, use is also made of an electrodeless discharge. The advantage of such a discharge over conductive discharges for the initiation of the reaction in a chemical laser is that it makes it possible to obtain F atoms in large volumes of plasma microwave generators with more uniform distribution of these atoms in the discharge volume. For the dissociation of SF_6 or F_2 in chemical lasers one uses radio-frequency [51] or microwave [52] radiation.

Figure 5.23 shows diagrams of a quasicontinuous chemical laser with microwave initiation of the reaction and the working chamber of this chemical laser. The working chamber 1, shown in Fig. 5.23b, is made of a solid aluminum block. In this chamber, the main channel for the flow of the active medium (shown by arrows) measures 6.4 mm in height, 5 cm in width, and 7.5 cm in length. Perpendicular to this channel is located an optical channel with the same cross section, which permits regulation of the position along the stream of the active medium of the cavity axis which is transverse to the screen. The H_2 injector consists of a large number of openings of 0.1 mm diameter located above and below the entry to the main channel. The two rows of transverse H_2 jets meet with the F atoms contained in the main gas stream of the reagents.

The entrance to the working chamber of the chemical laser is connected through a transition compartment with a quartz plasma tube 2 having an inside diameter 13 mm. In this tube the helium-diluted SF_6 is dissociated in the field of the microwave-radiation source [53] of 1.2 or 2.5 kW power at a frequency 2.45 GHz. The microwave energy is fed in pulses at a frequency of 120 Hz. For optimum transfer of the microwave-radiation energy inside the plasma tube and for the production in the tube of a homogeneous electrodeless discharge, this tube and the microwave radiaton source are mounted alongside each other at a certain adjustable angle θ.

The cavity is made up of two mirrors. One is gold-coated and has a curvature radius 10 m, and the other is made of germanium with dielectric coating having a transmission coefficient 4% in the wavelength range from 1.9 to 3.3 μm, and has a curvature radius of 4 m. The distance between mirrors is 43 cm. The Brewster angles were protected by helium jets against diffusion of HF molecules from the main stream of the active medium. Without this protection,

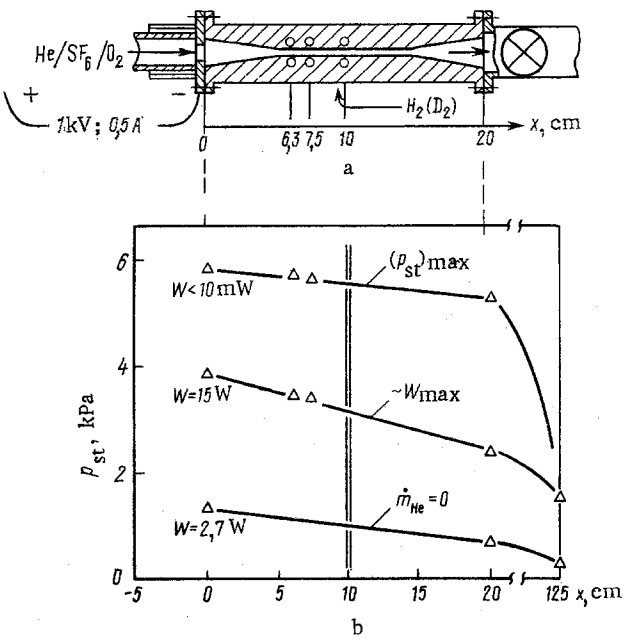

Fig. 5.21. Channel of small-size subsonic electric-discharge chemical laser (a) and distribution of the pressure p_{st} over the channel at different powers W of the generated radiation (b).

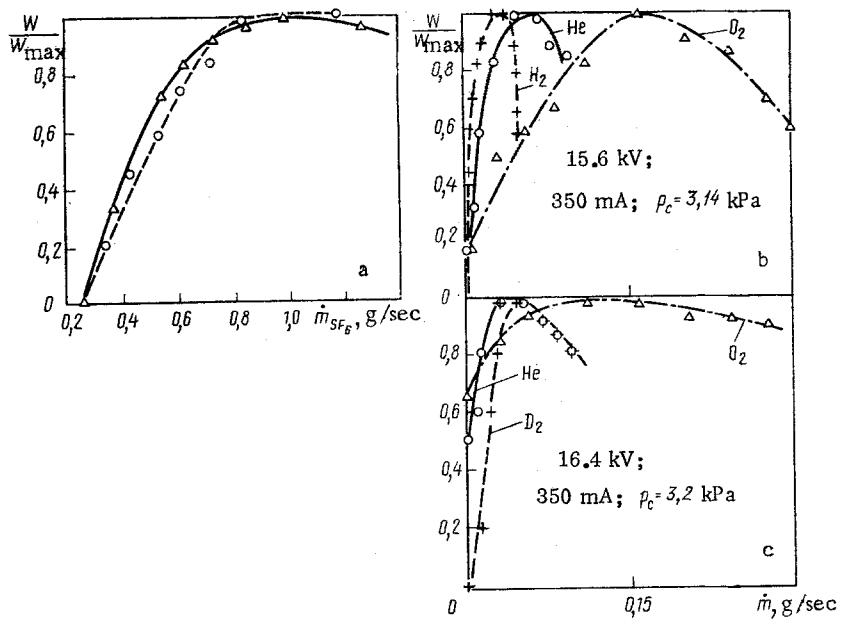

Fig. 5.22. Operating characteristics of small-size chemical laser: a) ——) 16.4 kV; 350 mA; $\dot{m}$: He — 0.0405, D_2 — 0.044, O_2 — 0.150 g/sec; p_c = 32 kPa; -----) 15.6 kV; 350 mA; $\dot{m}$: He — 0.054, H_2 — 0.03, O_2 — 0.18 g/sec; p_c = 3.14 kPa. b) $\dot{m}$: -----) He — 0.054, O_2 — 0.18, SF_6 — 0.87 g/sec; ——) H_2 — 0.03, O_2 — 0.18, SF_6 — 0.87 g/sec; -·-·-) He — 0.54, H_2 — 0.03, SF_6 — 0.87 g/sec. c) $\dot{m}$: ——) D_2 — 0.044, O_2 — 0.15, SF_6 — 0.98 g/sec; -·-·-) He— 0.0405, D_2 — 0.044, SF_6 — 0.98 g/sec; ----) He —0.04, O_2 — 0.15, SF_6 — 0.98 g/sec.

the chemical-laser radiation power would decrease to approximately one-half because of absorption of the radiation by the HF molecules in the ground state. When lasing was reached, the flow rates of the gas components were varied to optimize the radiation power W. The obtained optimum flow-rate ratio was: helium flow for the protection of the windows — 6 mmole/sec; main He flow — 21 mmole/sec; SF_6 — 0.4 mmole/sec; H_2 — 4 mmole/sec. The total pressure in the working chamber was 133 Pa.

The design of this chemical laser makes it possible to optimize not only the flow rates of the components, but also the angle θ, the distance x_c from the optical axis to the H_2 injector, and the rotation angle φ of this axis relative to the stream axis. Plots of these relations are given in Figs. 5.24, 5.25. Optimization [53] yielded for all the transition lines a maximum average power of 560 mW at a microwave-source power 2.5 kW, and 290 mW at a microwave-source power 1.2 kW.

A chemical laser with transverse flow operated with an electrodeless discharge source in the radiofrequency band, both on HCl [54] and on HF and DF [55]. The source of the F atoms was in this case a discharge in He/F_2 within a water-cooled quartz tube at an electromagnetic-field fource frequency 21 MHz. The activated flow from the discharge region passes through a number of small channels aligned with the outputs of the secondary-stream injectors. The primary stream of He/F_2 and F emerges with sonic velocity and is mixed with the secondary stream of H_2 (D_2). The cross section of the exit nozzle 3 × 0.5 cm determines the dimensions of a stream in which the optical axis of the cavity is located 0.5 cm downstream from the end section of the nozzle. The optimal consumptions in this chemical laser for He, F_2, and H_2 (D_2) are 2, 0.3, and 0.1 mmole/sec, respectively. The pressure in the cavity is approximately 130 Pa. The radiation power on all the lines of the chemical laser on HF and DF is, respectively, 0.3 and 0.12 W.

Microwave initiation of the reaction was investigated also in a CO chemical laser with subsonic flow transverse to the optical axis [49, 56-58]. As a result of the investigation, the following conditions were formulated for effective operation of a CO chemical laser as well as of chemical lasers using other active media:

1. High degree of dissociation and production of active atoms, in this case oxygen atoms.

2. Rapid mixing of the O/O_2 and CS_2 streams.

3. Sufficient inflow of diluent to regulate the temperature growth in the exothermic chemical reaction.

4. Organization of the stream geometry to ensure efficient interaction with the optical field of the cavity.

5. Rapid transport of the chemically excited CO into the optical field, and rapid removal.

In [56] a chemical laser is described in which atomic oxygen was produced by dissociation of O_2 with passage of a O_2/He mixture through the high-frequency discharge region. The cross section of such a chemical laser is shown in Fig. 5.26. The discharge was excited in quartz tube 2, which crossed at an angle $\theta = 10°$ a waveguide 3 connected to the output of a magnetron (2.45 GHz, 1 kW). The O/O_2/He mixture from the discharge region was fed to the oxygen injector 4. The flowrate G_o of the atomic oxygen through the cavity region was measured by titrating the working mixture with added NO_2. Figure 5.27 shows the dependence of G_o on the pressure p_c in the cavity, measured at constant flowrates of O_2, He, and H_2. At the input to the discharge gap, a small amount (0.0215 mmole/sec) of H_2 was added to the CO_2/He mixture.

Experiments have shown that at a mixture pressure 1.33 kPa this addition doubles the degree of dissociation of O_2. The flowrates of the atomic oxygen at the exit from the discharge tube and at the entrance to the cavity turn out to be the same. The value of G_o changed little when the O_2 consumption was increased from 1 to 7 mmole/sec and that of He from ~13 to 21 mmole/sec.

The injection system shown in Fig. 5.26 included one atomic-oxygen injector and two CS_2 injectors perpendicular to it. The two-dimensional injectors and the system for pumping out the working mixture had a length of 50 cm along the optical axis of the cavity. The brass CS_2 injectors were water-cooled.

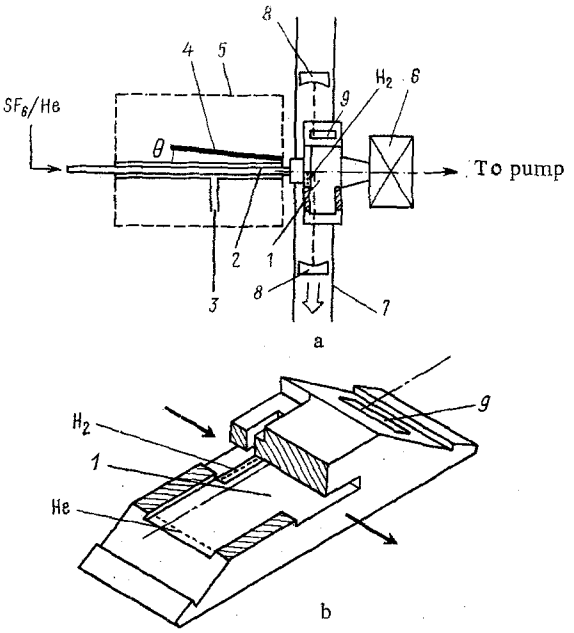

Fig. 5.23. Diagrams of a) the quasicontinuous chemical laser with microwave initiation of the reaction and b) the working chamber of this chemical laser: 1) working chamber; 2) quartz plasma tube; 3) air-cooling inlet; 4) microwave plasma generator; 5) microwave-radiation screen; 6) shutter; 7) optical bench; 8) mirrors; 9) Brewster windows.

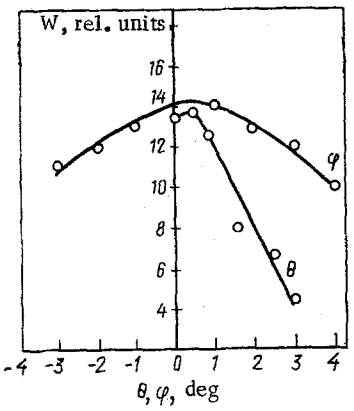

Fig. 5.24

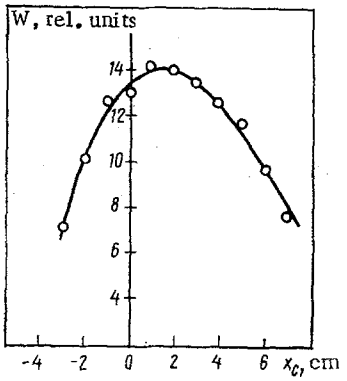

Fig. 5.25

Fig. 5.24. Dependence of the relative power of a chemical laser on the rotation angles φ and θ.

Fig. 5.25. Dependence of the relative power of a chemical laser with transverse flow on the distance from the optical axis to the H_2 injector.

The density profiles of the streams of the working gases were measured with a mass-spectrometer setup, the pickup of which could be moved along the gas-flow direction (the x axis). Figure 5.28 shows the measured distributions of the concentrations of Ar and He along the flow direction. The null point was taken to be the intersection point of the injected O and CS_2 streams. The same figure shows the gas-mixture temperature distribution. The temperature was measured with a thermocouple located at a distance 2 cm to the side of the mass-spectrometer pickup. Since Ar was used as the diluent of the CS_2 stream and the He was contained in the O/O_2 stream, the density profiles of the Ar and He streams can be used to assess the degree of mixing of the primary (O/O_2/He) and secondary (CS_2/Ar) streams. It can be seen from Fig. 5.28 that total mixing of the streams under the experimental conditions was reached already at a distance ~0.9 cm.

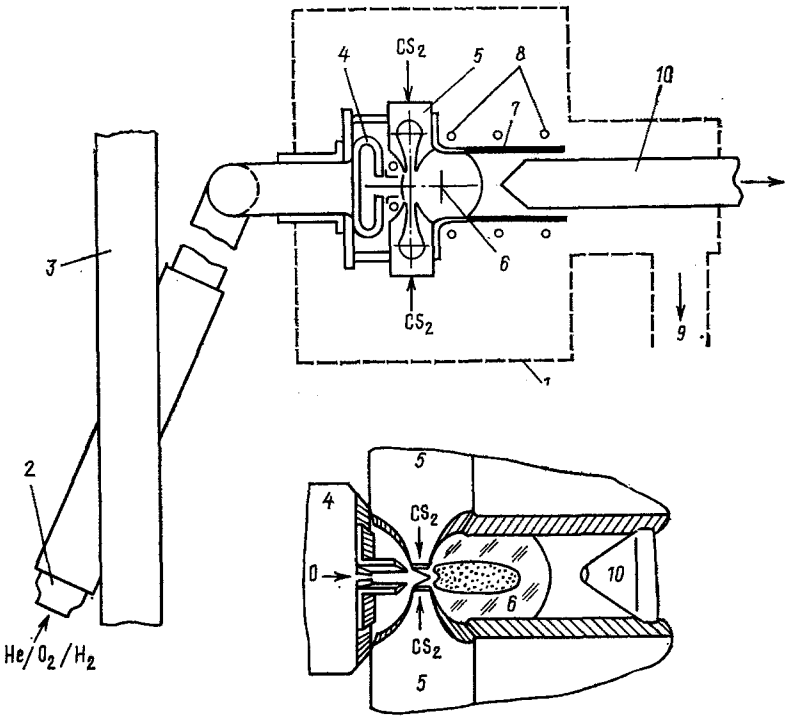

Fig. 5.26. Diagram of chemical laser with O_2 dissociation in a high-frequency discharge: 1) vacuum volume; 2) quartz discharge tube (2.7 cm diameter, wall thickness 0.1 cm); 3) waveguide; 4) oxygen injector; 5) CD_2 injector; 6) cavity; 7) extension; 8) water cooling; 9) evacuation; 10) mass-spectrometer pickup for the analysis of the flow (with an axial aperture of 0.1 mm diameter).

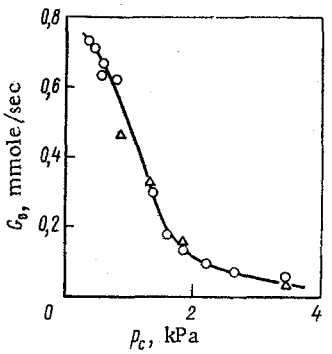

Fig. 5.27

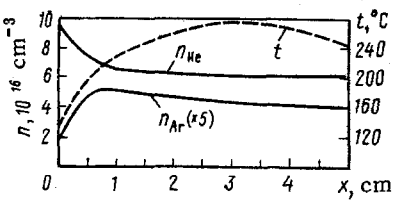

Fig. 5.28

Fig. 5.27. Dependence of the flow of atomic oxygen in the active region on the pressure in the resonator: ○) entry of NO_2 past the dissociator; Δ) entry of NO_2 through CS_2 injector; W = 1.4 kW; G_{O_2} = 5.6; G_{He} = 20.8; G_{H_2} = 0.0215 mmole/sec.

Fig. 5.28. Distribution of the concentrations of Ar and He along the flow direction in a chemical laser.

The excited CO* molecules in the cw chemical laser operating on a $O/O_2/CS_2$ mixture are produced in the course of the reactions already considered in Sec. 5.1:

$$O + CS_2 \rightarrow CS + SO; \quad (5.5)$$

$$O + CS \rightarrow CO^* + S. \quad (5.4)$$

Since the working mixture of the gases usually contains a large amount of molecular oxygen, the sulfur is rapidly oxidized:

$$S + O_2 \rightarrow SO + O. \tag{5.6}$$

In the analysis of the chemical kinetics of this mixture of reagents and in the simulation of a $O/O_2/CS_2$ mixture chemical laser, only the reactions (5.4)-(5.6) were usually considered. Sometimes account was also taken of the reaction

$$SO + O_2 \rightarrow SO_2 + O, \tag{5.24}$$

but estimates have shown that its rate at T ≃ 500 K is much less than the rate of the other reactions.

To determine the reactions that occur in the active medium of a $O/O_2/CS_2$ mixture chemical laser, the composition of the working gas mixture was investigated in [56] with a mass spectrometer under optimal excitation conditions. The measurements were performed only at the point x = 1.5 cm.

The mass-spectroscopic and flow-rate investigations of the composition of the working gas mixture have led to the following conclusions: 1) the CS_2 is effectively converted into CO in the employed reagent system; 2) reactions during which SO_2 and S_2O molecules are produced are quite rapid: 3) reactions in which SO molecules participate proceed intensively in the gas mixture.

The optimal parameters of the considered subsonic CO chemical laser with microwave initiation of the reaction are given in Table 5.2.

The power for the cavity with the total-reflection copper mirrors was determined from the heating of the mirrors, and the chemical efficiency was calculated from the relation

$$\eta_c = \frac{W_{out}}{G_{CS_2} \Delta H_e f_v}, \tag{5.25}$$

where W_{out} is the power lost to excitation of the vibrational levels of the CO; G_{CS_2}, flow rate of the CS_2, mole/sec; ΔH_e = −356 kJ/mole, specific heat of the reaction O + CS; f_v = 0.66, fraction of the pump energy consumed in the excitation of the vibration levels of the CO molecules.

The optimal parameters of the transverse-pumped CO chemical laser can be increased by introducing gas admixtures into the stream [56, 59]. The admixture gases are introduced into the working mixture, e.g., through the CS_2 injectors. The admixtures can produce several effects. First, they bind the atomic oxygen if their reaction rate with it is of the same order as the rate of the reaction CS_2 + O. This is observed, e.g., when OCS is added. Second, the admixtures can participate in the deactivation of the CO* molecules. For example, the molecules OCS, NO, N_2O and CO have large V—V exchange rates with CO molecules. Finally, in the employed injection system introduction of practically any gas initially at low admixture flux densities improves the mixing of the reagents and consequently increases the radiation power. At high admixture flow densities, the homogeneity of the primary flow of the working gases is disturbed, and this leads to a rapid decrease of the radiation power. This limits the permissible flow density of inert additives (such as Ar).

The dependence of the measured radiation power in relative units on the partial pressure p_i of various additives is shown in Fig. 5.29.

The N_2O gas turned out to be the best additive and its introduction into the working mixture doubled the radiation power. Introduction of additives changed the spectral distribution of the radiation power on account of the change of the rate of the V—V relaxation of the CO* molecules excited to various vibrational levels. In the collisions

$$CO(v) + M \xrightarrow{P_v} CO(v-1) + M \tag{5.26}$$

(M is the additive molecule, P_V is the probability of collision with energy transfer) there can be reached either an increase of the inversion on the v → v − 1 transition (without a decrease of the total population of the levels v and v − 1) at $P_V < P_{V-1}$, or a decrease of the inversion at $P_V > P_{V-1}$.

Such changes of the distribution of the populations of the vibration levels, and consequently, of the gains for different transitions, are primarily responsible for the observed

TABLE 5.2. Optimal Parameters of Subsonic CO Chemical Laser [56]

Parameter	Cavity with total-reflection mirrors	Cavity with transmitting exit mirror
Power, W	28,8	22,0
Flow rates of O_2/He/CS_2/N_2O, mmole/sec	5,59/19,9/0,58/3,11	12,6/21,5/0,50/4,0
Total mass flow rate, g/sec	0,44	0,70
Specific power, J/g	65,5	31,4
Chemical efficiency, %	21,1	18,7

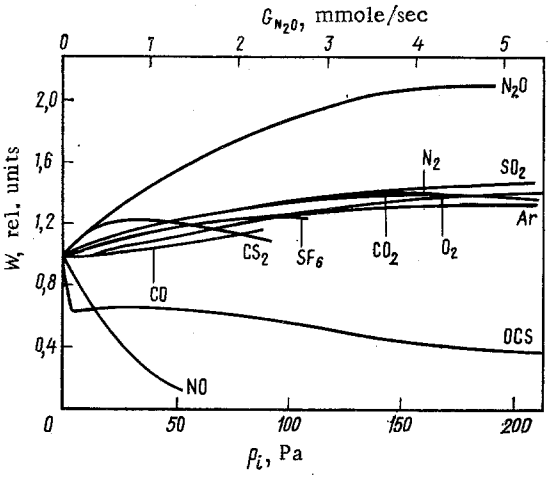

Fig. 5.29. Dependence of the relative power of the generated radiation on the partial pressure of additives of various gases.

changes in the lasing spectrum. The total optical gain upon introduction of the additives can be expressed in the form

$$g(G_M) = g_0|_{G_M=0} + \Delta g^M_{gd}(G_M) + \Delta g^M_{coll}(G_M) + \Delta g^M_{optic}(G_M), \quad (5.27)$$

$$g_0 = \exp(\alpha_0 L) - 1, \quad (5.28)$$

where α_0 is the specific gain; L, length of the gain region; G_M, molar flow rate of the additive M; and Δg^M_{gd}, Δg^M_{coll}, Δg^M_{optic}, changes of the optical gain due, respectively, to the action of the additive M on the gas-dynamic mixing, to the molecular collisions, and to absorption of the radiation by the additive M.

In [59] G_M was taken to be the independent variable, and estimates were made of the components of the total optical gain in (5.27). It was found that the term Δg^M_{optic} can be neglected, while Δg^M_{gd} can be separated experimentally by introducing into the stream an inert additive with negligibly small collisional effects. The result of this is also the possibility of estimating the remaining component Δg^M_{coll}.

The results of such an estimate [59] are given in Table 5.3, where the influences of a number of gas additives on the gain of a CO chemical laser are summarized.

It can be seen from the table that inversion on the lower levels is increased by the N_2O additive, while inversion on the medium levels is decreased by an NO additive. One more important effect of adding NO manifests itself in a collision-induced cascade of population from the higher to the lower levels. This effect is typical of the O + CS pump reaction in CO chemical lasers.

It follows from the plot in Fig. 5.29 and from Table 5.3 that introduction of various additives into a CO chemical laser makes it possible to control the spectrum of the output radiation and the total output power. Thus, N_2O increases the output power of a transverse-

TABLE 5.3. Influence of Gas Additives on the Gain of a CO Chemical Laser

Additive	Lower levels 3→2-5→4	Medium levels 6→5-9→8	Upper levels 10→9-13→12
N_2	*n*	*n*	*n*
SO_2	*n*	*n*	*q*
H_2	*n*	*n*	*q*
HF	*e*	*q*—*Q*	*Q*
CF_4	*e*	*q*—*Q*	*Q*
CCl_2F_2	*e*	*e*—*q*	*Q*
CO	*Q*	*q*—*e*	*e*
OCS	*Q*	*Q*	*e*—*Q*
N_2O	*e*	*e*—*n*	*n*—*q*
NO	*E*	*e*—*Q*	*Q*

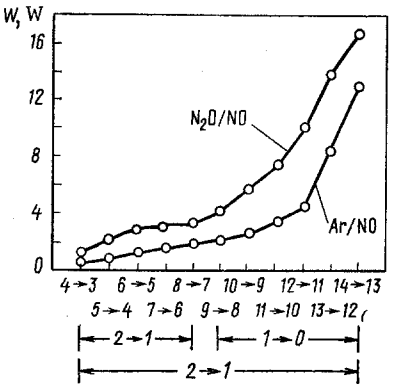

Fig. 5.30. Output power of a chemical laser on various transitions following the addition of NO.

flow chemical laser by approximately 50%. Such an increase of the power is due to the weak increase of the gain at low and medium energy levels without a considerable decrease at high levels.

It must be noted that the characteristics of the gain of a CO chemical laser are not very sensitive to many gas additives, so that it is possible to relax the requirements imposed on the diluents and to increase their number, as well as that of the reagents used, e.g., as fuel for the chemical laser. Another characteristic feature, as can be seen from Fig. 5.30, is that in a multilevel cascade chemical laser the total power decreases rapidly with decreasing length of the cascade [59].

5.3. Flame Chemical Lasers

Flame Model. Flame chemical lasers are devices in which the stimulated emission is obtained in free burning of the initial reagents in a flare. In this case a cw chemical laser with a self-maintaining flame is realized. Such a self-maintaining system is one of the examples of a purely chemical laser, which requires no electric or other power to maintain the process, other than for the system that feeds the reagents and pumps out the reaction products or for the ignition of the flame.

Consider [60] two gases A and B which enter in a chemical reaction with each other after they come in contact in a common vessel. The reacting mixture moves and has a total pressure of several hundred Pa. It is assumed that one of the newly produced types of molecules is partially or fully excited. Assume also that there are two energy levels corresponding to the reaction

$$\left.\begin{aligned} A + B \xrightarrow{k_1} C_1 + \ldots, \\ A + B \xrightarrow{k_2} C_2 + \ldots, \end{aligned}\right\} \qquad (5.29)$$

where k_1 and k_2 are the specific rate constants of the second-order reaction, and the indices 1 and 2 label, respectively, the lower and upper quantum states of C. The concentrations of the molecules in the states 1 and 2 (n_1 and n_2, respectively) are determined by radiative transitions characterized by a lifetime τ_{12}. The influence of the relaxation and damping processes is neglected.

An approximate solution of the rate equations yields for the steady-state population difference, which contains the characteristic time constants for different processes:

$$\left(\frac{n_2-n_1}{n_0}\right)_{\max} \cong (f_2-f_1)\frac{\tau_m}{\tau_m+\tau_r} - \frac{1}{\tau_{12}}\left[\tau_m - \tau_r \ln\left(1+\frac{\tau_m}{\tau_r}\right)\right], \tag{5.30}$$

where n_0 denotes identical initial concentration of the gases A and B; $f_{1,2} = k_{1,2}/(k_1 + k_2)$; $\tau = 1/n_0 (k_1 + k_2)$; τ is the time during which the difference $n_2 - n_1$ reaches a maximum value. Obviously, population inversion takes place only when $k_2 > k_1$. The pumping conditions can be obtained by comparing the population difference with the threshold conditions

$$n_2 - n_1 \geqslant \Delta N_{\text{vib}}, \tag{5.31}$$

where

$$\Delta N_{\text{vib}} = 8\pi c \frac{1-r}{l}\tau_{12}\omega^3\frac{\Delta\omega}{\omega}\ [61], \tag{5.32}$$

c is the speed of light; ω, wave number of the transition between C_1 and C_2; $(1 - r)$ and l are determined by the properties of the chemical-laser cavity. Thus, the requirement imposed on the relative reaction rate is given by the expression

$$f_2 - f_1 \geqslant \frac{\Delta N_{\text{vib}}}{n_0}\frac{\tau_r+\tau_m}{\tau_m} + \frac{\tau_r+\tau_m}{\tau_{12}}\left[1 - \frac{\tau_r}{\tau_m}\ln\left(1+\frac{\tau_m}{\tau_r}\right)\right]. \tag{5.33}$$

If it is assumed that the parameters of the system have the following values: $\omega = 2\cdot10^3$ cm^{-1}, $\Delta\omega/\omega = 10^{-6}$, $1 - r = 10^{-2}$, $l = 10$ cm; $\tau_{12} = 10^{-2}$ sec, $n_0 = 10^{16}$ cm^{-3}, and $\tau_m = 10^{-3}$ sec, then τ_r can vary in the range 10^{-2}–10^{-4} sec without causing large changes in the pumping conditions, i.e., $f_2 - f_1$ varies from $6\cdot10^{-2}$ to $9\cdot10^{-2}$. The reaction rate constants connected with these values of τ_r are equal to 10^{-14}–10^{-12} cm^3/sec or 10^7–10^9 $(mole\cdot sec)^{-1}$.

To create conditions under which stimulated emission from a flame becomes possible, it is important to have detailed data on the value of the absorption at different states of the flame. By way of a flame quantum system, an acetylene–oxygen flame was considered in [60]. It is well known that the reaction zone of this flame radiates in the visible and ultraviolet regions of the spectrum, and part of the radiation is of chemical and not of thermal origin [62]. Acetylene–oxygen flames of low pressure, burning at pressures 0.1-2 kPa, were investigated. Particular attention was paid to a determination of the population of the energy levels of components such as C_2 and CH. At a total pressure of 0.66 kPa, the (0–0) and (1–1) absorption bands of C_2 were observed together with five bands of the sequence (1–0). The lower limits were calculated for the absorption coefficients:

$$\begin{gathered}(0—0),\ 7\cdot10^{-4}\,cm^{-1};\ (1—1),\ 2\cdot10^{-4}\,cm^{-1};\ (1—0),\ 2\cdot10^{-4}\,cm^{-1};\\ (2—1),\ 3\cdot10^{-4}\,cm^{-1};\ (3—2),\ 3\cdot10^{-4}\,cm^{-1};\ (4—3),\ 2\cdot10^{-4}\,cm^{-1};\\ (5—4),\ 1\cdot10^{-4}\,cm^{-1}.\end{gathered}$$

Observations of higher vibrational components, particularly of the sequence (1–0), pointed to a larger degree of vibrational excitation of the $X'^3\Pi_u$ state of C_2 at the chosen experimental conditions. The same follows from the distribution of the intensity in the sequence (1–0) when radiation from the $A^3\Pi_g$ state is observed.

Absorption for CH was obtained in the 430-nm region. The effect is very insignificant and depends to a great degree on the state of the flame. The experimental determination of the optical gain of a free burning acetylene–oxygen flame was carried out in [63] in the pressure interval 0.4-2 kPa, the lower limit of the pressures being determined by the flame shut-off conditions, and the upper by the conditions of the decrease of the flare volume, increased energy release, etc.

The measurements have shown that the enhancement of the radiation proceeds directly in the front of the flame at a certain optimal interval of the flare parameters. It was shown that in an acetylene–oxygen plane the substantial part of the CO is obtained in a nonthermal vibrationally excited state. This agrees with results of investigations of the kinetics of the acetylene–oxygen reaction in [64-66]. In [63], however, no lasing with an acetylene–oxygen flame was obtained, since none of the transitions had a gain larger than the cavity losses, the latter being approximately 5%. Obviously, more promising is the CS_2/O_2 mixture, with which the first flame chemical laser was produced [67].

Examples of Realization of Flame Chemical Lasers. Besides the conditions that facilitate the development of flame chemical lasers, such as the presence of a self-maintaining process, and the absence of the need for energy sources, there are also difficulties. One is the high flame temperature, which lowers the gain. Another is that only some of the large number of high-temperature chemical reactions participate in the pumping of the upper energy levels.

In addition, the propagation velocity of fuel-oxygen flames are usually low, from several centimeters to several meters per second, and this imposes a limit on the enhancement of the bulk efficiency of flame chemical lasers. Nevertheless, flame chemical lasers are attractive because of the simplicity of the construction, and because of the absence or low value of the energy consumed from an extraneous source, inasmuch as the branched chain reactions take place in the laser itself. These reactions maintain an equilibrium concentration of the intermediate active center, replenishing their losses from the flame on account of diffusion and reactions that take place in the flame itself. The rates of these branched chain reactions determine to a considerable degree whether a particular system is suitable for use as a flame chemical laser. To produce a flame chemical laser it is usually desirable that the chain reaction be as fast as possible and have minimum activation energies.

The possible reactions in a CS_2/O_2 flame at low pressure [67] are similar to (5.4)-(5.6) and (5.24).

As already indicated, a high temperature is not desirable to obtain lasing, since this lowers the gain and facilitates the relaxation within the flame itself. Since the degree of impact relaxation depends strongly on the flame propagation velocity, which determines the time of interaction of the molecules and consequently the number of collisions within the chemical-laser cavity, preferable systems are those with rapid kinetics of all the processes, which presupposes, in turn, a high propagation velocity.

To lower the temperature and the rate of impact relaxation in the flame, it is desirable to operate at lower pressures. The results of experiments with chemiluminescence at a total pressure 66-80 Pa in a CS_2/O_2 flame were reported in [68], where it was assumed that inversion is present on certain V–R transitions of CO. At a higher pressure [69] it was found that in a free burning flame of CS_2/O_2 the gain on the CO V–R transitions $\mathcal{P}(12) - \mathcal{P}(14)$ in the bands 8-7, 9-8, and 10-9 is approximately 2%.

The constructions of flame lasers, while differing in details, are in the main quite similar to one another. A general diagram of such a chemical laser is shown in Fig. 5.31. The burner 1 is mounted in a vacuum chamber 3 equipped with a cooling system 2 and can be moved in a vertical direction. Located above the burner is a fine-mesh screen 4. The cavity mirrors 5 are located along the direction of the optical axis which passes through the reaction zone. The position of the reaction zone relative to the cavity axis is varied with the aid of a mechanism 6, so that it is possible to measure the gain at any height of the flame. In [67] the burner took the form of a set of mutually parallel tubes. Each tube, 60 cm long with outside diameter 6 mm, had 50 openings of 1 mm diameter. The tubes that injected the CS_2 and O_2 were transversely oriented. The dielectric mirrors of the cavity had a reflection coefficient of 99.2%. The radiation was extracted through a 0.5-mm hole in one of the mirrors; the total cavity losses were estimated to be less than 3%. The output radiation was modulated at a frequency of 150 Hz and detected with the aid of an Au–Ge detector at 77°K. The measurements were performed with a tunable amplifier. Inside the cavity, outside the flame zone, is mounted an electric-discharge CO_2 laser. With this laser turned on, the cavity was tuned and the gain was determined. The vacuum chamber, 120 cm in diameter and 270 cm long, was connected to a mechanical pump of capacity 9 m^3/min. The flame was ignited with a glow discharge located several centimeters above the burner. After ignition the burning continued autonomously.

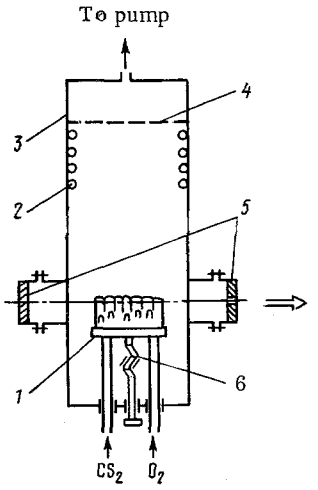

Fig. 5.31. Diagram of flame chemical laser: 1) burner; 2) cooling; 3) evacuated chamber; 4) screen; 5) mirrors; 6) burner-displacement mechanism.

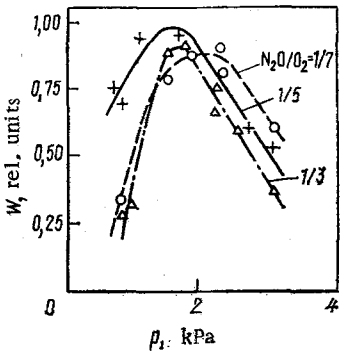

Fig. 5.32. Dependence of the lasing power W on the pressure in the evacuated chamber.

At pressures less than 266 Pa, the blue glow of the flame was diffuse and homogeneous. With increasing O_2 pressure with constant CS_2 pressure, starting with a ratio $p_{CS_2}/p_{O_2} = 0.5$, the flame broke up into several hundred tongues, equally distributed in the upper part of the burner. For a noticeable gain to be produced, it was necessary to raise the flame boundary somewhat, and this was done by further increase of the O_2 pressure. At O_2 and CS_2 pressure 1.2 kPa and 80 Pa, respectively, lasing took place, in which case the flame was inhomogeneous with attributes of a certain spatial instability. At a small change of the CS_2 pressure, by approximately 13 Pa, the lasing stopped.

The lasing spectrum was determined with the aid of a monochromator. Continuous lasing was observed in [67] on three CO transitions with wavelengths 5.216, 5.297, and 5.421 μm. The measured total output lasing power was 1 mW.

Mixing of the initial components in flame lasers of the type shown in Fig. 5.31 was effected both directly in the reaction volume and in a separate mixer placed at the enctrance of the gases into the burner or in the supply pipe.

In [70], nitrous oxide N_2O was added to the reacting CS_2/O_2 mixture in a flame chemical laser to increase the gain. In this case several variants of premixing the components were used: either two of them N_2O/O_2, or else all three components $CS_2/O_2/N_2O$. When the mixture N_2O/O_2 and the carbon disulfide were separately supplied, the coherent radiation power was approximately half the value obtained in the case when the three-component mixture was fed, this being due to insufficient mixing in the reaction region of the cavity.

Investigations of the optimal operating conditions of $CS_2/N_2O/O_2$ chemical lasers with respect to pressures and to the relative content of the reacting-mixture components have shown that these conditions are similar for a mixture which was prepared beforehand and kept in the

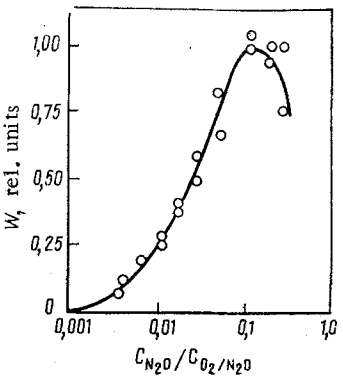

Fig. 5.33. Dependence of the lasing power on the relative N_2O concentration.

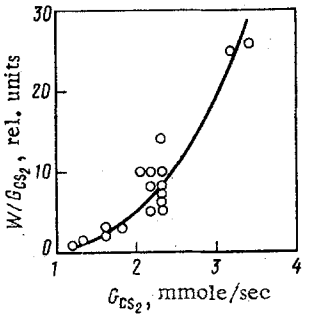

Fig. 5.34. Dependence of the power of a flame chemical laser on the CS_2 flow rate. The distance of the cavity optical axis from the burner is 1.1 cm.

mixer for 2-4 h and a mixture which was freshly prepared by mixing the streams in a mixer at the entrance to the burner. For this last case, Fig. 5.32 shows typical plots of the generated radiation power vs the pressure of the medium in the evacuated chamber. The maxima of the power are located in this case in the interval 2-2.66 kPa. The decrease of the radiation power at lower and higher pressures relative to the maximum value is explained, respectively, by the decrease of the density of the inverted population in the cavity volume and by the increase of the relaxation rate of the processes that equalize the nonequilibrium distribution over the vibrational levels of the CO molecules. The dependence of the lasing power on the mixture composition is characterized by curves with maxima in the region satisfying the relation

$$\frac{c_{N_2O}}{c_{N_2O/O_2}} = 1{,}10 - 0{,}13. \qquad (5.34)$$

There is also an optimum ratio with respect to the CS_2 concentration.

A characteristic feature of CO chemical lasers is that they operate with small additions of N_2O (Fig. 5.33). As the N_2O mixture is added, the radiation power increases rapidly compared with the power in the $c_{N_2O} = 0$ regime even at a ratio $c_{N_2O}/c_{O_2/N_2O} = 1/24$-, and when this latter ratio is further increased the power increases almost linearly. The abrupt change of the lasing power at small relative concentrations of N_2O, in the opinion of the authors of [70], cannot be attributed to peculiarities of the mechanism of the vibrational exchange of energy (see, e.g., [69]). At N_2O concentrations as low as $(3.5)\cdot10^{15}$ cm^{-3} the main contribution to the vibrational relaxation of the CO molecules with concentration of the order of 10^{16} cm^{-3} in the chemical-reaction zone is made by CO–CO collisions, in which the probability of vibrational-energy exchange is 2-4 times larger than in CO–N_2O collisions. It is assumed [70] that the rapid increase of the radiation power when small amounts of N_2O are added is due to dissociation of these molecules in the flame zone with temperature of the order of 1200°K. In fact, calculation of the equilibrium constant for

$$N_2O \rightleftarrows N_2 + O \qquad (5.35)$$

at $n_{N_2O} = 3\cdot(10^{15}-10^{17})$ cm^{-3} yields practically complete dissociation of the N_2O molecules at 1000-1200°K. An increase of n_o intensifies the formation of CO* in the course of the reaction

$$CS + O \rightarrow CO^* + S \tag{5.36}$$

and consequently increases the lasing power.

The use of a burner with a spacing 1.3 mm between the fuel and oxygen injection holes, with special screens, ensured rapid mixing of the gases on the burner surface [71]. Using such a burner, the operating characteristics of a CS_2/O_2 flame chemical laser and the influence on these characteristics of He, SF_6, N_2O, CO, CO_2, N_2, SO_2, NO_2 additives were investigated. The obtained dependence of the power on the flow rate of the CS_2 is shown in Fig. 5.34. The largest radiation power 0.6 W was obtained for a chemical laser using $CS_2/O_2/N_2O$ with corresponding molar flow rates of 3.9, 110, and 7.6 mmole/sec.

Considerably higher output powers of flame lasers were obtained in [72-74], on the order of 10-25 W with specific energy 13 J/g and with chemical efficiency 2.5%. Powers of the order of tens of watts were obtained also in systems with prior dissociation of the reagents, and the parameters and the operating conditions of flame lasers of kilowatt power were estimated [75].

5.4. Subsonic Metal-Vapor Chemical Lasers

With Ba, Ca, and Mg burning in $N_2O/He/CO_2$ mixtures, enhancement of the emission on the 00°1-10°0 transition of CO_2 was observed. On the same transition, continuous lasing was obtained in [76] by burning Mg vapor in a N_2O/CO_2 mixture. The pumping was effected by the fast exothermic reaction

$$Mg + N_2O \rightarrow MgO + N_2, \tag{5.37}$$

during which MgO molecules are produced in the $B^1\Sigma$ state.

Among the various possible methods of transferring energy from the reaction products to the CO_2 molecules, the most probable is the transfer of the energy of the excited electronic states of the MgO molecule to the vibrational levels of the ground electronic state of the CO_2 molecule (E–V transfer). This process can proceed in two ways: directly from the levels $B^1\Sigma$ and $b^3\Sigma$ to the high-lying vibrational levels of CO_2, or after decay of the excited $B^1\Sigma$ state of MgO into the $A^1\Pi$ state (3563 cm^{-1}) and subsequent population on account of internal conversion of the metastable level $a^3\Pi$ (2610 cm^{-1}) to the 00°1 level of CO_2 (2349 cm^{-1}). Both possible schemes are shown in Fig. 5.35.

V–V energy transfer from MgO and N_2 to CO_2 is not very likely, since the vibrational levels of MgO are separated by ~760 cm^{-1} [77] and do not coincide with the CO_2 levels, while the N_2 molecule produced as a result of the Mg + N_2O reaction is not excited in practice. E–V quenching of excited electronic states was observed earlier in mixtures of Na, Rb, Cs and Hg with H_2 and of Na with N_2 [78, 79].

The results of measurements of the gain in the flames offer evidence that the most probable process of E–V transfer is a transition between high-lying levels, since addition of nitrogen increased the gain on the 00°1-10°0 transition [76]. If the excitation were resonantly transferred to the upper level, the addition of nitrogen would cause part of the energy to land on the v = 1 level of N_2, and the population of the 00°1 level should decrease. If, however, the 00°1 level is populated as a result of V–V relaxation of the upper vibrational levels, then the entire energy of the vibrational nitrogen levels should ultimately go to the 00°1 level of CO_2. Consequently, an increase of the nitrogen content cannot decrease the gain in this case.

The construction of a subsonic metal-vapor chemical laser is shown in Fig. 5.36 and is similar in many respects to the setups used in [35, 80].

Heating metallic magnesium in aluminum crucibles 2 (depth 2.5 cm, inside diameter 2.5 cm) by tungsten heaters 1 produces Mg vapor, which is carried by the He stream into tube 3. At the entry of the active region, a CO_2/N_2O mixture is introduced in the Mg/He stream through radially disposed injectors 4. Additional weak He streams enter in tube 3 near mirrors 5 and 6 to protect them against deposition of reaction products. The reaction itself proceeds inside stainless-steel bellows 7 (inside diameter 1.9 cm, length 7.6 cm). Two such blocks are joined to form a single channel with a common exhaust 8.

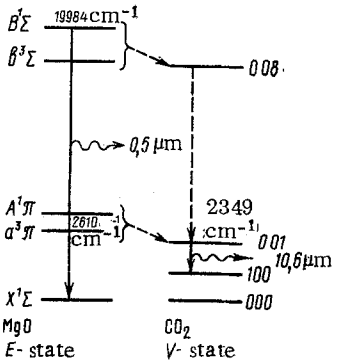

Fig. 5.35. States of MgO and CO_2 with possible E–V transitions.

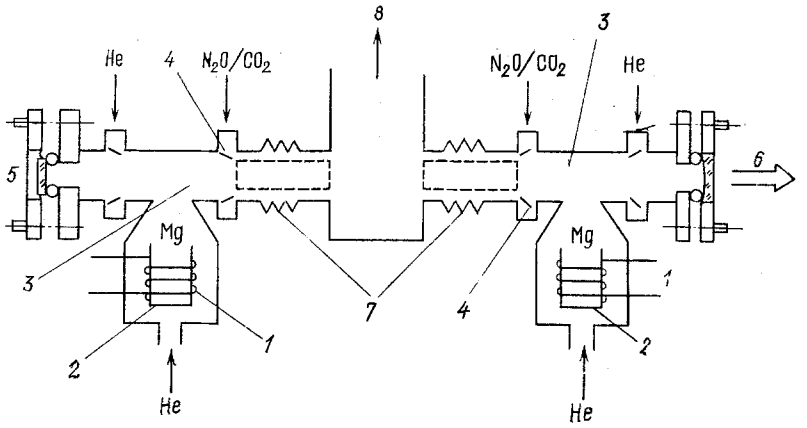

Fig. 5.36. Diagram of metal-vapor flame chemical laser: 1) heaters; 2) crucibles; 3) working tubes; 4) injector; 5) plane mirror; 6) concave mirror; 7) bellows; 8) exhaust channel.

The cavity is made up of a flat total-reflection mirror 5 on a silicon substrate and a concave mirror 6 with reflection coefficient 98% on a germanium substrate (dielectric mirrors were used). The diameter of the mirrors was 12.7 mm and the distance between them 65 cm. The mirror position is stabilized with the aid of three Invar rods. The coarse and fine adjustments of the cavity were effected with gas-discharge excitation, in the same tube 3, of lasing on CO_2 and N_2O, respectively.

Usually, 1.5 g of metallic magnesium was placed in each crucible and was evaporated within 3 min at a heating power 300 W. Approximately 50% of the produced magnesium vapor entered the active region (the remainder condensed on the walls). A homogeneous blue-green chemiluminescence glow was produced near the injectors 4 and filled the entire cross section of the tube 3. The chemiluminescence in the region of ~0.5 μm, corresponding to the transition of the MgO from the $B^1\Sigma$ state into the ground state, exists at a length ~1 cm at a stream velocity 1400 cm/sec, and consequently, the time of displacement of the gas mixture amounted to ~1 msec. The bellows in which the chemiluminescence takes place remained practically unheated.

The maximum lasing power was 5 mW and was reached under the same conditions as when the gain was a maximum (~10^{-2} cm^{-1}) in the absence of mirrors. The maximum was observed at a total pressure in the tube ~1.33 kPa and at the following ratio of the partial flow rates of the gases: $He/N_2/N_2O/CO_2/Mg$ = 50/15/15/15/5.

It is noted in [76] that many effects that determine the operation of the described chemical laser are still not clear. Thus, the rate of deactivation of the excited CO_2 and N_2 molecules by the alkali-metal atoms is quite low; therefore, the only channel for the losses in the tube is the extraction of the radiation through the output mirror. The radiation power

should in this case amount to 0.5 W/cm^3, corresponding to emission of one photon at a wavelength 10.6 μm for each Mg atom that enters the active region. In the experiment, however, much weaker lasing was observed, possibly as a result of either resonant absorption of the radiation by thermalized reaction products or the presence of additional losses inside the cavity due to scattering of the radiation by magnesium particles of 1 μm size, which are produced when the magnesium evaporates. E–V quenching of the luminescence of the atoms and molecules, which are the products of exothermic chemical reactions, also determines the lasing parameters in other gas mixtures. It turns out, e.g., that the vibrational CO levels, which are resonant to the electronic 3p state of the Na atom [81], are nonequilibrium populated in a $N_2O/CO/Na$ flame. In pulsed photolysis of CO_2/N_2O mixtures, lasing on CO_2 is observed and is most likely excited as a result of energy transfer from high-lying electronic levels of the NO molecule, which is one of the photolysis products [82].

The investigation of chemical lasers excited via E–V transfer is of great interest, since it makes it possible to find molecules, such as MgO, which store, when produced in the course of exothermic reactions, energy on metastable electronic levels. Molecules of this type can serve as a basis for chemical lasers that emit in the visible region of the spectrum. Certain problems connected with the development and production of chemical lasers that generate in the visible band on electronic transitions, particularly in the gas-phase reaction $Ba + N_2O \rightarrow BaO^* + N_2$ and others, are considered in the review papers [83, 84]. The study of processes in flame chemical lasers with periodically repeated pulses is the subject of [31, 85].

LITERATURE CITED

1. C. J. Ultee, "Compact pulsed HF laser," Rev. Sci. Instrum., 12, No. 8, 1174-1176 (1971); "Premixed CW electric-discharge CO chemical lasers," Appl. Phys. Lett., 19, No. 12, 535-537 (1971).
2. T. F. Deutsch, "Molecular laser action in hydrogen and deuterium halides," Appl. Phys. Lett., 10, 234-236 (1967).
3. C. J. Ultee, "Pulsed hydrogen fluoride laser," IEEE J. Quantum Electron., 6, 647-648 (1970).
4. J. H. Parker and G. C. Pimentel, "Vibrational energy distribution through chemical laser studies. I. Fluorine atoms plus hydrogen or methane," J. Chem. Phys., 51, 91-96 (1969).
5. J. C. Polanyi and D. C. Tardy, "Energy distribution in the exothermic reaction F + H_2 and the endothermic reaction HF + H," J. Chem. Phys., 51, No. 12, 5717-5719 (1969).
6. E. B. Gordon, V. S. Pavlenko, Yu. L. Moskvin, et al., "Kinetics of pulsed chemical CO laser photo-initiated by carbon-disulfide oxidation," Zh. Eksp. Teor. Fiz., 63, No. 4(10), 1159-1172 (1972).
7. M. A. Pollack, "Laser oscillation in chemically formed CO," Appl. Phys. Lett., 8, 237-238 (1966).
8. S. J. Arnold and G. H. Kimbell, "Chemical laser action in electrically pulsed flowing CS_2–O_2 mixture," Appl. Phys. Lett., 15, 351-353 (1969)
9. C. Wittig, J. C. Hassler, and P. D. Coleman, "Carbon monoxide chemical laser utilizing a fast flow system," Appl. Phys. Lett., 17, 117-118 (1970).
10. R. D. Suart, G. H. Kimbell, and S. J. Arnold, "Continuous-wave simulated emission in flowing carbon disulfide oxygen mixtures," Chem. Phys. Lett., 5, 519-520 (1970).
11. W. Q. Jeffers and C. E. Wiswall, "A transverse-flow CO chemical laser," Appl. Phys. Lett., 17, 67-69 (1970).
12. T. V. Jacobson and G. H. Kimbell, "Transversely spark-initiated chemical laser with high pulse energies," J. Appl. Phys., 41, No. 13, 5210-5212 (1970).
13. L. Alain and L. S. Nicole, "Etude d'un laser a oxyde de carbone forme chimiquement," C. R. Acad. Sci., 271, No. 25, 1212-1215 (1970).
14. B. Ahlborn, P. Gensel, and K. L. Kompa, "Transverse-flow transverse-pulsed chemical CO laser," J. Appl. Phys., 43, 2487-2489 (1972) .
15. M. C. Lin, "Chemical lasers produced from O(^{3}P) atom reactions. III. 5-μm CO laser emission from the O + CH reaction," J. Chem. Kinetics, 6, No. 1, 1-14 (1974).
16. S. Rosenwaks and I. W. M. Smith, "Laser emission from carbon monoxide formed in the flash-initiated reactions of O(^{3}P) atoms with carbon monosulfide and selenide," Trans. Faraday Soc., 69, No. 9, 1416-1424 (1973).
17. S. Tsuchiya, N. Nielsen, and S. H. Bauer, "Lasing action and the relative populations of vibrationally excited carbon monoxide produced in pulse-discharged carbon disulfide–oxygen–helium mixtures," J. Phys. Chem., 77, No. 20, 2455-2464 (1973).

18. M. C. Lin, "Chemical CO and CO_2 lasers produced from the CH + O_2 reaction," J. Chem. Phys., 61, No. 5, 1835-1843 (1974).
19. J. J. Tiee, C. R. Quick, Jr., C. D. Harper, et al., "High-energy pulsed CO chemical laser," J. Appl. Phys., 46, No. 12, 5191-5193 (1975).
20. A. N. Oraevskii, "Onset of negative temperatures in chemical reactions," Zh. Eksp. Teor. Fiz., 45, No. 2 (8), 177-179 (1963).
21. V. L. Tal'roze, "On the generation of coherent stimulated emission in chemical reactions," Kinet. Katal., 5, No. 2, 11-27 (1964).
22. A. N. Oraevskii, "Chemical laser based on branched reactions," Zh. Eksp. Teor. Fiz., 55, No. 4(10), 1423-1429 (1968).
23. O. M. Batovskii et al., "Chemical laser based on branched chain reaction of fluorine with oxygen," Pis'ma Zh. Eksp. Teor. Fiz., 9, No. 6, 341-343 (1969).
24. N. G. Basov, L. V. Kulakov, E. P. Markin, et al., "Emission spectrum of H_2 + F_2 chemical laser," Pis'ma Zh. Eksp. Teor. Fiz., 9, No. 11, 613-617 (1969).
25. L. D. Hess, "Pulsed laser emission chemically pumped by the chain reaction between hydrogen and fluorine," J. Chem. Phys., 55, 2466-2473 (1971).
26. N. G. Basov, V. T. Galochkin, V. I. Igoshin, et al., "Spectra of stimulated emission in hydrogen–fluorine reaction process and energy transfer from DF to CO_2," Appl. Opt., 10, No. 8, 1814-1820 (1971).
27. G. G. Dolgov-Savel'ev, V. A. Polyakov, and G. M. Chumak, "Lasing in the 2.8-μm region on vibrational–rotational transitions of the HF molecule," Zh. Eksp. Teor. Fiz., 58, No. 4, 1197-1203 (1970).
28. N. G. Basov, E. P. Markin, A. I. Nikitin, et al., "Branching reactions and chemical lasers," IEEE J. Quantum Electrom., QE-6, 183-184 (1970).
29. V. T. Galochkin, S. I. Zavorotnyi, V. N. Kosinov, et al., "Investigation of the characteristics of a chemical HF laser excited by a pulsed CO_2 laser," Kvantovaya Elektron. (Moscow), 3, No. 1, 125-130 (1976).
30. O. D. Krogh and G. C. Pimentel, "Chemical lasers from the reactions of ClF and ClF_3 with H_2 and CH_4: a possible chain-branching chemical laser," J. Chem. Phys., 56, No. 2, 969-975 (1972).
31. J. A. Woodroffe and R. Limpaecher, "Pulsed H_2–F_2 laser flameout," Appl. Phys. Lett., 30, No. 4, 195-196 (1977).
32. A. S. Bashkin, A. N. Oraevskii, V. N. Tomashev, et al., "Chemical CO_2 laser on CS_2 + O_3 mixture with photoionization," Kvantovaya Elektron., 3, No. 2, 362-368 (1976).
33. W. B. Lacina and M. M. Mann, "Transient oscillator analysis of a high-pressure electrically excited CO laser," Appl. Phys. Lett., 21, No. 5, 224-226 (1972).
34. T. A. Cool, R. R. Stephens, and T. J. Falk, "A continuous-wave chemically excited CO_2 laser," Int. J. Chem. Kinetics, 1, 495-497 (1969).
35. T. A. Cool, T. J. Falk, and R. R. Stephens, "DF–CO_2 and HF–CO_2 continuous-wave chemical laser," Appl. Phys. Lett., 15, 318-320 (1969).
36. N. G. Basov, V. G. Mikhailov, A. N. Oraevskii, and V. A. Shcheglov, "Thermal methods of laser excitation," Zh. Tekh. Fiz., 37, No. 2, 339-348 (1967).
37. T. A. Cool and R. R. Stephens, "A chemical laser by fluid mixing," J. Chem. Phys., 51, 5175-5176 (1969).
38. T. A. Cool, J. A. Shirley, and R. R. Stephens, "Operating characteristics of a transverse-flow DF–CO_2 purely chemical laser," Appl. Phys. Lett., 17, 278-281 (1970).
39. J. A. Shirley et al., "Purely chemical laser operation in the HF, DF, HF–CO_2 and DF–CO_2 systems," AIAA Paper No. 27, 9 (1971).
40. T. A. Cool, "The transfer chemical laser: A review of recent research," IEEE J. Quantum Electron., QE-9, No. 1, 72-83 (1973).
41. H. Brunet and M. Mabru, "Etude d'un laser **chimique** DF–CO_2 utilisant un ecoulement gazeux transversal," C. R. Acad. Sci., 272, 232-235 (1971).
42. T. A. Cool and R. R. Stephens, "Efficient purely chemical CW laser operation," Appl. Phys. Lett., 16, 55-58 (1970).
43. N. G. Basov, V. V. Gromov, E. L. Koshelev, et al., "CW chemical DF–CO_2 laser," Pis'ma Zh. Eksp. Teor. Fiz., 13, 496-498 (1971).
44. K. G. Anlauf, P. T. Kuntz, D. H. Maylotte, et al., "Energy distribution among reaction products," Discuss. Faraday Soc., 44, 183-193 (1967); "Vibrational population-inversion and stimulated emission from the continuous mixing of chemical reagents," Phys. Lett., 24A, No. 4, 208-210 (1967).
45. C. P. Wang, "Frequency stability of a CW HF chemical laser," J. Appl. Phys., 47, No. 1, 221-223 (1976).

46. C. P. Wang and R. L. Varwing, "Longitudinal mode beat intensities in a CW HF chemical laser," Appl. Phys. Lett., 29, No. 6, 345-347 (1976).
47. J. J. Hinchen and C. M. Banas, "CW HF electric discharge mixing laser," Appl. Phys. Lett., 17, No. 9, 386-388 (1970).
48. Y. Hirose, J. C. Hassler, and P. D. Coleman, "A CW-CO chemical laser from the reaction of active nitrogen with O_2 + CS_2," IEEE J. Quantum Electron., QE-9, No. 1, 114-116 (1973).
49. C. J. Ultee and P. A. Bonczyk, "Performance and characteristics of a chemical CO laser," IEEE J. Quantum Electron, QE-10, No. 2, 105-110 (1974).
50. D. J. Spencer, J. A. Beggs, and H. Mirels, "Small-scale CW HF (DF) chemical laser," J. Appl. Phys., 48, No. 3, 1206-1211 (1977).
51. R. R. Stephens and T. A. Cool, "Continuous wave chemical laser for laser-induced flourescence studies," Rev. Sci. Instrum. 42, No. 10, 1489-1494 (1971).
52. D. I. Rosen, R. N. Sileo, and T. A. Cool, "A spectroscopic study of CW chemical lasers," IEEE J. Quantum Electron., QE-9, No. 1, 163-167 (1973).
53. J. M. Gagne, S. Q. Mah, and Y. Conturie, "Transverse-flow quasi-CW HF chemical laser: Design and preliminary performance," Appl. Opt., 13, No. 12, 2835-2839 (1974).
54. J. A. Glaze, J. Finzi, and W. F. Krupke, "A transverse flow CW HCl chemical laser," Appl. Phys. Lett., 18, 173-175 (1971).
55. J. A. Glaze, "Gain and spectral characteristics of a CW HF/DF chemical laser," Appl. Phys. Lett., 19, No. 5, 135-136 (1971).
56. W. Q. Jeffers and C. E. Wiswall, "Experimental studies of the $O/O_2/CS_2$ CW CO chemical laser," IEEE J. Quantum Electron., QE-10, No. 12, 860-869 (1974).
57. R. D. Suart, P. H. Dawson and G. H. Kimbell, "CS_2/O_2 chemical laser: Chemistry and performance characteristics," J. Appl. Phys., 43, 1022-1032 (1972).
58. K. D. Foster, "Initial distribution of CO from the reaction O + CS → CO* + S," J. Chem. Phys., 57, 2451-2455 (1972).
59. W. Q. Jeffers, C. E. Wiswall and H. Y. Ageno, "Gas additive effects in CO chemical lasers," IEEE J. Quantum Electron., QE-12, No. 11, 693-697 (1976).
60. R. Bleekrode and W. C. Nieuwpoort, "Flame laser: Model and some preliminary experimental results," Appl. Opt., Suppl., No. 2, 179-180 (1965).
61. A. Shawlow and C. H. Townes, "Infrared and optical masers," Phys. Rev., 112, No. 6, 1940-1949 (1958).
62. K. G. Gaydon, The Spectroscopy of Flames, London, Chapman and Hall (1957).
63. S. K. Searles and N. Djeu, "Gain measurements on CO P-branch transition in a C_2H_2-O_2 flame," IEEE J. Quantum Electron., QE-9, No. 1, 116-120 (1973).
64. P. N. Clough, S. E. Schwartz, and B. A. Thrush, "Infrared chemiluminescence from carbon monoxide in the reactions of atomic oxygen with acetylene and carbon suboxide," Proc. R. Soc., 317A, 575-586 (1970).
65. D. M. Creek, C. M. Melliar-Smith and N. Jonathan, "Infrared emission from the reaction of atomic oxygen with acetylene," J. Chem. Soc., 1970A, 646-651 (1970).
66. D. Gutman and S. Matsuda, "Shock-tube study of the acetylene-oxygen reaction. I. $CH(A^2\Delta \rightarrow X^2\Pi)$ chemilumnescence and CO production during the induction period," J. Chem. Phys., 52, 4122-4132 (1970).
67. H. S. Pilloff, S. K. Searles, and N. Djeu, "CW CO laser from the CS_2-O_2 flame," Appl. Phys. Lett., 19, No. 1, 9-11 (1971).
68. K. D. Foster and G. H. Kimbell, "Vibrational population inversion of CO in a free burning CS_2/O_2 flame," J. Chem. Phys., 53, No. 6, 2539-2541 (1970).
69. R. G. Suart, S. J. Arnold, and G. H. Kimbell, "Power enhancement of a CO chemical laser by the addition of vibrationally cool gases," Chem. Phys. Lett., 7, No. 3, 337-340 (1970).
70. V. A. Dudkin, V. B. Librovich, and V. B. Rukhin, "Investigation of chemical CO laser based on a carbon-disulfide flame," in: Chemical Physics of Combustion and Explosion Processes. Kinetics of Chemical Reactions [in Russian], Inst. Chem. Phys. USSR Acad. Sci., Chernogolovka (1977), pp. 13-16.
71. S. K. Searles and N. Djeu, "Characteristics of a CW CO laser resulting from a CS_2-O_2 additive flame," Chem. Phys. Lett., 12, No. 1, 53-56 (1971).
72. M. J. Linevsky and R. A. Carabetta, "Continuous-wave (CW) laser power from carbon disulfide flames," Appl. Phys. Lett., 22, No. 6, 288-291 (1973).
73. K. D. Foster, G. H. Kimbell and D. R. Snelling, "Near single-line operation of a free-burning $CS_2/O_2/N_2O$ flame laser with a nondispersive optical cavity," IEEE J. Quantum Electron., QE-11, No. 6, 253-258 (1975).

74. S. Solimeno, "Chemical lasers," Phys. Bull., 517-520 (Nov. 1974).
75. W. Q. Jeffers, H. Y. Ageno and C. E. Wiswall, "CO chain-reaction chemical laser. I. Experimental," J. Appl. Phys., 47, No. 6, 2509-2510 (1976).
76. D. J. Benard, "CW chemical transfer CO_2 laser," Appl. Phys. Lett., 26, No. 10, 542-544 (1975).
77. J. Schamps and H. Lefebvre-Brion, "Vibrational relaxation of N_2 and CO_2(001) by alkali metal atoms," J. Chem. Phys., 61, No. 5, 1652-1657 (1974).
78. P. H. Lee et al., "Direct observation of vibrationally excited hydrogen produced by collisional energy transfer from electronically excited sodium, rubidium, cesium, and mercury," J. Photochem., 2, No. 2, 165-172 (1973).
79. H. E. Krause, J. Fricke and M. L. Fite, "Excitation of Na D-line radiation in collisions of sodium atoms with internally excited H_2, D_2, and N_2," J. Chem. Phys., 56, No. 9, 4593-4605 (1972).
80. D. J. Benard, R. C. Benson and R. E. Walker, "N_2O pure chemical CW flame laser," Appl. Phys. Lett., 23, No. 2, 82-84 (1973).
81. R. E. Walker et al., "Vibrational disequilibrium in a low-pressure sodium catalyzed carbon monoxide nitrous oxide flame," Chem. Phys. Lett., 20, 528-533 (1973).
82. M. C. Lin, "Photoexcitation and photodissociation lasers. Part I: Nitric oxide laser emissions resulting from $C(^2\Sigma) \rightarrow A(^2\Sigma^+)$ and $D(^2\Sigma^+) \rightarrow A(^2\Sigma^+)$ transitions," IEEE J. Quantum Electron., QE-10, No. 6, 516-521 (1974).
83. C. R. Jones and H. P. Broida, "Chemical lasers in the visible," Laser Focus, 10, No. 3, 37-47 (1974).
84. D. J. Benard, "Sensing chemically excited metastable populations by CO_2 laser gain measurements," in: Electron. Transit. Lasers, Cambridge, Mass., London, MIT Press (1976). pp. 60-67.
85. R. Limpaecher and J. A. Woodroffe, "Flameout in repetitively pulsed chemical lasers," AIAA J., 15, No. 11, 1612-1616 (1977).

CHAPTER 6

SUPERSONIC CHEMICAL LASERS

6.1. Diffusion Chemical Lasers with Thermal Initiation of the Reaction

Operating Principles and Structural Schemes of Supersonic Chemical Lasers. The feasibility, in principle, of obtaining inverted population in gases by thermal excitation methods (by rapid heating or by rapid adiabatic cooling) was considered in [1-10]. It was shown in [6-10], in particular, that a high-velocity stream of a two-component gas mixture in a Laval nozzle can be used to obtain inverted population of molecules and to set in operation a cw laser in the infrared band. If mixtures components capable of entering in a chemical reaction are used, then the gas dynamics, the chemical reaction, the optical radiation, as well as the convective transfer (if the components are separated beforehand) serve to convert the energy of the chemical reactions into molecule-excitation energy.

Conditions for the most effective conversion of the chemical-bond energy into coherent stimulated emission energy, with sufficiently high transport velocities of the components into the reaction zone and with sufficiently small backward diffusion from the reaction zone, as well as collisional deactivation in the active medium during the time preceding the lasing, can be created in supersonic streams. To obtain such streams, in turn, it is necessary to heat the gas mixture to a sufficiently high temperature, and this heating can simultaneously be used to dissociate the medium into chemically active centers, i.e., for thermal initiation of the reaction in supersonic chemical lasers.

The chemical reaction can be initiated here, just as in subsonic chemical lasers, also by the combustion process, by electric discharge, e.g., by a microwave induction discharge, or by shock waves. The different structural features of chemical lasers are governed by the different processes that take place in the chemical supersonic lasers and by the various methods used to initiate the chemical reactions.

The operating principle of supersonic diffusion (SD) chemical lasers with thermal initiation of the chemical reaction is based on successive realization of the following processes:

heating the heat-transfer agent to a temperature that ensures the required degree of dissociation of the chemical reagent;

mixing this chemical reagent with a heat-transfer agent and its dissociation into chemical active centers in the mixing process;

acceleration of the mixture of the heat-transfer agent with the chemically active centers to supersonic velocity;

injection and diffusion, into the supersonic stream, of this fuel mixture of molecules that enter into the pumping reaction with the chemically active centers contained in the stream;

excitation, in a downstream cavity, of lasing by the active molecules produced in the course of the pump reaction.

These processes are realized, e.g., in the SD chemical laser design shown schematically in Fig. 6.1 [11-13]. In such a cw SD chemical laser with thermal initiation of the reaction, N_2 or He is heated by an electric arc and causes, upon mixing, dissociation of the SF_6; as a result, F atoms appear in the expanding extension 7, in accordance with the reaction (5.1).

Inversion is obtained upon diffusion of H_2 or D_2 into the supersonic stream containing F atoms. On passing through the nozzle array, the gas is accelerated to supersonic velocities and H_2 is introduced into this stream. In analogy with the process (5.1), the pumping reaction

$$F + H_2 \rightarrow HF(v) + H\ (-134\ \text{kJ/mole},\quad v \leqslant 3) \tag{6.1}$$

produces vibrationally excited HF. The HF molecules approach a state of thermodynamic equilibrium because of the induced emission and the collisional deactivation process. The latter can be written in the form

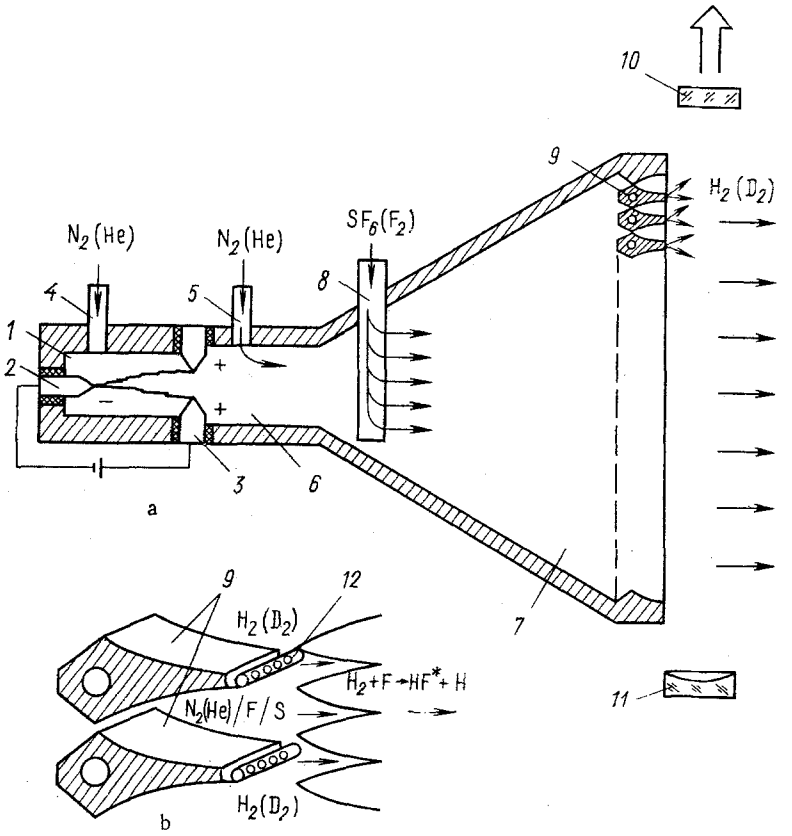

Fig. 6.1. Supersonic chemical laser with thermal initiation of the reaction: a) construction of chemical laser; b) element of nozzle array and flow diagram; 1) electric-discharge chamber; 2) cathode; 3) anode; 4) entry of transfer agent; 5) injector for additional heat-transfer agent; 6) secondary chamber; 7) expanding extension; 8) injector of chemical reagent (oxidizer); 9) supersonic-nozzle block; 10) semitransparent mirror or mirror opening for the extraction of the radiation; 11) total-reflection mirror; 12) fuel injectors.

$$\mathrm{HF}\ (v) + \mathrm{M} \rightarrow \mathrm{HF}\ (v-1) + \mathrm{M}; \tag{6.2}$$

$$\mathrm{HF}\ (v) + \mathrm{M}\ (v') \rightarrow \mathrm{HF}\ (v-1) + \mathrm{M}\ (v'+1), \tag{6.3}$$

where (6.2) and (6.3) are, respectively, V—T and V—V collisions. The gas-dynamic and energy parameters obtained for chemical lasers [12, 13] are listed in Table 6.1. (The subscript 0 denotes hereafter the parameters of the gas in the electric-discharge chamber, while j labels the parameters at the exit from the nozzle block.)

The constant conditions were $\dot{m}_{N_2} = 8.5$ g/sec; $\dot{m}_{H_2} = 1.0$ g/sec; and $p_0 = 0.166$ MPa; the arc power was 42.5 kW; the Mach number $M_j = 4.4$; $T_j = 0{,}205\ T_0$; $p_j = 3{,}92 \cdot 10^{-3}\ p_0$; $u_j = 2{,}03 \cdot 10^3 \cdot (T_0/2500)^{1/2}$ m/sec; $(c_F)_j = 1{,}55 \cdot 10^{-7} \cdot (p_F/p)_0\ (2500/T_0)$ mole/cm^3.

For effective conversion of the chemical-bond energy into coherent stimulated emission energy, it is necessary that the velocity of the diffusion of H_2 in the stream and the rate of the pump reaction (6.1) be large compared with the rates of the collisional deactivation (6.2), (6.3). These rates can be estimated by representing the flow in the diffusion region of H_2 as shown in Fig. 6.2, where $\delta(x)$ is the boundary of the diffusion region in the y direction. For laminar flow the following relation is satisfied:

$$\delta = k_l (Dx/u_j)^{1/2}, \tag{6.4}$$

where k_l is a constant of order of unity. For diffusion of H_2 in N_2 we have

$$D = 15{,}8 \cdot 10^{-4}\ T_j^{3/2}\ p_j^{-1}\ \mathrm{cm^2/sec} \tag{6.5}$$

TABLE 6.1. Example of the Gas-Dynamic and Electric Parameters of an SD Chemical Laser

$\dot{m}_{SF_6}$, g/sec	W, W	Conditions in prechamber				η_c, %
		T_0, K	$(p_F/p)_0$	G_F, mole/sec	$\frac{G_F}{6G_{SF_6}}$	
0,105	90	4150	0,014	0,00431	1,00	15,8
0,203	167	3970	0,0267	0,90833	1,00	15,2
0,297	236	3870	0,0387	0,0122	1,00	14,7
0,400	293	3660	0,0513	0,0164	1,00	13,5
0,505	357	3510	0,0639	0,0207	1,00	13,1
0,600	415	3400	0,075	0,0246	1,00	12,8
0,800	514	3200	0,0976	0,0328	1,00	11,9
1,00	586	2920	0,116	0,0396	0,96	11,2
1,25	648	2680	0,135	0,0473	0,92	10,4
1,40	692	2580	0,145	0,0515	0,90	10,2
1,60	722	2480	0,153	0,0548	0,83	10,0
1,80	738	2400	0,155	0,0555	0,75	10,1
2,00	732	2360	0,156	0,0560	0,68	9,9
2,20	710	2320	0,157	0,0564	0,62	9,7

(T_j, deg K, p_j, Pa). Let $h_{y,1/2}$ be the half-width of the stream (see Fig. 6.2). The characteristic diffusion length $x = L_D$ will then correspond to $\delta = h_{y,1/2}$, and from Eqs. (6.4) and (6.5), expressing u_j in terms of the Mach number M_j, we obtain

$$\frac{T_j p_0}{T_0 p_j}\left(\frac{\mu}{28}\right)^{1/2}\left(\frac{k_l}{2}\right)^2\frac{T_0}{2500}\left(\frac{10^4}{p_0}\right)h_{y,1/2}^{-2}L_D \sim M_j, \tag{6.6}$$

where μ is the molar mass.

When reagents are mixed at $x = 0$, the rate of the initial development of the process (6.1) can be represented in the form

$$u_j(dc_F/dx)_{x=0} = -(k_f c_{H_2} c_F)_{x=0}. \tag{6.7}$$

The characteristic length of the reaction along the stream is determined by the relation

$$L_R = \left[\frac{c_F}{dc_F/dx}\right]_{x=0}. \tag{6.8}$$

Here L_R is the longitudinal distance that the flux must negotiate in order for all the F atoms to react, if the total rate of the reaction remains equal to its initial value. If the local partial pressure of the F atoms is $p_F = 8\cdot10^6 c_F T$, we get from (6.7) and (6.8)

$$\left(\frac{\mu}{28}\frac{1.4}{\gamma}\right)^{1/2}\left[\frac{c_{H_2}}{c_F}\frac{5.0}{M}\frac{p_F}{10^4}\right]_j L_R \sim \frac{T_j^{3/2}}{k_f}. \tag{6.9}$$

The left-hand side includes the parameters that characterize the operating conditions of the SD chemical laser, while the right-hand side of (6.9) is a function of T_j, with

$$k_f = 12.0\cdot10^{13}\exp\left[-1710/(1.987\,T_j)\right]. \tag{6.10}$$

The relations $L_D = f_1(M_j)$ and $L_R = f_2(T_j)$ are used to estimate the order of magnitude of L_D and L_R, assuming that under typical operating conditions of SD chemical lasers we have $k_f/k_b \gg 1$. If at the same time $L_D/L_R \gg 1$, the reaction zone is governed by diffusion mixing, and if $L_D/L_R \ll 1$, we can assume that the H_2 has completely diffused in the stream at the section $x = 0$, so that the reaction should be regarded as in a one-dimensional flow. For typical operating conditions of an SD chemical laser with the parameters indicated in Table 6.1, at $T_j = 500°K$, $M_j = 4.4$ we find [12] that $L_D \approx 4$ cm and $L_R \approx 0.4$ cm. This means that the reaction zone is determined by the supersonic diffusion of the components.

The component-mixing picture depends also on the employed nozzle-block construction. Figure 6.3 shows some of the most widely used nozzle configurations. The advantage of nozzle blocks consisting of axisymmetric matrices over slit injectors is pointed out in [14] and consists in the fact that they are easier to prepare, have better initial-mixing characteristics, and have a small nozzle dimension at the exit (2-3 mm).

Greatest interest attaches to the study of such SD chemical-laser parameters as the power W and the chemical efficiency η_c. The influence of the changes of the flow rates of the working-mixture components and of the distance x_c from the optical axis of the cavity to the

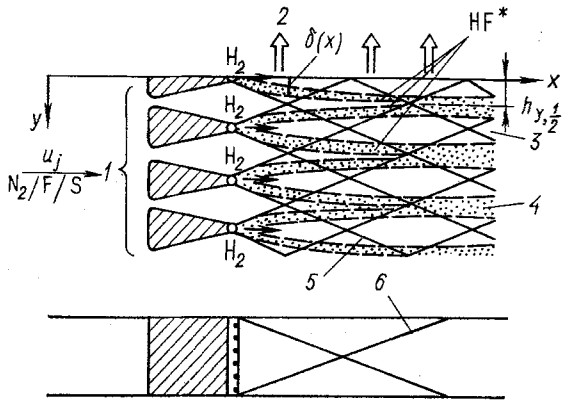

Fig. 6.2. Supersonic diffusion of fuel: 1) supersonic nozzles; 2) generated radiation; 3) region filled with hydrogen; 4) region of mutual diffusion of the components; 5) shock waves produced by chemical reaction; 6) shock waves reflected from the walls.

nozzle exit section was investigated in [12], together with the influence of the addition of various gases.

Plots of the chemical efficiency and of the lasing power of SD HF chemical lasers vs the mass flow rate $\dot{m}_{SF_6}$ at constant flow rate of N_2 and H_2 and at constant flow parameters are shown in Fig. 6.4. The power was measured in a cavity with total-reflection mirrors at x_c = 1.9 cm; the mirrors had a curvature radius 1.15 m; the distance between mirrors was 1 m. The chemical efficiency of the SD chemical laser was determined from the relation

$$\eta_c = \frac{W\,(\text{kW})}{133 G_F (\text{mole/sec})} \cdot 100\,. \tag{6.11}$$

Equation (6.11) is the ratio of the real lasing power to the power theoretically attainable if one starts with the reaction (6.1). The chemical efficiency decreases from 16 to 8-10% at maximum power. The shaded region in Fig. 6.4 corresponds to the scatter of the data on the chemical efficiency, obtained as a result of a large number of experiments. The scatter is due to errors in the estimates of G_F, connected with the determination of the SF_6 concentration, and to the errors in the determination of the electric energy given up by the arc to the gas. At small SF_6 flow rates these errors are smaller, inasmuch as under these conditions, SF_6 dissociates almost completely and the flow rate G_F corresponds to the flow rate of SF_6. The decrease of the chemical efficiency with increasing G_F can be due only to an increase in the HF–HF collisional dissociation.

The lasing power increases with increasing SF_6 flow rate and reaches a maximum at $\dot{m}_{SF_6}$ = 1.8 g/sec. The appearance of the maximum is due to the decrease of the chemical efficiency with decreasing degree of dissociation of the SF_6 ($G_F/6G_{SF_6}$) at large SF_6 flow rates. At maximum power, the flow rate of H_2 is nine times larger than the stoichiometric value needed for the reaction (6.1), i.e., $G_{H_2}/G_F = 9$. A decrease in the flow rate of H_2 leads to a decrease in the lasing power, as a result of the corresponding decrease of the rate of diffusion of H_2 into the supersonic flow.

The SD chemical-laser parameters can also be optimized by varying the heat-carrier material, the additives, and their flow rates. Since the SF_6 is incompletely dissociated even when the maximum lasing power is achieved, additional increase in power can be obtained by introducing oxygen into the high-pressure chamber. For example, at $T_0 \approx 2000°K$ and $p_0 \approx 0.1$ MPa the source of the F atoms can be, besides (6.1), also the reaction

$$SF_4 + O_2 \rightarrow SO_2F_2 + 2F. \tag{6.12}$$

In [15], besides investigating the influence of O_2 additions, the authors studied the change of the parameters of an SD HF chemical laser with the heat carrier N_2 replaced by He. The data obtained at x_c = 1.9 cm (see Fig. 6.4) are compared in Fig. 6.5 with other operating regimes of the HF SD chemical laser. A comparison shows that addition of a small amount of oxygen into the heat-transfer agent leads to an increase in the generated power by 20-30%. This is probably due to the reaction (6.12). An SD chemical laser with helium as the heat-

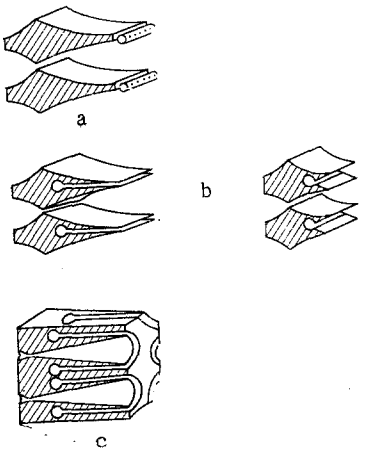

Fig. 6.3. Nozzle construction: a) with perforated tubes; b) with slits; c) nozzle block of axisymmetric matrices with annular supply of the component.

transfer agent has better parameters than that with nitrogen. It is typical that the use of helium makes the powers generated by SD chemical lasers with HF and DF practically identical, whereas when the heat carrier is nitrogen the maximum power of the SD chemical laser with DF is only 70% of the maximum power of the SD chemical laser with HF [15].

As already mentioned, the characteristics of flow-through chemical lasers are determined by competing processes, namely the formation of the excited molecules, the diffusion of two streams in each other, e.g., with reagents F and H_2, and deactivation of the excited molecules by collisions. It can be assumed that the HF* formation is fast compared with the remaining two. If the diffusion time is shorter than the deactivation time, chemical and quantum-mechanical processes should be controlled by the deactivation process, and the processes in the chemical laser should be independent of the mixing. If the deactivation time is shorter than or of the order of the diffusion time, the quantum-mechanical effect of the radiation generation decreases because of the absorption that takes place during the time preceding the total consumption of the reagents.

The properties, e.g., of an HF chemical laser with transverse flow and with microwave initiation of the reaction, improved substantially in the accelerated flow. Figure 6.6 shows an improvement, carried out in [16], of an earlier subsonic design. The zone A located between the microwave-discharge region and the H_2 injectors contains a mixture of F atoms, inert gas, and the SF_6 dissociation products. The hydrogen accelerated at the entrance of the nozzle in zone B diffuses rapidly into the fluorine jet. A homogeneous mixture of fluorine and molecular hydrogen is produced. The HF (v) is formed in zone C via the reaction (6.1). The generated radiation is extracted from a cavity made up of mirrors spaced 40 cm apart.

In such a chemical laser, the radiated power W increases linearly with the ionization potentials of the added rare gases. The higher their ionization potential, the higher the average electron energy and consequently the larger the SF_6 dissociation by inelastic electron collisions in accordance with the relation

$$SF_6 + e \rightarrow SF_i^+ + (6 - i)\,F + 2e \quad (i = 1, \ldots, 6). \tag{6.13}$$

This increase of W is explained in [17] as being due to the mechanism of SF_6 dissociation by electron impact, according to which up to three F atoms are produced from the one electron with kinetic energy close to the ionization potential of the helium, whereas only one F atom is produced from one electron with kinetic energy close to the ionization potential of Ar. On the other hand, a linear relation exists between W and the introduced microwave power. The strong dependence of W on the inert-gas additives and the weak dependence on the O_2 additive shows that dissociation of SF_6 with formation of chemically active centers (F atoms) is due to electron collisions. On the other hand, a contribution to the dissociation from atoms with a metastable state is impossible when Kr and Ar are used, and is small in He.

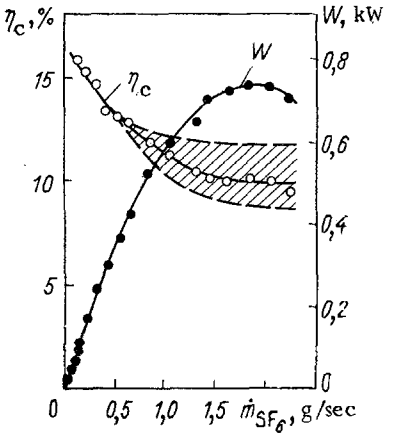

Fig. 6.4. Dependence of the chemical efficiency and of the lasing power on the mass flow rate of SF_6 at constant mass flow rates $\dot{m}_{N_2}$ = 8.5 g/sec and $\dot{m}_{H_2}$ = 1.0 g/sec.

The efficiency of the chemical laser increases substantially if the chemically active centers are used repeatedly, e.g., oxygen atoms, as a result of the chain reaction from (5.4) and (5.6):

$$\left.\begin{aligned} O + CS \rightarrow CO^* + S, \\ S + O_2 \rightarrow SO + O. \end{aligned}\right\} \tag{6.14}$$

Here CS is the fuel, while O and S are the active centers.

The efficiency of multiple use of each atom in a mixture of fuel and oxidizer is measured by the average chain length

$$l^* = G_{CO}^{end}/G_O^{init}. \tag{6.15}$$

Here G_{CO}^{end} is the CO flow rate at the exit from the cavity, and G_O^{init} is the flow rate of the O atoms that initiate the reaction. In essence, l^* is the average number of pump-reaction cycles in which the O atom participates until it is lost in the course of some quenching reaction (e.g., O + OCS → CO + SO).

The chain reaction (6.14) was realized in the experimental setup illustrated in Fig. 6.7. A stream of CS_2 passes through an electric heater 1, in which the CS_2 molecules are thermally dissociated into CS and S. The heating temperature is approximately 2400°C. The flow rate of the CS reaches in this case 1 mmole/sec; the ratio of the molar concentrations of the CS and CS_2 at the exit from the heater is 2.2. Introduction of helium into the hot CS/CS_2 gas through supersonic nozzles 2 and passage of the produced mixture through a supersonic diffusor 3 leads to a lowering of the gas-flow temperature and to an increase of the pressure.

At the exit from the diffusor is placed a ring injector 4 which makes it possible to uniformly introduce various impurities into the gas stream. Before entering the cavity 6, the stream passes through a transition section 5, in which its cross section changes from circular to rectangular (height 0.95 cm; length along the optical axis 9.84 cm). In the wedge-shaped region (length along the stream direction 15 cm) the stream is accelerated and expands from 0.95 to 3 cm.

The pumping reaction is initiated at the entrance to the cavity by injecting into the CS/CS_2/He stream with sonic velocity a mixture O/O_2/He through two oppositely placed rows of holes 7 (hole diameter 1.5 mm; distance between centers 2.0 mm; each row contains 48 holes). At the exit from the active region, the gas stream enters a large branched pipe 8, and the chemical composition of the stream in this region is determined with the aid of a quadrupole mass spectrometer 9 (the measurement procedure is similar to that used in [18]).

The principles of obtaining lasing by using low-toxicity reagents that are convenient to use, and simulation of the operation of continuous chemical lasers with large flow rates of the reagents, are being developed also for compact shock-wave chemical lasers, of the

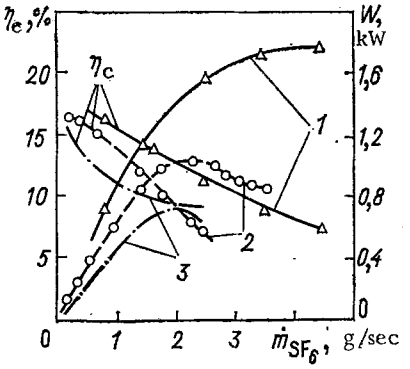

Mixture	$\dot{m}$, g/sec	Curves	Reference
$He/H_2/O_2$	2,06/1,25/0,75	1	[14]
$N_2/H_2/O_2$	8,5/1,0/0,4	2	[12,15]
corresponds to Fig. 6.4		3	[14]

Fig. 6.5. Dependence of the generated power and the chemical efficiency on the mass flow rate of SF_6.

shock-tube type with a supersonic nozzle and with mixing of the stream at the exit of this nozzle, where the fuel is injected into it [19]. In such a device (Fig. 6.8) the oxygen dissociates in a three-section tube 1 behind the shock-wave that is reflected from the constriction at the entrance to the nozzle 2.

A supersonic wedge-shaped nozzle with critical cross section 0.3 × 70 mm was equipped in its expanding section with an injector 3. The stream passed into the cavity 4, which was connected with receiver 5.

A mixture of oxygen with argon was admitted into the low-pressure chamber, which was separated from the nozzle by a diaphragm. The injected gas, a CS_2/He mixture, was fed through an electromagnetic valve, which opened 5 msec after the startup of the shock tube and had an opening time shorter than 0.5 msec. The outflow of the $O/O_2/Ar$ mixture from the shock tube started 3 msec after the opening of the valve. To prevent contamination, helium was blown over the cavity mirrors through another electromagnetic valve synchronized with the startup of the setup.

One other shock-wave chemical-laser setup with mixing of the reagents was proposed in [20], where, in the configuration of the shock waves reflected from the constriction at the entrance of the supersonic continuous stream into the cavity, the mixture was heated and the following chemical reaction took place:

$$N_2 + CF_3I + Q \rightarrow CF_3 + I^* + N_2. \qquad (6.16)$$

The excited iodine atom produced a photon downstream in the cavity region: $I^* \rightarrow I + h\nu$.

The examples of the shock-wave chemical lasers presented here should be supplemented by the suggestion [21] for initiating a reaction by a shock-wave, and by the developed SD chemical laser that starts continuous operation within 1.8 msec and is based on reflected-shock-wave geometry [22] in a F_2/HCl mixture. In this wave, the fluorine dissociated partially, $F_2 + M \rightarrow 2F + M$, and then the resultant stream expanded in a nozzle with a Mach number M = 4. The HCl was expanded in a nozzle with M = 2 until its static pressure reached the same as in the foregoing stream. The gas streams were mixed in a two-dimensional diffusion zone with the reaction $F + HCl \rightarrow HF^* + Cl$, and the output power was generated in an optical cavity transverse to the stream. Also used in the SD chemical laser was the pumping reaction $Cl + HI \rightarrow HCl^V + I$. In this case $\eta_C \approx 3.5\%$ for the mixture $He/ClO_2/NO/HI$.

The thermal energy needed for the SD chemical laser is obtained by combustion in the high-pressure chamber [23], into which some of the F_2 flows for the reaction with H_2, and by obtaining a temperature that ensures dissociation of the remaining part of the F_2 flow.

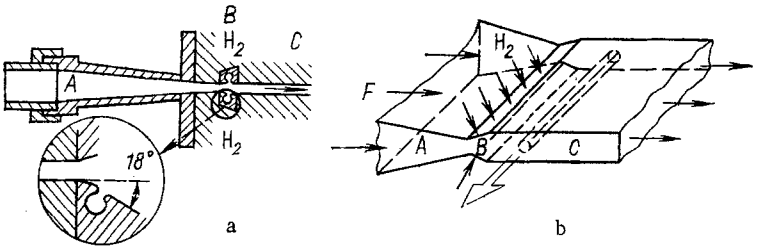

Fig. 6.6. Schematic diagram of the working chamber (a) and of the entry of the gases (b) in a HF diffusion chemical laser.

An attempt at simultaneously using electric heating in the high-pressure chamber and combustion at the exit from the nozzle is described in [24]. Here, under the action of a discharge temperature of approximately 6000°K, the N_2 was transformed into a stream of active nitrogen in the form of a mixture of vibrationally and electronically excited molecules. This mixture expanded through the nozzle into the reaction chamber at a velocity up to 15 km/sec. The pressure in the chamber was 1.33 kPa. When hydrocarbon was injected into the supersonic stream of active nitrogen, a bright flame was produced at the exit from the nozzle. An investigation of the chemiluminescence of this flame yielded a photon yield of 18.5% for the CN $A^2\Pi \rightarrow X^2\Sigma^+$ radiation using C_2F_4 as the reagent. Estimates [24] have shown that under conditions of vibrational cooling of the populations of the electron-excited states it is possible to reach a positive gain in such a system.

A mixture of oxygen with argon up to temperatures in the interval 1000-4000°K at a pressure 20-50 kPa was heated in the electric-discharge chamber, and a mixture CS_2/Ar/He [25] was injected into the produced supersonic screen with the O atoms at the exit from the nozzle. This ensured effective production of CO* and generation, in the cavity placed transverse to the stream, of radiation with power 34 W in the V–R transition band from 4.9 to 5.7 μm.

A search for substances that can be conveniently used to obtain chemically active centers has led, in particular, to the use of liquid fuels such as toluene ($C_6H_5 \cdot CH_3$) or C_6F_6, which reacts with NF_3 [26]. In such a liquid-fuel SD chemical laser, combustion of the reagent produces excited fluorine, which after dilution with helium expands through the nozzles from 0.3-1 MPa in the combustion chamber to 0.133-1.33 kPa in the cavity. The fluorine-containing stream is mixed in the nozzles with the injected material, and excited DF* molecules are produced and cause lasing up to 8 kW for 120 sec.

6.2. Supersonic Chemical Lasers with Energy Transfer

The method of obtaining lasing in the cw regime with an auxiliary component was proposed in [7, 27]. Such a purely chemical laser, in which rapid replacement of the reagents makes it possible to use components that react at a high rate without initiation, was first realized in [28]. The process is based on the reaction of D_2 (H_2) with F_2, followed by transfer of the excitation energy to CO_2, i.e., the same reaction (5.9) as in the chemical lasers described in Secs. 4.1, 5.2. Examples of other reactions are given in [29].

The gas-dynamic laser described in [2, 6] is an example of a device capable of working at sufficiently high static pressures up to atmospheric at the exit of the diffusor. In the case of supersonic chemical lasers, however, the use of a similar open cycle of a gas-dynamic laser would make it possible to dispense with the spent-gases evacuation system which is needed to maintain a low pressure in the cavity. The system of a hybrid supersonic chemical laser described in [30] (Fig. 6.9) is similar, with respect to the flow conditions, to the gas-dynamic CO_2 laser [31]. This system is, in principle, the same as that shown in Fig. 6.1, but the electric-discharge chamber is replaced by combustion chamber 1, and a supersonic diffusor 2 is placed at the exit of the stream. The stream passes through nozzles 3 into a cavity made up of mirrors 4. Approximately half of the gas flow rate is produced by its arrival from the chamber where CO is burned in oxygen diluted with helium to raise the temperature to 1400°K at a pressure of 1.5 MPa. The hot gases at the entrance to the block of the supersonic nozzles form a mixture of He, CO_2, F_2, and F. This mixture, on passing through the nozzle, is accelerated to the supersonic velocity, is mixed with deuterium, and enters the resonator. By choosing the nozzle parameters it is possible to ensure a pressure ~8 kPa in the cavity region. A diffusor placed behind the resonator makes it possible to raise the

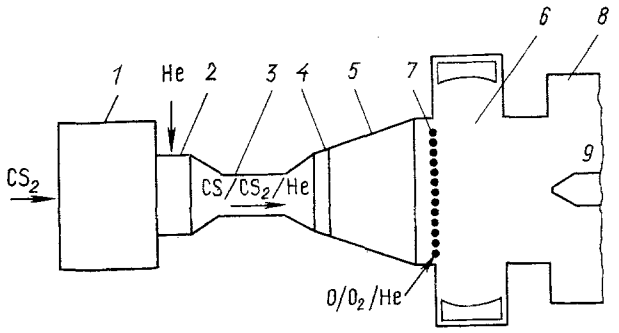

Fig. 6.7. Diagram of CO diffusion chemical laser: 1) electric heater; 2) supersonic-nozzle block; 3) supersonic diffusor; 4) annular injector; 5) transition section; 6) cavity; 7) rows of holes; 8) pipe; 9) mass spectrometer.

static pressure to atmospheric. A small model of a supersonic hybrid chemical laser [30] yielded a total lasing output power higher than 500 W at η_c = 3%, at a specific power of approximately 30 $kW \cdot (kg \cdot sec)^{-1}$, and at a pressure p_c = 3 kPa in the cavity.

A large-scale DF/CO_2 chemical laser with energy transfer was constructed in both a subsonic (IRIS-I) and a supersonic (IRIS-II) variant [32]. The fuel used was nitrous oxide mixed with CO_2, and the oxidizer was fluorine diluted with helium. These two variants differ from each other only in the presence of a supersonic-nozzle block in IRIS-II, which ensured acceleration of the stream to a Mach number of the order of M = 1.75. This Mach number is due to the degree of expansion 6:1, which in turn is caused by the pressure in the combustion chamber and in the cavity. The pressure in the combustion chamber must not exceed approximately 13 kPa, in order to minimize the formation of NOF which noticeably lowers the output characteristics of the chemical laser, and the pressure in the cavity should be higher than 2 kPa to ensure that the chemical reaction takes place. The output powers obtained in the subsonic and supersonic regimes are, respectively, approximately 5-15 kW at cavity pressures p_c = 8-4.7 kPa and 6-7.7 kW at p_c = 3-1.8 kPa.

Thus, a substantial restriction on the operation of both subsonic and supersonic hybrid chemical lasers is that they can produce generation only at cavity pressures not more than 8 kPa. It was found, however, that a radical change in the evolving opinions concerning the designs of supersonic chemical lasers and the conditions of their operations makes it possible to produce chemical lasers with cavity pressures higher than 27 kPa [33]. The construction of such a chemical laser differs from ordinary supersonic lasers in that one nozzle is used rather than a block of numerous small nozzles, and that the gas in the high-pressure section is at room-temperature, in contrast to chemical lasers with electric-arc heating or with combustion to obtain atomic F.

Let us examine in greater detail such an unusual, compared with the prevailing notions, chemical laser, shown in Fig. 6.10. The primary gas stream in it consists of the mixture $F_2/CO_2/He$ produced in the mixing section 1. This primary stream, which is at room temperature, passes through a grate 2 intended to destroy the large-scale vortices in the stream. Downstream is located an injector 3 for the gases NO and D_2; the exit from this injector is located on the axial line of the two-dimensional nozzle 4 whose exit end section and throat have an area ratio 1.14. This ensures a Mach number of approximately 1.5 at the exit from the nozzle. The dimensions of the exit end section are 1.488 × 4.445 cm and their longer side is in the direction of the cavity axis 5. The NO/D_2 mixture is injected in the primary stream inside the nozzle through 20 small tubes with inside diameter 0.122 cm and outside diameter 0.183 cm. Each tube is terminated with 17 holes of 0.024 cm diameter. These holes ensure outflow of the gas with a maximum angle 20° to the primary-stream direction. The entire construction is made of aluminum and teflon.

The jet exits into a large cavity chamber evacuated with a mechanical pump. Two 10 × 10 cm water-cooled gold-coated mirrors made up a cavity with total-reflection mirrors for the measurement of the power of the optical radiation at 10.6 μm wavelength.

Directly near the jet are mounted tubes that feed helium to keep the strongly absorbing CO_2 (100) contained in the hot surrounding gas from landing in the optical path of the stable cavity.

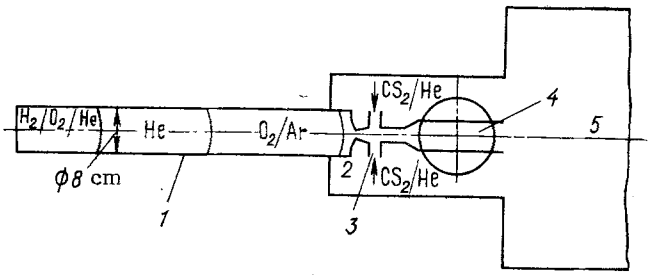

Fig. 6.8. Diagram of chemical laser with shock-wave initiation of the reaction: 1) three-section tube; 2) nozzle; 3) injector; 4) cavity; 5) receiver.

The curved mirror was made movable to determine the change of the power as a function of the position of the optical axis.

When the NO/D_2 gas is mixed with the primary stream, F atoms are obtained via the reaction $F_2 + NO \rightarrow F + NOF$. These F atoms then excite the DF chain which was considered in detail in Sec. 4.1:

$$F + D_2 \rightarrow DF^*(v) + D;\ D + F_2 \rightarrow DF^*(v) + F,$$

and the excited DF (v) pumps the CO_2 to the state (001), which then produces the lasing. To increase the efficiency of this effect it is necessary to have a high CO_2 concentration. Without CO_2, the excited DF is deactivated too rapidly by the collisions, and no lasing sets in.

Measurements of the power when using a cavity with total-reflection mirrors have revealed a sufficient gain, 0.7 cm^{-1}. The power, 1.45 kW, was measured in a chemical laser with optical axis located 3.89 cm downstream from the nozzle exit section. This power corresponds to $\eta_c = 1.9\%$. Under these conditions the pressure was 84 kPa in the forechamber and 31 kPa in the cavity proper. The stream in the jet consisted of 5.29 g/sec F_2, 57.8 g/sec CO_2, 15.1 g/sec He, 1.61 g/sec D_2, and 1.53 g/sec NO. It should be noted that all these mass flow rates, the pressure in the cavity, and the position of the optical axis were not the optimal values for maximum power.

Hybrid supersonic chemical lasers can also be constructed, in which molecular deuterium mixed with argon is dissociated behind a reflected shock-wave [34]. This set-up (see Fig. 6.8) also produced lasing on the mixture $D/O_3/CO_2$ in the quasicontinuous regime. The mixture $D/D_2/Ar$ obtained behind the reflected shock-wave passed through a supersonic flat wedge-shaped nozzle into an injector, where it was mixed with a subsonic stream of a mixture of ozone, carbon dioxide, and helium, fed through an electromagnetic valve. The mixing of the streams led to the basic reactions

$$D + O_3 \rightarrow OD^*(v) + O_2;$$
$$OD^*(v) + CO_2(00^00) \rightarrow OD^*(v-1) + CO_2(00^01).$$

The stream proceeded from the mixing chamber of the injector into a cavity with optical axis perpendicular to the stream. The operating time of such a chemical laser was determined by the time of outflow of the gas heated behind the shock-wave, and amounted to 4.5 msec. The lasing duration was almost four times longer than the lifetime of a quasistationary state behind the reflected shock-wave front.

Lasing was obtained in the following regime: initial pressure of the mixture $D_2/Ar = 1/15$ in the low-pressure channel of the shock tube 9 kPa; the velocity of the incident shock-wave 1.48 km/sec; pressure of the $O_3/CO_2/He = 1/3/17$ mixture in the valve at the instant of the start of its outflow 50 kPa. The cavity consisted of a gold-coated total-reflection spherical mirror with curvature radius 3 m, and a flat dielectric coupling mirror with transmissivity ~1%.

In this regime, lasing was obtained with a peak power 1.5 W at a power 0.4 W averaged over 4.5 msec. To prove the chemical mechanism of the population inversion of the CO_2 molecules, control experiments were performed with deuterium or ozone excluded from the mixtures. In these two cases there was no lasing. When the deuterium was replaced by hydrogen, lasing was also obtained, but at a noticeably lower lasing power.

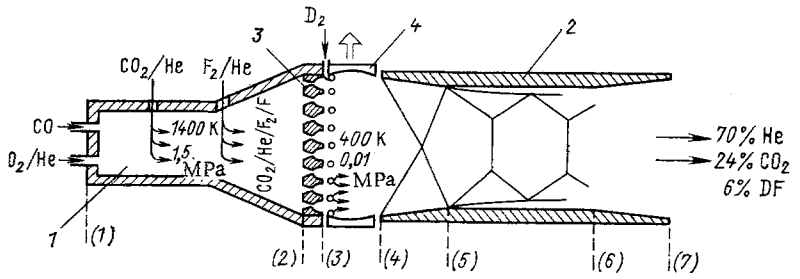

Fig. 6.9. Diagram of supersonic chemical laser with energy transfer. 1) Combustion chamber; 2) diffusor; 3) nozzle block; 4) cavity mirrors; the numbers (1)-(7) in the parentheses designate the sections of the chemical-laser channel.

6.3. Gas-Dynamic Chemical Lasers

The real conditions of the processes in gas-dynamic lasers are frequently such that chemical reactions take place in them, depending on the method of producing the working medium and on the construction of the gas-dynamic laser. This is particularly the case when the gas-dynamic lasers are optimized by choosing special mixtures, by selecting the proper conditions for fuel ignition and gas mixture, and by stimulation of definite reactions [35]. Included among the chemical gas-dynamic lasers are, e.g., facilities in which nonequilibrium chemical combustion reactions produce vibrationally excited molecules that are used as a working medium of the gas-dynamic laser [36]. Thus, combustion of CO in air produces vibrationally excited CO_2 molecules with vibrational temperature exceeding the gas temperature. When CO or hydrocarbons are burned, more than 20% of the heat is realized in the infrared band. Part of this radiation constitutes the 4.4-μm V–R band, with the aid of which the energy is pumped to the upper level [37]. The excited CO_2 molecules can be produced also by additional burning of the mixture in the nozzle. Thus, Fig. 6.11 shows a diagram of a similar cw chemical laser with supersonic flow of the medium [38], operating on a reaction whose products are not toxic. The oxidation reaction $CO + 0.5\ O_2$ in the $CO/0.5O_2/H_2/He$ mixture is used. The working mixture was admitted into the combustion chamber 2, after which it was ignited with a spark. A pneumoelectric valve 1 made it possible to feed the ignited mixture into nozzle 3 at practically any instant of the ignition process.

For comparison, the pure gas-dynamic regime was investigated in addition to the chemical gas-dynamic lasing regime. It was found that the power in the former case decreases substantially when the combustion chamber is opened on the ignition leading front, which is responsible for the most intense burning of the mixture. The decrease in the power can be atrributed to the fact that on the leading front in the mixture there is still not enough CO_2 and the temperature is low.

In contrast to the gas-dynamic regime, the maximum power in the chemical gas-dynamic regime was realized precisely in the region where the conditions for thermal pumping are far from optimal. The maximum power in this case is observed when the combustion chamber is opened on the leading front of the conflagration, when the temperature in it is 600-900°K. When the combustion chamber is opened on the trailing edge and at the same temperatures, there is no lasing. Thus, this experiment shows that the excited CO_2 molecules are produced as a result of additional burning of the mixture in the nozzle.

When the cavity axis is moved away from the throat of the nozzle, the power decreases much more smoothly than in the gas-dynamic regime; this can likewise be explained only as being due to the formation of the excited CO_2 molecules via a chemical reaction in the cavity region. The chemical-laser power W_1 slightly exceeded the gas-dynamic laser power W_2 ($W_1/W_2 \approx 1.25$) at the same calorie content of the mixture.

The use of chemical reactions for additional pumping of gas-dynamic lasers based on the reaction products of carbon monoxide with nitrous oxide was investigated also in [39]. It was found that for a reacting mixture in the temperature range 1500-2000°K, the gain increases noticeably compared with the previously made up mixture that models the products of the same chemical reaction.

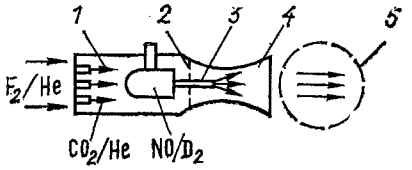

Fig. 6.10

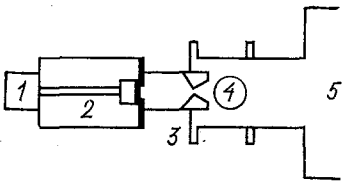

Fig. 6.11

Fig. 6.10. Diagram of the construction of a hybrid supersonic chemical laser with increased pressure in the cavity: 1) mixing section; 2) grating; 3) injector; 4) two-dimensional nozzle; 5) cavity.

Fig. 6.11. Diagram of combustion chemical laser: 1) pneumoelectric valve; 2) combustion chamber; 3) nozzle; 4) cavity; 5) receiver.

6.4. Analysis of the Efficiency of Diffusion Chemical Lasers

Features of the Analysis of Chemical Diffusion Lasers. Only part of the chemical-reaction energy is used up in cw diffusion lasers. Thus, the chemical efficiency of energy conversion of the reagents into radiation energy does not exceed 10-20%, and the total efficiency, with allowance for the thermal energy lost in the preparation of the working mixture, is still quite low, $\eta \leqslant 2$-4%. The reason is that there exists an equilibrium reserve of vibrational energy in the presence of radiation, and this does not make it possible to convert the total vibrational energy of the molecules into radiation-field energy, even in the absence of V—T relaxation. A rapid relaxation of the working molecules on the reaction products also takes place, as well as an incomplete mixing of the reagents in the cavity volume during the lasing cycle. The need for simultaneous account of these phenomena greatly complicates the theoretical analysis of the operation of diffusion cw chemical lasers.

In SD chemical lasers, inversion is produced either as a result of a direct chemical reaction upon diffusion of one component, such as H_2, into the supersonic jet containing another component—diluent (He) [15], or else as a result of energy transfer to an auxiliary reagent such as CO_2 [27, 40]. In the diffusion regime the time of convective passage of the reacting particle (τ_{conv}) should exceed the time of diffusion passage of the particle (τ_d), i.e.,

$$\tau_{conv} > \tau_d. \tag{6.17}$$

Introducing the Schmidt and Reynolds numbers Sc and Re, respectively, and using [41] $\tau_{conv} = l_\parallel/u$, $\tau_d = l_\perp^2/D$, where $l_\parallel$ and $l_\perp$ are the characteristic longitudinal and transverse dimensions of the channel, D is the diffusion coefficient, and u is the characteristic stream velocity, we obtain

$$\mathrm{Sc\,Re} < e_\parallel/e_\perp. \tag{6.18}$$

In the case of the pure diffusion regime we have ScRe << 1, i.e., e.g., ScRe $\leq$ 0.1.

For continuous lasing it is necessary that the lasing time τ exceed the time of passage τ_c of the reagents, i.e., $\tau > \tau_c = l_\parallel/u$, whence $u > l_\parallel/\tau$.

For the smallest value $l_\parallel = 1$ cm and $\tau = 10^{-4}$-10^{-5} sec, which are typical of pulsed chemical lasers at reagent pressures up to several kPa, we have

$$v > 10^4 \div 10^5 \text{ cm/sec}.$$

The longitudinal channel dimension is as a rule larger than 1 cm, and τ decreases with increasing pressure and with increasing specific lasing power. For successful operation of real chemical cw lasers it is necessary to have high-speed reagent streams, with a speed close to that of sound or higher. These high speeds, on the one hand, create additional technical difficulties due to the need of having high-power exhaust systems, and on the other they make it possible to use components that react very rapidly when mixed with one another without any initiation.

In addition, for effective operation it is necessary that the component mixing time τ_d and the chemical reaction time τ_{ch} be smaller than the time of collision relaxation τ_{rel}, i.e.,

$$\tau_d, \tau_{ch} < \tau_{rel}.$$

For a purely chemical laser operating without preliminary external initiation, exchange reactions of atoms or of radicals with molecules, considered in Chap. 2, are suitable. It is more convenient, however, to use chain reactions such as $H_2 + F_2$, and to initiate the reaction by introducing auxiliary reagents that react with the basic component and create priming atoms or radicals.

Laminar Model of Mixing. The highest efficiency of SD chemical lasers can theoretically be achieved at relatively low presures in the cavity and at small Reynolds numbers, i.e., when the flow regime is laminar. In real cw chemical lasers, however, where high pressures are used, the velocity of the laminar mixing becomes insufficient to compete with deactivation of the excited particles. As a result, it becomes desirable to obtain faster mixing, namely turbulent. We begin with consideration of a laminar mixing model. It is possible [41] to solve the linear differential equations of multicomponent diffusion with account taken of the off-diagonal diffusion coefficients:

$$\frac{\partial n_i}{\partial t} + \mathbf{u}\nabla n_i - \sum_{k=1}^{p} D_{ik}\nabla^2 n_k + \alpha_{si} n_i = 0. \tag{6.19}$$

Here $\mathbf{u}$ is the vector of the average flow velocity; α_{si}, dissipative coefficients; and D_{ik}, diffusion coefficients connected with one another by the Onsager relations.

On the basis of (6.18), the second term of (6.19) can be neglected for a pure diffusion regime. In addition, when the inequality

$$|\alpha_{si} - \alpha_{sk}| < \tau_d^{-1}, \tag{6.20}$$

which is realized in practice frequently, is satisfied, we can disregard the difference between the dissipative coefficients. We then have, in place of (6.19),

$$\frac{\partial n_i}{\partial t} = \sum_{k=1}^{p} D_{ik}\nabla^2 n_k - \alpha_s n_i. \tag{6.21}$$

This sum of equations reduces to a system of p independent equations by diagonalization of the matrix D. Multiplying the equations of the system (6.21) by the elements g_{ij} of the auxiliary nonsingular quadratic matrix g, summing over i, and replacing i by the index k in the terms with single summation, we obtain

$$\frac{\partial}{\partial t}\sum_{k=1}^{p} g_{kj} n_k = \operatorname{div}\operatorname{grad}\sum_{k=1}^{p} n_k \sum_{i=1}^{p} g_{ij} D_{ik} - \alpha_s \sum_{k=1}^{p} g_{kj} n_k, \quad j = 1, 2, \ldots, p. \tag{6.22}$$

Introducing the notation

$$G_j = \sum_{k=1}^{p} g_{kj} n_k, \quad H_j = \frac{1}{g_{kj}} \sum_{i=1}^{p} g_{ij} D_{ik}, \tag{6.23}$$

we obtain from (6.22)

$$\partial G_j/\partial t = H_j\nabla^2 G_j - \alpha_s G_j. \tag{6.24}$$

The elements of the matrix H_j are obtained from the condition

$$\det(D_{ik} - H\delta_{ik}) = 0, \tag{6.25}$$

and the solution of the system of equations (6.21) is

$$n_i = \sum_{j=1}^{p} g_{ij}^{-1} G_j, \tag{6.26}$$

where g_{ij}^{-1} are elements of the inverse matrix g^{-1}.

Reduction of this problem of multicomponent convective diffusion was carried out in [41] with allowance for the geometry of the system. For a diffusion-type amplifier using HF it was shown that a gain of the output power of the chemical laser can be achieved by asymmetric injection of the reacting molecules.

Turbulent Mixing. The description of the macroscopic characteristics of turbulent mixtures is based on the time-averaged Navier–Stokes equations. Representing each quantity f in the form of a sum of a time-averaged part $\bar{f}$ and a pulsation part f'

$$f = \bar{f} + f' \quad (\bar{f}' = 0), \tag{6.27}$$

we obtain [42] mass, momentum, mixture-enthalpy, and individual-mass-component conservation equations

$$\partial \bar{\rho}\tilde{u}_j / \partial x_j = 0; \tag{6.28}$$

$$\bar{\rho}\tilde{u}_j \frac{\partial \tilde{u}_i}{\partial x_j} + \frac{\partial \bar{p}}{\partial x_i} + \frac{\partial}{\partial x_j}\left(\overline{\rho u_i'' u_j''} - \overline{P_{ij}^L}\right) = 0; \tag{6.29}$$

$$\bar{\rho}\tilde{u}_j \frac{\partial \tilde{h}_e}{\partial x_j} - \tilde{u}_j \frac{\partial \bar{p}}{\partial x_j} + \frac{\partial}{\partial x_j}\left(\overline{\rho u_j'' h_e''} + \overline{q_j^L} - \sum_s h_{f,s}\overline{\rho Y_s D_{sj}^L}\right) - \overline{P_{ij}^L}\frac{\partial \tilde{u}_i}{\partial x_j} - \overline{u_j''\frac{\partial p}{\partial x_j}} - \overline{P_{ij}^L \frac{\partial u_i''}{\partial x_j}} = -\sum_s h_{f,s}\bar{w}_s; \tag{6.30}$$

$$\bar{\rho}\tilde{u}_j \frac{\partial \tilde{Y}_s}{\partial x_j} + \frac{\partial}{\partial x_j}\left(\overline{\rho u_j'' Y_s''} + \overline{\rho Y_s D_{sj}^L}\right) = \bar{w}_s. \tag{6.31}$$

Here Y_s is the mass fraction of the component s; D_{sj}^L, P_{ij}^L, q_j^L, diffusion velocity, stress tensor, and thermal flux for laminar flow; and w_s, rate of the chemical reaction of the component s.

In a fully developed turbulent flow, the laminar transport coefficients are negligibly small compared with the turbulent ones.

In the simplest approximation of an incompressible turbulent boundary layer, with allowance for the velocity component v directed along the y axis, we have

$$\left.\begin{aligned} -\overline{\rho u'' v''} = \eta^T \frac{\partial \tilde{u}}{\partial y}, \ \overline{\rho v'' h_e''} = -\frac{\eta^T}{\mathrm{Pr}^T}\frac{\partial \tilde{h}_e}{\partial y}; \\ \overline{\rho v'' Y_s''} = -\frac{\eta^T}{\mathrm{Sc}^T}\frac{\partial \tilde{Y}_s}{\partial y}. \end{aligned}\right\} \tag{6.32}$$

The numbers Pr^T, Sc^T are assumed constant here, and the turbulent viscosity η^T is determined by the mixing length l or by the shear excess velocity $|\tilde{u}_{max} - \tilde{u}_{min}|$:

$$\eta^T = C_1 \bar{\rho} l^2 \left|\frac{\partial \tilde{u}}{\partial y}\right|; \tag{6.33}$$

$$\eta^T = C_2 \bar{\rho}\delta\,|\tilde{u}_{max} - \tilde{u}_{min}|, \tag{6.34}$$

where δ is the boundary-layer thickness.

For a heterogeneous mixture, the best agreement with experiment takes place at

$$\eta^T = C_3 \bar{\rho}_\infty \tilde{u}_\infty \delta^*, \tag{6.35}$$

where $\delta^* = \int_{-\infty}^{\infty}\left|1 - \frac{\bar{\rho}\tilde{u}}{\bar{\rho}_\infty \tilde{u}_\infty}\right| dy$, and the coefficients C_1, C_2, and C_3 in (6.33)–(6.35) are determined from experiment.

Enhancement of the Radiation in the Flame-Front Model. In the analytic description of the hydrodynamics and of the optical properties of chemical lasers with diffusion, convection, and chemical reactions it is possible to take into account the presence of nonequilibrium population distribution if one considers each long-lived vibrational level of the active molecule as a separate mixture component. To this end one uses, in the flame-front model [43], the equations of the laminar boundary layer, in which account is taken of the chemical reactions with conversion of the excited particles into radiation. In these equations one neglects the axial pressure gradient and it is assumed that $D_{ij} = D$ and that the Lewis number is $\mathrm{Le} = \rho D c_p/\lambda = 1$, an assumption valid for most gases. We then have from (3.38)–(3.41)

$$\partial \rho u/\partial x + \partial \rho v/\partial y = 0; \tag{6.36}$$

$$\rho u \frac{\partial u}{\partial x} + \rho v \frac{\partial u}{\partial y} = \frac{\partial}{\partial y}\eta \frac{\partial u}{\partial y}; \tag{6.37}$$

$$\rho\left(u\frac{\partial h_e}{\partial x}+v\frac{\partial h_e}{\partial y}\right)=\frac{\partial}{\partial y}\left\{\frac{\eta}{\mathrm{Pr}}\left[\frac{\partial h_e}{\partial y}+(\mathrm{Pr}-1)\frac{1}{2}\frac{\partial(u^2)}{\partial y}\right]\right\}; \tag{6.38}$$

$$\rho\left(u\frac{\partial Y_i}{\partial x}+v\frac{\partial Y_i}{\partial y}\right)=\frac{\partial}{\partial y}\left(\rho D\frac{\partial Y_i}{\partial y}\right)+w_i,\ i=0,1,\ldots,n-1; \tag{6.39}$$

$$p=\rho RT\sum_i(Y_i/\mu_i), \tag{6.40}$$

where

$$\mathrm{Pr}=\eta c_p/\lambda;\quad c_p=\sum_i Y_i c_{pi}.$$

In analogy with (1.22) and (1.6), for N chemical reactions of n gas components we have

$$w_i=\mu_i\sum_{j=1}^{N}(r'_{ij}-r_{ij})\left[k_{fj}\prod_{k=0}^{n-1}(c_k)^{r_{kj}}-k_{bj}\prod_{k=0}^{n-1}(c_k)^{r'_{kj}}\right],\ j=1,\ldots,N. \tag{6.41}$$

If the transport coefficients are expressed in terms of the flow parameters, then Eqs. (6.36)-(6.40), with account taken of (6.41), constitute equations for the unknowns ρ, u, v, h_e, T, and Y_i.

To solve the problem one changes over to the variables x and

$$\tilde{y}=\left(\frac{u_\infty}{2D_\infty x}\right)^{1/2}\int_{y_f(x)}^{y}\frac{\rho(x,\bar{y})}{\rho_\infty}d\bar{y}. \tag{6.42}$$

Starting from the definition of the stream function, an expression is obtained for the stream velocity, and a solution of (6.36)-(6.40) is sought for the corresponding boundary conditions under the conditions:

$$K_p=(k_b/k_f)_p\to 0;\ x/x_p\to\infty,\ (x/x_{cd})^2\ll 1.$$

Here x_p and x_{cd} are, respectively, the characteristic distances of the chemical pumping and the deactivation. As a result, expressions for the power per unit flow area and for the chemical efficiency were obtained [43] and good qualitative agreement was observed between theory and experiment. At low temperature, when the collisional deactivation can be neglected compared with the radiative deactivation, it follows from the calculation that the chemical efficiency should exceed 30%, but collisional deactivation effects decrease the efficiency to 10-20% at an H_2 diffusion time comparable with the HF collisional-deactivation time.

Simplified Analysis of a Saturated Chemical Amplifier on the Basis of the Analytic Solution [44]. In an analysis in terms of the coordinates x (along the stream velocity **u**) and y (in the propagation direction of the radiation) one uses the equations

$$\frac{\partial}{\partial y}I^{v,J_v-1}_{v-1,J_v}=G^{v,J_v-1}_{v-1,J_v}I^{v,J_v-1}_{v-1,J_v}\quad(v=1,2,\ldots,m); \tag{6.43}$$

$$\frac{\partial}{\partial x}(n_v y_f)=y_f\left\{P_v\frac{n_F}{x_x}+Q_{VT}(v)+Q_{VV}(v)+\frac{1}{u}\left[\alpha^{v+1,J_{v+1}-1}_{v,J_{v+1}}I^{v+1,J_{v+1}-1}_{v,J_{v+1}}-\alpha^{v,J_v-1}_{v-1,J_v}I^{v,J_v-1}_{v-1,J_v}\right]\right\}(v=0,1,\ldots m); \tag{6.44}$$

$$\frac{d}{dx}(n_F y_f)=N_0\frac{dy_f}{dx}-\frac{n_F y_f}{x_x}. \tag{6.45}$$

Here $I^{v',J'}_{V,J}$ is the radiation intensity for the transition v', J' → v, J; n_V, n_F, N_0 are the respective concentrations of the HF molecules on the v-th level and of the F atoms in the active zone inside the flame-front surface $y_f(x)$, and the initial concentration of the F atoms in the stream; $\alpha_{V,J^{v',J'}}=\sigma_{V,J^{v',J'}}(n_V-B_{J_V}n_{V-1})$ is the specific gain in the active zone for the transition v', J' → v, J; $\beta_J=\exp(-2\theta_{rot}J/T)$; $\sigma_{V,J^{v',J'}}$, cross section of the induced transition; $G_{V,J^{v',J'}}=y_f\alpha_{v,J^{v',J'}}/h_y$, gain averaged over the height h_y of the jet; P_V, probability of populating the v level of the HF molecule in the course of the reaction; $x_c=u/(k_c n_{H_2})$, characteristic length of the chemical reaction; k_c, rate constant of the chemical reaction; m, number of the highest vibration level populated in the course of the reaction (m = 3 for an HF chemical laser); and terms QVV, QVT describe the V—V exchange and the V—T relaxation of the HF molecules.

For simplicity it is assumed that

$$I_{1,0} = I_{2,1} = \ldots = I_{m,m-1} = I/m, \text{ где } I = \sum_{v=1}^{m} I^J_{v,v-1};$$

$$\alpha_{v,v-1} = \alpha_{v+1,v} \ (v = 1, 2, \ldots, m-1);$$

$$J_{1,0} = J_{2,1} = \ldots = J_{m,m-1} = \ldots = J.$$

For the density $q_v = \sum_{v=0}^{m} v n_v$ of the vibrational quanta we obtain under the indicated assumptions

$$q_v = N\varepsilon_J + B_J \alpha/\sigma_{1,0}, \tag{6.46}$$

where

$$B_J = \frac{1}{m(1-\beta_J)} \sum_{v=1}^{m} \left(\frac{\sigma_{1,0}}{\sigma_{v,v-1}}\right)\left[v-(m+1)\frac{\beta_J^{m+1}}{1-\beta_J^{m+1}}\left(\frac{1}{\beta_J^v}-1\right)\right];$$

$$\alpha = \sum_{v=1}^{m} \alpha^J_{v,v-1}; \ \varepsilon_J = \frac{\beta_J}{1-\beta_J}\left[1-(m+1)\beta_J^m\left(\frac{1-\beta_J}{1-\beta_J^{m+1}}\right)\right].$$

The values m = 1 and $\beta_J = 1$ correspond to a two-level system. From (6.44) and (6.46) we have an equation for $\alpha(J)$:

$$\frac{d}{dx}(\alpha y_f) = y_f\left\{\frac{\sigma_{1,0}}{B_J}\left(\frac{\varepsilon_c-\varepsilon_J}{x_c}+\frac{\varepsilon_J}{x_{VT}}\right)n_F - \frac{\sigma_{1,0}}{B_J}\frac{N_0}{x_{VT}}\varepsilon_J - \alpha\left[\frac{1}{x_{VT}}+\frac{\sigma_{1,0}I}{muB_J}\right]\right\}, \tag{6.47}$$

where $x_{VT} = u/(\sum_i k_{VT_i} n_i)$ is the characteristic length of the V–T relaxation zone; $\varepsilon_c = \sum_{k=1}^{m} kP_k$ is the reserve of vibrational energy (per molecule) produced in the course of the reaction ($\varepsilon_c \approx 2.1$ for the $F + H_2$ reaction).

For the coordinate of the flame-front surface in a laminar mixture we have

$$y_f(\xi) = \begin{cases} h_y\sqrt{\xi/\xi_d}, & (\xi<\xi_d); \\ h_y, & (\xi>\xi_d) \end{cases} \tag{6.48}$$

($\xi = x/x_{VT}$, $\xi_d = x_d/x_{VT}$, x_d is the characteristic diffusion length).

From (6.47), with allowance for (6.46) and (6.48) we have

$$\frac{\alpha y_f}{h_y}\left(\frac{\sqrt{\xi_d}}{\sigma_{1,0}N_0\gamma_J}\right) = \begin{cases} \dfrac{\varepsilon_\zeta D(\sqrt{\zeta\xi})}{(t-\zeta)\sqrt{\zeta}} - \dfrac{\sqrt{\xi}}{t} + \left(\dfrac{1}{t}-\dfrac{\varepsilon_\zeta}{t-\zeta}\right)\dfrac{D(\sqrt{t\xi})}{\sqrt{t}}, \\ \qquad \xi \leqslant \xi_d; \\ \dfrac{\varepsilon_\zeta D(\sqrt{\zeta\xi_d})}{(t-\zeta)\sqrt{\zeta}}\exp[-\zeta(\xi-\xi_d)] - \dfrac{\sqrt{\xi_d}}{t} + \left(\dfrac{1}{t}- \right. \\ \left. -\dfrac{\varepsilon_\zeta}{t-\zeta}\right)\dfrac{D\sqrt{t\xi_d}}{\sqrt{t}}\exp[-t(\xi-\xi_d)], \ \xi>\xi_d. \end{cases} \tag{6.49}$$

Here

$$D(z) = \exp(-z^2)\int_0^z \exp(x^2)\,dx \tag{6.50}$$

is the Dawson integral;

$$\zeta = \frac{x_{VT}}{x_x}; \ \gamma_J = \frac{\varepsilon_J}{B_J}; \ \varepsilon_\zeta = 1+\zeta\left(\frac{\varepsilon_c}{\varepsilon_J}-1\right); \ t = 1 + x_{VT}\sigma_{1,0}\frac{I}{muB_j}.$$

In the case of an instantaneous reaction on the flame front, $x_c \to 0$ and $\xi \to \infty$, so that

$$\frac{\alpha y_f}{h_y}\left(\frac{\sqrt{\xi_d}}{\sigma_{1,0}N_0\gamma_J}\right) = \begin{cases} \left(\dfrac{1}{t}+\dfrac{\varepsilon_c}{\varepsilon_J}-1\right)\dfrac{D(\sqrt{t\xi})}{\sqrt{t}} - \dfrac{\sqrt{\xi}}{t}, \ \xi\leqslant\xi_d; \\ \left(\dfrac{1}{t}+\dfrac{\varepsilon_c}{\varepsilon_J}-1\right)\dfrac{D(\sqrt{t\xi_d})}{\sqrt{t}}\exp[-t(\xi-\xi_d)] - \dfrac{\sqrt{\xi_d}}{t}, \ \xi>\xi_d. \end{cases} \tag{6.51}$$

In the absence of radiation I = 0 (t = 1 is the unsaturated gain of the medium), the width of the inversion zone is

$$\Delta x_{\text{inv}} \approx x_{VT} \frac{\varepsilon_c}{2\varepsilon_J} \approx x_{VT} \frac{1-\beta_J}{\beta_J\left[1-(m+1)\beta_J^m \dfrac{(1-\beta_J)}{1-\beta_J^{m+1}}\right]}. \tag{6.52}$$

We see therefore that in a multilevel system with partial inversion ($\beta_J < 1$) the width of the inversion zone is much larger than in a two-level medium ($m = \varepsilon_c = \beta_J = 1$), where $\Delta x_{\text{inv}} \approx x_{VT}$.

At high radiation intensity ($t \gg 1$) relation (6.51) makes it possible to determine the inversion band width of a saturated amplifier. At $\xi > \xi_d$ the gain decreases exponentially with increasing ξ, so that the width of the inversion band is limited to the value ξ_d or $\Delta x_{\text{inv}} \approx x_d$. In the region $\xi \leqslant \xi_d$ for a multilevel medium we have

$$\Delta x_{\text{inv}} \approx \frac{1}{2} x_{VT}\left(\frac{\varepsilon_c}{\varepsilon_J} - 1\right), \tag{6.53}$$

and for a two-level medium $\Delta x_{\text{inv}} \approx {}^1/_2 x_{VT}$. We see from this that in the region $\xi \leqslant \xi_d$ the inversion band in a multilevel medium is larger than in a two-level medium. With increasing J, the inversion band increases all the way to $\Delta x_{\text{inv}} = x_d$.

In the case of an instantaneous reaction on the flame front, the useful relative power W_{rel} per square centimeter of the area of the throat of the nozzle block is given by

$$W_{\text{rel}}(\xi) = \frac{h_y \nu_J \sigma_{1,0} \gamma_J I_0 N_0 x_{VT}}{m\sqrt{\xi_d}}\left\{\frac{1}{t^{3/2}}\left(\frac{1}{t} + \frac{\varepsilon_c}{\varepsilon_J} - 1\right)\left[\sqrt{t\xi} - D\left(\sqrt{t\xi}\right)\right] - \frac{2}{3t}\xi^{3/2}\right\} \quad (\xi \leqslant \xi_d). \tag{6.54}$$

In a saturated amplifier, the maximum power from the entire generation zone is equal to

$$W_{\max}(\xi^*) = h_y \nu_J u N_0 \varepsilon_J \sqrt{\frac{\xi^*}{\xi_d}}\left[\left(\frac{\xi_c}{\varepsilon_J} - 1\right) - \frac{2}{3}\xi^*\right], \tag{6.55}$$

whence

$$\eta_c(\xi^*) \approx \frac{N_A h_y \nu_J \varepsilon_J}{Q}\left[\left(\frac{\varepsilon_c}{\varepsilon_J} - 1\right) - \frac{2}{3}\xi^*\right] T\sqrt{\frac{\xi^*}{\xi_d}}. \tag{6.56}$$

It can be seen from (6.56) that in accordance with [45] the efficiency of a diffusion chemical amplifier increases with increasing number J of the working transition. Indeed, according to the calculations in [44] using reduced formulas, at T = 400°K, p = 0.66 kPa, u = 3 km/sec, $n_{He}/n_F = 5$, $h_y = 0.2$ cm, and $T_{H_2} = 100$°K we obtain that the transition from J = 4 to J = 8 makes it possible to raise the efficiency of a chemical laser by 2-2.5 times (from 8 to 20%). The displacement of the emission spectrum into the region of higher values of the rotational number J can also be effected without using selective mirrors.

To this end it is proposed [44] to use in the master oscillator a working mixture with a degree of dilution by a rare gas (e.g., helium) lower than in the amplifier itself. The average temperature of the laser mixture will then turn out to be higher, so that the frequency spectrum applied to the input of the amplifier shifts into the region of values of J that do not coincide with the maximum-gain band, but ensures a higher chemical-amplifier efficiency. It is possible, however, that this increase in efficiency will be obtained only in a sufficiently powerful amplifier with large volume of the active medium, which compensates the gain loss due to the decreased cross section for the induced transition with increasing J.

Numerical Investigation of a DF Chemical Laser When the Rotational Equilibrium Is Violated. The Boltzmann equilibrium distribution over the rotational levels, assumed in a number of theoretical investigations, is not justified. More accurate ideas concerning the role of the rotational relaxation have shown that in cw chemical lasers the violation of the rotational equilibrium leads to a decrease in power by 20-30% [45]. A theoretical investigation of the operation of a cw chemical laser was carried out in [46] without assuming an equilibrium distribution of the rotational-level populations. It was assumed that the gas dynamics and the reagent-mixing processes are described by quasi-one-dimensional equations along individual jets, in which the mixing had already taken place and whose widths vary in accordance with the formula

$$\delta l = \frac{L_c}{i}\operatorname{tg}\left(\frac{x}{L_d}\right)^{1/2}, \tag{6.57}$$

where L_c is the cavity length; i, number of nozzles; and L_d, length of the mixing zone. The reagent concentration was determined with the aid of the equation

$$\frac{dc_s}{dx} = \frac{\dot{c}_s}{u} + (c_s^0 - c_s)\frac{dw}{wdx}, \tag{6.58}$$

where $\dot{c}_s$ is the rate of change of the concentration as a result of the chemical reaction, of V—V exchange, and of vibrational relaxation, of rotational relaxation, and of the induced transitions. Similar equations were also used for the reaction products in excited V—R states of DF ($v \leqslant 4$), in excited V states of DF ($v > 4$), for excited D_2 molecules ($v \geqslant 1$).

It was assumed that the only pumping reaction is

$$F + D_2 \rightarrow DF(v, J) + D, \tag{6.59}$$

whose integral rate constant was taken from [47]. The distribution of the relaxation products over the levels v and J was taken from [48], according to which the maximum of the distribution for v = 1, 2, 3, and 4 takesplace, respectively, at J = 13, 11, 9, and 5. The numerical calculations were performed for the active medium $F/He/HF/D_2$ = 3/6/3/14 at T = 300°K, u = 2.13 km/sec, pL_d = 1.66 kPa•cm, pL_c = 13.3 kPa•cm, and p = 133 Pa.

The large gain on transitions of strongly rotating molecules immediately after the start of the mixing manifests itself experimentally in the fact that lasing evolves in this region simultaneously on several lines. Calculations of the lasing intensity show also that after the start of the mixing the lasing proceeds immediately on many lines, but lines having small J cease to emit in the course of time and the maximum of the spectrum shifts towards larger J. Gain on purely rotational transitions of DF (v = 2) can increase appreciably. Thus, at p = 0.66 kPa we have $\alpha > 1$ cm^{-1} at a distance $x \leqslant 0.3$ cm.

Violation of the rotational equilibrium decreases the power in a nonselective cavity by 14%, and by 35% in the case of selection of one mode. According to calculations, when individual lines are selected the output power depends noticeably on the choice of the rotational-relaxation rate constant.

Other Numerical Investigations of SD Chemical Lasers. An idealized picture of flow with laminar diffusion of the H_2 stream of finite width in a semiinfinite stream containing fluorine and a diluent was considered in [49] in a coherent-radiation field. To simplify the numerical solution of the boundary-layer system of equations of the type (3.38)-(3.41), which take into account the multicomponent diffusion, emission, and chemical reactions, the Mises transformation was used. At a constant initial stream velocity, temperature, H_2 stream width, and initial partial pressure of the fluorine, direct dependences on the pressure of the integral gain and of the effective specific output power of a chemical laser were obtained, as well as inverse pressure dependences of the length of the active region and of the chemical efficiency.

Similar limitations on the length of the active zone and on the efficiency with increasing pressure, due to reagent mixing in the laminar regime of the operation of SD HF chemical lasers, were obtained by numerical calculation in [50]. The total chemical-laser efficiency, however, with account taken of the thermal losses in the mixture preparation, increases when a chain excitation mechanism is used; an analysis of this mechanism for chemical lasers with low degrees of dissociation of molecular fluorine is given in [51]. An estimate of the comparative efficiency of different fuel compositions of chemical lasers based on the H_2/F_2 mixture is possible by using a calculation [52] on the basis of the instantaneous-mixing model.

From the numerical analysis of the efficiency of energy conversion in diffusion HF chemical lasers [53] it follows that the use of turbulent injectors in chemical lasers increases the pressure in the cavity. This ensures a high rate of mixing of the components of the mixture under conditions of advanced turbulent flow.

HF chemical lasers, especially those with a chain reaction mechanism, are characterized by multilevel excitation with kinetic processes in the active zone, which occur against the background of diffuse flow with refractive-index gradients in the stream past the exit section of the nozzle. Calculation of the structure of the amplitude and phase diagrams of the radiation field in the near and far zones [54], for typical HF chemical laser operating conditions, has shown that an increase in the directivity of the radiation at a moderate decrease of the efficiency results from the use of telescopic cavities.

A numerical analysis of the kinetics of physical processes was also carried out for chemical gas-dynamic lasers with mixture $CS_2/CS/O_2/O$ [55]. From a joint solution of the equations

of chemical kinetics, vibrational relaxation, and gas-dynamics for a logarithmic nozzle it follows that the effective chemical pumping and gas-dynamic cooling should yield relatively high values of the total inversion (~10^{14} cm^{-3}) and of the gain (~0.1 cm^{-1}).

6.5. Open-Cycle Chemical Laser with Restoration of the Pressure in a Diffusor

Inasmuch as in a supersonic chemical laser the gas flows at the entrance to the cavity with a Mach number M > 1, it follows, as already stated in Sec. 6.2, that a diffusor can be used to restore the pressure from the range required in the cavity 0.66-3.33 to 26.7-53.3 kPa at the diffusor exit. From this level it is possible to raise the exhaust pressure, with the aid of a mechanical pump or an ejector [56], to the value required, e.g., when the chemical laser operates in the atmosphere. To increase the overall efficiency, the energy consumed in the evacuation should be a minimum. It can be seen therefore that the requirements for restoring the pressure in the diffusor are important in the design and construction of supersonic chemical lasers.

In the open-cycle chemical lasers (see Fig. 6.9), a primary fuel mixture is produced on sections (1)-(2). This mixture is accelerated in the nozzle (2)-(3) to supersonic velocity at low static pressure. In the cavity (3)-(4) heat is released from the stream when the primary and secondary mixtures are combusted, and in the diffusor (4)-(7) the stream slows down, starting with supersonic velocities, and the gas pressure is correspondingly lowered. A one-dimensional analysis of such a flow in a chemical laser is given, e.g., in [57], in which are considered the chemical and thermochemical processes in the cavity, the hydrodynamics of the flow with account taken of the boundary layer, and the slowing down of the stream in a diffusor with constant cross section at the entrance and at the throat (4)-(6) and with a subsonic expanding diffusor (6)-(7) at the exit.

If the variable parameters of the primary stream of the oxidizer are designated by the index p, and those of the secondary fuel flow by s, then the molar flow rates of the oxidizer in the nozzle are G_{pF} and G_{pF_2}. The relative dissociation of the fluorine is then defined as $\alpha_F = {}^1/_2 G_{pF}/\hat{G}_{pF_2}$, where $\hat{G}_{pF_2} = {}^1/_2 G_{pF} + G_{pF_2} = \hat{G}$ is a normalization parameter which characterizes the flow of the entire fluorine in molecular form. Dilution of the components i (F, F_2, D, D_2, He, DF, etc.) in the cavity is described by the degree of dilution $\psi_{pi} = G_{pi}/G$, and complete dilution of the primary stream of the oxidizer is expressed as $\psi_p = \Sigma\psi_{pi}$. The molar flow rates of F and F_2 are, respectively, $G_{pF} = 2\alpha_F\hat{G}$ and $G_{pF_2} = (1 - \alpha_F)\hat{G}$.

The normalized molar flow rate of the fuel, with allowance for the ratio R_c of the mixture components in the cavity, will be $G_{SD_2} = R_c\hat{G}$, and the flow rate of the dilute secondary stream is $\psi_s\hat{G}$. The total molar flow rate of the fuel is $G_S = \hat{G}(R_c + \psi_s)$.

The total molar flow rate at the entrance to the cavity (3) (see Fig. 6.9), with account taken of the dilution, is equal to the sum of the flow rates of the fuel and of the oxidizer

$$G_3 = \hat{G}(1 + \alpha_F + \varphi_p + \varphi_s + R_c). \tag{6.60}$$

Inasmuch as F and F_2 react completely at the entrance to the cavity up to DF, and the diluent does not take part in the chemical reaction, it follows that the equality $G_{4DF} = 2\hat{G}$ is satisfied in the cross section (4), and for atomic deuterium we have $G_{4D} = \alpha_D G_{pF} = 2\alpha_F\alpha_D\hat{G}$, where α_D is the relative dissociation of the D atoms. The flow rate of the molecular deuterium at the exit from the cavity is $G_{4D_2} = \hat{G}(R_c - 1 - \alpha_F\alpha_D)$, and the total molar flow rate at the exit of the cavity is

$$G_4 = \hat{G}(1 + \alpha_F\alpha_D + \psi_p + \psi_s + R_c). \tag{6.61}$$

The thermochemical processes in the cavity (3)-(4) are described by the expressions $H_{e3} = G_3 h_{e3}$ and $H_{e4} = G_4 h_{e4}$, which are equal to each other in the adiabatic regime. However, the cavity delivers a lasing-radiation power $W = G_3\mu_3 w_{sp}$, where μ_3 is the molar mass; $w_{sp} = W/\dot{m}_3$, specific power of the generated radiation; and $\dot{m}_3$, mass flow. Then $H_{e3} = H_{e4} + W$ or

$$(G_4 h_{e04} - G_3 h_{e03}) + G_3\mu_3 w_{sp} = Q = \sum_i (G_{3i} h_{fi} - G_{4i} h_{fi}), \tag{6.62}$$

where h_{fi} is the specific heat of formation of the i-th component. For the diluents $G_{3i} = G_{4i}$, and for F_2 and D_2, $h_{fF_2} = h_{fD_2} = 0$; therefore

$$Q = G_{pF} h_{fF} - G_{4DF}\, h_{fDF} - G_{4D} h_{fD}. \tag{6.63}$$

The specific energy release in terms of the oxidizer F_2 in the cavity is

$$\hat{q} = Q/\hat{G} = 2\alpha_F(h_{fF} - \alpha_D h_{fD}) - 2h_{fDF}. \tag{6.64}$$

From (6.60)-(6.62) we can obtain the ratio of the specific stagnation enthalpies of the flow in the cavity:

$$h_{e04}/h_{e03} = 1 + \frac{1}{\lambda_s}\left[\frac{\hat{q}/h_{e0p}}{1+\alpha_F+\psi_p} - \frac{\mu_3 w_{sp}}{X_p h_{e0p}}\right], \tag{6.65}$$

where $X_p = G_p/G_3$ is the molar fraction of the oxidizer; h_{e0p}, specific stagnation enthalpy of the primary stream at the exit from the nozzle; and λ_s, parameter that describes the influence of the secondary stream,

$$\lambda_s = 1 + \frac{X_s h_{e0s}}{X_p h_{e0p}}. \tag{6.66}$$

In general, as can be seen from Fig. 6.2, the stream at the exit from the nozzle is not uniform and can have a complicated system of shock discontinuities. These effects, however, which are connected with the energy release and with the mixing, play the principal role only in the entrance section of the cavity, while in the remaining part of the cavity they can be neglected. The contour of the walls on the section (4)-(5) is usually small with a large curvature radius, so that there are no large pressure gradients. Thus, inasmuch as over the entire extent of the channel the transverse stream velocities are small compared with the axial velocities, we can assume the deviations from uniform flow to be quantities of second order of smallness. The homogeneous stream parameters at the exit from the nozzle grating were obtained in [57] by integrating the inhomogeneous distributions across the nozzle by the method given in [58]. The diffusor (4)-(6) is provided with a throat having a constant cross-sectional area and a length sufficient to convert the stream in the shock-wave system from a supersonic stream to a subsonic one, and also to equalize the inhomogeneities of the stream at the diffusor exit. Thus, in the analysis of the flows in the cross section (6) it is also possible to use the one-dimensional approximation.

The equation for the momentum in the nonviscous control volume I of the cavity in the region (3)-(4) is written in the form

$$[pS(1+\gamma M^2)]_{4I} = [pS(1+\gamma M^2)]_3 + \int_3^4 p\,dS. \tag{6.67}$$

Here the cross section of the nonviscous control volume $S_{4I} = S_4 - S_\delta$, S_δ characterizes the boundary layer in the cavity, determined by the crowding-out thickness δ and by the hydraulic diameter D_H as $S_\delta = S_4 4\delta/D_H$.

From the solutions of the equations for the momentum, energy, and continuity follow expressions for the stream velocity u_3, enthalpy h_{e3}, and pressure p_3:

$$u_3 = Y_p u_p + Y_s u_s + \dot{m}_3^{-1}[p_p S_p + p_s S_s - p_3(S_p + S_s)]; \tag{6.68}$$

$$h_{e3} = X_p h_{ep} + X_s h_{es} + (2\mu_3)^{-1}[Y_p u_p^2 + Y_s u_s^2 - u_3^2]; \tag{6.69}$$

$$p_3 = \dot{m}_3 R_3 T_3/(u_3 S_3) \tag{6.70}$$

(R is the gas constant; $h_{ej} = \sum_i \int_0^{T_j} C_{pi}\,dT$ is the enthalpy of the j-th state of the medium, e.g., j = p, s, 3; $Y_{ji} = m_{ji}/m_j$ is the mass fraction of the component i), iteractionsof which using the temperature dependences of the gas properties determine p_3, u_3, T_3 and then p_{03} and M_3. For the general case p = f(S) one substitutes in (6.67) the relation

$$pS^{\zeta/(\zeta-1)} = \text{const}\ (0 \leqslant \zeta \leqslant 1)\ [59] \tag{6.71}$$

and one estimates the integral of the pressure and the quantities

$$p_{4I}/p_3 = \left[\frac{\zeta+\gamma M_3^2}{\zeta+\gamma M_{4I}^2}\right]^{\zeta}; \tag{6.72}$$

$$S_{4I}/S_3 = [(\zeta+\gamma M_3^2)/(\zeta+\gamma M_{4I}^2)]^{(1-\zeta)}; \tag{6.73}$$

$$T_{4I}/T_4 = [M_{4I}(\zeta+\gamma M_3^2)/M_3(\zeta+\gamma M_{4I}^2)]^2. \tag{6.74}$$

For the ratio of the stagnation pressures we have

$$p_{04}/p_{03} = (p_{4I}/p_3)\left[\left(1+\frac{\gamma-1}{2}M_{4I}^2\right)\Big/\left(1+\frac{\gamma-1}{2}M_3^2\right)\right]^{\gamma/(\gamma-1)}. \tag{6.75}$$

The stagnation temperature at the exit from the cavity is

$$T_{04}=T_{4I}\left(1+\frac{\gamma-1}{2}M_{4I}^2\right). \tag{6.76}$$

A similar expression also holds for T_{03}. Dividing (6.76) by T_{03} and substituting the result in (6.74) we obtain

$$T_{04}/T_{03}=\left[\left(1+\frac{\gamma-1}{2}M_{4I}^2\right)\Big/\left(1+\frac{\gamma-1}{2}M_3^2\right)\right]\left[\frac{M_{4I}(\zeta+\gamma M_3^2)}{M_3(\zeta+\gamma M_{4I}^2)}\right]^2. \tag{6.77}$$

The ratio T_{04}/T_{03} is obtained from (6.65) and (6.66), and Eq. (6.77) with ζ given is solved relative to M_{4I}, after which it is easy to determine the quantities in (6.72)-(6.75). The transition from nonviscous parameters to those averaged over the cross section (4), with allowance for the boundary layer, can be carried out by using the data of [58].

The parameters in the cross sections (4) and (5) for a diffusor with a throat of constant cross section and without a constriction at the entrance can be assumed to be equal to one another: $S_5 \approx S_4$, $M_5 \approx M_4$, $p_5 \approx p_4$, etc. From section (5) to section (6) the transitions of the stream from $M > 1$ to $M < 1$ take place at a throat length $(8\text{-}13)D_H$ via a complicated system of oblique shocks identified as one direct shock-wave. Consequently, the parameters of the current in section (6) are calculated from the parameters in section (5) using the known relations for a direct shock-wave.

This is followed by a determination of the sought pressure at the exit of the diffusor of a supersonic open-cycle chemical laser

$$p_7 = p_6\left[1+\delta\left(p_{06}/p_6-1\right)\right], \tag{6.78}$$

where δ is the coefficient of the restoration of the static pressure of the subsonic diffusor (6)-(7). Since the number M_7 is small, we can assume here $p_7 \approx p_{07}$.

The characteristics of the described diffusor can be improved by using an inlet (4)-(5) with decreasing width as in Fig. 6.9, which compresses the stream and decreases the Mach number ahead of the constant-section throat (5)-(6).

The indicated one-dimensional analysis [57] agrees with the results of experimental investigations of a chemical-laser nozzle block with a diffusor having constant throat cross-section area. In these experiments the pressure at the exit from the diffusor (7) is restored to 35 kPa. Data were obtained about a linearly increasing dependence of the exit pressure in the diffusor on the increase of the pressure in the combustion chamber (1)-(2). A considerable influence on the restoration of the pressure σ is exerted by the change of the temperature of the medium in the combustion chamber. Thus, an increase of T_{02} from 1700 to 2100°K leads to an increase of p_{07} by 25%.

LITERATURE CITED

1. N. G. Basov and A. N. Oraevskii, "Obtaining negative temperatures by heating and cooling a system," Zh. Eksp. Teor. Fiz., 44, No. 5, 1742-1745 (1963).
2. I. R. Hurle and A. Hertzberg, "Electronic population inversions by fluid-mechanical techniques," Phys. Fluids, 8, No. 9, 1601-1607 (1965); "On the possible production of population inversions by gas-dyanmic techniques," Minutes of the 1963 Annual Meeting of the Division of Fluid Dynamics, Cambridge, Mass., Nov. 25-27, 1963, Bull. Am. Phys. Soc., 9, No. 5, 582-595 (1964).
3. W. H. Wells, "Proposed gas maser pumping scheme for the far infrared," J. Appl. Phys., 36, No. 9, 2838-2843 (1965).
4. K. Shimoda, "Thermally pumped infrared masers," Institute of Phys. and Chem. Research, Papers 59, No. 2, 53-68 (1965).
5. N. G. Basov, A. N. Oraevskii, and V. A. Shcheglov, "Beam driven infrared laser," Pis'ma, Zh. Eksp. Teor. Fiz., 4, No. 2, 61-62 (1966).
6. V. K. Konyukhov and A. M. Prokhorov, "Population inversion in adiabatic expansion of a gas mixture," Pis'ma Zh. Eksp. Teor. Fiz., 3, No. 11, 436-439 (1966).
7. N. G. Basov, A. N. Oraevskii, and V. A. Shcheglov, "Thermal methods of laser excitation," Zh. Tekh. Fiz., 37, No. 2, 339-348 (1967).
8. A. N. Oraevskii, "Obtaining population inversion by thermal dissociation of molecules in a shock wave," Zh. Eksp. Teor. Fiz., 48, No. 4, 1150-1154 (1965); "Onset of negative temperatures in chemical reactions," ibid., 45, No. 2(8), 177-179 (1963).

9. G. Makhov and I. Wieder, "Vibrational excitation of the CO_2 by transfer from thermally excited nitrogen," IEEE J. Quantum Electron., QE-3, No. 9, 378 (1967).
10. N. G. Basov et al., "Obtaining inverted population of molecules in a supersonic stream of a binary gas in a Lavel nozzle," Zh. Tekh. Fiz., 38, 2031-2041 (1968).
11. D. J. Spencer et al., "Preliminary performance of a CW chemical laser," Appl. Phys. Lett., 16, No. 6, 235-237 (1970).
12. H. Mirels and D. J. Spencer, "Power and efficiency of a continuous HF chemical laser," IEEE J. Quantum Electron., 7, No. 11, 501-507 (1971).
13. D. J. Spencer et al., "Continuous-wave chemical laser," Int. J. Chem. Kinetics, 1, No. 5, 493-494 (1969).
14. W. R. Warren, Jr., "Chemical lasers," Astron. Aeron., 13, No. 4, 36-49 (1975).
15. D. J. Spencer, H. Mirels and D. A. Durran, "Performance of CW HF chemical laser with N_2 or He diluent," J. Appl. Phys., 43, 1151-1157 (1972).
16. L. Bertrand, J. M. Gagne, B. Mongeau, et al., "A continuous HF chemical laser: Production of fluorine atoms by a microwave discharge," J. Appl. Phys., 48, No. 1, 224-229 (1977).
17. W. Q. Jeffers and H. Y. Ageno, "CO chain reaction chemical laser," Appl. Phys. Lett., 27, No. 4, 227-229 (1975).
18. W. Q. Jeffers and C. E. Wiswall, "Experimental studies of the $O/O_2/CS_2$ CW CO chemical lasers," IEEE J. Quantum Electron., QE-10, No. 12, 860-869 (1974).
19. A. S. Bashkin, N. M. Gorshunov, Yu. A. Kunin, et al., "Obtaining lasing on a CS_2–O mixture in a shock tube with a supersonic nozzle," Kvantovaya Elektron., 3, No. 2, 463-465 (1976).
20. A. W. Blackman, "Laser device," Pat. USA N 3566297, Nov. 3 (1970).
21. N. G. Basov et al., "Dynamics of chemical lasers," Kvantovaya Elektron. (Moscow), No. 2, 3-24 (1971).
22. J. R. Airey and S. F. McKay, "A supersonic mixing chemical laser," Appl. Phys. Lett., 15, No. 12, 401-403 (1969); S. J. Arnold, K. D. Foster, and D. R. Snelling, "A supersonic HCl chemical laser," J. Opt. Soc. Am., 68, No. 5, 652 (1978).
23. R. A. Meinzer, "A continuous-wave combustion laser," Int. J. Chem. Kinetics, 2, 335 (1970).
24. G. A. Capelle and S. N. Suchard, "CN* production efficiencies from active nitrogen–hydrocarbon flames," IEEE J. Quantum Electron., QE-12, No. 7, 417-421 (1976).
25. L. R. Boedeker, J. A. Shirley, and B. R. Bronfin, "Arc-excited flowing CO chemical laser," Appl. Phys. Lett., 21, No. 6, 247-249 (1972).
26. "Studying liquid-fuel chemical lasers, a group of TRW works up from 8 kW," Laser Focus, 12, No. 6, 38 (1976).
27. N. G. Basov and A. N. Oraevskii, "Laser," Inventor's Certificate No. 436413 (Priority 24 April 1967), Byull. Izobret., No. 26, 146 (1974).
28. T. A. Cool, R. R. Stephens, and T. J. Falk, "A continuous-wave chemically excited CO_2 laser," Int. J. Chem. Kinetics, 1, 495-496 (1969).
29. A. N. Oraevskii, "Chemical lasers," Khim. Vys. Energ., 8, No. 1, 3-20 (1974).
30. T. A. Cool, "The transfer chemical laser. A review of recent research," IEEE J. Quantum Electron., QE-9, No. 1, 72-83 (1973).
31. E. T. Gerry, "Gasdynamic CO_2 lasers," Bull. Am. Phys. Soc., 15, 563 (1970).
32. G. W. Tregay et al., "DF–CO_2 transfer laser development," IEEE J. Quantum Electron., QE-11, No. 8, 672-678 (1975).
33. G. Emanuel, W. G. Gaskill, R. J. Reiner, et al., "High-pressure operation of a CW DF–CO_2 transfer laser," IEEE J. Quantum Electron., QE-12, No. 11, 739-740 (1976).
34. A. S. Bashkin, N. M. Gorshunov, Yu. A. Kunin, et al., "Supersonic chemical CO_2 laser on mixture of atomic deuterium with ozone and carbon dioxide," Kvantovaya Elektron. (Moscow), 3, No. 5, 1142-1143 (1976).
35. A. S. Biryukov, "Kinetics of physical processes in gasdynamic lasers," in: Theoretical Problems of Spectroscopy and Gasdynamic Lasers [in Russian], Izd. Akad. Nauk SSSR, Moscow, Vol. 83 (1975), pp. 13-86.
36. A. S. Biryukov and L. A. Shelepin, "Chemical-mechanical molecular laser," Zh. Tekh. Fiz., 40, No. 12, 2575-2577 (1970).
37. J. Wieder, "Flame pumping and infrared maser action in CO_2," Phys. Lett., 24A, No. 13, 759-760 (1967).
38. N. G. Basov, V. V. Gromov, E. P. Markin, et al., "Chemical lasers based on oxidation of CO + 0.5 O_2 with supersonic flow of medium," Kvantovaya Elektron. (Moscow), 3, No. 5, 1154-1155 (1976).

39. N. N. Kudryavtsev, S. S. Novikov, and I. B. Svetlichnyi, "Effect of nonequilibrium chemical pumping on the amplification of CO_2-laser emission in the products of the reaction $CO + N_2O$," Dokl. Akad. Nauk SSSR, 231, No. 5, 1113-1115 (1976).
40. N. G. Basov, V. V. Gromov, E. L. Koshelev, et al., " Chemical CW laser on DF–CO_2," Pis'ma Zh. Eksp. Teor. Fiz., 13, No. 9, 496-498 (1971).
41. N. G. Preobrazhenskii, " Diffusion problems arising in the linear theory of gasdynamic and chemical lasers," Zh. Prikl. Mekh. Tekh. Fiz., No. 2, 32-37 (1974).
42. G. L. Grohs, "Turbulent cavity mixing in continuous-wave chemical lasers: Status of theory," Combust. Sci. Technol., 13, 257-267 (1976).
43. R. Hofland and H. Mirels, "Flame-sheet analysis of CW diffusion-type chemical lasers. I. Uncoupled radiation," AIAA J., 10, No. 4, 420-428 (1972).
44. A. N. Oraevskii et al., "Efficiency of a CW diffusion chemical amplifier," Kvantovaya Elektron. (Moscow), 3, 9, 1896-1908 (1976).
45. J. G. Skifstad and C. M. Chao, "Rotational relaxation in a line selected continuous HF chemical laser," Appl. Opt., 14, 1713-1718 (1975); L. H. Sentman, "Chemical laser power spectral performance: a coupled fluid dynamic, kinetic and physical optics model," Appl. Opt., 17, No. 14, 2244-2449 (1978).
46. R. J. Hall, "Rotational nonequilibrium and line-selected operation of CW DF-chemical lasers," IEEE J. Quantum Electron., 12, No. 8, 453-462 (1976).
47. K. H. Homann et al., "Eine Methode zur Erzeugung von Fluorstammer in inerten Atmosphäre," Berichte Bunsen Gesellschaft, Physicalische Chemie, 74, 585-589 (1970).
48. J. C. Polanyi and K. B. Woodall, "Energy distribution among reaction products. VI. F + H_2, D_2," J. Chem. Phys., 57, No. 4, 1574-1586 (1972).
49. W. S. King and H. Mirels, "Numerical study of a diffusion-type chemical laser," AIAA J., 10, No. 12, 1647-1654 (1972).
50. V. G. Krutova et al., "Numerical analysis of CW diffusion chemical laser at arbitrary degree of dissociation of molecular fluorine," Kvantovaya Ekektron. (Moscow), 3, No. 9, 1919-1931 (1976).
51. A. N. Oraevskii et al., "Analysis of lasing regime of CW diffusion chemical laser with chain-reaction excitation at low degrees of dissociation of molecular fluorine," Kvantovaya Elektron. (Moscow), 3, No. 1, 136-146 (1976).
52. V. A. Pospelov, "Calculation of flow in a CW chemical laser on a hydrogen–fluorine mixture," Izv. Akad. Nauk SSSR, Mekh. Zhidk. Gaza, No. 2, 203-205 (1978).
53. V. I. Golovichev and N. G. Preobrazhenskii, "Numerical analysis of turbulent chemical HF laser of diffusion type in the amplification regime," in: Gas Lasers [in Russian], R. I. Soloukhin and V. P. Chebotaev (eds.), Novosibirsk, Nauka (1977), pp. 83-104.
54. Ya. Z. Virnik et al., "Diffraction effects in CW chemical HF laser with unstable telescopic cavity," Kvantovaya Elektron. (Moscow), 6, No. 1, 236-248 (1979).
55. A. S. Biryukov, Yu. A. Kulagin, and L. A. Shelepin, "Kinetics of physical properties in a supersonically pumped chemical CO laser," Kvantovaya Elektron. (Moscow), 5, No. 7, 1444-1455 (1978).
56. P. J. Ortwerth, "On the rational design of compressible flow ejectors," AIAA Paper 1217, 1-9 (1978).
57. R. J. Driscoll and L. F. Moon, "Pressure Recovery in Chemical Lasers," AIAA J., 15, No. 5, 665-673 (1977).
58. R. J. Driscoll, "A study of the boundary layers in chemical laser nozzles," AIAA J., 14, 1571-1577 (1976).
59. L. Crocco, "One-dimensional treatment of steady gasdynamics," in: Fundamentals of Gasdynamics, Vol. III, Princeton Univ. Press, Princeton, New Jersey (1958).

CHAPTER 7

DETONATION CHEMICAL LASERS

7.1. General Information on Detonation Processes

It is known that detonation of solid explosives (see, e.g., [1]) and of explosive gas mixtures [2, 3] can be used for optical laser pumping. Here the chemical energy of the substance is directly converted into optical pumping energy, and then into the lasing energy. Even more effective conversion of chemical energy should take place in detonation chemical lasers, whose operating principle is based on obtaining lasing directly from the chemical-reaction zone behind the detonation front [4, 5], or else from the region of the free expansion of detonation products [6], or else from the region of exhaust of the detonation products through a nozzle [7]. In general, we shall use the term "detonation" for a chemical laser in which the active medium or a component of this medium is a detonation product.

Let us present some information of general character concerning detonations.

A *detonation* is a explosive conflagration wave, one of the known basic properties of which is its propagation with constant supersonic average velocity, typical of the particular explosive and of its initial parameters. If we choose a coordinate frame connected with the front of the detonation wave, then, in accordance with one-dimensional detonation theory, the flow can be represented as shown in Fig. 7.1. The gas flows along the x axis in its positive direction, and the wave parameters remain constant in planes perpendicular to the x axis. Equations describing such a flow are given, e.g., in [8]. From these equations one obtains, in the coordinates p and V, a curve called the Hugoniot adiabat, which describes the solution for all values of the wave velocity D (Fig. 7.2):

$$V/V_0 = \frac{(p/p_0)+[(\gamma+1)/(\gamma-1)]+(2\gamma Q/c_0^2)}{[(p/p_0)(\gamma+1)/(\gamma-1)]+1}. \tag{7.1}$$

Here $V = 1/\rho$ is the specific volume; $\gamma = c_p/c_V$, ratio of the specific heats; Q, heat of combustion per unit mass of the mixture; and c_0, speed of sound in the initial mixture.

The condition that the detonation velocity be unique is substantiated in [9] and is called the Chapman–Jouguet condition:

$$(p - p_0)/(V_0 - V) = -(\partial p/\partial V)_S. \tag{7.2}$$

It follows from this condition that *normal* detonation corresponds to the lowest of all possible velocities D, which is represented on the p(V) plot (see Fig. 7.2) by the Michelson straight line AB, which is tangent to the Hugoniot curve CMNE at the point called the Jouguet point, G. A feature of the process is that in the state corresponding to the point G the detonation velocity is equal to the sum of the velocities of the stream and of the propagation of the perturbation in the explosion products, i.e.,

$$D = u + c. \tag{7.3}$$

In addition to the normal detonation regime, which corresponds to the straight line AB tangent to the detonation-product adiabat, the curve CM describes two other detonation regimes: overdriven (CG) and underdriven (GM) detonations. For the first regime $u + c > D$, and for the second $u + c < D$.

According to the *classical-one-dimensional detonation theory* [10, 11], after compression of the initial mixture by the shock-wave, the state of the mixture corresponds to the point B (see Fig. 7.2) for normal detonation and to the point B_1 in the overdriven detonation regime. Then, as the chemical reaction proceeds, the state of the medium shifts along the Michelson line BG or B_1C. Completion of the chemical reaction corresponds to states described, respectively, by the points G or C. Thus, an increase of pressure should occur at the points B or B_1.

The detonation-wave theory that presupposes the presence of a smooth front is based on the solution of the one-dimensional equations of gas dynamics and chemical kinetics.

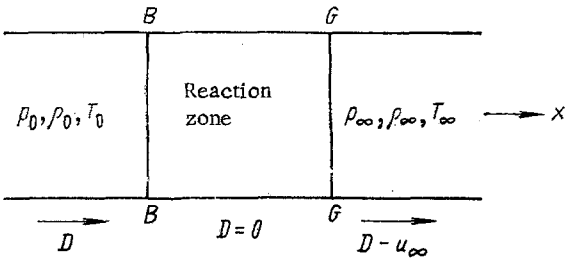

Fig. 7.1. Flow in a coordinate frame connected with the detonation front velocity D.

A deviation from such a one-dimensional model takes place in the so-called *spin* detonation [12], namely a helical motion near the wall of the tube of one site of the chemical conflagration reaction, a site produced upon splitting of the wave front [13]. Spin detonation always takes place at the propagation limits of the detonation wave [14].

The *detonation propagation limits* are those critical initial conditions, with respect to the pressure p_0 or density ρ, to diameter d of the explosive charge, and also to the concentration of the component and the composition of the initial mixture, whose change (either towards lower pressure or diameter or towards enrichment or depletion of the initial mixture of the combustion component) leads to the impossibility of propagation of the detonation process.

Far from the limits, according to the classical concepts, a detonation wave should have a plane smooth front. However, using increased-resolution photorecording and an advanced tracking method, a *non-one-dimensional high-frequency structure* of real detonation waves was observed under these conditions [15, 16], with periodic inhomogeneities in a nonsmooth leading front of the wave.

Thus, whereas spin detonation near the limit of its propagation corresponds to a track imprint of Fig. 7.3a, with a thickened helical track of only one conflagration site whose trajectory makes an angle χ to the generatrix of the detonation channel, displacement away from the limits leads to a jumplike restructuring of the process. Not one but 2n (n = 1, 2, 3 ...) conflagration sites are produced in the detonation front. These move over the front opposite to each other with spacing Δx, collide, and are reflected (Figs. 7.3b, c). A streak photograph (Fig. 7.3d) makes it possible to determine the pulsation frequency of the process

$$\nu = D/\Delta x. \tag{7.4}$$

It is convenient to characterize such a periodic process as a *detonation mode*

$$\Omega = \nu/\nu_0 \ (\Omega \approx n), \tag{7.5}$$

where ν_0 is the minimum frequency of the pulsations in the region next to the limit of the existence of a detonation wave with $\Omega \approx n = 1$. The pulsation interval decreases with increasing initial pressure of the mixture p_0 or when its reactivity is decreased, e.g., if the chemical composition is changed (Fig. 7.4) [15-19]. The results of an extrapolation of the data of [20] correspond here to $\Delta x \approx 5 \cdot 10^{-3}$ and $2 \cdot 10^{-3}$ mm and to $\nu \approx 7 \cdot 10^8$ and $11 \cdot 10^8$ Hz.

Pulsations also exist in a spherical-detonation wave [21]. All this is evidence that the pulsation mechanism, as a property of a detonation wave, is universal.

One of the distinguishing features of detonation is the *discrete* dependence of the pulsation interval Δx, of the frequency ν, and of other parameters that characterize the detonation-wave structure, on the initial pressure p_0.

An analysis of the sequences of Δx for neighboring n in [22] yielded a relation for the discrete spectrum Δx in the form

$$\pi d/\Delta x = 1/n + \zeta_* (1 + 1/n)(n - 1), \ n = 1, 2, 3, \ldots \tag{7.6}$$

Here $\zeta_* = \tan(\chi)_{\min}$, i.e., the tangent of the smallest angle χ reached far from the detonation limits.

Each of the intersecting lines on the track records of Figs. 7.3b, c was interpreted in [15, 16] as the trajectory of the so-called *kink*. A kink was considered in [23] in the form of three intersecting shock discontinuities: an *oblique* shock-wave, a *direct* shock-wave normal to the generatrix of the detonation channel, and a shock-wave moving *tangentially* to the

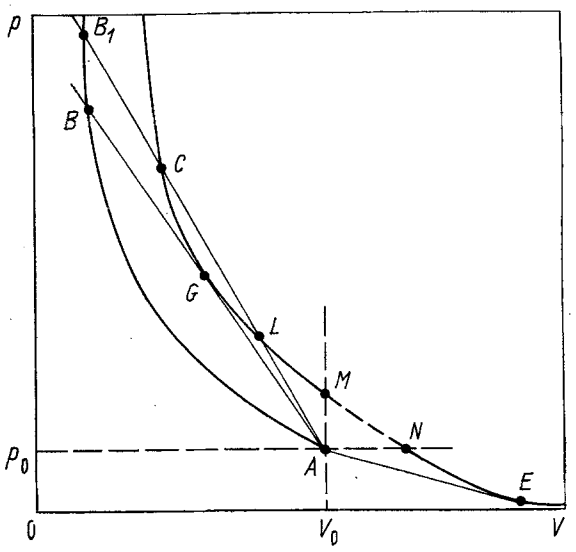

Fig. 7.2. Hugoniot adiabat.

straight shock-wave. Gas-dynamic calculation of such a model, which is a *Mach configuration*, leads to the need for the existence of also a fourth *tangential discontinuity*, which emerges from the point of intersection of the other three discontinuities — the *triple point*.

Each of the kink track lines is drawn precisely through the triple point [24]. The three-dimensional structure of the real detonation wave for the case with n = 2, which is registered on the track imprint of Fig. 7.3b, is shown clearly in Fig. 7.5 [24] for three successive instants of time t_0, t_1, and t_2. The change from the concave wavefront to convex takes place at the collision points of the triple points marked by crosses. Such a pulsating character of the change of the leading front of the detonation wave is observed only by Toepler photography of the detonation in a planar channel [25, 17]. Behind the leading front, however, as shown in [25], the structure of the flow for detonation with small n is even more complicated and includes the *transverse* detonation wave, which was proposed in [26] for spin detonation, and observed experimentally in the structure of this detonation [27-29], and investigated in [30-32].

Calculation of planar Mach configurations in a detonation wave and their collisions with one another was carried out first by the method of *shock and detonation polars* in [24, 33, 34]. To this end, equations were derived connecting the relative change of the pressure in the i-th jump $\Delta P = (p_i - p_0)/p_0 = \Delta p/p_0$ with the angle of inclination η of the stream behind the jump:

of the *detonation polar*

$$\operatorname{tg}\eta=\frac{\Delta P}{\gamma M^2-\Delta P}\sqrt{\frac{M^2(1-q/\Delta P)}{\Delta P/(\mu^2+1)+1}-1} \tag{7.7}$$

[M is the Mach number; $q = Q/E_0 = Q(\gamma - 1)(p_0/\rho_0)^{-1}$ is the effective energy released in fractions of the internal energy of the gas; $\mu^2 = (\gamma - 1)/(\gamma + 1)$];

and of the *shock polar*

$$\operatorname{tg}\eta=\frac{\Delta P}{\gamma M^2-\Delta P}\sqrt{\frac{M^2}{\Delta P/(\mu^2+1)+1}-1}\,. \tag{7.8}$$

The solution has shown that for a detonation with $\Omega > 1$, the collisions of the Mach configurations and the formation, in these collisions, of new pulsations in the wave should be of substantial significance. The real interaction of the perturbations in the detonation wave far from the limits is even more complicated than that usually considered in the planar model, and is connected with the influence of the *bulk effect* on the structure of the detonation front [35]. Indeed, what is important is that the process is essentially three-dimensional and that the most intense sources of the disturbances which are renewed by the pulsations with Mach configurations in the wave are the places of the "triple" and more collisions of the Mach configurations. As a result, the pulsation multiplication coefficient

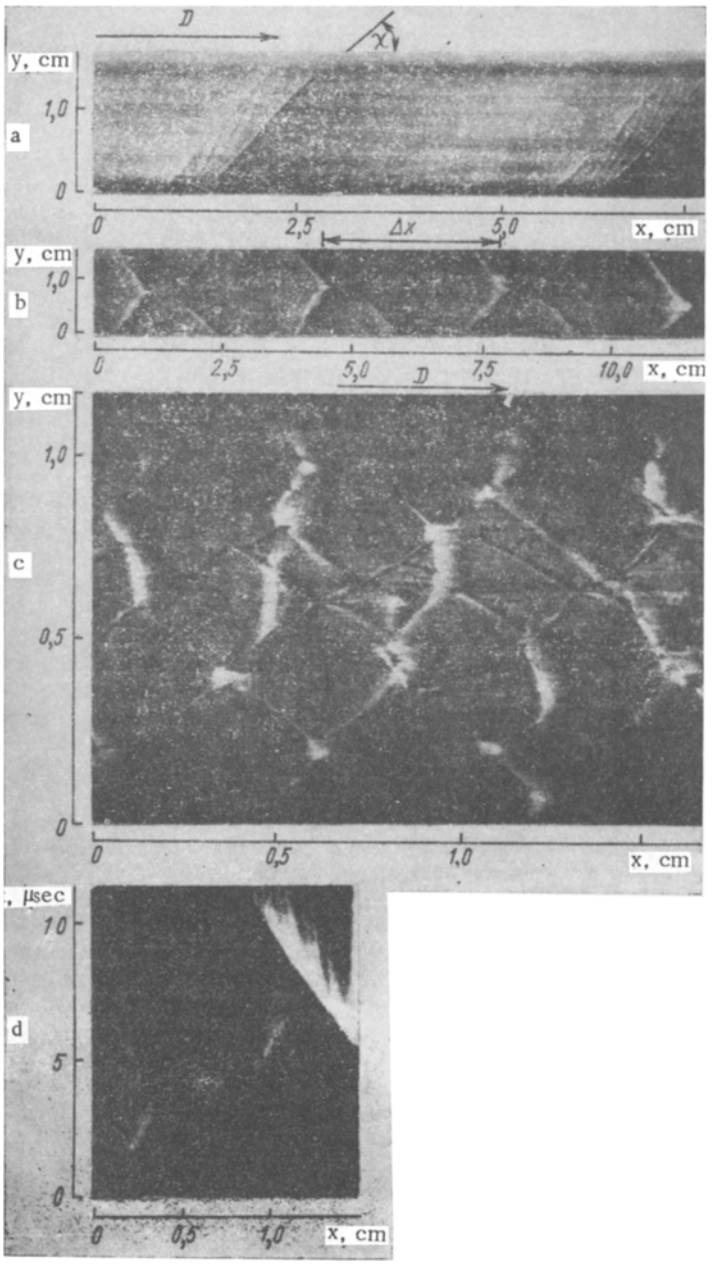

Fig. 7.3. Recording of detonation inhomogeneities in the mixture $2H_2/O_2$. Trackprints of the detonation: a) spin, n = 1; b) pulsating, $\Omega = 2$; c) pulsating, $\Omega \approx 20$; d) increased resolution x–t streak photograph of the emission of a pulsating detonation, $\Omega = 30$.

$$K = 1 + [(1 + N)/(n^* + N)], \tag{7.9}$$

at a sufficiently large number of initial pulsations N, tends to two ($n^* = 3$ for detonation in round channels, $n^* = 5$ for spherical detonation). The realization of such a multiplication is due to the reaction-kinetic data of the detonation medium [21]. At a small number of pulsations in the wave ($<n^*$) their multiplication can be due to the formation of new triple points with nonequal change of the intensity of the jumps that are contained in the Mach configuration [36].

Of importance for the understanding of the mechanism of the detonation is the question of the localization of the *leading elements of the ignition zone*. In [37] is proposed a chemical-reaction mechanism that takes place in the adiabatic explosion regime, where the role of the induction zone is played by a shock discontinuity in which several collisions of atoms or molecules lead to a chemical transformation of a small fraction of the explosive, and

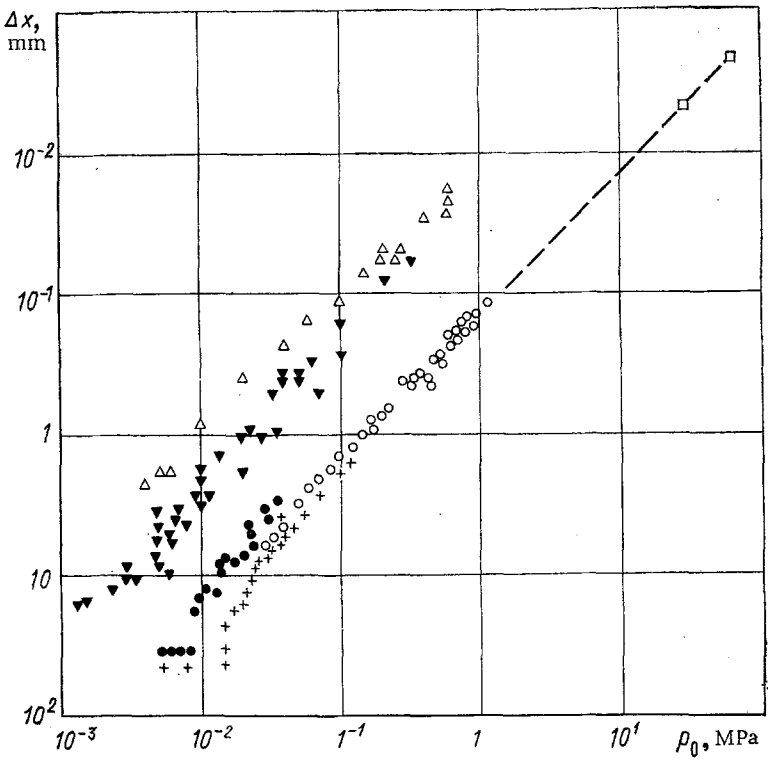

Fig. 7.4. Pulsation scale vs. the initial pressure p_0 of the primary explosives: ○ $2H_2/O_2$ – O[18], +[15, 16], ●[19]; $2C_2H_2/O_2$ – ▼ [17–19]; C_2H_2/O_2 – △[18]; $2H_2/O_2$ – □ extrapolation of the data of [20].

this prepares the conditions for the concluding stages of the reaction. It can therefore be assumed that in the case of detonation there exists a thin layer – a shock-discontinuity film in which conflagration sites are intruded. The presence of such a structure of the reaction zone in a detonation wave was demonstrated by a correlation analysis, by experimental study of the perturbations of the fine structure of the spin detonation, and by comparison of the obtained data with the calculated sizes of the zone of vibrational relaxations of the molecules [38, 39]. The leading elements of the ignition zone upon detonation are localized in a narrow forward layer of the detonation wave with thickness of the order of the size of the zone of vibrational relaxations of the mixture. Consequently, the scale of the detonation pulsations can reach considerable values, likewise of the order of the size of this zone.

7.2. "Optical" Properties of Detonation Waves and the Phase Character of Their Propagation

The detonation wavefront, according to Fig. 7.5, can be represented as consisting of elementary fronts, which oscillate about a certain average position that propagates with constant velocity. The interaction between neighboring elementary fronts serves as the source of new fronts. If the initial explosive is isotropic, the propagation of such a front in it should also obey the laws of geometric and wave optics.

On the basis of this one can apply [40] the analytic Fermat principle and the Huygens–Fresnel principle to the propagation of detonation waves in an unbounded medium.

The principle states: In an isotropic medium the propagation of a wavefront f from a point P_1 (x_1, y_1) to a point P_2 (x_2, y_2) corresponds to the extremal value of the integral

$$T = \int_{P_1}^{P_2} \frac{ds}{D(x, y)}, \tag{7.10}$$

where T is the time of passage of the section of the wavefront from P_1 to P_2, and s is the length of the trajectory arc of the point of the wavefront.

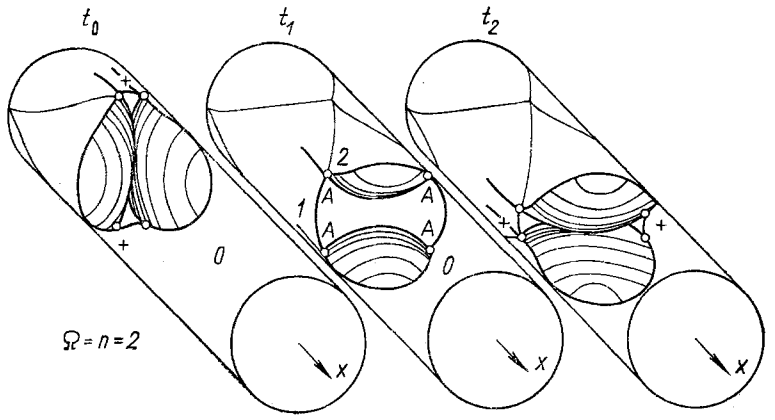

Fig. 7.5. Diagram of three-dimensional structure of detonation for $\Omega \approx n = 2$: thin lines — trajectories of triple points; thick lines — shock discontinuities; circles — triple points A; 0, 1, 2) states of the gas: initial and behind the straight and oblique shock waves, respectively.

The integral curve is determined from the differential Euler equation for the extremum

$$\frac{d}{dx}\frac{y'}{D(x,y)\sqrt{1+(y')^2}}+\frac{\sqrt{1+(y')^2}}{D^2(x,y)}\frac{\partial D(x,y)}{\partial y}=0. \tag{7.11}$$

The constants of the general integral y (x, C_1, C_2) are determined from the conditions

$$\left.\begin{aligned} y_1 &= y(x_1, C_1, C_2),\\ y_2 &= y(x_2, C_1, C_2).\end{aligned}\right\} \tag{7.12}$$

In many cases the Fermat principle reduces to simple algebraic expressions for the conditions of the minimum time of propagation of wavefronts, e.g., those shown in Figs. 7.6a, b. For simultaneous emergence, in the planar case, of all the points of the detonation front f_1 from one initiation point I on a straight line P_1P_2 (see Fig. 7.6a), in the case when a compound charge consisting of two media 1 and 2 is used, with different detonation velocities D_1 and D_2, the shape of the line separating the media 1 and 2 is calculated from the equations

$$T = \sqrt{x^2+y^2}/D_1+(x^*-x)/D_2; \tag{7.13}$$

$$T_{min} = x_0/D_1 + (x^* - x_0)/D_2. \tag{7.14}$$

At $D_1/D_2 > 1$ the line C separating the media is a hyperbola. This type of generator of a straight-line detonation front (collimator) can be of importance for detonation chemical lasers, as a device for simultaneously introducing the gaseous detonation products into the cavity region. The same function can also be performed by a detonation wave generator, shown in Fig. 7.6b.

Here the line M_1M_n is a channel filled with a detonating medium having a detonation velocity D_1, while the lines M_iN_i (i = 1, 2, ..., n) are channels with a medium detonating with velocity D_2. The condition for simultaneous arrival of the detonation fronts in all the channels M_iN_i to the level of the straight line M_1N_n is

$$T = \frac{IM_i}{D_1}+\frac{M_iN_i}{D_2} \quad \text{or} \quad T=\frac{IM_1}{D_1}\Big|_{M_iN_i=0} = \frac{IN_n}{D_2}\Big|_{IM_i=0}, \tag{7.15}$$

whence

$$D_1 = D_2 \sin\beta/\sin\alpha. \tag{7.16}$$

If $\alpha = \beta$, then $D_1 = D_2$ and $IM_1 = IN_n$. Such a scheme was realized, e.g., in linear-detonation generators filled with gaseous explosives and constructed in the form of detonation channels of equal length [3]. A similar principle serves as the basis for a system, used to focus a detonation wave, of hollow cumulating cylindrical lenses made in the form of a packet of cylindrical partitions which are rough at the central part and smooth in the peripheral part. A number of detonation wave generators developed on the basis of the Fermat principle are shown in Figs. 7.7a-t [40]. Here are shown: a, b, i, p) schemes with focusing of the detonation fronts into a point; c, d, e, g, h, t) straight-line detonation fronts; f, m) focusing

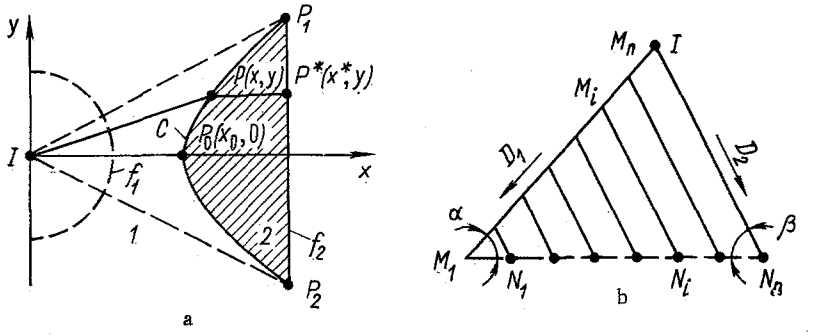

Fig. 7.6. Examples of application of the Fermat principle to the detonation process — detonation collimators: a) with two solid explosives 1 and 2 ($D_1/D_2 > 1$); b) with separated explosion channels.

of the detonation on the axis of the system; k, l) generation of a planar detonation front; n, o) generation of a curvilinear detonation front; r, s) diffraction of detonation fronts. The schemes r, s, and t are based on the diffraction properties of detonation waves that are no longer governed by the geometrical optics, but by the physical optics of the system.

Within the frame of the physical optics of detonation, the Huygens–Fresnel principle makes it possible to construct the front of the detonation wave for a certain instant of time, if the front of the wave at the preceding instant is known. This construction is based on the fact that each point of the medium at which a wavefront has arrived is considered as a new source of oscillations.

These new sources of pulsations in a detonation wave are the points of the collisions of the kinks — of the triple Mach configurations. The presence of sources of new pulses in a detonation front gives rise to the *phase character* of its propagation. After each collision of the kinks, a new pulsation is produced and its parameter is determined only on the initial conditions. This can explain the existence of diffraction of the detonation waves, e.g., when they flow around corners, or else the phenomenon of refraction by interfaces between media [41]. A schematic picture of the phase propagation of a detonation front is shown in Fig. 7.8, where the numbers 1-8 show the pulsation-front positions corresponding to the instants of time from t_1 to t_8. The thick lines arbitrarily show the regions of maximum energy release, which renew the pulsations in the wave.

The phase propagation of such a structure with velocity D, as can be seen from Fig. 7.3b and c, forms patterns similar to those observed in hydrodynamics in the flow of "shallow water", namely motion in the gravitational field of an incompressible liquid with a free surface and having a layer depth that is small compared with the characteristic dimensions of the flow.

It is known (see, e.g., [42]) that wave processes on shallow water are described by the Korteweg–de Vries equation

$$\psi_t + D\psi_x + b\psi_{xxx} + \psi\psi_x = 0 \qquad (7.17)$$

(D is the wave velocity, $b = Dl^2$, l is a scale parameter), particular cases of which for the propagation of small and finite perturbations in a medium with a chemical reaction were considered, e.g., in [43]. Longwave perturbations for the case of acoustic detonation and reacting media were analyzed for the purpose of obtaining an equation that describes the structure of a finite perturbation propagating in a reacting medium in one direction. The general system of equations of a reacting gas, indicated in Sec. 1.7, is reduced in [43] to a single equation from which, in limiting cases $\tau_c/T < 1$ (τ_c is the time of the chemical reaction; T, characteristic period of the initial perturbation), one obtains the Korteweg–de Vries–Burgers equation for waves on the surface of a liquid with positive viscosity. The conditions $\tau_c/T \sim 1$ corresponds in this case to medium frequencies and $\tau_c/T > 1$ to the high-frequency approximation. It follows from the analysis that when the long wave perturbation propagates in a medium with exothermic reaction, it increases in amplitude and decreases in duration, i.e., amplification of the signal takes place.

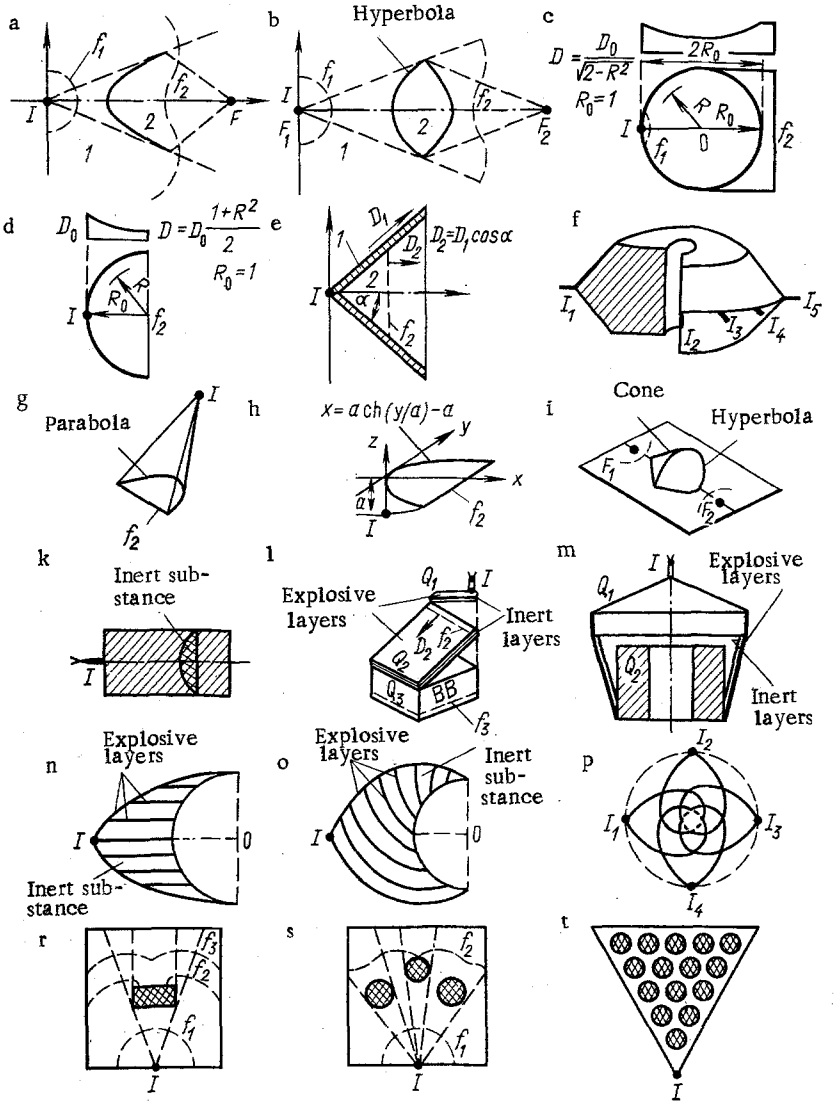

Fig. 7.7. Diagrams of detonation wave generators.

The energy method and the formalism of elementary quantum mechanics [42], in which the state of a medium is described by a normalized function $\psi(x, t)$ that satisfies an equation of the Schrödinger type, as a particular case of Eq. (7.17), make it possible to obtain the frequency characteristics of wave packets in each of the possible detonation regimes for given initial conditions of the initial explosive medium. Such a set of possible eigenfrequencies of the detonation process can be obtained in the following manner [44]. The energy release Q(T) is taken into account by the second law of thermodynamics:

$$Tds = dT - (\gamma - 1)Td\rho/\rho = (1/c_V)Q(T)dt. \tag{7.18}$$

Here $s = S/c_V R$ is the dimensionless specific entropy.

To simplify the problem, we assume that the dependence of Q on T is linear, i.e., $Q(T) = (\partial Q/\partial T)T$, where $\partial Q/\partial T = \text{const}$. We then have from (7.18)

$$T = T_a \exp(\omega t), \tag{7.19}$$

where $\omega = ds/dt = 1/c_V\ \partial Q/\partial T = 1/\tau$; τ is the period of the induction of ignition; $T_a = T_0(\rho/\rho_0)^{\gamma-1}$ is the ignition temperature.

Each wave packet in a detonation wave is described on the average by the transported mass m, the momentum $\mathbf{p} = m\mathbf{u}$, and the energy E in the phase space $\mathbf{r}$, t. In analogy with the quantum-mechanical formalism [42] we write

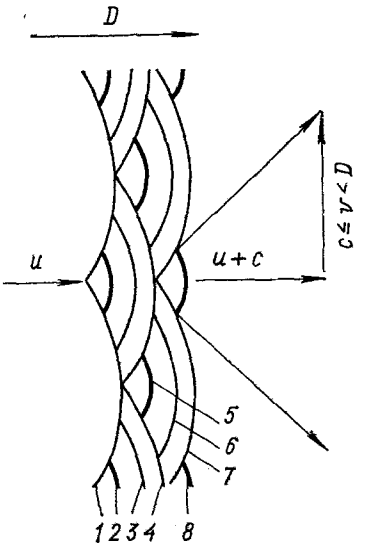

Fig. 7.8. Phase propagation of a detonation wave. For the tangential velocity of the pulsation propagation, $c \leqslant v < D$ ($v = D$, spin detonation; $n = 1$).

$$ih_D \frac{\partial \psi}{\partial t} = -\frac{h_D^2}{2m} \nabla^2 \psi + \left(\frac{\gamma T_a e^{\omega t}}{\gamma - 1} - \int T ds \right) \psi. \tag{7.20}$$

Here h_D is a constant that depends on the thermodynamic properties of the medium, and $\psi(\mathbf{r}, t)$ is a wave function that characterizes the wave packet in the detonation front.

To determine the constant h_D, we use one of the solutions of (7.20) in the form of a plane wave

$$\psi(\mathbf{r}, t) \sim \exp[-(i/h_D)(Et - \mathbf{pr}) - is_0(t)], \tag{7.21}$$

where s_0 is the initial phase of the wave.

The energy conservation law in such a wave is

$$E = mu^2/2 + [T_a/(\gamma - 1)] \exp \omega t. \tag{7.22}$$

We determine the constant h_D by substituting (7.21) in (7.20). We obtain

$$E + h_D ds_0/dt = mu^2/2 + [T_a/(\gamma - 1)] \exp(\omega t) + T_a. \tag{7.23}$$

From (7.22) and (7.23) it follows that

$$ds_0/dt = T_a/h_D = \omega \quad \text{or} \quad h_D = T_a/\omega. \tag{7.24}$$

In accordance with the physical meaning, the initial phase of the wave s_0 coincides here with the concept of the specific entropy, and therefore when a new wave packet is produced a jump takes place not only in the phase but also in the entropy.

We verify now whether Eq. (7.20) satisfies the basic mass and momentum conservation laws. Expressions for these laws can be obtained from (7.20) by averaging. Thus, the mass conservation law

$$\frac{\partial |\psi|^2}{\partial t} = -\operatorname{div} \mathbf{j} \tag{7.25}$$

is written in the form $\partial/\partial t \int |\psi|^2 d\mathbf{u} = -\operatorname{div} \int \mathbf{j} d\mathbf{u}$, where $|\psi|^2 \sim \rho/\rho_0$, while $\mathbf{j} = (ih_D/2m)(\psi \nabla \psi^* - \psi^* \nabla \psi)$ is the probability flux density. Integration over the physical volume $\mathbf{r}$, t yields the averaged mass conservation law. The momentum conservation law is written in the form

$$\frac{\partial j_i}{\partial t} = -\frac{\partial}{\partial x_j} \hat{\Pi}_{ij}. \tag{7.26}$$

Here the tensor of the momentum probability flux density is

$$\hat{\Pi}_{ij} = \frac{h_D^2}{4m} [(\nabla_i \psi \nabla_j \psi^* + \nabla_i \psi^* \nabla_j \psi) - (\psi \nabla_i \nabla_j \psi^* + \psi^* \nabla_i \nabla_j \psi)] + \delta_{ij} (p_0/\rho_0) \gamma \exp(\omega t)/(\gamma - 1). \tag{7.27}$$

Analogously, integrating (7.26) using (7.21) we obtain an expression for the momentum conservation law.

Let us analyze the structure of the detonation front on the basis of Eq. (7.20). To this end we consider the two-dimensional problem with longitudinal transport of the wave energy in the x direction, and with transverse transport along the y axis. We seek solutions periodic in y and arbitrary in x and t, in the form

$$\psi = \psi(x, t) \exp(iky), \tag{7.28}$$

where $k = 2\pi/\Delta y$ is the wave number and Δy is the transverse scale of the pulsations in the detonation front. From (7.20) we obtain

$$ih_D \frac{\partial \psi}{\partial t} = -\frac{h_D^2}{2m} \frac{\partial^2 \psi}{\partial x^2} + \left[T_a \left(\frac{e^{\omega t} + \gamma - 1}{\gamma - 1} \right) + \frac{k^2 h_D^2}{2m} \right] \psi. \tag{7.29}$$

We seek self-similar solutions of (7.29) for the steady-state motion, in analogy with the procedure used in the theory of steady-state shock waves [45]:

$$\psi(x, t) = \psi(x - Dt).$$

Making the self-similar substitution $\partial/\partial x \to -1/D\ \partial/\partial t$, we obtain

$$\frac{\partial^2 \psi}{\partial t^2} + \frac{2imD^2}{h_D} \frac{\partial \psi}{\partial t} - \frac{2mD^2}{h_D^2} \left[T_a \frac{\exp(\omega t) + \gamma - 1}{\gamma - 1} + \frac{k^2 h_D^2}{2m} \right] \psi = 0 \tag{7.30}$$

To solve the eigenvalue equation we use the conditions $|\psi|^2_{t=0} = 1$, $|\psi|^2_{t\to\infty} = 0$.

Following the substitution

$$\psi(x, t) = \Phi(x, t) \exp(-imD^2 t/h_D) \tag{7.31}$$

Eq. (7.30) is transformed into

$$\Phi''_{tt} - \Phi \left(\frac{2mD^2}{h_D^2} \right) \left[\frac{T_a (e^{\omega t} + \gamma - 1)}{\gamma - 1} - \frac{1}{2} mD^2 + \frac{k^2 h_D^2}{2m} \right] = 0. \tag{7.32}$$

We solve this equation at $\Phi_{t=0} = 1$, $\Phi_{t\to\infty} = 0$. The solution can be represented as a cylindrical function $K_\nu(z)$ of imaginary argument, and then

$$\psi(x, t) = \exp\left[-\frac{imD^2}{h_D} \left(t - \frac{x}{D} \right) \right] C K_\nu \left\{ a \exp\left[\frac{\omega}{2} \left(t - \frac{x}{D} \right) \right] \right\}, \tag{7.33}$$

where $a = (2D/\omega h_D)[2mT_a/(\gamma - 1)]^{1/2}$ and C is obtained from the normalization condition

$$\int_{-\infty}^{+\infty} |\psi|^2 d\nu = 1.$$

From the solution follows a dispersion relation for the pulsating process

$$\Omega = \frac{2D}{\omega} \left(\frac{2mT_a}{h_D^2} + k^2 - m^2 \frac{D^2}{h_D^2} \right)^{1/2}. \tag{7.34}$$

Figure 7.9 shows a model obtained in this manner for the wave packet, in the form of the function ψ in the coordinates y and $t - x/D$, at a fixed value of Ω. An estimate of the time scale of the x-pulsation in the detonation wave yields

$$\Delta t \simeq \frac{2}{\omega} \ln \left[\frac{8mD^2}{(\gamma - 1) T_a} \right]^{-1/2}. \tag{7.35}$$

Using expression (7.33) for the wave function ψ and the representation of the energy in accordance with Eq. (7.22) in operator form, we obtain, after averaging,

$$\bar{E} = \rho_0 T_a + \rho_0 D^2 \left[1 - \frac{\Omega^2 T_a^2}{4\rho_0^2 D^4} \right]. \tag{7.36}$$

From this it follows, e.g., that at $\Omega > \bar{\varepsilon} - 1$ the detonation-wave Mach number is

$$M = \left[\frac{\Omega}{2\gamma} + \frac{\bar{\varepsilon} - 1}{2\gamma} \right]^{1/2} (\rho/\rho_0)^{\frac{\gamma - 1}{2}}, \tag{7.37}$$

where $\bar{\varepsilon} = Q\bar{\mu}/RT_a^{(0)}$; $Q = \bar{E}/\rho_0$.

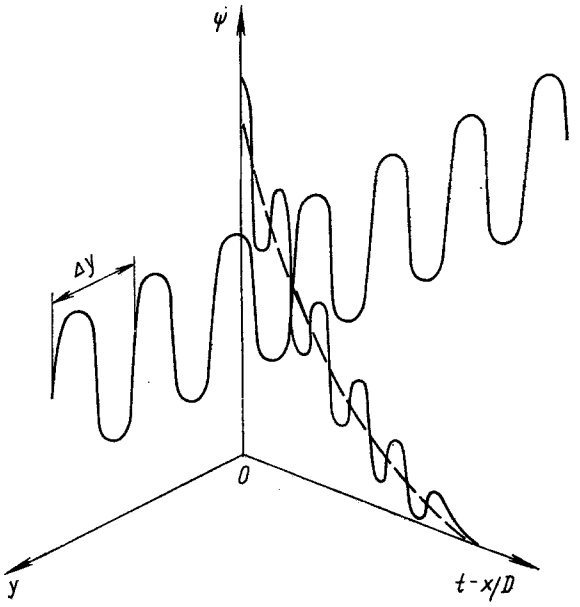

Fig. 7.9. Model of wave packet of the detonation process.

If the detonation-frequency spectrum is represented in accordance with (7.5) as $\nu = \Omega\nu_0$, where ν_0 is the minimum frequency of the pulsations in the near-limiting region of the detonation, while Q, $T_\alpha^{(\circ)}$, and μ are taken to be, respectively, the specific thermal effect of the chemical ignition reaction, the ignition temperature, and the average molar mass of the mixture, then the relation (7.37) qualitatively follows the spectrum of the experimentally observed connection between the longitudinal mode and the Mach number M. This can be seen, e.g., from the comparison in Fig. 7.10 of the experimental discrete detonation frequency spectrum (shown by vertical strokes and a dashed curve; the cross marks the value calculated from the data of [18]) and the results calculated from (7.37) (strokes and dash-dot curve) for a stoichiometric hydrogen–oxygen mixture.

Although the comparison of experiment and theory in Fig. 7.10 shows only a qualitative correspondence between the directions of the parameter changes, the developed theoretical analysis can serve as an illustration of the phase process, based on "physical optics" of their propagation. The condition for the applicability of such a treatment should naturally be that the frequency $\nu = \Omega\nu_0$ of the process be less than the natural frequency of the molecule vibrations.

The fundamental harmonics of the detonation pulsations were obtained also in [46] by treating the periodic instability as the theoretical basis of an intrinsic property of detonations – the pulsational structure of the wave.

A detailed mechanism of detonation phase propagation was proposed in [47]. It is based on equality of the average tangential velocities D_2 of collision and D_3 of reflection of the triple points, regarded as *ignition points* (*lines*) in the relaxation layer (film).

Indeed, the conditions for stable existence of detonation should be

$$D_3/D_2 = 1, \tag{7.38}$$

$$M_2 = D_2/c_1 \gtrsim 1, \tag{7.39}$$

where the last condition means that the tangential velocity of the point A is close to the speed of sound in the initially compressed gas in state 1.

Assume that shock waves collide and Chapman–Jouguet waves are reflected. If condition (7.38) is satisfied, the conservation equations yield

$$M_2^2 = \frac{\gamma_1+1}{2\gamma_1}\,\frac{2\gamma_3(3-\gamma_1)+\gamma_1(4-\gamma_1)-3}{\{[\gamma_3(\gamma_1-1)+2\gamma_1(\gamma_1-2)]^2-4\gamma_1(\gamma_1-3)[2\gamma_3(\gamma_1-3)+\gamma_1(\gamma_1-4)+3]\}^{1/2}-\gamma_3(\gamma_1-5)+\gamma_1^2-3}+\frac{\gamma_1-1}{2\gamma_1}. \tag{7.40}$$

The motion of the ignition point A in detonation was treated in [38, 47], in a coordinate frame connected with this point, as a supersonic flight in a gas by a pointed-wedge body in which an isothermic reaction takes place. The flow in the immediate vicinity of the point A

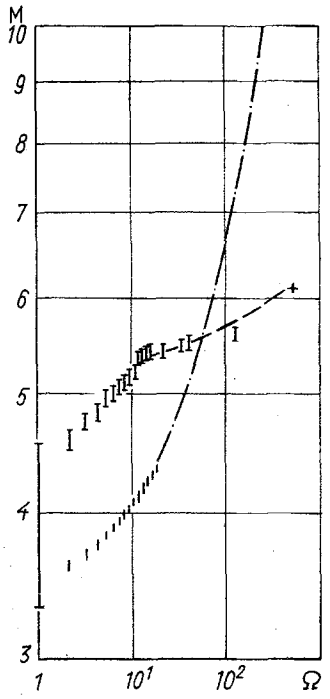

Fig. 7.10. Comparison of the experimental and calculated discrete detonation spectra.

can be represented as shown in Fig. 7.11. Owing to the symmetry of the ignition points (lines) relative to the direction of the average velocity D, the symmetry axis of the process can be taken to be the absolutely rigid wall x—x. We regard AB as the front of the incident wave of an irregular Mach reflection, AN as the Mach disk of this reflection, and the dash-dot line as the direction of the "flight" of the ignition point A with the exothermic reaction products diverging to both sides of this line at angles $\varphi_1 \approx \varphi_2$, while AK is the spreading boundary in the form of a shock wave that goes over into a Mach wave. For an irregular Mach reflection to be formed anew after collision with x—x, the following condition must be satisfied:

$$\psi \geqslant \operatorname{arcctg} \sqrt{\frac{\gamma_2+1}{2}\frac{\rho_0}{\rho_2}\left(1-\frac{\rho_0}{\rho_2}\right)}. \tag{7.41}$$

Using the equal sign in (7.41) and assuming the transition 0—2 to be strong enough, such that $\rho_0/\rho_2 \approx (\gamma_2 - 1)/(\gamma_2 + 1)$, we obtain from (7.41)

$$\psi = \operatorname{arcctg} \sqrt{(\gamma_2-1)/(\gamma_2+1)}. \tag{7.42}$$

The angles φ_1 and φ_2 satisfy the relation

$$\varphi_1 \approx \varphi_2 = \alpha + \varkappa = \frac{\pi}{2} - \psi + \varkappa \approx \varphi, \tag{7.43}$$

where

$$\varkappa = \operatorname{arctg}(D/D_2) = \operatorname{arctg}(M_1 c_0/M_2 c_1); \tag{7.44}$$

$$c_0/c_1 = \{(\gamma_1+1)^2(\gamma_0-1)/2\gamma_1(\gamma_1-1)[2+(\gamma_0-1)M_1^2]\}^{1/2}. \tag{7.45}$$

From (7.44) and (7.45), taking (7.43) into account, we have

$$\varphi = \operatorname{arctg}\left\{\left(\frac{\gamma_1+1}{m}+\mu_2\right)\Big/\left[1-\frac{(\gamma_1+1)\mu_2}{m}\right]\right\}, \tag{7.46}$$

where

$$m = M_2\{2\gamma_1(\gamma_1-1)[1+2/M_1^2(\gamma_0-1)]\}^{1/2};$$
$$\mu_2 = [(\gamma_2-1)/(\gamma_2+1)]^{1/2}.$$

The following relation [48] holds for the pressure in region 2:

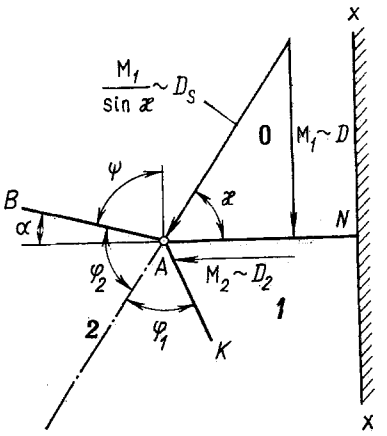

Fig. 7.11. Diagram of flow in the vicinity of the ignition point in a detailed structure of a detonation wave.

$$p_2 = \frac{2}{n_2+1} \rho_0 D_s^2 \sin^2 \varphi, \tag{7.47}$$

which is transformed, recognizing that $D_S = D/\sin \varkappa$ (see Fig. 7.11), into

$$\frac{p_2}{p_0} = \frac{2\gamma_0 M_1^2}{n_2+1} \frac{\sin^2 \varphi}{\sin^2 \varkappa}. \tag{7.48}$$

Here, according to [48],

$$n_2 = \gamma_2 \frac{1+(\gamma_2-1)\,q/2\gamma_2}{1+(\gamma_2-1)\,q/2} \quad \left(q = \frac{2Q}{p_2/\rho_2}\right). \tag{7.49}$$

To determine in these calculations the connection between M_1 and p_1/p_0 and ρ_1/ρ_0, respectively, we use the equations

$$\frac{p_1}{p_0} = \frac{\gamma_0 M_1^2+1}{\gamma_1+1} + \left[\left(\frac{\gamma_0 M_1^2+1}{\gamma_1+1}\right)^2 + \frac{2\gamma_0 M_1^2 (\gamma_0-\gamma_1)}{(\gamma_1+1)(\gamma_0-1)} - \frac{2\gamma_0 M_1^2-(\gamma_1-1)}{\gamma_1+1}\right]^{1/2}; \tag{7.50}$$

$$\rho_1/\rho_0 = \left\{1 + \frac{\gamma_1+1}{\gamma_1-1}\left[\left(\frac{2\gamma_0 M_1^2}{\gamma_0+1}\right) - \frac{\gamma_0-1}{\gamma_0+1}\right]\right\}\left[\frac{4\gamma_0}{\gamma_0^2-1} + \frac{2\gamma_0 M_1^2}{\gamma_0+1}\right]^{-1}. \tag{7.51}$$

The equations for p_2/p_1 and ρ_2/ρ_1 are similar.

From (7.40), (7.44), and (7.45) we obtain, e.g., for a stoichiometric hydrogen–oxygen mixture at $\gamma_0 = 7/5$, $\gamma_1 = 8/6$, $\gamma_2 = 9/7$, the values $\varkappa = 55$-$56°$, which are close to the experimental ones at the Mach numbers $M_1 = 5$-6 which are typical of a pulsating detonation.

The Mach number M_1 for a detonation wave in the same mixture is conveniently determined from the graphic solution of Eqs. (7.48), (7.49) in Fig. 7.12, where the experimental spectrum of the detonation frequencies in terms of the coordinates M_1 and $\Omega = \nu/\nu_0$ is shown for comparison. For a pulsating detonation the region of this spectrum on the plot is bounded by hatched dash-dot lines. The solutions L_1 and L_Ω of (7.48) and (7.49) for $Q_1 = 3.77$ and $Q_\Omega = 13.44$ MJ/kg, respectively, differ little from the indicated region of the experimental spectrum of the detonation frequencies. Here Q_1 is the energy release at near-limiting pulsating detonation with a fundamental mode $\Omega = 1$, and Q_Ω is the maximum possible theoretical energy release in the case of a chemical reaction in the detonation wave. The point L_{30} corresponds to detonation of a $2H_2 + O_2$ mixture under normal initial conditions with a natural frequency characterized by a mode $\Omega = 30$ and by $\nu = 1.5$ MHz.

In region 2, in the centered-rarefaction-wave fan produced by expansion of the reaction products from the ignition point A, the incoming stream may turn around to the extent that compression is produced in region 1 (see Fig. 7.11), so that the process becomes self-regulating via this so-to-speak feedback. This is the reason why the detonation wave "knows" in which geometry tangential to itself it propagates, whether the channel has a round or, say, rectangular cross section; at the same time it "does not know" the geometry of the space in the direction normal to itself, e.g., whether the channel ends are closed or open.

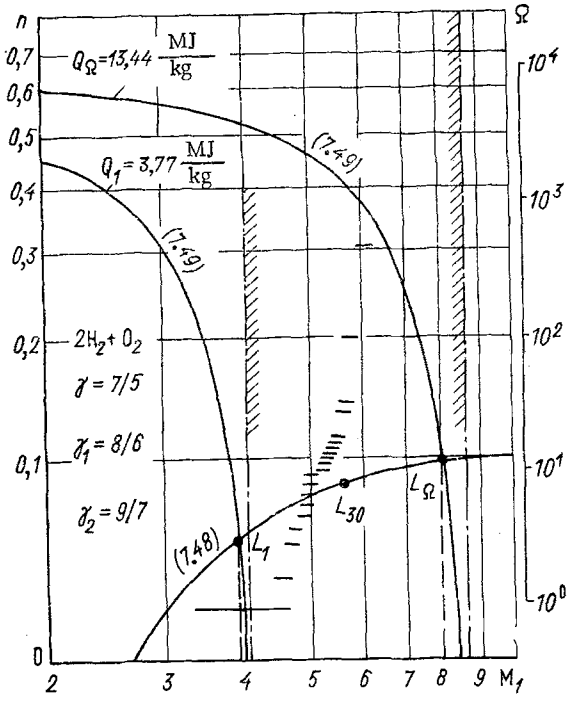

Fig. 7.12. Graphic solution of Eqs. (7.48), (7.49) for Q_1 = 3.77 and Q_Ω = 13.44 MJ/kg, and comparison with the limits of the experimental spectrum of the detonation frequencies.

7.3. Overdriven Detonation

As applied to detonation chemical lasers, it is of interest to consider overdriven-detonation regimes, for these are the only ones in which direct generation of coherent radiation was obtained so far [4]. Corresponding to overdriven detonation regimes are states on the Hugoniot diagram that lie above the Chapman–Jouguet point, e.g., on the CG curve (Fig. 7.2). These regimes can be realized by preventing the formation of a rarefaction wave behind the detonation-wave front, say by compressing the reaction products with a piston or by some other method [10]. An overdriven detonation is obtained, e.g., by changing the geometry, tangential to the wave, of the channel in a narrow tube to which a detonation goes over from a wide tube, by producing in the explosive mixture a thin electric-discharge layer that assumes the role of an impermeable piston that drives the shock-wave [49].

An overdriven detonation wave can also be produced by "crossing" of a detonation wave from a high-pressure section into a low-pressure section separated by a destructible membrane and containing an explosive medium. The velocity of overdriven waves decreases in the absence of support and they should in essence not be regarded as detonation waves, one of the main properties of which being a quasistationary behavior at constant initial conditions.

Account must be taken, however, of one more attribute of a detonation, namely a periodic structure identified by a wake method [15]. The presence of such a structure in a mixture capable of reacting is evidence of the existence of energy release directly in the front of the front of the wave, particularly also in the case of overdriven detonation.

From the character of the variation of the pulsation interval Δx on the wake prints, knowing the initial conditions p_0 and d_t, one can determine whether an overdriven detonation process exists and select smooth-front structures that are of interest for chemical lasers. Figure 7.13 shows schemes of such imprints for a number of methods of exciting an overdriven detonation and plots of the variation of the pulsation interval Δx in the course of transition of the detonation waves from the overdriven state to the steady-state Chapman–Jouguet regime over a length LCG from a section in the detonation channel corresponding to overcompression at the point C of the Hugoniot adiabat to the point G corresponding to the steady detonation regime (see Fig. 7.2). The overdriven-detonation regime with velocity D_C is produced both by stimulated excitation (dashed curves of Fig. 7.13) and by natural onset of detonation from a nonstationary complex of an accelerated flame H with a shock-wave Sh in front of it (solid line) propagating with velocity D_{Sh}.

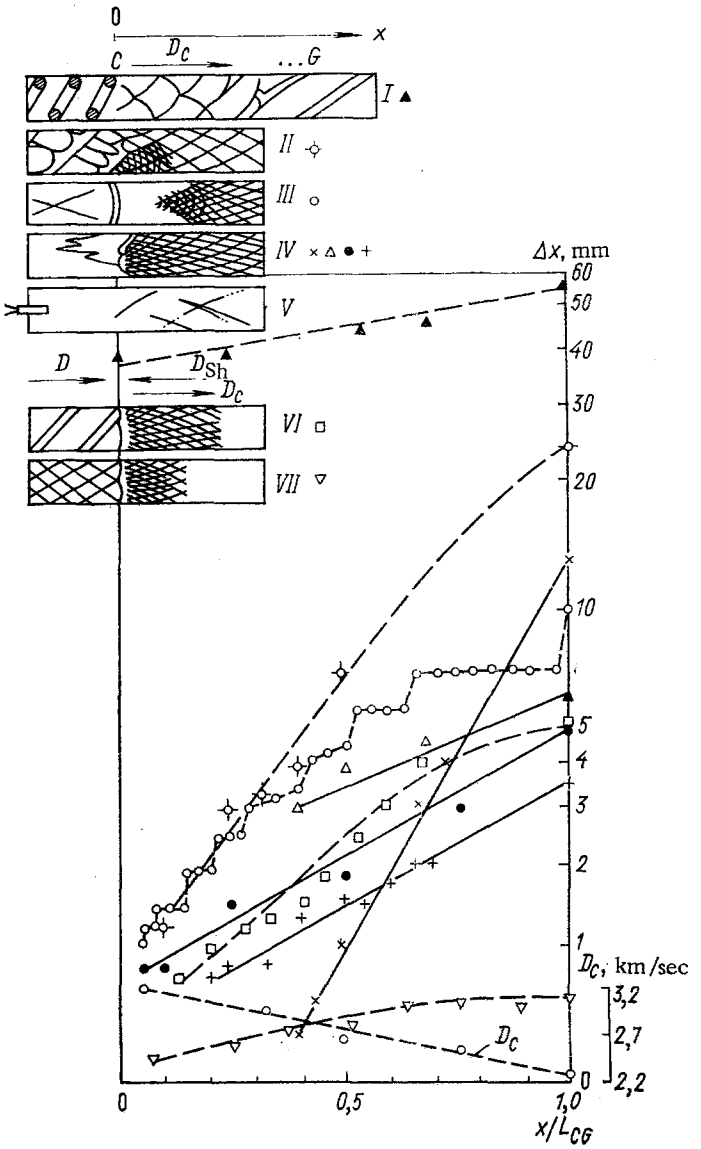

Mixture	Experiment	p_0, kPa	d_t, mm	L_{CG}, mm
$CH_4/2O_2$	×	40	20	90
$2H_2/O_2$	▲	13,3	16	400
	☼	17,3	18	50
	○	26,6	18	800
	Δ	40	20	30
	●	53,3	20	40
	+	66,6	20	50
	□	9,3	16	30
	▽	40	16	8

Fig. 7.13. Track imprints and plots of the pulsation scale Δx on the line L_{CG} of the transition of overdriven detonations to the steady-state regime: I) transition of artificially produced pulsating detonation, under overdriven conditions in a tube with a wire coil, into a spin-detonation wave [24, 50]; II) transition of stimulated spin detonation, obtained in a tube with a coil, into a pulsating detonation at constant initial mixture parameters (a similar result was obtained in [36] by changing the initial mixture density); III) strong initiation by electric discharge [51]; IV) onset of detonation from the nonstationary complex H — Sh; V) strong initiation with an electric detonator or with a batch of silver azide; VI) collision of a spin detonation; VII) collision of a pulsating detonation with nonstationary complexes H–Sh.

It can be seen from the foregoing schemes that in detonation chemical lasers it is possible to use the processes shown in schemes I, III, and V on the sections corresponding to overcompression above the limit, i.e., from sections C downstream to the places where high-frequency detonation pulsations take place. It is possible to also use the overdriven processes with smooth fronts, obtained in [52].

The onset of detonation under overdriven conditions is identical with generation in lasers, and is characterized by amplification of a shock-wave and coherent emission of energy (e.g., IV in Fig. 7.13) – a phenomenon called "swacer" in [53].

7.4. Mechanisms of Inversion Formation in Detonation Chemical Lasers

Pumping of Active Medium by Chemical Bond Energy. To increase the coefficient of utilization of the pump energy, it is proposed in [4] to directly convert the explosion energy on account of dissociation (including photodissociation), shock dissociation, or some other chemical reaction, via premixing the laser working medium with the initial explosive. This method of producing a medium with a negative absorption coefficient is based on the fact that any explosive in its initial state can be regarded as a medium with inverted population, for which the state of the ignition products is the stable state. Inversion can be realized in detonation of an explosive by various modifications of reactions in the detonating explosive medium. We now consider some of these reactions.

a. Two-component mixture: explosive + working (radiating) substance.

For this case the energy is converted in the following manner. The explosive XY decomposes:

$$XY \rightarrow \sum_{j=1}^{m} (XY_j + \Delta E_j + h\nu_j), \tag{7.52}$$

where XY_j are the decay products of the initial substance; ΔE_j, kinetic energy of the reaction products; $h\nu_j$, energy of the quantum radiated upon decay of the initial substance XY into the components XY_j; and m, number of final products.

When the explosion occurs, the energy of the decay products is consumed in dissociation and radiation of the introduced working substance AB:

$$AB + \Delta E_j \rightarrow AB^*; \tag{7.53}$$

$$AB + h\nu_j \rightarrow AB^*. \tag{7.54}$$

In turn, AB* can emit a quantum as a result of the reactions

$$AB^* \rightarrow A + B^* \rightarrow A + (B + h\nu); \tag{7.55}$$

$$AB^* \rightarrow A + B + h\nu + \Delta E. \tag{7.56}$$

The reaction (7.55) corresponds to emission of the dissociation product (B*) of the excited molecule AB*, and the reaction (7.56) corresponds to the transition of the working medium from the excited state to the repulsive state.

In place of the diatomic working molecule AB it is possible to introduce into the working medium a monatomic substance A that produces in the excited state a metastable molecule with a dispersive lower state. The reaction scheme for this case is

$$\left.\begin{matrix} A + \Delta E_j \\ A + h\nu_j \end{matrix}\right\} A^*; \tag{7.57}$$

$$A + A^* \rightarrow A_2^*; \tag{7.58}$$

$$A_2^* \rightarrow A + A + \Delta E + h\nu. \tag{7.59}$$

Whereas in reactions (7.53)-(7.56) it is more profitable in energy to use substances with low dissociation potentials, such as metal salts, in reactions (7.57) and (7.58), the substance A can be a noble gas or a metal such as Zn, Cd, and Hg, capable of forming dissociative molecules .

b. Pure explosive. The most interesting method of energy conversion in one in which the initial substance XY, one of the explosion fragments XY_j, and an intermediate decay product XY_j are excited or deactivated in accord with the reactions (7.53)-(7.56) or (7.57)-(7.59).

Let us consider each reaction separately. The initial substance XY breaks up into

$$XY \rightarrow \sum_{j=1}^{m} (XY_j + \Delta E_j). \tag{7.60}$$

When the initial substance collides with the fragment XY_j, the molecule of this substance XY is excited:

$$XY + \Delta E_j \rightarrow XY^* \tag{7.61}$$

and emits a light quantum, while the molecule goes over into the repulsive state:

$$XY^* \rightarrow XY^1 + XY^2 + h\nu + \Delta E_1 + \Delta E_2. \tag{7.62}$$

When the repelling fragments interact with one another, they are transformed into the final products of the decay of the initial substance XY, i.e.,

$$XY^1 + XY^2 \rightarrow \sum_{j=1}^{m} (XY_j + \Delta E_j). \tag{7.63}$$

The products XY_j of the decay reaction, in turn, react with the initial substance XY, and a chain reaction continues until the entire supply of XY is exhausted, with the greater part of the energy stored in the substance converted into radiation energy in the reaction (7.61). The end products of this reaction have a low temperature, since the kinetic energy of the reaction products XY_j is converted into light in reaction (7.61).

Another mechanism of converting the chemical-bond energy into light is the decay of the initial explosive XY in accordance with the scheme (7.60). One of the explosion fragments, say XY_i, having a sufficiently low dissociation energy, emits a photon in accordance with the scheme of reactions (7.53)-(7.56), i.e.,

$$XY_i + \Delta E_j \rightarrow XY_i^* \rightarrow X_i + Y_i^*; \tag{7.64}$$

$$Y_i^* \rightarrow Y_i + h\nu_i; \tag{7.65}$$

$$X_i + Y_i \rightarrow XY_i. \tag{7.66}$$

Thus, the kinetic energy of the fission fragments is converted into optical radiation, and the final chemical composition of the mixture remains unchanged.

Definite interest can attach also to the following reaction mechanism, wherein the chemical-bond energy is converted into light, namely: the initial explosive splits up into several (in the case considered here, two) intermediate fragments:

$$XY \rightarrow XY^{(1)} + XY^{(2)}. \tag{7.67}$$

The fragments break up further into the end products of the decomposition reaction

$$XY^{(1)} \rightarrow \sum_{j=1}^{k} (XY_j + \Delta E_j); \tag{7.68}$$

$$XY^{(2)} \rightarrow \sum_{j=k+1}^{m} (XY_j + \Delta E_j). \tag{7.69}$$

The unstable intermediate decay products (complexes) can emit a light quantum via the following reaction schemes in the medium:

one of the complexes $XY^{(j)}$ is produced in an electron-excited state, and becomes deactivated via a radiative transition of the composition into the repulsive state:

$$XY^{(j)*} \rightarrow \sum_{j=1}^{k} (XY_j + \Delta E_j) + h\nu \tag{7.70}$$

or as a result of spontaneous emission with transition to the ground state

$$XY^{(j)*} \rightarrow XY^{(j)} + h\nu \tag{7.71}$$

with further decay in accordance with reactions (7.68), (7.69);

an intermediate complex is excited by collision with the end products of the reaction

$$XY^{(j)} + \Delta E_j \rightarrow XY^{(j)*} \tag{7.72}$$

and emits a quantum on going to the repulsive state

$$XY^{(j)*} \rightarrow \sum_{j=1}^{k} (XY_j + \Delta E_j) + h\nu \tag{7.73}$$

or on going into the ground state

$$XY^{(j)*} \rightarrow XY^{(j)} + h\nu \tag{7.74}$$

with further decay

$$XY^{(j)} \rightarrow \sum_{j=1}^{k} (XY_j + \Delta E_j). \tag{7.75}$$

The two cases considered do not cover all the possible reactions in which the chemical-bond energy is converted into radiation. Their characteristic feature is that they are non-equilibrium, and population inversion with generation of coherent radiation can take place in a medium in which these reactions occur.

Possibility of CO Molecule Lasing behind an Overdriven Detonation Front [54]. The detonation process, as already indicated in Sec. 7.1, is characterized by constant average parameters that are high within the confines of the detonation propagation. This makes it difficult to vary the temperature or the reaction-product density, e.g., when using mixtures whose component ratios are beyond the detonation concentration limits. So far, no methods have been found of using in chemical lasers the high-frequency processes in the detonation-wave structure described in Sec. 7.1. They are very difficult to calculate, and all that one obtains now is the assumption that the non-one-dimensionality of the detonation structure, the local inhomogeneities of the temperature and density fields, and the alternation of zones of non-reacting mixture with ignition products should all decrease the maximum possible radiation gain. These restrictions can be lifted by using overdriven detonation from a plane shock-wave followed by a combustion zone. The time of induction of the chemical reaction can in this case exceed by five times the time of establishment of thermodynamic equilibrium in the gas behind the shock-wave. Under these conditions, it is possible as shown by calculation [54], to construct detonation CO chemical lasers using the $CS_2 + O_2$ mixture.

The parameters behind the shock-wave front are first calculated without allowance for the chemical transformations. A computer is used to calculate by the Runge–Kutta method, from the chemical-kinetics equations, the concentrations of all the components. Each vibrational level (v) of the CO molecule, from the zeroth to the seventeenth, was regarded as a separate component. The thermodynamic quantities p, ρ, and T and the wave velocity were assumed constant at a heat release Q less than a certain given value Δq. After calculating the new values of the thermodynamic quantities and of the velocity, corresponding to the obtained concentrations, the rate constants of the chemical reactions were calculated at the new values of the temperature. The dependence of the specific heats on the temperature were taken into account by iteration.

The principal among the more than 40 elementary reactions known from the literature data for the considered mixture were selected with account taken of their role during the first 75 μsec from the instant of action of the shock-wave on the mixture. Reactions whose initiation during this time changed the component concentrations by less than 0.1% were disregarded. This time interval completely covers the lifetime of the inversion under the conditions assumed for the given problem with respect to: a) the mixture composition, $CS_2/O_2/Ar$ = 1/2.5/40; 1/1/30; 2.5/1/10; b) the temperature interval T = 1400-3400°K; c) the pressure p ~ 0.1 mPa; d) the chemical kinetics determined in the indicated time interval 75 μsec by the selected 16 basic equations of the reactions with the following rate constants of these reactions (k, $cm^3 \cdot mole^{-1} \cdot sec^{-1}$; E, $kJ \cdot mole^{-1}$; R, $kJ \cdot mole^{-1} \cdot deg\ K^{-1}$):

1. $CS_2 + CS_2 \rightleftarrows CS + S + CS_2$, $k_1 = 0.166 \cdot 10^{15} \times \exp(-183/RT)$; [55]
2. $CS_2 + Ar \rightleftarrows CS + S + Ar$, $k_2 = 0.364 \cdot 10^{16} \times \exp(-336/RT)$; [55]
3. $CS_2 + O \rightleftarrows CS + SO$, $k_3 = 0{,}12 \cdot 10^{14} \times \exp(-4.4/RT)$; [56]

$$
\begin{aligned}
&4.\ CS_2+O \rightleftarrows OCS+S, && k_4=0{,}1\cdot10^{15}\times\\
&&&\times\exp(-33{,}6/RT);\ [58]\\
&5.\ CS_2+S \rightleftarrows CS+S_2, && k_5=0{,}1\cdot10^{15}\times\\
&&&\times\exp(-16{,}7/RT);\ [58]\\
&6.\ O_2+SO \rightleftarrows SO_2+O, && k_6=0{,}35\cdot10^{12}\times\\
&&&\times\exp(-27{,}2/RT);\ [57]\\
&7.\ O_2+S \rightleftarrows SO+O, && k_7=0{,}1\cdot10^{14}\times\\
&&&\times\exp(-23{,}4/RT);\ [57]\\
&8.\ O+OCS \rightleftarrows CO+SO, && k_8=0{,}19\cdot10^{14}\times\\
&&&\times\exp(-18{,}9/RT);\ [58]\\
&9.\ O+S_2 \rightleftarrows SO+S, && k_9=0{,}4\cdot10^{13}\ \text{at}\ T=\\
&&&=1100\ \text{K};\ [57]\\
&10.\ O+OCS \rightleftarrows CO_2+S, && k_{10}=0{,}16\cdot10^{13}\ \text{at}\ T=\\
&&&=1270\,\text{K};\ [58]\\
&11.\ CS+O_2 \rightleftarrows OCS+O, && k_{11}=0{,}1\cdot10^{14}\times\\
&&&\times\exp(-50{,}3/RT);\ [58]\\
&12.\ S+OCS \rightleftarrows CO+S_2, && k_{12}=0{,}19\cdot10^{14}\times\\
&&&\times\exp(-18{,}9/RT);\ [58]\\
&13.\ SO+SO \rightleftarrows SO_2+S, && k_{13}=0{,}45\cdot10^{12}\times\\
&&&\times\exp(-15{,}9/RT);\ [57]\\
&14.\ OCS+Ar \rightleftarrows CO+S+Ar, && k_{14}=0{,}398\cdot10^{20}\,T^{-1{,}37}\times\\
&&&\times\exp(-299/RT);\ [55]\\
&15.\ O_2+CS \rightleftarrows CO^*(v)+SO, && k_{15}=0{,}55\cdot10^{11}\times\\
&&&\times\exp(-8{,}36/RT);\ [58]\\
&16.\ O+CS \rightleftarrows CO^*(v)+S, && k_{16}=0{,}24\cdot10^{15}\times\\
&&&\times\exp(-8{,}36/RT).\ [58]
\end{aligned}
\qquad (7.76)
$$

Equations (1)-(16) characterize a complicated chain reaction for which Fig. 7.14 shows the dependences, obtained in [54], of the reagent concentration c_i and of the temperature T on the time t of motion of the gas volume relative to the leading shock front of the overdriven detonation. The calculations were performed for the mixture $CS_2/O_2/Ar$ = 1/2.5/40 at an initial gas pressure 2 kPa and a shock-wave velocity 1500 m/sec. It can be seen that the temperature changes insignificantly in the reaction zone. The dashed curves show the change of the concentrations of O_2, CS_2, CS and CO, which were calculated by assuming that the CS_2 dissociation rate constants (k_1, k_2) are zero starting with 6 μsec. After this instant of time the reaction can be maintained by the chain branching processes, but the chain-initiation processes accelerate the combustion considerably. At lower dilutions or in the case of an undiluted working mixture, the temperature may rise during the reaction. Thus, Fig. 7.15 shows the calculated chemical kinetics of the reaction in the mixture CS_2/O_2 = 1/9 at an initial mixture pressure 2 kPa and at a shock-wave velocity 1700 m/sec. In this case the temperature changes from 1510 to 2800°K in the course of the reaction.

Reactions (15), (16) determine the populations of the vibrational levels of the CO molecules [59], as well as the V—V exchange processes with the molecules CO (v), O_2, OCS, CS_2, and the V—T exchange with the molecules CO, O, and Ar. The molecules O_2, OCS (v_3) and CS_2 (v_3) can go over from the ground to the first excited level by collision with CO (v). In this calculation no account was taken of the transfer of excitation from O_2, OCS (001) and CS_2 (001) to CO.

A numerical computer calculation of the system of equations for the chemical, relaxation, and gas-dynamic processes yielded the dependences of the populations of the vibrational levels of the CO molecules on the time behind the leading shock front of the overdriven detonation wave. The results of such a dependence for total inversion of the CO vibrational levels are shown in Fig. 7.16. The relaxation rate constants as functions of the vibrational number v were calculated in this case using the formulas from [60], while the gain of the radiation at the line centers for individual V—R transitions of the $\mathcal{P}$ and $\mathcal{R}$ branches was calculated at the instants of time corresponding to the maximum of the total inversion between each pair of vibrational levels. A Maxwell—Boltzmann population of the rotational level was assumed at a temperature equal to the translational one; it was also assumed that the line half-width corresponds to impact broadening and that the line width is independent of the quantum numbers

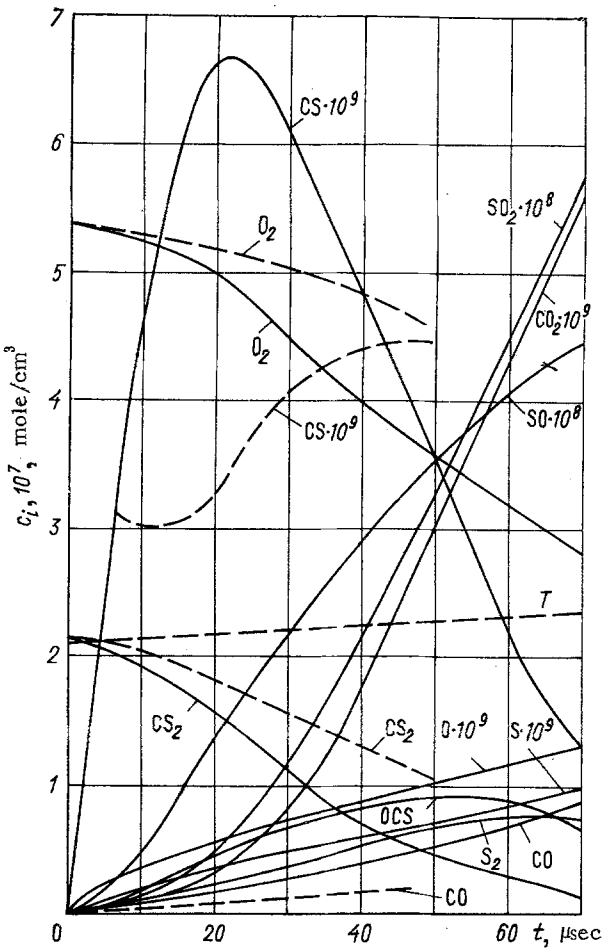

Fig. 7.14. Calculation of the change of the reagent concentration c_i and of the temperature T as a function of the time t in an overdriven-detonation wave.

and of the type of molecules that cause the broadening. The obtained maximum gains α_{max} on a given vibrational level v for the mixture CS_2/O_2 = 1/9 at T = 2495°K are listed in Table 7.1. The table also gives the populations of the vibrational levels n_v and n_v/n_{v-1}, corresponding to the rotational quantum number J and the wave number $\omega^{v,J}_{v-1,J+1}$ of the transition on which α_{max} is reached for the $\mathcal{P}$ and $\mathcal{R}$ branches.

Analysis of the calculated data shows that during the first 1.5 μsec the first inversion wave passes over all the vibrational levels from 13 through 1. This wave, as follows from Table 7.1, is characterized by low populations of the CO-molecule vibrational levels and by low gains (10^{-7}-10^{-5} cm^{-1}). The second inversion wave is due to the intense chemical reactions, and extends under the given conditions over only three vibrational levels (7, 8, 9). It is characterized by large values of the maximum gain (10^{-3}-10^{-2} cm^{-1}) and long inversion lifetimes. The calculated maximum gains α_{max}, the inversion lifetime τ_i, the inversion zone size Δx_i corresponding to this time, the values of the velocity D, the temperature in the inversion zone, and the maximum vibrational and rotational transition quantum numbers corresponding to α_{max} are listed in Table 7.2 for p_0 = 2 kPa.

From the results of such a numerical analysis of the possibilities of obtaining lasing on the CO molecule behind an overdriven detonation front in the $CS_2 + O_2$ mixture, the following conclusions were drawn in [54]:

a change of pressure causes an inversely proportional change of all the characteristic times of the chemical and relaxation processes, including τ_i;

the maximum radiation gain is not changed thereby so long as the impact approximation remains valid for the line-width calculation;

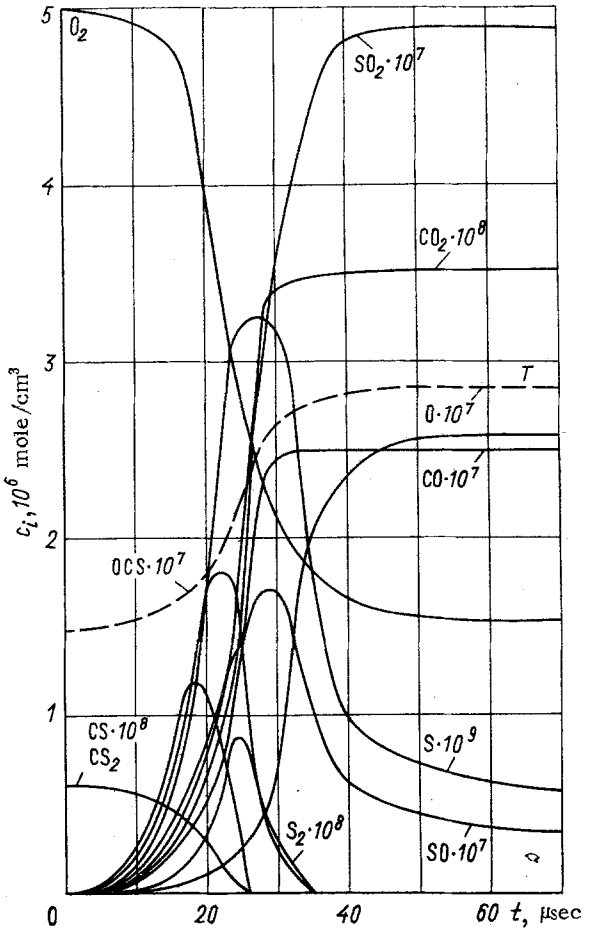

Fig. 7.15. Results of calculation of the chemical kinetics of the reaction behind the leading shock front of an overdriven detonation.

the inversion lifetime increases as the composition approaches stoichiometry, and raising the temperature from 1800 to 2495°K for the same composition (regimes 2, 4) increases both the gain and the inversion lifetime;

the calculations performed for an idealized one-dimensional model yield relatively high values of the gain.

Population Inversion in Adiabatic Cooling of Detonation Products. The chemical energy of the detonation of the initial combustion mixture can serve also simply as a source of thermal energy to heat the mixture of the produced products with the added gases before they are cooled in the course of the subsequent adiabatic expansion. Detonation lasers in which such processes are used are quite similar to shock-wave and chemical—gas-dynamic lasers described in Chap. 6, and to the gas-dynamic shock-tube lasers [61]. What distinguishes them, however, is that in detonation lasers the thermal pumping takes place in a regime with more intense energy released in the detonation wave than in ordinary combustion, and the components required for the formation of the active medium, as well as the density ratios of these components needed for lasing, are produced directly in the course of the chemical reaction in the detonation wave. In all other respects production of population inversion in such lasers is similar to the method of obtaining negative temperatures by cooling a medium, first described in [62] and later in [63, 64]. This method can help consider, e.g., a three-level system with different relaxation times between subsystems — levels 1, 2, 3 placed successively one above the other. If the time of relaxation between the subsystems is substantially longer than the time of relaxation within each subsystem, and radiative transitions are possible between them, equilibrium is established quite rapidly within each subsystem if the thermodynamic state changes rapidly enough, but there will be no equilibrium between the subsystems. A state is then possible with negative temperature with respect to transitions from the energy levels of one system to levels of another.

This method of obtaining inverted population by abruptly changing the temperature in the medium was used in [65] to demonstrate the possible existence, within a certain state, of

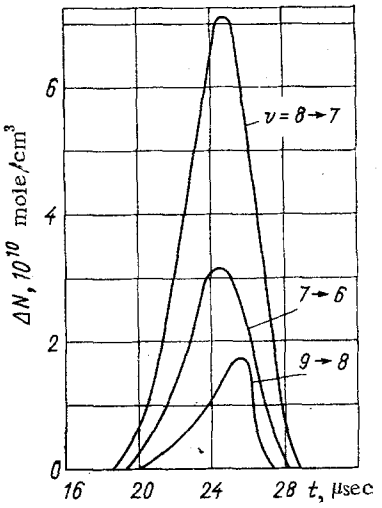

Fig. 7.16. Calculated dependences of the CO-molecule vibrational levels behind the leading shock front of an overdriven detonation.

inverted population with respect to the vibrational levels upon adiabatic expansion of mixtures whose molecules have substantially different vibrational relaxation times and can exchange vibrational-excitation energy. Such an exchange is effective if the energies of the vibrational levels are close to one another, or if the energy deficit

$$|\Delta E| \ll kT. \tag{7.77}$$

Mixtures satisfying the condition (7.77) for resonant exchange of vibrational excitation were taken in [65] to be N_2/CO_2 and N_2/NO_2. In these mixtures the process takes place without chemical transformations and is typical only for purely gas-dynamic lasers. In detonation chemical lasers with adiabatic expansion, however, the mixtures N_2/CO_2 and N_2/NO_2 can serve either as added gases, or be components of the detonation products produced in the course of the reaction. It is therefore of interest here to describe the analysis of [65].

The probability of energy transfer in the N_2/CO_2 mixture in one collision of the molecule at room temperature is $\beta \sim 10^{-5}$ [66]. The exchange process is considered under the assumption that there is an excess concentration of the molecules, which carry the vibrational excitation, over the concentration of the working molecules, whose levels are subject to inversion, $n_{N_2^*} \gg n_{CO_2}$, i.e., the concentration $n_{N_2^*}$ is assumed to be constant in time. On the other hand, the time variation of the number of molecules of the working gas CO_2 on the three vibrational levels (Fig. 7.17) among which the 00°1 level can exchange with the v = 1 level of the N_2^* molecule can be written in the form

$$\left.\begin{aligned} dn_3/dt &= -P_{ab}' n_3 + P_{ba} n_1 - P_{31} n_3 + P_{13} n - P_{32} n_3 + P_{23} n_2; \\ dn_2/dt &= P_{32} n_3 + P_{12} n_1 - P_{23} n_2 - P_{21} n_2. \end{aligned}\right\} \tag{7.78}$$

Here $n_1 + n_2 + n_3 = n$ is the concentration of the working molecules; P_{ba}, P_{ab}, proper probabilities of the direct and reverse transfer of excitation between the working molecule CO_2 and the energy-transfer molecule N_2^*; and P_{31}, P_{13}, P_{32}, etc., probabilities of thermal relaxation of the working molecule among the corresponding vibrational levels.

Let the rate of adiabatic expansion of the gas mixture be such that the time of its cooling from the initial temperature T_1 to the final T_2 is substantially shorter than the time of the proper vibrational relaxation of the energy-transfer gas. After the end of the gas-mixture expansion a stationary distribution over the vibrational levels of the working molecules is established. Consequently, equating to zero the right-hand sides of Eqs. (7.78) and designating the relaxation probabilities per collision by β_{21}, β_{32}, β_{31}, we can determine the population inversion between levels 3 and 2:

$$\frac{n_3 - n_2}{n_1} = \frac{\beta(\beta_{21} - \beta_{32})}{\beta_{21}(\beta + \beta_{32} + \beta_{31})} \exp\left(-\frac{E_b - E_a}{kT_1}\right). \tag{7.79}$$

TABLE 7.1. Calculated Population Kinetics and Gains [54]

Time from start of reaction, μsec	v	n_v, cm^{-3}	$\frac{n_v}{n_{v-1}}$	$J_{\mathcal{P}}$	$\omega^{v, J_{\mathcal{P}}}_{v-1, J_{\mathcal{P}}+1}$, cm^{-1}	$\alpha_{\mathcal{P}\max}$, cm^{-1}	$J_{\mathcal{R}}$	$\omega^{v, J_{\mathcal{R}}}_{v-1, J_{\mathcal{R}}-1}$, cm^{-1}	$\alpha_{\mathcal{R}\max}$, cm^{-1}
0,04	13	$0,42\cdot10^{-7}$	1,004	32	1699,31	$1,7\cdot10^{-7}$	—	—	—
0,08	12	$0,19\cdot10^{-6}$	1,044	28	1741,71	$1,2\cdot10^{-6}$	8	1882,08	$1,4\cdot10^{-7}$
0,11	12	$0,37\cdot10^{-6}$	1,062	27	1770,91	$2,5\cdot10^{-6}$	12	1920,64	$5,4\cdot10^{-7}$
0,15	10	$0,73\cdot10^{-6}$	1,075	26	1800,22	$4,9\cdot10^{-6}$	14	1953,02	$1,4\cdot10^{-6}$
0,22	9	$0,17\cdot10^{-5}$	1,092	25	1829,64	$1,2\cdot10^{-5}$	15	1982,47	$4,2\cdot10^{-6}$
0,31	8	$0,36\cdot10^{-5}$	1,109	25	1854,74	$2,5\cdot10^{-5}$	17	2015,01	$1,1\cdot10^{-5}$
0,38	7	$0,54\cdot10^{-5}$	1,127	24	1884,36	$3,7\cdot10^{-5}$	17	2041,68	$1,8\cdot10^{-5}$
0,43	6	$0,67\cdot10^{-5}$	1,147	24	1909,63	$4,4\cdot10^{-5}$	18	2071,44	$2,3\cdot10^{-5}$
0,48	5	$0,81\cdot10^{-5}$	1,169	23	1939,47	$4,9\cdot10^{-5}$	19	2101,30	$2,8\cdot10^{-5}$
0,57	4	$0,17\cdot10^{-4}$	1,176	23	1964,92	$6,1\cdot10^{-5}$	19	2128,25	$3,6\cdot10^{-5}$
0,67	3	$0,18\cdot10^{-4}$	1,203	23	1990,43	$7,5\cdot10^{-5}$	19	2165,26	$4,8\cdot10^{-5}$
0,81	2	$0,30\cdot10^{-4}$	1,258	22	2020,58	$1,0\cdot10^{-4}$	20	2185,43	$7,2\cdot10^{-5}$
5,49	7	$0,22\cdot10^{-3}$	1,220	23	1888,80	$2,2\cdot10^{-3}$	20	2050,51	$1,5\cdot10^{-3}$
5,74	8	$0,31\cdot10^{-3}$	1,417	22	1867,93	$5,0\cdot10^{-3}$	21	2026,57	$4,1\cdot10^{-3}$
6,14	9	$0,32\cdot10^{-3}$	1,087	26	1825,21	$2,1\cdot10^{-2}$	15	1982,47	$7,2\cdot10^{-3}$

TABLE 7.2. Calculated Characteristics of the Inversion Zone for Different Detonation Regimes [54]

Regime No.	Mixture composition CS_2/O_2	D, m/sec	T, K	$v\to \to v-1$	$J\to \to J-1$	$\alpha_{\max}$, cm^{-1}	τ_i, μsec	Δx_i, cm
1	0,05/0,95	1700	1700	8—7	20—21	$6,1\cdot10^{-3}$	3,7	0,9
2	0,10/0,90	1700	1800	8—7	19—21	$9,2\cdot10^{-3}$	4,2	1,0
3	0,20/0,80	2000	2495	8—7	22—23	$3,8\cdot10^{-3}$	6,9	1,7
4	0,10/0,90	—	2495	8—7	22—23	$5,0\cdot10^{-3}$	3,5	—

In the derivation of (7.79) we neglected the thermal perturbation of the molecule, i.e., the probabilities P_{13}, P_{23}, P_{12}, but took into account the deactivating collisions and the condition (7.77) for the temperature T_2. It follows from (7.79) that the inversion is zero at $\beta_{32} > \beta_{21}$ and a maximum at $\beta_{21} >> \beta_{32}$ and that the probability β of transferring the vibrational excitation is much larger than the probability of deactivating the level 3 of the working molecule. In this case the inversion is equal to the relative concentration of the excited molecules of the carrier gas with initial temperature T_2.

In [65] a concrete numerical example is given of obtaining an inverted population using a supersonic nozzle with continuous adiabatic expansion of the gas mixture. Thus, under conditions of population inversion between the levels (00°1) and (10°0) of the CO_2 molecule at $T_1 = 1000$ and $T_2 = 300$°K it follows that $(n_3 - n_2)/n_1 \sim 1$-3.5%.

Following [62-65], many investigations were published devoted to the process of rapid expansion of a preheated mixture of molecular gases as they escape through a nozzle or a slit, thus producing conditions for inversion of the population of the vibrational states of molecules (e.g., [67-74]).

Such an effect can also be obtained in a strongly exothermic chemical reaction in a detonation with free expansion of the reaction products [6] without using gas-dynamic devices such as a nozzle or a slit.

As already mentioned, the composition of the detonation products should correspond in this case to a relaxation scheme analogous to that used in gas-dynamic lasers of the type

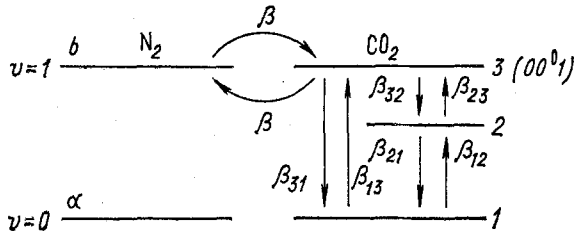

Fig. 7.17. Time variation of the number of CO_2 molecules on three vibrational levels.

described, e.g., in [67, 75, 76]. Such a composition of detonation products is possessed by many gaseous and condensed explosives [77, 78]. The rate of expansion of detonation products heated, depending on the type of explosive, to $(2-5)\cdot10^3$ °K is comparable with or larger than the stream velocity in gas-dynamic lasers, and reaches 10^5-10^6 cm/sec. For an acetylene–air mixture, the process is described in this case by the exothermic chemical reaction [79]

$$0.081C_2H_2 + 0.202\,(O_2 + 3.76N_2) = 0{,}162CO_2 + 0.081H_2O + 0.757N_2 + 108.9\ \text{kJ/mole}. \qquad (7.80)$$

This process was analyzed in [6]. Thus, it is known from [79] that at a pressure higher than 0.05 MPa a detonation is excited in an initial mixture with a volume concentration 8-14% C_2H_2 by a spark in tubes of $d \geqslant 18$ mm diameter. The detonation velocity is then $1.8\cdot10^3$ m/sec. Under the conditions of reaction (7.80), the temperature of the reaction products is 2000-2400°K. The walls of the detonation tube are assumed to be rapidly destroyed by the pressure in the detonation wave. The reaction products are then adiabatically expanded and cooled, the calculated expansion velocity amounting to about $0.9\cdot10^5$ cm/sec. Expansion in vacuum changes the parameters of the state of the reaction products, resulting in population inversion of the 2 (00°1) and 1 (10°0) states of the CO_2 molecule.

The relaxation of the excited CO_2 molecules is subject here to the kinetic equation

$$\frac{dn_\alpha}{dt} = P_{N^*-C}N^*n_0\delta_{2\alpha} - [n_\alpha/\tau_\alpha(t)], \qquad (7.81)$$

where $\alpha = 1.2$; $\delta_{2\alpha}$ is the Kronecker delta; N^*, n_0, n_α, concentrations of the excited N_2 and CO_2 molecules in the ground and α states; P_{N^*-C}, probability of excitation transfer from the N_2 to the CO_2; $\tau_\alpha(t)$, time of collisional relaxation.

The time dependences of the gas temperature and of the molecule concentration were calculated [6] for a cylindrical expansion geometry (Fig. 7.18). Also determined [80] was $\tau_\alpha(t)$ with allowance for the temperature dependence of the collisional relaxation of the CO_2 molecule. The initial conditions were chosen here from the following considerations. Below 1000°K the relaxation of the excited CO_2 molecules depends on the collisions with the H_2O molecules and is most probable for the lower level. Owing to the relatively high water concentration in the reaction products, the relaxation times are short and at initial-mixture pressures above 0.1 MPa the relaxation is faster than the cooling of the gas. On the other hand, at initial-medium pressures lower than 0.05 MPa, as already mentioned, it is difficult to excite a detonation in the acetylene–air mixture. The conditions chosen were therefore: pressure 0.05-0.1 MPa and tube diameter $d \approx 2$ cm.

Integration of the kinetic equation (7.81) makes it possible to obtain the time dependence of the population of the excited states. It is possible here to disregard the energy transfer from N_2 to CO_2, and approximate $\tau_\alpha(t)$ by exponentials. It is found that the relaxation of level 1 is faster than its depletion because of the cooling of the gas, i.e., its population is determined by the Boltzmann factor. The relaxation of level 2, however, starting with a certain instant, is slower, and the vibrational temperature deviates from the temperature of the random motion in the gas. It can be seen from the calculation results in Fig. 7.18 that the vibrational temperature of level 2 begins to differ at $t = 200$ μsec, and population inversion sets in at 650 μsec after the start of the expansion. The time dependence of the density of the population of the excited level of the nitrogen N^* is determined mainly by the relaxation in collisions with the CO_2 molecules. It is indicated in [6] that allowance for the energy transfer from the nitrogen to the CO_2 should lead to an increase of the inversion and to a decrease of the time prior to its onset, and should furthermore take place at high pressures in the initial mixture. An increase of the inversion is also possible when an explosive mixture with a lower water concentration in the explosion products is used.

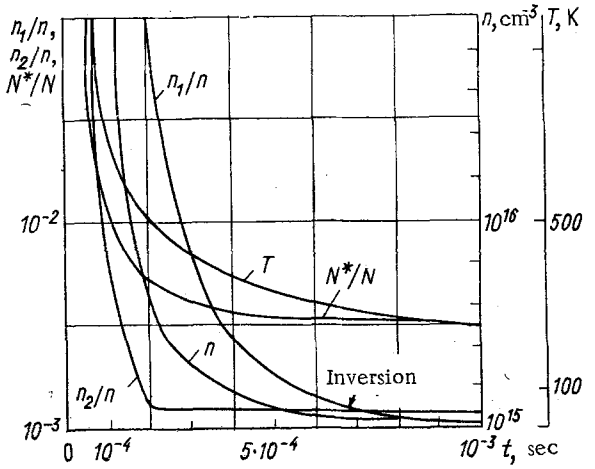

Fig. 7.18. Time dependences of the gas temperature and of the molecule concentration in cylindrical expansion of the detonation products of an acetylene–air mixture; T) temperature of detonation products; n) concentration of the CO_2 molecules; n_1/n, n_2/n, and N^*/N) relative populations of the excited states of the CO_2 and nitrogen molecules, respectively.

7.5. Experimental Realization of Lasing in Detonation Chemical Lasers

Lasing in an Overdriven Detonation Wave. Realization of lasing in detonation, just as in a thermal explosion, remains a complicated problem. The pertinent experimental data include the use of overdriven detonation for direct lasing and the use of normal Chapman–Jouguet and of explosion detonation for thermal pumping of the active medium.

Stimulated emission was first obtained directly from a detonation wave in the gas mixture $F_2O/H_2/Ar$ = 1/1/20. Before that, lasing of vibrationally excited HF was obtained by a chain reaction initiated by pulsed photolysis [82]:

$$\left.\begin{aligned} &F + H_2 = HF + H \quad (-134\ \text{kJ/mole});\\ &OF + H_2 = HOF + H;\\ &H + F_2O = HF + OF;\\ &H + HOF = HF + OH;\\ &H + OF = FH + O \ \text{or} \ OH + F. \end{aligned}\right\} \qquad (7.82)$$

For better stabilization of the zone of the reaction (7.82) in a detonation wave, the process was excited at a wave propagation velocity exceeding the Chapman–Jouguet velocity, i.e., in the overdriven detonation regime. In this case, notwithstanding the strong dilution of the mixture with argon and the relatively low initial pressure (about 0.66 kPa), the wave velocity was 1.8-2 km/sec at a temperature higher than 2000°K behind the wave front. The authors of [5, 81] assume that under these conditions the reaction zone is obviously quite narrow, so that the diffraction losses in the cavity are low, i.e., such a chemical laser operates near critical temperature and pressure.

In [5, 81] the authors used a detonation tube of the type shown in Fig. 7.19a with 16.7 cm diameter, with a nearly confocal cavity mounted flush against the tube walls. The coherent radiation leaving the cavity was recorded with a photoelectric InSb detector using a narrow-band filter for spectral resolution. A typical record of the radiation is illustrated by the two-trace oscillogram of Fig. 7.19b. Here the upper curve is the radiation of the gas heated by the detonation wave, observed through a CaF_2 window placed upstream relative to the cavity. The lower trace is a record of the radiation from the optical cavity using an InSb photoelectric detector with aperture 1.5 mm. Comparison of these curves shows that the amplitude of the curve characterizing the coherent radiation is 10^5 times larger. This is convincing proof of the reliability of the observation of emission of coherent radiation.

A theoretical analysis of the processes in the detonation chemical laser described above was briefly reported in [83] as a numerical calculation for the most realistic chemical model

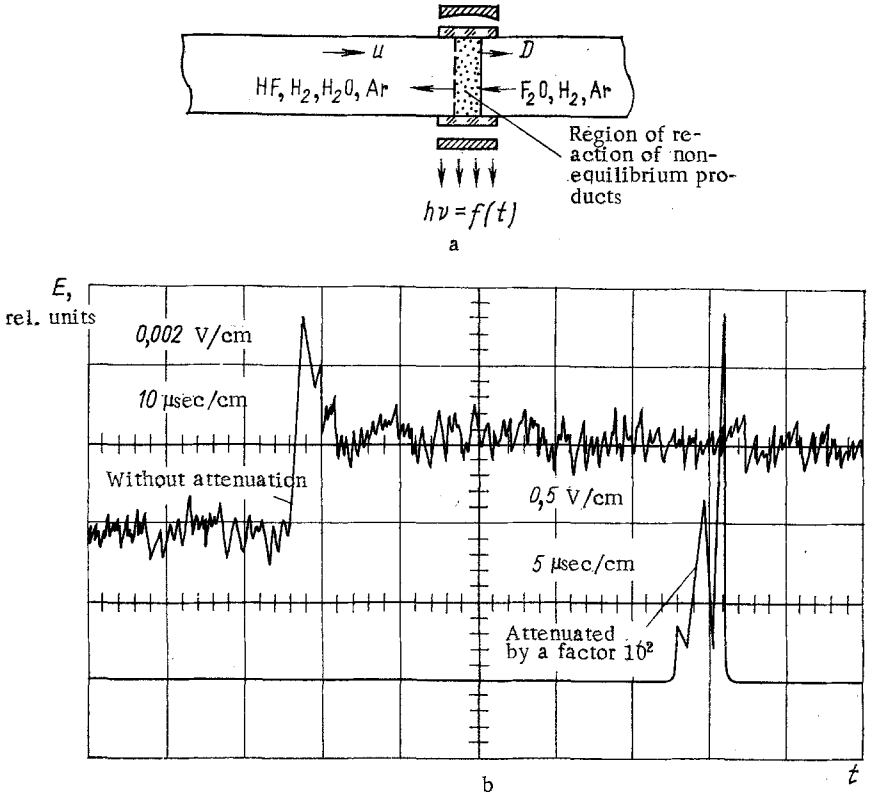

Fig. 7.19. Diagram of detonation chemical laser (a) and record of its emission (b).

of the reaction. A number of chemical reactions were excluded, and the difficulty in allowing for the processes in the cavity was circumvented by considering the nonequilibrium radiation only for "zero" gain, i.e., for the process characterized by the upper curve of Fig. 7.19b. It is stated that the data used in the calculation were the results of experiments with $F_2O/H_2/Ar$ mixtures with respective concentrations from 1/1/10 to 1/1/200, and with heating in the wave from 2200 to 3500°K. The calculations have shown that in the course of the chemical reaction the concentrations of HOF, F_2O, and OF decrease rapidly to negligible values, so that reactions that include these components can be neglected. Thus, only the first reaction of (7.82) remains, giving excited HF. In addition, it was found for this reaction that the deactivation is controlled by V—V energy transfer processes, and that the V—T processes are of no importance.

Use of Detonation and Explosion to Produce and Pump Active Laser Media. The choice of the initial composition of the mixture for detonation lasers operating on the principle of adibatic expansion of the detonation products through a nozzle is governed by the relaxation scheme described in Sec. 7.4. This leads to a variety of employed reagents and of structural features of the detonation lasers based on these reagents.

Here we describe the constructions and operating principles of the most typical of these lasers.

One of the first experimental lasers in which detonation was used to obtain a high-temperature gas mixture at the entrance into the nozzle or slit was a detonation laser using the exothermic explosive decomposition of hydrazoic-acid molecules in a mixture with carbon dioxide and xenon [7]. The mechanism of this reaction is determined mainly by the following processes [84]:

$$\left.\begin{aligned} &HN_3^* \to NH + N_2 \quad (-41{,}9 \text{ kJ/mole});\\ &NH + HN_3 \to H_2 + N_2 + N_2^* (+635 \text{ kJ/mole});\\ &N_2^* + \varkappa HN_3 \to \varkappa HN_3^* + N_2;\\ &N_2^* + M \to N_2 + M^*;\\ &M + HN_3^* \to HN_3 + M^*. \end{aligned}\right\} \qquad (7.83)$$

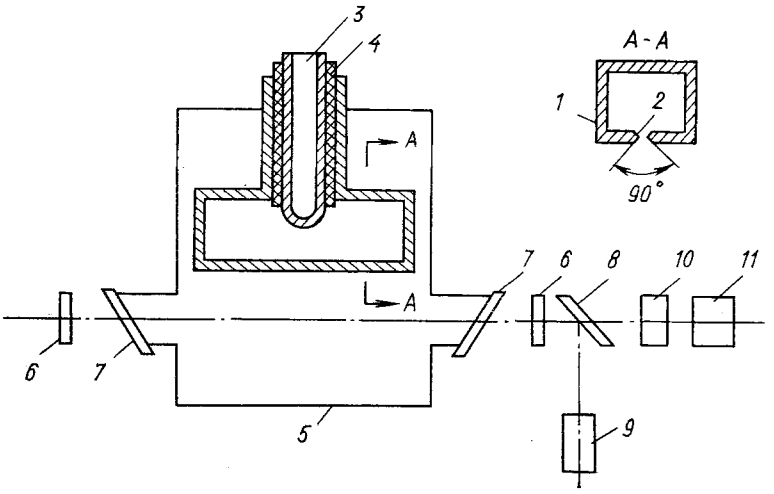

Fig. 7.20. Hydrazoic-acid detonation laser: 1) 0.3-liter high-pressure chamber; 2) 200 × 0.4 mm slit; 3) metal rod with hollow; 4) thermal insulation; 5) 0.012 m^3 ballast volume; 6) gold-coated mirrors of 25 mm diameter, one with an output aperture of 2.5 mm diameter; 7) NaCl Brewster windows; 8) plane-parallel germanium plate; 9) calorimeter; 10) photoreceiver; 11) oscilloscope.

If carbon dioxide is used as the diluent M, the excited nitrogen gives up its energy to the CO_2 molecule on account of quasiresonance between the vibrational levels of the nitrogen and the vibrational (00°1) mode of the carbon dioxide. The production of population inversion in the course of such a chemical reaction was analyzed in detail in [85] and was investigated in [86].

The structure of an experimental detonation laser using hydrazoic acid [7] is shown in Fig. 7.20.

The gas mixture is admitted into volume 5 and is then frozen on the outside of the hollow metallic rod 3 filled with liquid nitrogen. The detonation was initiated with an electric spark. The pressure and temperature in the high-pressure chamber, after expansion of the detonation products, were approximately 1-2 MPa and 2000-3000°K, depending on the amount and composition of the mixture. The time of outflow of the detonation products and of the diluents through the slit was estimated as the ratio of the volume of the high-pressure chamber to the product of the slit area by the speed of sound at the critical section, and amounted to about 1 msec. The distance from the slit to the cavity axis was regulated in the experiment. The optimal distance was about 3 cm. The duration of the lasing pulse at optimal mixture composition was close to the time of escape of the gas through the slit.

Figure 7.21 shows the experimentally obtained dependences of the output energy: a) on the CO_2 in the HN_3/CO_2 mixture at a given amount of HN_3 (0.5 g); b) on the Xe content in the $HN_3/CO_2/Xe$ mixture for the same amount of HN_3 and CO_2 (0.33 g). The maximum energy (~1 J) was obtained at a component ratio corresponding to an initial detonation product temperature of about 2500°K, much higher than the temperatures that are optimal for $N_2/CO_2/He$ mixtures according to [69]. The reason is believed in [7] to be the difference between the parameters of the experimental setups, as well as the dependence of the mixture temperature on the change of the composition of this mixture.

A thermodynamic calculation and an analysis of the detonation products have shown that practically all the hydrogen (~90%) is oxidized to form water and reduces part of the carbon dioxide to carbon monoxide. The water content in the mixture reached 15-20%. The addition, to the investigated mixtures, of chlorine in amounts close to stoichiometric for the reaction with hydrogen lead to a strong (approximately threefold) increase of the generated energy. The water content in the products decreased to 2-4%.

The H_2O molecules deactivate the symmetric and deformational vibrational modes of the CO_2 molecule, so that small amounts of water in the detonation products improve the radiative characteristics of the active medium. In the main, however, the fuels used in explosive lasers

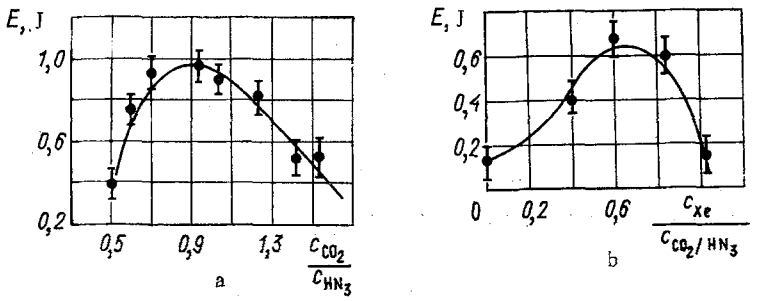

Fig. 7.21. Energy characteristics of HN_3 laser as functions of the contents of CO_2 (a) and Xe (b) in the mixture.

are hydrocarbons, and their reaction products contain enough water to also deactivate the antisymmetric vibrational mode of CO_2 as well as the vibrationally excited N_2 molecules, i.e., to cause loss of vibrational energy. To lower this loss, additives that interact with hydrogen are introduced and form compounds that cause less loss of vibrational energy from the antisymmetric CO_2 mode and from the vibrational N_2 mode than the water molecules.

The effect of chlorine additives on the gain of a hydrocarbon-fuel (methane—oxygen mixtures) explosive laser has been investigated and reported in [87]. It is noted there that under the experimental conditions of [7] the almost threefold increase in the lasing power cannot quite be unambiguously attributed to the lower water content. In fact, when the chlorine was bound to the hydrogen, the CO_2 content was higher than in the preceding experiment. It is also possible that the conditions (sufficiently high water-vapor content) were close to the lasing threshold, in which case even a small increase of the gain due to the increase of the CO_2 concentration could substantially increase the lasing power.

The influence of additives was investigated in [87] with an explosion laser consisting of an explosion chamber (500 cm^3), a wedge-shaped nozzle (throat height 1 mm, half-angle 15°), and a receiver. The gas stream was 400 mm wide. At a degree of expansion 18, the nozzle wedge-shaped profile became plane-parallel. The gain (absorption coefficient) of the medium was measured with an electric-discharge CO_2 laser at a distance of 80 mm from the nozzle throat. The mixture partial pressures were 30.6, 61.3, and 288 kPa for CH_4, O_2, and N_2, respectively. Chlorine was added in amounts of 25, 50, 75, and 100% of stoichiometric relative to hydrogen, and the gains obtained were compared with those without the chlorine. The results of the thermodynamic calculation of the composition of the explosion products as a function of the chlorine content are shown in Fig. 7.22. The experimental dependence of the maximum gain on the chlorine content in the initial mixture is shown in Fig. 7.23. The pressure in the nozzle prechamber, corresponding to the maximum gain, increases with increasing chlorine content of the initial mixture and ranges from 0.15 MPa in mixtures without Cl_2 to 0.25 MPa when the Cl_2 additive is stoichiometric relative to the hydrogen. At equal prechamber pressures, however, the gain increases monotonically with increasing Cl_2 content in the initial mixture, up to an amount stoichiometric relative to hydrogen. It was concluded in [87] that addition of chlorine to a hydrocarbon fuel decreases the loss of vibrational energy from the upper energy level of a laser based on the explosion products of these fuels, and consequently improves the energy properties of these lasers.

Another detonation laser using hydrocarbon fuel was proposed in [88]. The experiments aimed at obtaining lasing on the gas-detonation products were performed for the following explosive reactions:

$$\left.\begin{aligned} &1)\ C_2H_2 + 2{,}5\,O_2 + \varkappa N_2 \rightarrow 2\,CO_2 + H_2O + \varkappa N_2 + Q_\varkappa;\\ &2)\ CO + N_2O + \varphi\,He \rightarrow CO_2 + N_2 + \varphi\,He + Q_\varphi, \end{aligned}\right\} \qquad (7.84)$$

where $Q_{\varkappa,\,\varphi}$ is the energy released, and $\varkappa$ and φ are the fraction of the nitrogen and helium impurities, respectively. The properties of the initial gas mixtures are listed in Table 7.3.

The relative concentrations of the initial components were chosen to satisfy contradictory requirements with respect to the compositions of the final mixtures and to the detonation properties of the initial mixtures. In reaction 2) of Eqs. (7.84) the catalyst is the trace of hydrogen. The experiments were performed with a detonation laser illustrated schematically in Fig. 7.24.

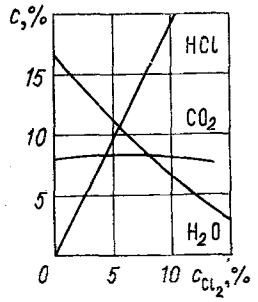

Fig. 7.22

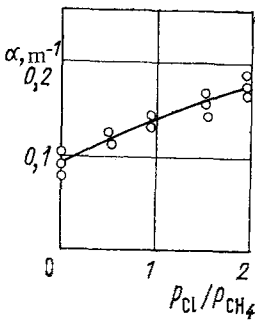

Fig. 7.23

Fig. 7.22. Thermodynamic calculation of the concentrations of CO_2, H_2O, and HCl in the explosion products of $CH_4/O_2/N_2/Cl_2$ mixtures vs the chlorine content in the initial mixture.

Fig. 7.23. Maximum gain in the explosion products of the $CH_4/O_2/N_2/Cl_2$ mixture vs the ratio of the chlorine and methane pressures (p_{CH_4} = 30 kPa).

TABLE 7.3. Properties of Explosive Mixtures [88]

Partial composition of mixture	Q, J/g	Detonation velocity D, m/sec
$C_2H_2/O_2/N_2$ 16,7/41,6/41,7	5650	2150
12,6/31,4/56,5	4030	1920∓20
$CO/N_2O/He/H_2$ 35/35/28/2	6340	2240∓20

The explosive gas mixture is ignited at atmospheric pressure in tube 2 by a spark, igniter, or an electrically exploding wire 15. The resultant self-accelerating burning changes into detonation whose direction is shown in Fig. 7.24 by arrows. Double entry of the detonation wave into the detonation chamber 1 is used to ensure a more simultaneous rupture of Lavsan* film 14 glued on a slit 3 of length 40 cm. When the film is broken, the gas mixture of given composition, heated behind the detonation-wave front, flows through the slit into vacuum chamber 6 and is cooled by rapid expansion. The populations of the V–R levels 00°1 and 10°0 of the CO_2 molecules are inverted in the gas stream. The active-medium jet shown dashed in Fig. 7.24 passes transversely through an optical cavity 1.5 m long, consisting of two copper or gold-coated mirrors — plane 11 and spherical 4 with curvature radius 5 m. The distance from the cavity axis to the slit is 4 cm. The radiation is extracted to a Ge–Au photoresistor 9 through a round opening in the flat mirror 11. An InSb filter 12 placed ahead of the photoresistor 9 cuts off wavelengths shorter than 8 μm.

Lasing was obtained with all three mixtures listed in the table when the detonation product escaped through a slit 1 mm wide. For the $CO/N_2O/He$ mixture, lasing was also obtained when the product escaped through a slit up to 4 mm wide.

It was pointed out in [88] that each lasing pulse has its own more detailed structure, governed apparently by the complicated gas-dynamic process of nonstationary outflow of the detonation products.

It can be seen from the considered designs of lasers that use detonation to produce and pump the active media that one decisive property of the general design of a detonation laser is the *method of containing* the initial substance in the reaction volume and providing a seal between this volume and the vacuum chamber of the cavity during the time prior to the start of the outflow of the detonation or explosion products.

In [7] this problem was solved by a phase transformation of the working medium into an initial condensed state. In [88] this was done by separating the explosion chamber from the evacuated region by a diaphragm in the form of a Lavsan polyester film that is broken by the detonation wave.

*Soviet equivalent of Dacron — Publisher.

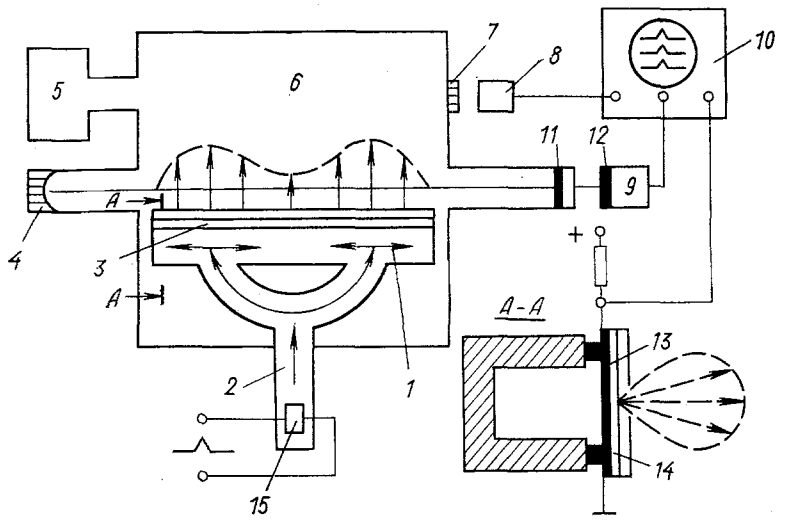

Fig. 7.24. Diagram of detonation laser with destructible diaphragm: 1) explosion chamber, 2) tube with explosive gas mixture; 3) slit; 4) opaque mirror; 5) vacuum pump; 6) vacuum chamber; 7) NaCl window; 8, 9) Ge–Au photodevices; 10) oscilloscope; 11) output mirror; 12) InSb filter; 13) contact pickup; 14) Lavsan polyester film; 15) ignition.

Properties of this kind also determine, in the main, the constructions of other detonation lasers. Thus, in [89, 90] was investigated the operation of a laser (Fig. 7.25) in which a high-pressure hermetic valve 4 is opened by an electric release 3 when an explosion induced by a spark igniter 1 in a mixture $CO/O_2/H_2/N_2$ contained in chamber 2 is terminated. This ensures rapid expansion of the heated explosion products in the two-dimensional slit nozzle 5 and population inversion and lasing in the region of the optical cavity 6, followed by escape of these products into the vacuum chamber 7.

The most typical conditions in such experiments were: explosion-product composition $CO_2/N_2/H_2O$ = 15/83.5/1.5; stagnation temperature and pressure 1500°K and 1 MPa, respectively. The temperature and pressure in the cavity region were, respectively, 300°K and about 13 kPa, and the Mach number was M = 4.5. The approximate repetition period was 3 min.

The changes of the pressure in the explosion chamber 2 and of the lasing power in the cavity 6 are illustrated by the synchronized oscillograms in Fig. 7.26. It can be seen that lasing begins at the instant when the valve is opened (upper trace), whereas the pressure p in the explosion chamber decreases relatively slowly (lower trace) as the explosion products flow out and are cooled.

The measured [89] dependences of the energy output on the CO_2 concentration (Fig. 7.27) are of interest. Three types of nozzle inserts were used in the experiments and are shown in Fig. 7.28: wedge-shaped nozzle (a), contoured nozzle (b), and block of axisymmetric nozzles (c). It was found that the energy output is approximately 2.5 times larger for the contoured nozzle than for the wedge-shaped one (Fig. 7.29). The dark points in the last figure correspond to lasing with gas expansion in the wedge-shaped nozzle, and the light circles, to expansion in the contoured nozzle. The stagnation temperature was 1400°K. This output-energy difference is due in part to the decrease of the relaxation rates of the molecules in the more intense expansion of the stream in the contoured nozzle.

The output energy is a function of the optical-cavity mirror transmissivity. Such an experimental dependence for the contoured nozzle insert is shown in Fig. 7.30 for stagnation pressure and temperature 0.54 MPa and 1100°K, respectively. The gain determined from these data was approximately 0.7 m^{-1}, as against ~0.4 m^{-1} for the wedge-shaped nozzle insert, although the stagnation temperature was substantially higher, 1400°K. This shows that the conditions for quenching the upper energy level population are better for contoured nozzles. The maximum energy obtained in the described detonation laser is 110 J when a contoured nozzle is used. This amounts to 0.06% of the thermal energy contained in the initial gas. From experiments with a block of axisymmetric nozzles it was found that shock-waves and turbulent wakes

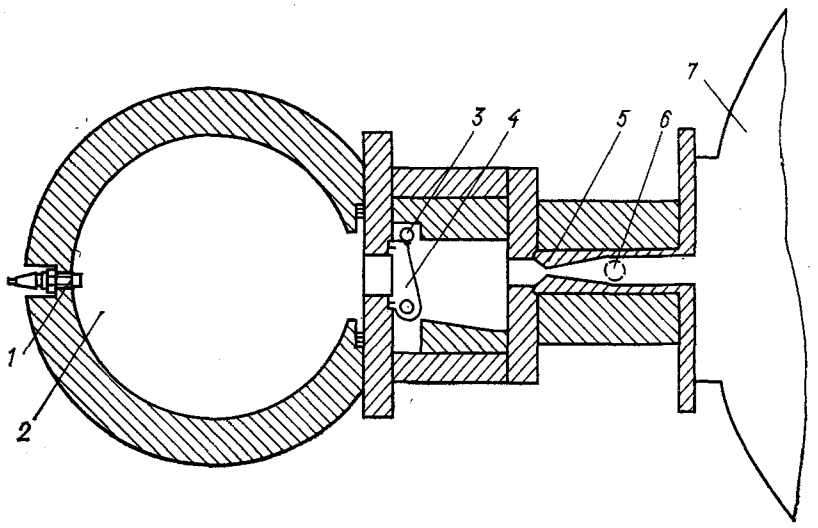

Fig. 7.25. Diagram of detonation laser with an electrically released valve: 1) ignition; 2) explosion chamber; 3) electric release; 4) valve; 5) nozzle; 6) cavity; 7) vacuum chamber.

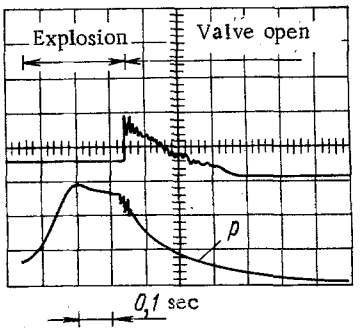

Fig. 7.26. Variation of gas pressure and lasing power in detonation lasers.

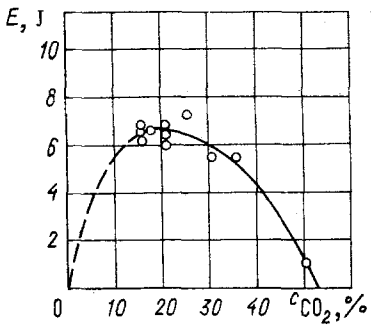

Fig. 7.27. Energy output vs CO_2 concentration.

in the stream, from the nozzle boundaries, cause heating of the gas and optical inhomogeneity of the medium in the cavity.

The high energy losses in the described laser can be attributed to the following factors:

1. About 50% of the gas still remains in the explosion chamber after the end of the laser pulse. This is due to the pressure rise in the vacuum chamber — an effect that can be decreased by using a diffusor.

2. Heat is lost to the walls when the gas expands.

3. Losses due to relaxation in the nozzle.

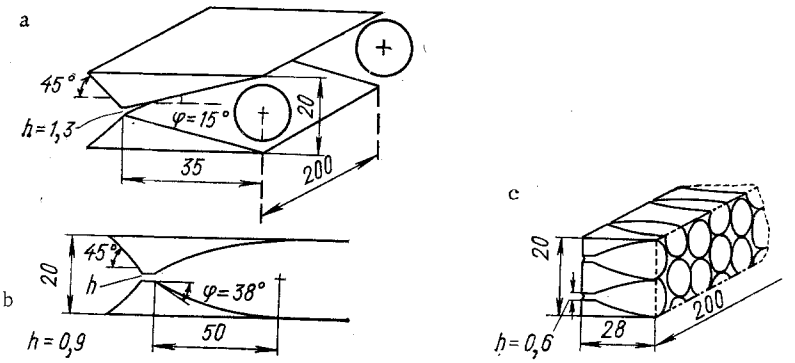

Fig. 7.28. Types of nozzle inserts: a) wedge-shaped, b) contoured; c) block of axisymmetric nozzles.

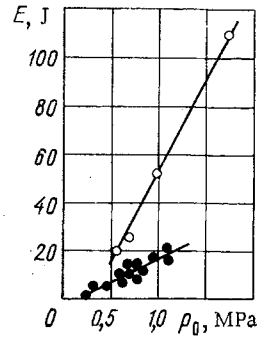

Fig. 7.29

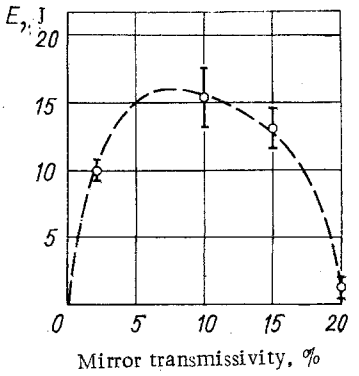

Fig. 7.30

Fig. 7.29. Comparison of the energy output of lasers with different types of nozzles: o) contoured; ●) wedge-shaped.

Fig. 7.30. Output energy vs cavity mirror transmissivity.

4. The small dimensions of the cavity in the flow direction (~1 cm) do not permit full utilization of the energy contained in the N_2, owing to the slow energy transfer from $N_2(v)$ to CO_2 (00v), and the lower energy level cannot transfer all its energy to the translational mode because of the short time of passage of the gas through the interior of the cavity. Estimates show that these factors cause about 50% of the energy entering the cavity to be lost.

5. Flow loss due to nonoptimal cavity parameters.

It is proposed in [90] that with reduction of all or some of these losses a total efficiency of about 0.5% can be reached, and further improvement is possible by raising the stagnation temperature.

In contrast to the described laser design, the question of containing the initial substance in the reaction volume and separating this volume from the evacuated optical cavity was solved by using a periodically acting electromagnetic valve, for periodic operation of the setup (2 cycles/min). Figure 7.31 shows a schematic diagram of such an explosion-pumped laser.

When the explosion chamber is filled with the gas mixture to the required pressure, electromagnet 1 is turned off and the mixture is ignited. When the burning gas reaches maximum temperature and pressure, the valve 5 opens and the gas rushes through the nozzle 6. The pressure ahead of the nozzle is recorded by sensor 4, and the temperature in this zone is calculated from the pressure rise in the chamber. Direct measurements of the temperature in this zone have shown good agreement between the measured and calculated quantities.

After passing through the electromagnetic valve, the explosion products expand in the nozzle and are then exhausted into reservoir 8, in analogy with the design described above. The optical cavity 7, of 20 cm active length, is placed transverse to the gas stream at the exit from the nozzle. The two mirrors of the cavity are displaced 76 mm away from the gas stream to prevent contamination during the laser operation.

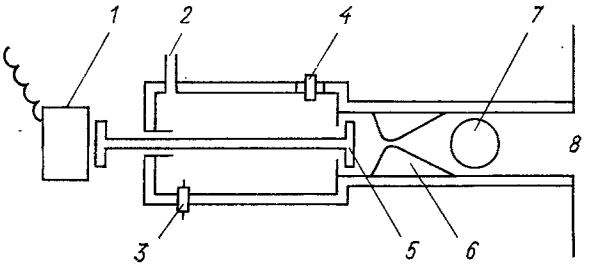

Fig. 7.31. Detonation laser with periodically acting electromagnetic valve: 1) electromagnet; 2) entry of mixture; 3) spark ignition; 4) pressure sensor; 5) valve; 6) nozzle; 7) cavity; 8) reservoir for the spent gas mixture.

For a nozzle with h = 1.5 mm, a cross-sectional area $S/S^* = 15$, and half-angle $\varphi = 15°$, the gas stream leaves the nozzle at $M \approx 4$, while at h = 0.75 mm, $S/S^* = 30$, and $\varphi = 15°$, we have $M \approx 5$.

In the case of the explosive mixture CO/H_2 and the mixture $CO_2/N_2/H_2O = 1.5/8.3/0.2$ it was found that the amplification in the system starts at the instant the valve is opened. For the area ratio $S/S^* = 15$ the pressure in the explosion chamber increased from 0.2 to 0.5 MPa within 0.15 sec after the initiation of the explosion, and during the succeeding 0.15 sec after the opening of the valve the pressure decreased to zero and then slowly increased again to the initial value 0.2 MPa. At the instant when the valve was opened, the optical gain increased and simultaneously the power of the generated output radiation increased to 60 W at a pulse duration of this radiation of 0.8 sec.

After the pressure in the combustion chamber decreased to zero, a rapid growth of the optical absorption in the active medium was observed. In addition, it was noted that the amplification in the active medium and the generation of the stimulated emission were accompanied by fluctuations of the gain of the active medium and of the output power; these were due to a change in the conditions of gas expansion through the nozzle, and apparently also to some gas-dynamic instabilities inherent in this design.

Obviously, it is desirable to examine the possibility of using ordinary hydrocarbons as fuels for the described lasers. The large amount of water vapor released when such fuels are burned can hinder the lasing to a considerable degree, since the cross section for relaxation of antisymmetric oscillation modes of CO_2 molecules under the action of H_2O molecules is large. To determine the influence of water vapor on the characteristics of the described lasers, several types of CO/H_2 mixtures with varying amounts of water vapor in their combustion products were investigated [91]. Figure 7.32 shows the results of these investigations in the form of a plot of the gain vs the percentage water-vapor content.

It can be seen that for a nozzle with h = 1.5 mm ($S/S^* = 15$) the gain reaches a maximum at water-vapor content ~1% and decreases to approximately one-half at a water-vapor content ~8%. At a faster expansion of the gas, i.e., at h = 0.75 mm ($S/S^* = 30$), the gain decreases much more slowly with decreasing water-vapor content than in the first case. A laser with h = 0.75 mm turned out to be less sensitive to the water-vapor content; several types of hydrocarbon fuels were therefore used in this laser to check how the additional combustion products, which are inevitably present in such a fuel, influence the properties of the system. The use of three such fuels — acetylene, propane, and natural gas — leads to generation of intense pulsed stimulated emission in the cases of both oxygen excess and deficiency. For example, when the fuel was natural gas and the active medium was the mixture $CO_2/N_2/H_2O = 0.66/8.0/1.34$, the output radiation power reached 60 W at a pulse duration of the order of 0.03 sec. When the fuel was acetylene and the active medium $CO_2/N_2/H_2O = 1.2/8.2/0.6$, the power was 70-75 W at a pulse duration of ~0.08 sec. If the fuel was propane and the active medium the mixture $CO_2/N_2/H_2O = 0.85/8.0/1.15$, the output radiation had a pronounced form of a series of very short beams, some with 100 W power.

Further progress in the development of the described lasers is possible by increasing the working pressure and temperature. At high temperature the energy fraction connected with the vibrational states of the molecules increases strongly, so that the power and energy of the generated coherent radiation should increase considerably. Higher pressures, in turn, are needed to obtain higher temperatures and higher gas-flow velocities. The increasing coherent-

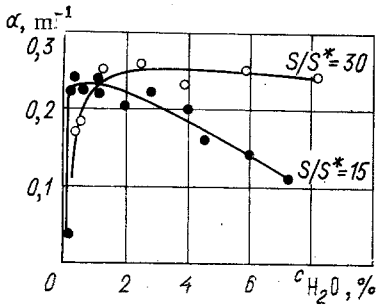

Fig. 7.32. Dependence of the gain α on the content c_{H_2O} of the water vapor in the active medium.

radiation energy will then be released in shorter periods of time, and the peak power of the output radiation will substantially increase as a result.

LITERATURE CITED

1. B. B. Dunne, "Shock wave optically pumped laser," USA Patent No. 3451008 (1969).
2. Problems of Combustion Electrophysics, No. 36, G. M. Krzhizhanovskii Power Research Institute (1975); Ref. Zh. Mekh., No. 11, 101 (1976).
3. V. K. Ablekov, Yu. N. Denisov, F. N. Lyubchenko, et al., "Laser," Inventors' Certificate No. 589841, Priority 2 February 1976, Byull. Izobret., No. 4, 251 (1979).
4. V. K. Ablekov, "Method of producing a medium with a negative absorption coefficient," Inventor's Certificate No. 475964, Priority 27 February 1964, Byull. Izobret., No. 4, 251 (1979).
5. R. W. F. Gross, R. R. Giedt, and T. A. Jacobs, "Stimulated emission behind overdriven detonation waves in F_2O–H_2 mixtures," J. Chem. Phys., 51, No. 3, 1250 (1969).
6. V. M. Marchenko and A. M. Prokhorov, "Possibility of producing an inverted medium for lasers by explosion," Pis'ma Zh. Eksp. Teor. Fiz., 14, No. 2, 116-120 (1971).
7. M. S. Dzhidzhoev, V. V. Korolev, V. N. Markov, et al., "Detonation gasdynamic laser," Pis'ma Zh. Eksp. Teor. Fiz., 13, 73-76 (1971).
8. F. A. Williams, Combustion Theory: the Fundamental Theory of Chemically Reacting Flow Systems, Addison-Wesley (1965).
9. D. L. Chapman, "On the rate of explosion in gases," Philos. Mag. J. Sci., 47, Ser. 5, No. 284, 90-104 (1899).
10. Ya. B. Zel'dovich, "On the theory of detonation propagation in gaseous svstems," Zh. Eksp. Teor. Fiz., 10, No. 5, 542-568 (1940); "Pressure and velocity distributions in detonation explosion products, particularly for spherical detonation-wave propagation," Zh. Eksp. Teor. Fiz., 12, No. 9, 389-406 (1942); Theory of Combustion and Detonation of Gases [in Russian], Izd. Akad. Nauk SSSR, Moscow–Leningrad (1944).
11. J. Neuman, Theory of Detonation Waves, Office of Scientific Research and Development, Report N 549 (1942); W. Doring, "Uber den Detonationsvorgang in Gasen," Ann. Physik, 43, 421-436 (1943).
12. C. Campbell and D. W. Woodhead, "The ignition of gases by an explosion wave. I. Carbon monoxide and hydrogen mixtures," J. Chem. Soc., 129, 3010-3012 (1926); "Striated photographic records of explosion waves," J. Chem. Soc., 130, 1572-1578 (1927).
13. Yu. N. Denisov, B. V. Voitsekhovskii, et al., "Wave splitting (fine structure) of spin detonation," Discovery Diploma No. 134, Priority 12 February 1957, 24 February 1958, Byull. Izobret. Otkrytii, No. 48, 4-5 (1973).
14. M. A. Rivin and A. S. Sokolik, "Explosion limits of gas mixtures. 3. Limits in mixtures of carbon monoxide and methane," Zh. Fiz. Khim., 8, 767-773 (1936); Ya. K. Troshin and K. I. Shchelkin, "Spin in limits of gas detonation," Izv. Akad. Nauk SSSR, Otd. Tekh. Nauk, No. 8, 142-143 (1957).
15. Yu. N. Denisov et al., "Instability of detonation wave in gases," Discovery Diploma No. 111, Priority 5 November 1957, Byull. Izobret. Otkrytii, No. 24, 4-5 (1972); Yu. N. Denisov and Ya. K. Troshin, "Pulsating and spin detonation of gas mixtures in tubes," Dokl. Akad. Nauk SSSR, 125, No. 1, 110-113 (1959).
16. Yu. N. Denisov and Ya. K. Troshin, "Structure of gas detonation in tubes," Zh. Tekh. Fiz., 30, No. 4, 450-459 (1960).
17. B. V. Voitsekhovskii, V. V. Mitrofanov, and M. E. Topchiyan, Structure of Detonation in Gases [in Russian], Sib. Otd. Akad. Nauk SSSR, Novosibirsk (1963), p. 168.

18. V. I. Manzhalei, V. V. Mitrofanov, and V. A. Subbotin, "Measurements of inhomogeneities of a detonation front in gas mixtures at increased pressures," Fiz. Goreniya Vzryva, No. 1, 102-110 (1974).
19. R. A. Strehlow and C. D. Engel, "Transverse waves in detonations: II. Structure and spacing in H_2—O_2, C_2H_2—O_2, C_2H_4—O_2, and CH_4—O_2 systems," AIAA J., 7, No. 3, 492-496 (1969).
20. A. Schmidt, "Über den Nachweis der Gültigkeit der hydrodinamisch-thermodynamischen Theorie der Detonation fur feste und flüssige Sprengstoffe," Z. Phys. Chem., A189, 88-94 (1941).
21. B. P. Volin et al., "Reaction-kinetics nature of inhomogeneities in a shock front and their role in the propagation of a gas detonation," Zh. Prikl. Mekh. Tekh. Fiz., No. 2, 78-89 (1967).
22. Yu. N. Denisov and Ya. K. Troshin, "Discrete character of change of structure of a gas detonation," Zh. Prikl. Mekh. Tekh. Fiz., No. 2, 90-92 (1967).
23. K. I. Shchelkin, "Fast combustion and spin detonation of gases," Voenizdat, Moscow (1949).
24. Yu. N. Denisov and Ya. K. Troshin, "Mechanism of detonation burning," Zh. Prikl. Mekh. Tekh. Fiz., No. 1, 21-35 (1960).
25. V. V. Mitrofanov, "Structure of detonation wave in a planar channel," Zh. Prikl. Mekh. Tekh. Fiz., No. 4, 100-105 (1962).
26. A. N. Voinov, "Mechanism of onset of detonation spin," Dokl. Akad. Nauk SSSR, 73, No. 1, 125-128 (1950).
27. B. V. Voitsekhovskii, "Spin detonation," Dokl. Akad. Nauk SSSR, 114, 717-720 (1957).
28. B. V. Voitsekhovskii, "Investigation of the structure of the front of a spin detonation," in: Trudy MFTI, Oborongiz, Moscow (1958), pp. 81-91.
29. B. V. Voitsekhovskii and B. V. Kotov, "Optical investigation of the front of a spin detonation wave," Izv. Sib. Otd. Akad. Nauk SSSR, No. 4, 74-80 (1958).
30. B. V. Voitsekhovskii, V. V. Mitrofanov, and M. E. Topchiyan, "Structure of flow in a spin detonation wave," Zh. Prikl. Mekh. Tekh. Fiz., No. 3, 27-30 (1962).
31. M. E. Topchiyan, "Experimental investigations of spin detonation by pressure sensors," Zh. Prikl. Mekh. Tekh. Fiz., No. 4, 94-99 (1962).
32. V. V. Mitrofanov, V. A. Subbotin, and M. E. Topchiyan, "Contribution to the measurement of pressure in a transverse spin wave," Zh. Prikl. Mekh. Tekh. Fiz., No. 3, 45-48 (1963).
33. Yu. N. Denisov and Ya. K. Troshin, "Thermogasdynamic model of pulsating detonation," in: Third All-Union Conf. on Combustion Theory [in Russian], Izd. Akad. Nauk SSSR (1960), Vol. 1, pp. 200-207.
34. Yu. N. Denisov and Ya. K. Troshin, "On the mechanism of detonative combustion," in: Eighth Symp. on Combustion, Baltimore (1962), pp. 600-610.
35. Yu. N. Denisov, "Influence of volume effect on the structure of a detonation front," Dokl. Akad. Nauk SSSR, 187, No. 2, 358-361 (1969).
36. V. E. Gordeev, "Cause of multiplication of kinks of detonation front," Dokl. Akad. Nauk SSSR, 226, No. 2, 288-291 (1976).
37. A. N. Dremin, "Contemporary problems in research into detonation in condensed media," in: Sci. Papers of Mechanics Inst. of Moscow State Univ., No. 21, Moscow State Univ. (1973), pp. 150-157.
38. Yu. N. Denisov, "High-frequency processes in the core of a spin detonation," Fiz. Goreniya, Vzryva, No. 3, 386-392 (1974).
39. Yu. N. Denisov and I. I. Podtynkov, "Elements of high-frequqency process in detonation waves," in: Fourth All-Union Symposium on Combustion and Explosion, Abstract of Papers, Chernogolovka, Inst. Khim. Fiz. Akad. Nauk SSSR (1974), p. 45; in the book: Combustion and Explosion [in Russian], Nauka (1977), pp. 454-460.
40. M. Busco, "Optical properties of detonation waves (optics of explosives)," in: Proc. Fifth Symp. (Int.) on Detonation, Pasadena, Calif.—Arlingt., 513-522 (1970); W. B. Benedick, "Detonation wave shaping," in: Behav. and Util. Explos., Eng. Des. and Biomech. Princip. Appl. Clin. Med., Proc. 12th Ann. Symp., Albuquerque, New Mexico (1972), pp. 47-56.
41. T. V. Bazhenova, L. V. Gvozdeva, Yu. S. Lobastov, et al., Shock Waves in Real Gases [in Russian], Nauka (1968).
42. I. A. Kunin, Theory of Elastic Media with Microstructure [in Russian], Nauka (1975).
43. A. A. Borisov, "Long-wave perturbations in reacting media," in: Research into Hydrodynamics and Heat Exchange [in Russian], S. S. Kutateladze (ed.), Izd. Sib. Otd. Akad. Nauk SSSR, Novosibirsk (1976), pp. 94-95.

44. V. I. Aref'ev and Yu. N. Denisov, "Contribution to the phase theory of propagation of detonation waves in plasmalike media," in: Electromagnetic Processes in Inhomogeneous Media [in Russian], Izd-vo DVNTs, Vladivostok (1977), p. 48.
45. Ya. B. Zel'dovich and Yu. P. Raizer, Physics of Shock Waves and High-Temperature Hydrodynamic Phenomena, Academic Press (1966, 1967).
46. S. K. Aslanov, "Periodic instability as a theoretical basis for the pulsating structure of detonation," Dokl. Akad. Nauk Ukr. SSR, Ser. "A," No. 4, 318-321 (1977).
47. Yu. N. Denisov, "Investigation of detailed mechanism of detonation," in: Twelfth All-Union Conf. on Problems of Evaporation, Combustion, and Gasdynamics of Disperse Systems, Abstract of Papers, Odessa (1976), p. 41; "Detailed detonation mechanism," Dokl. Akad. Nauk SSSR, 251, No. 3, 628-632 (1980).
48. F. A. Baum, S. A. Kaplan, and K. P. Stanyukovich, Introduction to Cosmic Gasdynamics [in Russian], Fizmatgiz, Moscow (1958).
49. J. H. Lee, R. Knystautas, and C. M. Guirao, "Critical power density for direct initiation of unconfined gaseous detonation," in: 15th Symp. (Int.) Combust., Tokyo, 1974, Pasadena, 53-66 (1974).
50. Yu. N. Denisov, P. I. Kopeika, and S. K. Aslanov, "Onset of spin detonation," in: Physics of Aerodispersed Systems [in Russian], No. 11, Visha Shkola, Kiev (1974), pp. 66-71.
51. V. E. Gordeev, "Limiting velocity of overdriven detonation and stability of discontinuities in detonation spin," Dokl. Akad. Nauk SSSR, 226, No. 3, 619-622 (1976).
52. V.I. Manzhelei and V. A. Subbotin, "Experimental investigations of the stability of overdriven detonation in a gas," Fiz. Goreniya Vzryva, 12, No. 6, 935-942 (1976).
53. J. H. S. Lee, "Recent advances in gaseous detonations," AIAA Paper, No. 0287 (1979).
54. V. M. Akulintsev, A. S. Bashkin, N. M. Gorshunov, et al., "Possibility of lasing on the CO molecule behind the front of an overcompressed detonation wave in a $CS_2 + O_2$ mixture," Fiz. Goreniya Vzryva, 12, No. 5, 739-744 (1976).
55. V. N. Kondrat'ev, Rate Constants of Gas-Phase Reactions (Handbook) [in Russian], Nauka (1971).
56. R. D. Suart, P. H. Dawson, and G. H. Kimbell, "CS_2/O_2 chemical lasers: Chemistry and performance characteristics," J. Appl. Phys., 43, No. 3, 1022-1032 (1972).
57. K. H. Von Homann, G. Krome, and H. G. Wagner, "Schwefelkohlenstoff—Oxydation Geschwindigkeit von Elementarreaktionen. Teil I," Berichte der Bunsen-Gesellschaft fur Physikalische Chemie, 78, 998-1004 (1968); "Schwefelkohlenstoff-Oxydation. II. Zur Oxydation von Carbonylsulfid," ibid., 73, No. 10, 967 (1969); "Schwefelkohlenstoff-Oxydation. III. Die isotherme-oxydation von Schwefelkohlenstoff," ibid., 74, No. 7, 654-659 (1970).
58. D. W. Howgate and T. A. Barr, Jr., "Dynamics of the CS_2—O_2 flame," J. Chem. Phys., 59, No. 6, 2815-2829 (1973).
59. G. Hancock, C. Morley, and W. M. Smith, "Vibrational excitation of CO in the reaction: $O + CS \rightarrow CO + S$," Chem. Phys. Lett., 12, No. 1, 193-196 (1971).
60. B. F. Gordiets, A. I. Osipov, et al., "Vibrational relaxation in gases, and molecular lasers," Usp. Fiz. Nauk, 108, No. 4, 655-699 (1972).
61. J. D. Anderson and M. T. Madden, "Population inversions behind normal shock waves," AIAA J., 9, No. 8, 1630-1632 (1971).
62. N. G. Basov and A. N. Oraevskii, "Obtaining negative temperatures by heating and cooling of a system," Zh. Eksp. Teor. Fiz., 44, No. 5, 1742-1745 (1963).
63. I. R. Hurle and A. Hertzberg, "On the possible production of population inversions by gas dynamic techniques," Minutes of the 1963 Annual Meeting of the Division of Fluid Dynamics, Cambridge, Mass., Nov. 25-27, 1963, Bull. Am. Phys. Soc., 9, No. 5, 582-595 (1964).
64. I. R. Hurle and A. Hertzberg, "Electronic population inversion by fluid-mechanical techniques," Phys. Fluids, 8, No. 9, 1601-1607 (1965).
65. V. K. Konyukhov and A. M. Prokhorov, "Population inversion in adiabatic expansion of a gas mixture," Pis'ma Zh. Eksp. Teor. Fiz., 3, No. 11, 436-439 (1966).
66. J. E. Morgan and H. I. Schiff, "The study of vibrationally excited N_2 molecule with the aid of an isothermal calorimeter," Can. J. Chem., 41, No. 4, 903-912 (1963).
67. V. K. Konyukhov, I. V. Matrosov, A. M. Prokhorov, et al., "Gasdynamic CW laser on a mixture of carbon monoxide, nitrogen, and water," Pis'ma Zh. Eksp. Teor. Fiz., 12, No. 10, 461-464 (1970).
68. N. G. Basov, A. N. Oraevskii, and V. A. Shcheglov, "Thermal methods of laser excitation," Zh. Tekh. Fiz., 37, No. 2, 339-348 (1967).
69. D. M. Kuehn and D. J. Monson, "Experiments with a CO_2 gas-dynamic laser," Appl. Phys. Lett., 16, No. 1, 48-51 (1970).

70. A. P. Dronov et al., "Gasdynamic laser with escape of a mixture heated in a shock tube through a slit," Pis'ma Zh. Eksp. Teor. Fiz., 11, No. 11, 516-519 (1970).
71. B. R. Bronfin, L. R. Boedeker, and J. P. Cheyer, "Thermal laser excitation by mixing in a highly convective flow," Appl. Phys. Lett., 16, No. 5. 214-216 (1970).
72. A. S. Biryukov, B. F. Gordiets, and L. A. Shelepin, "Nonstationary methods of producing an inverted population of the levels of the CO_2 molecule," FIAN Preprint No. 41, 51 (1969).
73. A. S. Biryukov and L. A. Shelepin, "Chemical–mechanical molecular laser," Zh. Tekh. Fiz., 40, No. 12, 2575-2577 (1970).
74. N. G. Basov et al., "Obtaining inverted population of molecules in a supersonic stream of binary gas in a Laval nozzle," Zh. Tekh. Fiz., 38, No. 12, 2031-2041 (1968).
75. "Avco describes gasdynamic system that attains 60-kW pulses," Laser Focus, 6, No. 7, 16-18 (1970).
76. E. Gerry, "The gas-dynamic laser," Laser Focus, 6, No. 12, 27-31 (1970).
77. F. A. Baum, K. P. Stanyukovich, and B. I. Shekhter, Physics of Explosions [in Russian], Fizmatgiz (1959).
78. K. K. Andreev and A. F. Belyaev, Theory of Explosives [in Russian], Oborongiz, Moscow (1960).
79. B. A. Ivanov, Physics of Acetylene Explosion [Russian translation], Khimiya, Moscow (1969).
80. R. L. Taylor and S. Bitterman, "Survey of vibrational relaxation data for processes important in the CO_2–N_2 laser system," Rev. Mod. Phys., 41, 26-47 (1969).
81. R. W. F. Gross, R. R. Giedt, and T. A. Jacobs, "Stimulated emission behind overdriven detonation waves in F_2O–H_2 mixtures," IEEE J. Quantum Electron., QE-6, 168 (1970).
82. R. W. F. Gross, N. Cohen, and T. A. Jacobs, "Chemical laser produced by flash photolysis of F_2O–H_2 mixtures," J. Chem. Phys., 48, No. 8, 3821-3822 (1968).
83. N. Cohen, R. Wilkins and T. A. Jacobs, "Theoretical calculations of detonation initiated chemical lasers," IEEE J. Quantum Electron., QE-6, 168-169 (1970).
84. V. G. Voronkov and A. S. Rozenberg, "Explosive properties of mixtures of gaseous hydrazoic acid with inorganic diluents," Dokl. Akad. Nauk SSSR, 177, No. 4, 835-838 (1967).
85. M. S. Dzhidzhoev, M. I. Pimenov, V. G. Platonenko, et al., "Production of population inversion in polyatomic molecules by the energy of a chemical reaction," Zh. Eksp. Teor. Fiz., 57, No. 2, 411-420 (1969).
86. N. G. Basov, V. V. Gromov, E. L. Koshelev, et al., "Stimulated emission in the explosion of HN_3 in CO_2," Pis'ma Zh. Eksp. Teor. Fiz., 10, No. 1, 5-8 (1969).
87. N. Ya. Vasilik, V. M. Shmelev, and A. D. Margolin, "Effect of chlorine on the gain of a gasdynamic CO_2 laser operating on the products of methane–mixture combustion," Kvantovaya Elektron. (Moscow), 3, No. 10, 2171-2175 (1976).
88. Yu. A. Bokhon, I. I. Davletchin, V. M. Marchenko, et al., "Observation of lasing in a gasdynamic laser on the products of gas detonation," Kratk. Soobshch. Fiz., No. 11, 52-56 (1972).
89. S. Jatsiv, E. Greenfield, F. Dothan-Deutsch, et al., "Pulsed CO_2 gasdynamic laser," Appl. Phys. Lett., 19, No. 3, 65-68 (1971).
90. S. Jatsiv et al., "Experiments with a pulsed CO_2 gas-dynamic laser," IEEE J. Quantum Electron., QE-8, No. 2, 161-163 (1972).
91. J. Tulip and H. Seguin, "Explosion-pumped gas-dynamic CO_2 laser," Appl. Phys. Lett., 19, No. 8, 263-265 (1971).